

UC San Diego

UC San Diego Electronic Theses and Dissertations

Title

Identification and Targeting of Stem Cell Signals in Cancer

Permalink

<https://escholarship.org/uc/item/04r9b96f>

Author

Lytle, Nikki

Publication Date

2018

Peer reviewed|Thesis/dissertation

UNIVERSITY OF CALIFORNIA SAN DIEGO

Identification and Targeting of Stem Cell Signals in Cancer

A dissertation submitted in partial satisfaction of the requirements for the degree Doctor of Philosophy

in

Biomedical Sciences

by

Nikki K. Lytle

Committee in charge:

Professor Tannishtha Reya, Chair
Professor David Cheresh
Professor Scott Lippman
Professor Andrew Lowy
Professor Maïke Sander
Professor Jing Yang

2018

Copyright

Nikki Katherine Lytle, 2018

All rights reserved.

This Dissertation of Nikki K. Lytle is approved, and it is acceptable in quality and form for publication on microfilm and electronically:

Chair

University of California San Diego

2018

DEDICATION

To my companion, Scott, who has been by my side for the last 8 years of excitement, joy, disappointment, and dejection. You've seen my ugliest side during grad school and chose to stay with me. I can't wait for the next 50 years with you.

To the friends I lean on most: Kelli, Sam, Gwen, and Claire. You have been a critical support system. I am grateful for your infinite patience. I can always count on you.

To Dolly Parton, who is the love of my life. I would not have finished grad school without your sweet face. To FC, you are a confusing and funny chicken.

EPIGRAPH

“We just can’t seem to break our addiction to the kinds of fuel that will bring back a climate last seen by the dinosaurs, a climate that will drown our coastal cities and wreak havoc on the environment and our ability to feed ourselves. All the while, the glorious sun pours immaculate free energy down upon us, more than we will ever need... The dinosaurs never saw the asteroid coming. What’s our excuse?”

Neil deGrasse Tyson

TABLE OF CONTENTS

Signature Page	iii
Dedication	iv
Epigraph	v
Table of Contents	vi
List of Figures	ix
List of Tables	xi
List of Abbreviations	xii
Acknowledgements	xiv
Vita	xvi
Abstract of the Dissertation	xviii
Chapter 1: Introduction	1
Preface	2
Abstract	3
Introduction	4
Stem cell states in cancer initiation	4
Transcriptional context and the cell of origin	4
Epigenetic mechanisms and the cell of origin	7
Stem cell states in tumor propagation	8
Genetic and epigenetic control of cell fate in cancer	8
Asymmetric division and stem cell fate	13
Stem cell states in metastasis	14
Stem cell programs and epithelial-mesenchymal transition	14
Metastatic stem cells	16
Stem cell states in therapy resistance	18
Resistance to chemotherapy and radiotherapy	18
Targeted and immuno-therapies	19
The microenvironment in resistance	20

New technologies	21
Perspectives	22
Acknowledgements	24
References	25
Chapter 2: Image based detection and targeting of therapy resistance in pancreatic adenocarcinoma..	44
Preface	45
Abstract	46
Results	47
Methods	56
Supplemental Figures.....	67
Acknowledgements	77
References	79
Chapter 3: A multiscale map of the stem cell state in pancreatic adenocarcinoma	83
Preface	84
Abstract	85
Introduction	86
Results	88
Discussion	103
Methods	105
Supplemental Figures.....	119
Acknowledgements	126
References	127
Chapter 4: Examination of tumor cell behavior in response to target inhibition using intravital imaging	135
Preface	136
Abstract	137
CD98-mediated adhesive signaling enables the establishment and propagation of acute myelogenous leukemia	138
Introduction	138
Results	139

Methods	143
Supplemental Figures	145
Acknowledgements	146
Tetraspanin 3 is required for the development and propagation of acute myelogenous Leukemia	147
Introduction	147
Results	148
Methods	152
Supplemental Figures	153
Acknowledgements	154
Ubiquitin-conjugating enzyme Ubc13 controls breast cancer metastasis through a TAK1-p38 MAP kinase cascade	155
Introduction	155
Results	156
Methods	159
Supplemental Figures	161
Acknowledgements	163
Epigenetic and transcriptomic profiling of mammary gland development and tumor models disclose regulators of cell state plasticity	165
Introduction	165
Results	166
Methods	171
Supplemental Figures	173
Acknowledgements	174
References	175

LIST OF FIGURES

Figure 1.1. Impact of the cell of origin on cancer development	6
Figure 1.2. Epigenetic regulation of the stem cell state in cancer	9
Figure 1.3. Asymmetric division in cancer	11
Figure 1.4. Metastasis and cancer stem cells	15
Figure 1.5. Therapy resistance in cancer stem cells	17
Figure 2.1. Msi reporter positive pancreatic cancer cells are enriched for tumor initiating capacity	48
Figure 2.2. Loss of <i>Msi</i> impairs tumor initiation and progression in a mouse model of PDAC	50
Figure 2.3. Msi controls expression of key oncogenic and epigenetic signals	52
Figure 2.4. Targeting MSI inhibits pancreatic cancer growth in patient-derived xenografts	53
Figure Supplement 2.1. The Musashi genes <i>MSI1</i> and <i>MSI2</i> are expressed in human PDAC	67
Figure Supplement 2.2. Validation of Msi1 and Msi2 reporter mice	69
Figure Supplement 2.3. Analysis of stem cell traits in Msi1 and Msi2 reporter+ KP ^{fl} C populations	70
Figure Supplement 2.4. Analysis of tumor from Msi null KP ^{fl} C mice	71
Figure Supplement 2.5. Selection for escaper Msi expressing cells in Msi knockout KP ^{fl} C mice	72
Figure Supplement 2.6. Genome wide analysis of Msi controlled programs in pancreatic cancer	73
Figure Supplement 2.7. Molecular targets of Msi signaling	74
Figure Supplement 2.8. Analysis of impaired pancreatic cancer growth with shMSI and MSI1-ASOs ...	75
Figure Supplement 2.9. Elevated expression of Msi in pancreatitis	76
Figure 3.1. Transcriptomic and epigenetic tumor cell map reveals a unique stem cell state	89
Figure 3.2. Genome-scale CRISPR screen identifies core stem cell programs in PDAC	92
Figure 3.3. Identification of novel pathway dependencies of pancreatic cancer stem cells	94
Figure 3.4. Pancreatic cancer stem cells are dependent on immune-type signaling	96
Figure 3.5. The immune-regulatory gene ROR γ is a critical dependency of PDAC propagation	97
Figure 3.6. ROR γ controls expression of super-enhancer associated oncogenes	99
Figure 3.7. Pharmacologic blockade of ROR γ depletes pancreatic cancer stem cells	101
Figure 3.8. ROR γ is amplified in and required for human pancreatic cancer growth	102
Figure Supplement 3.1. REM2+ tumor cells preferentially drive organoid establishment	119

Figure Supplement 3.2. H3K27ac ChIP-seq is concordant with RNA-seq in stem and non-stem cells .	120
Figure Supplement 3.3. Cell line establishment for CRISPR screen	121
Figure Supplement 3.4. Identification of novel regulators of cancer stem cells	122
Figure Supplement 3.5. Transcription factors identified in CRISPR interactome	123
Figure 4.1. AML is dependent on CD98-mediated integrin signaling	142
Figure Supplement 4.1. CD98 loss impairs AML growth and propagation	145
Figure 4.2. Tspan3 is required for normal migration and SDF responsiveness of AML cells	150
Figure Supplement 4.2. Loss of Tspan3 impairs the development and propagation AML	153
Figure 4.3. Ubc13 is not required for BCa tumorsphere formation, intravasation, or extravasation	158
Figure Supplement 4.3. Ubc13 is required for lung colonization by BCa cells	161
Figure 4.4. Sox10+ tumor cells exhibit de-differentiation and mesenchymal features	170
Figure Supplement 4.4. Sox10+ tumor cells exhibit mammary stem/progenitor features	173

LIST OF TABLES

Table 1.1. Asymmetric division genes in cancer 12

Table 3.1. Selected genes from the stem cell networks124

Table 3.2. Novel drug targets in pancreatic cancer125

Table 4.1. Summary of circulating tumor cells in shCtrl and shUbc13 breast tumors162

LIST OF ABBREVIATIONS

ALL	Acute lymphoblastic leukemia
AML	Acute myeloid leukemia
ASO	Anti-sense oligonucleotide
ATAC-seq	Assay for transposase-accessible chromatin using deep sequencing
B-ALL	B Cell acute lymphoblastic leukemia
BCa	Breast cancer
BCP-ALL	B Cell progenitor acute lymphoblastic leukemia
BLI	Bioluminescence imaging
ChIP-seq	Chromatin immunoprecipitation with deep sequencing
CLIP-seq	Crosslinking immunoprecipitation with deep sequencing
CML	Chronic myeloid leukemia
CSC	Cancer stem cell
CTC	Circulating tumor cell
DNMT	DNA methyltransferase
ECM	Extracellular matrix
EMT	Epithelial-mesenchymal transition
FACS	Fluorescence activated cell sorting
fMaSCs	Fetal mammary stem cells
GFP	Green fluorescent protein
HCC	Hepatocellular carcinoma
HH	Hedgehog
HDAC	Histone deacetylase
KLS	Markers of murine hematopoietic stem/progenitor cells (cKit+/Lin-/Sca-1+)
KP ^{ff} C	Kras ^{G12D/+} ;p53 ^{ff} ;Ptf1a ^{Cre/+} mouse model of pancreatic cancer
LPs	Luminal progenitors
MaSCs	Mammary stem cells (adult)
MET	Mesenchymal-epithelial transition

MLs	Mature luminal cells
NOD/SCID	NOD.CB17- <i>Prkdc^{scid}</i> /J mice (immunocompromised)
NSG	NOD.CB17- <i>Prkdc^{scid}Il2rg^{tm1Wjl}</i> /SzJ mice (immunocompromised)
PanIN	Pancreatic intraepithelial neoplasia
PDAC	Pancreatic ductal adenocarcinoma
REM	Reporter of Musashi
RFP	Red fluorescent protein
RIP-PCR	RNA immunoprecipitation with quantitative real-time PCR
SE	Super-enhancer
T-ALL	T Cell acute lymphoblastic leukemia
TF	Transcription factor
UAR	Uniquely open (chromatin) region
URR	Uniquely repressed (chromatin) region

ACKNOWLEDGEMENTS

I would like to first acknowledge Dr. Tannishtha Reya, who has been a wonderful mentor throughout the past 5 years. By training under Tannishtha, I have gained invaluable insight into how to think critically, develop questions, and present findings. She has made me a better scientist. I would also like to thank my thesis committee for providing tremendous insight and guidance as my projects have evolved.

Additionally, I am indebted to the entire Reya lab and I am unsure how I would have finished my doctorate without them. To Claire, Paige, and Alison, thank you for making me laugh on a daily basis and for talking through the big questions in cancer. You all provided motivation when I felt like I wanted to quit. To Ray, Jeevisha, Fred, Long, and Nirakar, you are amazingly helpful and talented scientists that helped me work through difficult scientific questions and experimental approach. I will always have the deepest respect for you. To Marcie: as I've always said, the world would be a much better place if there were a million Marcie's. I will miss you all so much.

I would also like to thank the highly skilled bioinformaticists that were critical for my studies. Roman, Brin, Katie, Kathryn, and Neil, you are all so proficient and exceptionally patient. I benefited tremendously from your insight and direction.

Chapter 1, in full, has been submitted for publication of the material as it may appear in *Nature Reviews Cancer*. Lytle NK, Barber A, Reya T. Stem cell fate in cancer growth, progression and therapy resistance. The dissertation author is the primary author of this work.

Chapter 2, in full, is a reprint of the material as it appears in *Nature*. Fox RG*, Lytle NK*, Jaquish DV, Park FD, Ito T, Bajaj J, Koechlein CS, Zimdahl B, Yano M, Kopp J, Kritzik M, Sicklick J, Sander M, Gradgenett PM, Hollingsworth MA, Shibata S, Pizzo D, Valasek M, Sasik R, Scadeng M, Okano H, Kim Y, MacLeod AR, Lowy AM, Reya T. Image-based detection and targeting of therapy resistance in pancreatic adenocarcinoma. *Nature*. 2016 June 16;534(7607):407-411. The dissertation author was a co-primary author of this paper.

Chapter 3, in part, has been submitted for publication. Lytle NK, Ferguson LP, Fox RG, Gilroy K, Robertson N, Deshpande A, Rajbhandari N, Gilderman T, Esparza LA, Shima Y, Kritzik M, Spahn P, French R, Lin W, Noel P, Han H, Von Hoff D, Lewis N, Fisch KM, Sasik R, Rosenthal SB, Ideker T, Deshpande A,

Lowy AM, Adams P, Reya T. A multiscale map of the stem cell state in pancreatic adenocarcinoma. The dissertation author is the primary author of this work.

Chapter 4, in part, is a compilation of reprints of material as it appears in (1) *Cancer Cell*. Bajaj J*, Konuma T*, Lytle NK, Kwon HY, Ablack JN, Cantor JM, Rizzieri D, Chuah C, Oehler VG, Broome EH, Ball ED, van der Horst EH, Ginsberg MH, Reya T. CD98-mediated adhesive signaling enables the establishment and propagation of acute myelogenous leukemia. *Cancer Cell*. 2016 Nov 14;30(5):792-805. (2) *Cell Stem Cell*. Kwon HY*, Bajaj J*, Ito T, Blevins A, Konuma T, Weeks J, Lytle NK, Koechlein CS, Rizzieri D, Chuah C, Oehler VG, Sasik R, Hardiman G, Reya T. Tetraspanin 3 is required for the development and propagation of acute myelogenous leukemia. *Cell Stem Cell*. 2015 Aug 6;17(2):152-164. (3) *Proc Natl Acad Sci*. Wu X, Zhang W, Font-Burgada J, Palmer T, Hamil AS, Biswas SK, Poidinger M, Borchering N, Xie Q, Ellies LG, Lytle NK, Wu LW, Fox RG, Yang J, Dowdy SF, Reya T, Karin M. Ubiquitin-conjugating enzyme Ubc13 controls breast cancer metastasis through a TAK1-p38 MAP kinase cascade. *Proc Natl Acad Sci U.S.A.* 2014 Sep 23;111(38):13870-13875. The dissertation author was a co-author on these publications. Additionally, chapter 4, in part, has been accepted for publication of the material as it may appear in *Cancer Cell*. Dravis C*, Chung C-Y*, Lytle NK, Herrera-Valdez J, Luna G, Trejo CL, Reya T, Wahl GM. Epigenetic and transcriptomic profiling of mammary gland development and tumor models disclose regulators of cell state plasticity. The dissertation author was a co-author of this work.

VITA

- 2010 Bachelor of Arts, Biology and Religious Studies, Willamette University, Salem, OR
- 2010 - 2012 Research Assistant, Robert S. Dow Neurobiology Laboratories Legacy Research Institute, Portland, OR. Principal Investigator: Dr. Detlev Boison
- 2013 - 2014 Howard Hughes Medical Institute Med-into-Grad Initiative
- 2013 - 2015 NIH T32 Pharmacological Sciences Training Grant
- 2016 - 2018 NIH Ruth L. Kirchstein NRSA Individual Predoctoral Fellowship
- 2018 Doctor of Philosophy, University of California San Diego

PUBLICATIONS

Lytle NK, Ferguson LP, Fox RG, Gilroy K, Robertson N, Deshpande A, Rajbhandari N, Gilderman T, Esparza LA, Shima Y, Kritzik M, Spahn P, French R, Lin W, Noel P, Han H, Von Hoff D, Lewis N, Fisch KM, Sasik R, Rosenthal SB, Ideker T, Deshpande A, Lowy AM, Adams P, Reya T. A multiscale map of the stem cell state in pancreatic adenocarcinoma. *In preparation*.

Lytle NK, Barber A, Reya T. Stem cell fate in cancer growth, progression and therapy resistance. *Nature Reviews Cancer*; In Revision.

Shi Y, Gao W*, **Lytle NK***, Huang P, Dann AM, Ridinger M, DelGiorno KE, Erikson G, Sun H, Meisenhelder J, Terenziani E, Santisakultarm P, Manor U, Leblanc M, Umetsu SE, Collisson EA, Lowy AM, Reya T, Donahue TR, Downes M, Wahl GM, Evans RM, Pawson T, Tian R, Hunter T. Targeting LIF-mediated paracrine communication for pancreatic cancer therapy. *Nature*. In Revision.

Dravis C*, Chung C-Y*, **Lytle NK**, Herrera-Valdez J, Luna G, Trejo CL, Reya T, Wahl GM. Epigenetic and transcriptomic profiling of mammary gland development and tumor models disclose regulators of cell state plasticity. *Cancer Cell*. In Revision.

Todoric J, Antonucci L, Di Caro G, Li N, Wu X, **Lytle NK**, Dhar D, Banerjee S, Fragman JB, Browne CD, Umemura A, Valasek MA, Kessler H, Tarin D, Goggins M, Reya T, Diaz-Meco M, Moscat J, Karin M. (2017) Stress-activated NRF2-MDM2 cascade controls neoplastic progression in pancreas. *Cancer Cell*. 32(6):824-839.

Bajaj J*, Konuma T*, **Lytle NK**, Kwon HY, Ablack JN, Cantor JM, Rizzieri D, Chuah C, Oehler VG, Broome EH, Ball ED, van der Horst EH, Ginsberg MH, Reya T. (2016) CD98-mediated adhesive signaling enables the establishment and propagation of acute myelogenous leukemia. *Cancer Cell*. 30(5):792-805.

Fox RG*, **Lytle NK***, Jaquish DV, Park FD, Ito T, Bajaj J, Koechlein CK, Zimdahl B, Yano M, Kopp J, Kritzik M, Sicklick J, Sander M, Grandgenett PM, Hollingsworth MA, Shibata S, Pizzo D, Valasek M, Sasik R, Scadeng M, Okano H, Kim Y, MacLeod AR, Lowy AM, Reya T. (2016) Image based detection and targeting of therapy resistance in pancreatic adenocarcinoma. *Nature*. 534(7607):407-11.

Kwon HY, Bajaj J, Ito T, Blevins A, Konuma T, Weeks J, **Lytle NK**, Koechlein CS, Rizzieri D, Chuah C, Oehler VG, Sasik R, Hardiman G, Reya T. (2015) Tetraspanin 3 is required for the development and propagation of acute myeloid leukemia. *Cell Stem Cell*. 17(2):152-164.

Shen HY, van Vliet EA, Bright KA, Hanthorn M, **Lytle NK**, Gorter J, Aronica E, Boison D. (2015) Glycine transporter 1 is a target for the treatment of epilepsy. *Neuropharmacology*. 99:554-565.

Wu X, Zhang W, Font-Burgada J, Palmer T, Hamil AS, Biswas SK, Poidinger M, Borchering N, Xie Q, Ellies LG, **Lytle NK**, Wu LW, Fox RG, Yang J, Dowdy SF, Reya T, Karin M. (2014) Ubiquitin-conjugating enzyme Ubc13 controls breast cancer metastasis through a TAK1-p38 MAP kinase cascade. *Proc Natl Acad Sci U.S.A.* 111(38):13870-13875.

Yoo HS, Qiao L, Bosco C, Leong LH, **Lytle N**, Feng GS, Chi NW, and Shao J. (2014) Intermittent cold exposure enhances fat accumulation in mice. *PLoS One.* 9(5):e96432.

Williams-Karnesky RL, Sandau US, Lusardi TA, **Lytle NK**, Farrell JM, Pritchard EM, Kaplan DL, and Boison D. (2013) Epigenetic changes induced by adenosine augmentation therapy prevent epileptogenesis. *J Clin Invest.* 123(8):3552-3563.

Duncan JE, **Lytle NK**, Zuniga A, and Goldstein LSB. (2013) The microtubule regulatory protein Stathmin is required to maintain the integrity of axonal transport in *Drosophila*. *PLoS ONE.* 8(6):e68324.

Shen HY, Singer P, **Lytle N**, Wei CJ, Lan JQ, Williams-Karnesky RL, Chen JF, Yee BK, and Boison D. (2012) Adenosine augmentation ameliorates psychotic and cognitive endophenotypes of schizophrenia. *J Clin Invest.* 122(7):2567-2577.

Lusardi TA, **Lytle NK**, Szybala C, Li T, and Boison D. (2011) Caffeine prevents acute mortality after TBI in rats without increased morbidity. *Exp Neurol.* 234(1):161-168.

Li T, **Lytle N**, Lan J, Sandau US, and Boison D. (2011) Local disruption of glial adenosine homeostasis in mice associates with focal electrographic seizures: a first step in epileptogenesis? *Glia.* 60(1):83-9

ABSTRACT OF THE DISSERTATION

Identification and Targeting of Stem Cell Signals in Cancer

by

Nikki K. Lytle

Doctor of Philosophy in Biomedical Sciences

University of California San Diego, 2018

Professor Tannishtha Reya, Chair

It is common to hear scientists equate targeting cancer to playing whack-a-mole: hitting one “mole” (or pro-tumorigenic signal) will lead to the emergence of another mole, then another, and so on. This analogy is far too simple and disregards the elegant evolution observed in cancer. In this respect, I propose that cancer is more comparable to a pin art board. At one moment the pins are in the shape of a hand. If asked to describe the pin art board, all would agree that fingers and a palm are critical components. In the next moment the hand is replaced with a face defined by eyes and a mouth. Although these two snapshots seem quite different, there are underlying mechanics that can explain the fluidity that permits the hand to morph to a face, and those mechanics are shared across all pin art boards. In a similar way, cancer is quite fluid. At one moment the tumor is addicted to a signaling axis that can be therapeutically targeted. Upon blockade of that addiction, the tumor is able to elegantly morph into a new state with an entirely new set of defining features. This “new tumor state” is not a random “mole” that sporadically pops up in an unpredictable manner; rather, the tumor can predictably hijack mechanisms that permits fluid state changes. Instead of focusing on the mole, or better yet the shape of the pin art board, here we try to understand the mechanics and drivers of what defines the observed tumor phenotype. What allows tumor cells to overcome toxic insults, and adapt to novel and harsh environments?

To this end, tumor initiation, therapy resistance, and metastasis are highly dependent on the ability for cells to adapt and survive, and thus represent processes that select for the most adaptable, aggressive cell type. The following thesis aimed to identify and characterize tumor cells with the intrinsic capacity to thrive during those processes. Particular focus was given to tumor cells with stem cell properties, as these are characteristically able to respond to stresses and regenerate tumors accordingly. Using pancreatic cancer as a model system, we identified a population of tumor cells, functionally marked by the stem cell fate determinant Musashi, with cancer stem cell characteristics: Musashi+ cells were enriched for tumor propagating capacity, highly resistant to cytotoxic therapies, and preferentially survived in circulation. Further, we carried out unbiased screens to understand the landscape that defined these pancreatic cancer stem cells. This led to the discovery of targetable signals required for maintenance of a stem cell state, and thus represents an exciting new therapeutic approach designed to collapse mechanisms that promote an adaptable, aggressive cell phenotype. Finally, I highlight the power of using intravital imaging to track tumor cell behaviors *in vivo*, and apply this tool to better understand intrinsic and extrinsic dependencies.

CHAPTER 1

Stem cell fate in cancer growth, progression, and therapy resistance

Nikki K. Lytle^{1,2,3}, Alison Barber^{1,2,3}, and Tannishtha Reya^{1,2,3}

¹Departments of Pharmacology and Medicine

²Sanford Consortium for Regenerative Medicine

³Moore's Cancer Center

Submitted, in full, for publication in *Nature Reviews Cancer*

July 2018

PREFACE TO CHAPTER 1: INTRODUCTION

Chapter 1, in full, has been submitted for publication as an invited review for *Nature Reviews Cancer*, entitled “Stem cell fate in cancer growth, progression and therapy resistance” by Nikki K. Lytle, Alison Barber, and Tannishtha Reya. This review discusses current and historical evidence for the existence of cancer stem cells, and the role of cancer stem cells in disease progression. Particular focus is given to how aberrant activation of stem cell signals can define transformation susceptibility, promote therapy resistance, and drive metastasis. Finally, we highlight the need to understand and identify molecular signals that are essential for the maintenance of the stem cell state in order to improve therapy response and patient outcome.

ABSTRACT

Although we have come a long way in our understanding of the signals that drive cancer growth, and how these signals can be targeted, effective control of this disease remains a key scientific and medical challenge. The therapy resistance and relapse that is commonly seen is driven in large part by the inherent heterogeneity within cancers that allows drugs to effectively eliminate some, but not all of the malignant cells. Here we have focused on the fundamental drivers of this heterogeneity by examining emerging evidence that show that these traits are often controlled by the disruption of normal cell fate and aberrant adoption of stem cell signals. We discuss how undifferentiated cells are preferentially primed for transformation and often serve as the cell of origin for cancers. We also consider evidence that activation of stem cell programs in cancers can lead to progression, therapy resistance and metastatic growth, and that targeting these attributes may enable better control over a difficult disease.

KEYWORDS

Cancer stem cells, stem cell signals, stem cell fate, cell of origin, asymmetric division, tumor heterogeneity, therapy resistance, epithelial-mesenchymal transition

INTRODUCTION

Over the last several decades, cancer has largely been treated as a disease of aberrant proliferation and survival, and the therapies most commonly used today- radiation and chemotherapy- mainly target these properties. Despite the successes of cytotoxic therapies which include cures achieved in childhood acute lymphoblastic leukemia (ALL)¹ and lymphoma², it is also clear that we are reaching the limits of how effective these approaches can be, at least in their current form. Thus, it has become important to examine aspects of oncogenesis beyond aberrant survival and proliferation.

One critical aspect of the changes that occur as benign lesions transition to malignant ones is the progressive acquisition of the undifferentiated state. Benign lesions are often more differentiated while malignancies more undifferentiated, suggesting a reversal of the differentiation signals put in place during development. As many of the signals that drive the undifferentiated state are also key to conferring a stem cell fate, it is perhaps not surprising that many cancers show an acute dependence on these signals to maintain their more aggressive state.

In addition, stem cell signals are also integrally linked to cancer initiation, propagation and therapy resistance. While driver mutations are key to initiating oncogenesis, the cells in which these mutations occur are of equal importance; thus, mutations that cannot transform differentiated cells can transform undifferentiated ones³⁻⁶, suggesting that the stem or progenitor cell state provides a more permissive context for transformation. Even after cancer establishment, perpetuation of a stem cell state in some cells creates cancer stem cells, 'driver cells' that are preferentially aggressive and pose a high risk for therapy resistance and disease relapse⁷. Thus, understanding and targeting the signals critical to sustaining these cells is essential to improving outcomes. Here we focus on how regulation of stem cell fate can influence not only cancer initiation, but serve as a driver event for disease progression, therapy resistance and metastatic growth.

STEM CELL STATES IN CANCER INITIATION

Transcriptional context and the cell of origin

Key studies have shown that subsets of cells with stem and progenitor characteristics in normal tissues are particularly susceptible to oncogenic transformation. Beginning with work in hematologic

malignancies where chronic myeloid leukemia (CML) arose only when the *BCR-ABL* mutation occurred in stem cells^{8,9}, this paradigm has now been extended to other hematological^{10,11} and solid cancers^{3,12}. Defining the cell of origin can be critical for both understanding environments that are permissive for transformation and the signals required for transformation. *BCR-ABL* provides an interesting example of an oncogene that produces different outcomes depending on the cell in which it is expressed. While *BCR-ABL* rapidly triggers CML when introduced into stem cells, it triggers B cell ALL (B-ALL) when expressed in progenitor cells¹³. Interestingly, this difference in cell of origin is closely coupled to differential signal dependencies: while loss of β -catenin blocks CML propagation, it does not impact B-ALL to the same extent¹³. Thus, the cell of origin can define both the nature of the cancer, and its dependencies.

The link between the cell of origin and tumor types holds true across some solid cancers. For example, expression of *Kras* in the context of *p53* loss triggers squamous cell carcinoma¹⁴ when targeted to either interfollicular epidermis cells or hair follicle cells. Despite both cell types giving rise to squamous cell carcinoma, interfollicular epidermis-derived tumors are largely epithelial in nature with limited metastatic potential, and hair follicle-derived tumors contain a mixture of both epithelial and mesenchymal tumor cells and are associated with higher incidence of metastasis. Interestingly, transplantation of epithelial tumor cells from either tumor resulted in secondary tumors that histologically mirrored the primary tumor, suggesting that the balance between mesenchymal and epithelial phenotype was determined by the cell of origin¹⁴. Similarly, the cell of origin in glioblastoma can dictate sensitivity to transformation and the type of tumor formed. Concurrent inactivation of *Trp53*, *Nf1*, and *Pten* in neural stem cells, neural progenitor cells, or in oligodendrocyte progenitors triggers the development of unique subtypes of glioblastoma with distinct gene expression profiles that are predictive of differential molecular dependencies^{15,16}. These studies suggest that the transcriptional context of the cell of origin can be selectively permissive for specific tumor types and can be at least as strong a determinant of tumorigenesis as the driver mutations themselves (Figure 1.1A).

In contrast, activation of Hedgehog signaling via genetic deletion of its receptor Patched (*Ptch1*) in either neural stem cells or granule neural precursors leads to development of aggressive medulloblastomas

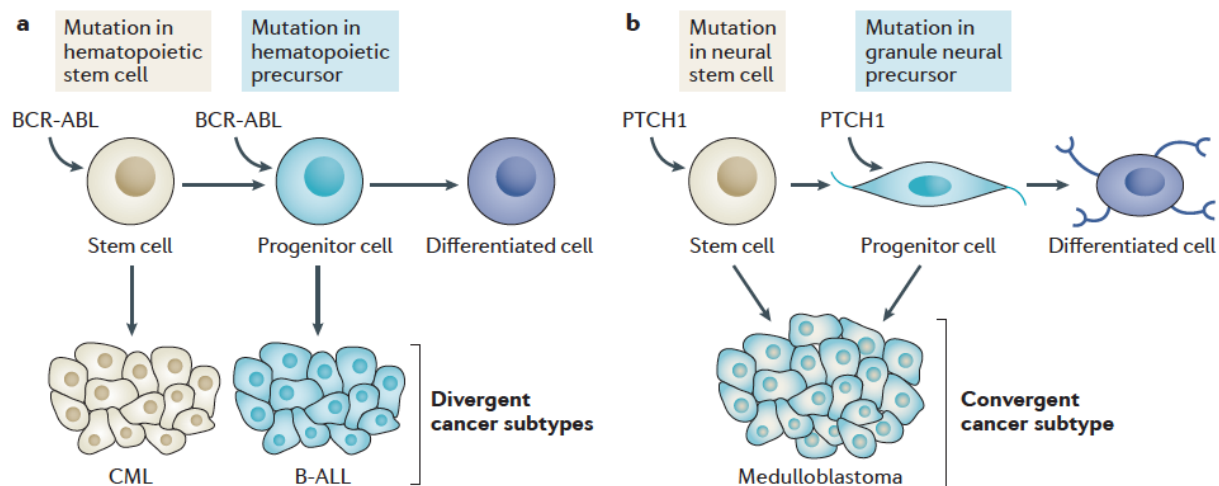


Figure 1.1. Impact of the cell of origin on cancer development

(A) Oncogenic mutation can drive distinct cancer subtypes depending on the epigenetic and transcriptomic profile of the cell of origin. For example, in hematologic malignancies, when BCR-ABL is introduced into stem cells it results in CML, however when this same mutation is introduced into progenitor cells it results in B-ALL. **(B)** Alternatively, oncogenic mutation in distinct cells of origin can lead to a convergence of cell states that results in the same cancer subtype. For example, in medulloblastoma deletion of Patched (PTCH1) in either neural stem cells or granule neural precursors leads to the development of aggressive medulloblastoma.

with similar molecular profiles¹⁷. This suggests that in some cases certain driver mutations, rather than the cell of origin, define the tumor profile by leading to a convergence of cell states^{17,18} (**Figure 1.1B**).

However, it remains unclear which tumors are predominantly determined by the cell of origin versus the relevant mutations. It is possible that certain mutations are powerful enough in terms of defining cell fate that they can override the transcriptional context of the cell of origin; for example, in the cases above, mutations in the Hedgehog pathway could have a dominant impact on fate because they can control stem cell programs (**Figure 1.1B**). Given the impact of these early tumorigenic events in determining tumor evolution, it may be important to better understand the factors that control tumor cell fate.

Epigenetic mechanisms and the cell of origin

In addition to the transcriptional context dictating susceptibility to transformation, epigenetic states may also direct tumor-initiating capacity and mutational state. Recent studies have shown that changes in DNA¹⁹ or histone²⁰ methylation patterns can override oncogene-induced senescence programs. Moreover, transformed cells that escape senescence have increased DNA methylation, leading to inactivation, at promoters of differentiation-associated genes¹⁹. This suggests that the epigenetic landscape may be a critical determinant of both transformation susceptibility and the acquisition of a stem or progenitor phenotype.

Work in zebrafish models has shown that there is an early permissive epigenetic signature within tumor initiating cells in melanoma²¹. In a field of melanocytes expressing driver mutations, only cells harboring an epigenetic profile that enabled Sox10-driven expression of the fetal oncogene *crestin* were sensitive to transformation²¹. Further, chromatin accessibility in melanocytes significantly overlaps with mutational density in human melanoma samples, suggesting that the combination of mutations that drive tumorigenesis may mirror the permissive epigenetic landscape of the cells within the tissue of origin²². Consistent with this, the epigenetic landscape of normal cells and the mutational status of tumors from the same tissue was also congruent in liver cancer, multiple myeloma, colorectal cancer esophageal cancer, glioblastoma, lung adenocarcinoma, and lung squamous cell carcinoma²². Highlighting the significance of the tumor initiating cell in defining the molecular profile of the tumor, a survey of over 10,000 tumor samples across cancers revealed that the methylome, transcriptome and proteome all cluster by the tissue of origin²³.

Importantly, the epigenetic alterations that precede transformation may act as the functional equivalent of a driver mutation. Bronchial epithelial cells chronically exposed to cigarette smoke display altered methylation patterns that lead to aberrant KRAS, WNT, and EGFR signaling²⁴. The altered epigenetic state sensitized the cells to transformation with just one mutation instead of the three normally required²⁴. Thus a deeper understanding of how epigenetic mechanisms contribute to the acquisition or maintenance of a stem cell phenotype is critical for developing strategies to disable the early permissive states for effective early intervention or prevention strategies.

STEM CELL STATES IN TUMOR PROPAGATION

Genetic and epigenetic control of cell fate in cancer

Beyond their role in establishing the cell of origin and initiating oncogenesis, programs that control cell fate are critical for cancer propagation via both genetic and epigenetic mechanisms. Multiple stem cell signals such as WNT, Notch or Hedgehog are activated in various cancers through mutations. For example, loss of APC in colon cancer activates the WNT pathway²⁵, activating mutations in Smoothed or GLI1, or loss of Patched 1 trigger aberrant Hedgehog signaling in medulloblastoma²⁶ and basal cell carcinoma²⁷, and Notch mutations are prevalent in T-ALL²⁸; in each of these contexts the signals serve as driver mutations highlighting the powerful influence of stem cell signals in promoting oncogenic growth.

While in some cancers, genes encoding members of stem cell signaling pathways are recurrently mutated, in other cancers these same genes are often activated epigenetically (**Figure 1.2A**). For example, *NOTCH1* is epigenetically activated in breast cancers and pancreatic cancer^{29,30}, and WNT signaling in leukemias³¹, and targeting these factors therapeutically using monoclonal antibodies against the Notch ligand delta-like protein 4 (DLL4) or antagonists of CREB binding protein (CBP) and β -catenin, respectively, is currently being tested in clinical trials^{32,33}. More recently defined stem cell signals, such as Musashi (MSI), have also been shown to be both genetically and epigenetically modified in cancers; for example blast crisis CML can harbor translocations in *MSI2*³⁴, but *MSI2* can also be epigenetically activated in the absence of

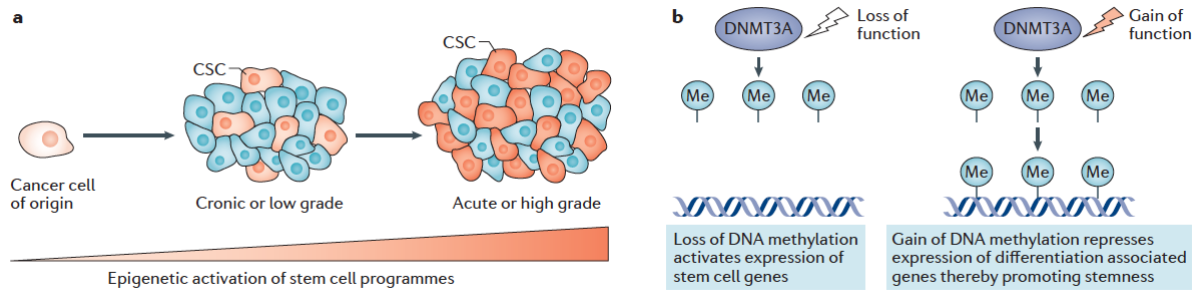


Figure 1.2. Epigenetic regulation of the stem cell state in cancer

(A) During normal development, stem cell programs are extinguished during differentiation; in cancers, such as myeloid leukemia, epigenetic re-activation of stem cell programs can promote propagation and progression to an aggressive state. The activation of these programs in a subpopulation (cancer stem cells (CSCs), shown in orange) is associated with chronic myeloid leukemia (CML), a low-grade disease, while widespread activation of these programs – illustrated by the expanded pool of cancer stem cells in the figure – is associated with blast crisis CML, an aggressive, high-grade disease. **(B)** Epigenetic regulation of stem cell programs may also be mediated through modification of DNA. For example, mutation of the DNA methyltransferase DNMT3A can promote the stem cell state through either loss of function mutations (which can lead to hypomethylation and activation of genes that promote the stem cell state shown at left) or gain of function mutations (which can lead to hypermethylation and silencing of genes associated with differentiation shown at right).

mutations³⁴. The discussion below focuses on how epigenetic mechanisms can influence expression and activation of stem cell signaling pathways to support cancer propagation.

DNA methylation can also influence the acquisition of the stem cell state in cancer. Alterations in DNA methylation may occur early in tumor development: inactivating mutations in gene encoding DNA methyltransferase 3A, *DNMT3A*, leads to altered methylation and leukemia onset^{35,36} and *DNMT3A* deletions can trigger a spectrum of hematologic malignancies in mouse models³⁷⁻³⁹ (**Figure 1.2B**). At a molecular level, mutant DNMT3A leads to decreased DNA methylation⁴⁰ which may confer stem cell fate by activating stem cell genes such as *HOXB*⁴¹, and leaving pro-differentiation genes hypermethylated³⁷. Promoter hypomethylation may also be a mechanism by which other key stem cell genes are reactivated in high grade cancer: for example, hypomethylation of the *MS11* locus is linked to high expression in triple-negative breast cancer⁴² and of the *CD133* locus in glioblastoma stem cells⁴³. Although many studies suggest DNMT3A promotes differentiation and acts as a tumor suppressor, DNMT3A and methylation status may have different consequences depending on the cellular context as it can be found overexpressed in multiple cancers, including breast, colon, and liver cancer⁴⁴. Functionally, DNMT3A can also lead to a differentiation blockade such as in HCC⁴⁵, and its deletion blocked tumor progression in a model of colon cancer⁴⁶. Consistent with these, hypomethylating agents have been shown to promote differentiation and increase sensitivity to chemotherapies in some cancer cells⁴⁷. Given the context specific impact of de novo DNA methylation, further work is clearly needed to define the programs that differentially inhibit or promote tumorigenesis and identify cellular contexts most responsive to disruption of methyltransferase activity.

As a result of efforts to pharmacologically target epigenetic states, several broad acting modulators such as EZH2⁴⁸, BRD4⁴⁹ and histone deacetylases (HDACs)⁵⁰ inhibitors have been shown to have a profound impact on tumor burden by promoting differentiation or by eroding stem cell programs^{49,51-55}. Interestingly perturbation of epigenetic programs via either gain or loss of histone acetylation using HDAC inhibitors or Bromodomain inhibitors, respectively, can deplete cancer stem cells^{53,56}. Similarly, loss or gain of DNA methylation via deletion or activation of DNMT3A can trigger a collapse of oncogenic programs, and can impact cancer stem cells preferentially relative to bulk tumor cells^{39,57}. The bidirectional nature of these dependencies suggests that cancer cells harboring stem cell traits may depend on tightly regulated

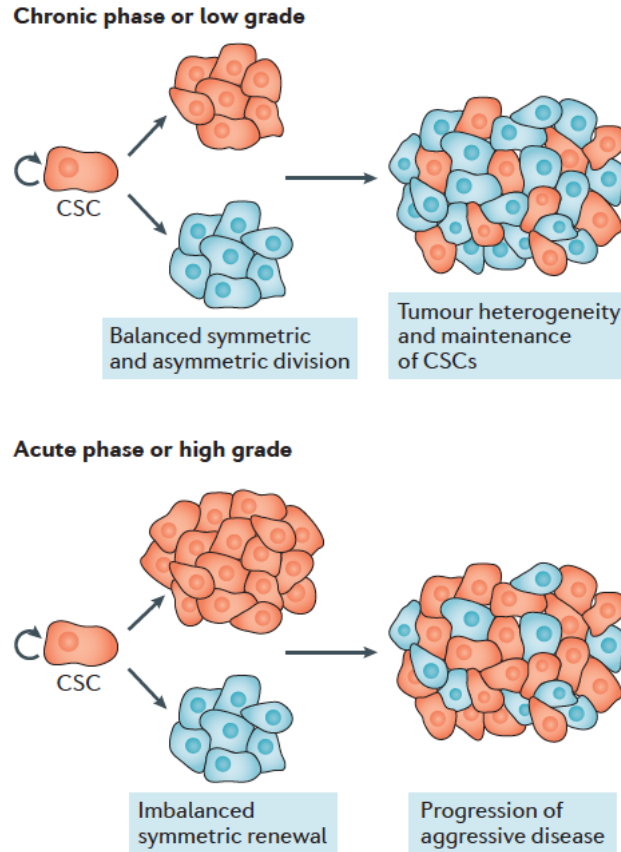


Figure 1.3. Asymmetric Division in Cancer

The disruption of asymmetric division is one way in which cancer may progress to an aggressive state. In low-grade cancers, symmetric renewal and asymmetric divisions are fairly balanced, resulting in both tumor heterogeneity and the maintenance of cancer stem cells (CSCs). However, in high-grade cancers this balance may be shifted towards increased symmetric renewal, which results in the expansion of CSCs which may result in a more aggressive disease state. While imbalances in asymmetric division leading to the progression of cancer have been clearly demonstrated in hematologic malignancies, there is evidence to suggest that disruption of asymmetric division can promote an aggressive state in some solid tumors as well.

Table 1.1. Asymmetric Division Genes in Cancer⁵⁸⁻⁶⁴

Protein	Function in Asymmetric Division	Cancer Type	Effect on Asymmetric Division	Dysregulation in Cancer	Refs
Lgl	Cell Polarity	Leukemia	Promotes asymmetric division	Decreased expression	Ref 58
Numb	Cell fate	Leukemia, colon, breast	Promotes differentiation	Decreased expression	Refs 62, 70, 72
Msi	Cell fate	Leukemia	Promotes stemness	Increased expression	Ref 70
Lis1	Dynein Binding Spindle orientation	Leukemia	Promotes symmetric renewal	N/A	Ref 71
Trim3	Cell fate	Brain	Promotes asymmetric division	Decreased expression	Ref 64
p53	Cell fate	Brain, colon, breast	Promotes asymmetric division	Decreased expression	Refs 72, 75
miR-34a	Cell fate	Colon Brain	Promotes differentiation [Targets Notch]	Decreased expression	Refs 60-62
miR-146a	Cell fate	Colon	Promotes symmetric renewal [Targets Numb]	Increased expression	Ref 62
Lnc34a	Cell fate	Colon	Promotes symmetric renewal [Targets miR-34a]	Increased expression	Ref 63

networks, and either gain or loss of epigenetic modifications can be deleterious. Further, because epigenetic regulators control large-scale programs, targeting them may be particularly effective for perturbing the stem cell state in cancers.

Asymmetric division and stem cell fate

In addition to epigenetic programs, a key way in which stem cell fate can be controlled is through asymmetric division, a posttranslational mechanism critical for diversification through differential segregation and inheritance of proteins during cell division. Misappropriation of asymmetric division by oncogenic events can be a potential force in driving cancer. When asymmetric divisions are balanced, tumours are heterogeneous, containing both cancer stem cells and bulk cancer cells. However, when the balance is shifted towards symmetric division, this results in the expansion cancer stem cells that subsequently drive a more aggressive, undifferentiated state.

The connection between aberrant asymmetric division and cancer was originally identified in *Drosophila*⁶⁵⁻⁶⁸, and has since been linked to mammalian cancers as well. The possibility that the differentiation arrest in aggressive cancers may be driven by disrupted asymmetric division was initially suggested by observations in hematologic malignancies (**Figure 1.3 and Table 1.1**). While division patterns were not altered in chronic phase CML, introduction of a second mutation leading to blast crisis CML triggered an imbalance favoring symmetric renewal⁶⁹. Mechanistically this shift was driven by MSI⁷⁰ which repressed the pro-differentiation signal Numb to promote an aggressive undifferentiated state. Though dysregulation of asymmetric division may result in a more aggressive cancer, the balance can be corrected: thus, both increased expression of Numb or loss of MSI, as well as inhibition of the dynein-binding protein LIS1, which leads to increased asymmetric division, served to halt the progression of aggressive myeloid disease *in vivo*⁷¹.

As in leukemia, a common theme in solid cancers involves disruption of Numb leading to enhanced self-renewal. ERBB2-mutant breast cancer cells display increased symmetric renewal divisions⁷² triggered by symmetric Numb inheritance. MSI signaling has also been implicated in other aggressive cancers such as pancreatic cancer, where it is an indicator of poor prognosis^{53,73}. p53 may also act in part by influencing symmetric renewal, with p53 loss reducing the frequency of asymmetric divisions, thus reducing differentiation in cells in the brain^{74,75}. These data suggest that hijacking asymmetric division can be a point

of control for classic tumor suppressors and oncogenes, and raise the possibility that enforced asymmetric division could be a strategy for controlling certain aggressive cancers.

STEM CELL STATES IN METASTASIS

Stem cell programs and epithelial-mesenchymal transition

The conventional paradigm for metastasis was based originally from observations in breast cancer, and postulated that cancer cells within primary tumors undergo epithelial-mesenchymal transition (EMT), and that this was necessary to enter circulation and transit to secondary sites⁷⁶. Although recent studies have raised doubts about the necessity of EMT during metastasis^{77,78}, there is significant evidence for a gradient of tumor cells^{79,80} expressing both epithelial and mesenchymal markers within the primary tumor, in circulation, and at the secondary site⁸¹⁻⁸³. However, in order for these mesenchymal cells to establish an epithelial tumor at the secondary site, genes responsible for maintaining a mesenchymal cell state must be switched off^{84,85}. These findings led to the idea that EMT occurs at the primary site and is followed by mesenchymal to epithelial transition (MET) at the secondary site for successful metastatic growth. This model bears striking parallels with the stem cell model, which postulates that a subpopulation of cells within the tumor has preferential capacity for driving tumor growth and regrowth at a new site, and can effectively recreate tumor heterogeneity (**Figure 1.4**).

The congruence between the stem cell and EMT-MET models of metastasis are supported by multiple observations showing that a great majority of disseminated tumor cells expressed stem cell markers^{53,86,87}, and that functionally cells expressing stem cell markers like ALDH were highly enriched in their ability to form metastases^{88,89}. Consistent with the idea that the stem cell state is a critical part of EMT and metastatic potential, genome wide analysis of cells undergoing EMT⁹⁰ and circulating tumor cells⁹¹ revealed a remarkably congruent transcriptomic profile between these cells and primary cancer stem cells⁹². Circulating tumor cells isolated from breast cancer patients⁹⁰ or breast cancer patient xenografts⁹¹ overexpress both EMT markers (such as TWIST1, AKT2, PI3K) and stem cell markers (such as ALDH, EPCAM, CD44, CD47, and C-MET), or exhibit stem cell properties such as chemoresistance. Genes associated with EMT are also highly expressed in cancer stem cells⁹³. Vimentin⁹⁴, TGF- β ⁹⁵, and transcription factors TWIST1⁹⁶, SNAI1 and SNAI2^{97,98}, and ZEB1 and ZEB2⁹⁹ are enriched in and support

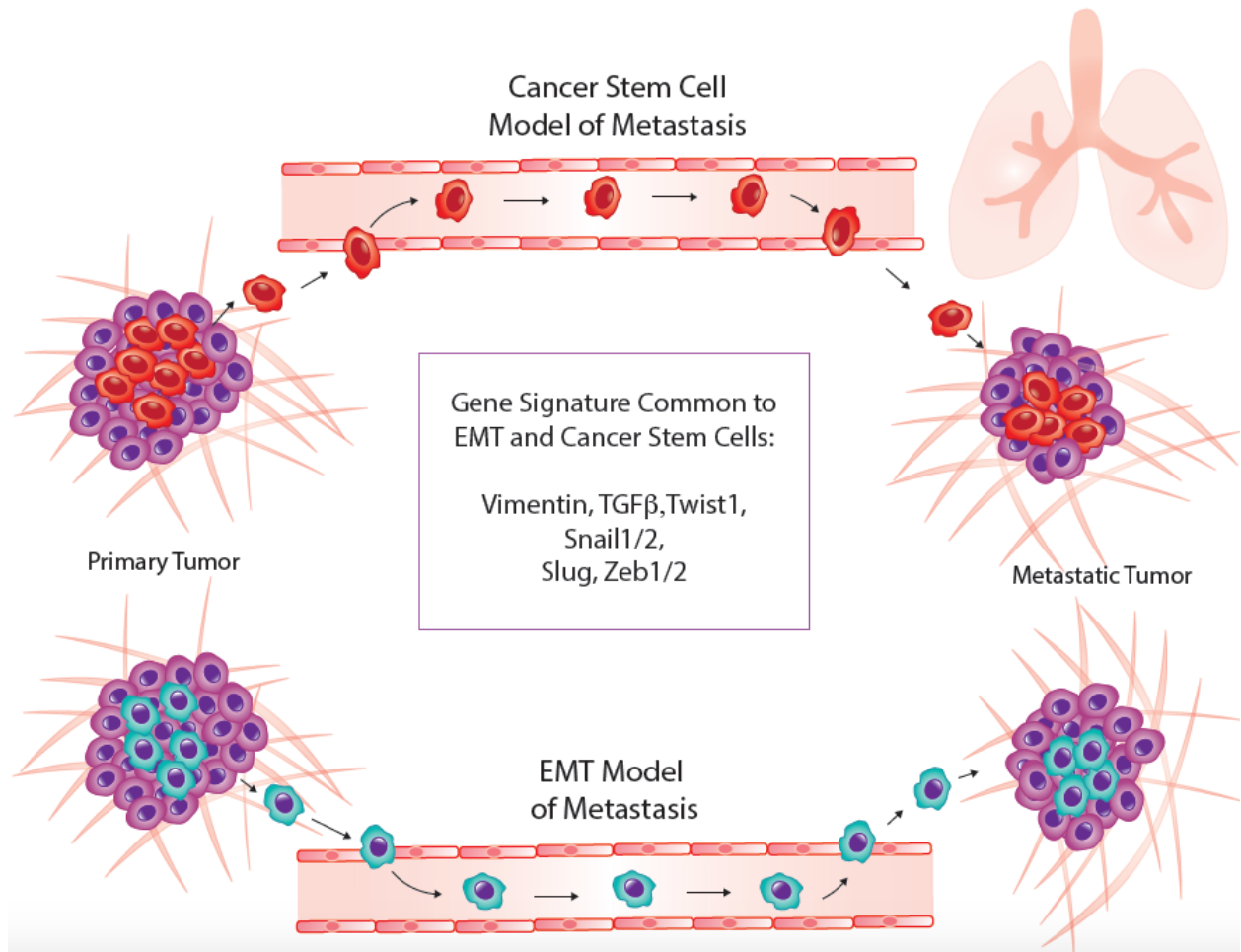


Figure 1.4. Metastasis and cancer stem cells

The classic EMT model of metastasis (top) posits that the dissemination of cancer cells requires loss of epithelial cell traits commensurate with gain of mesenchymal cell traits (dark blue), which enables the cells to detach from the primary tumor and invade surrounding tissue, intravasate and survive in circulation, and, finally, extravasate and localize to a distant metastatic site. Several genes (shown in the center box) have been shown to drive EMT, and their expression serves as markers of the process. Interestingly, cancer stem cells (CSCs) (bottom) are also enriched in disseminated tumor cells, and express the EMT gene signature. Further, the capacity for tumor propagation, which is required for establishment of a tumor at a distant site, is a salient feature of CSCs. The parallels between EMT cells and CSCs raise the possibility that they represent overlapping concepts.

maintenance of cancer stem cells from multiple cancers. Conventional EMT factors such as TWIST1, SNAI1, SNAI2 and ZEB1 can lead to acquisition of stem cell traits such as tumorsphere formation^{100,101}, and activate expression of stem cell programs driven by SOX2 and KLF4¹⁰².

Metastatic stem cells

Although the discussion above strongly suggests that the stem cell state and EMT are in fact overlapping concepts developed by different fields, it is possible that these cells represent populations with substantial but not complete overlap. A “metastatic stem cell”¹⁰³ has been proposed as a population with enhanced metastatic capabilities that may not overlap with other cancer stem cell properties such as therapy resistance or immediate capacity to propagate tumors. The metastatic stem cell could in fact be a subpopulation of stem cells, or one that evolves with new mutations needed to trigger metastasis. For example, CD133+ pancreatic cancer stem cells isolated from primary patient samples preferentially propagate tumors and are highly resistant to chemotherapy¹⁰⁴. At the invasive front of tumor growth, CD133+ cells are enriched for CXCR4 expression and this double-positive population is more migratory than CD133+/CXCR4- cells. Patients with more CD133+/CXCR4+ cells had more metastatic disease, indicating the relevance of these cells for human disease¹⁰⁴. A similar subpopulation of colorectal cancer stem cells expressing CD26 was identified as the population responsible for liver metastasis and predictive of distant metastasis in patients¹⁰⁵.

Exposure to spatially distinct microenvironmental cues throughout the tumor could be one trigger for heterogeneity within cancer stem cells. In this regard, CD133+/CXCR4+ or CD133+/CXCR4- cells may not be two distinct populations but rather represent a gradient of stem cell programs that are expressed at higher or lower levels in response to intra- and inter-cellular signals. Emerging technologies using unbiased single-cell sequencing have independently supported the existence of intratumoral heterogeneity among cells with stem-like properties¹⁰⁶⁻¹⁰⁹. New insights into the state of tumor cells driving metastasis and which programs and cues may promote functionally distinct capacities will likely develop by applying these same unbiased technologies to metastatic tumor cells.

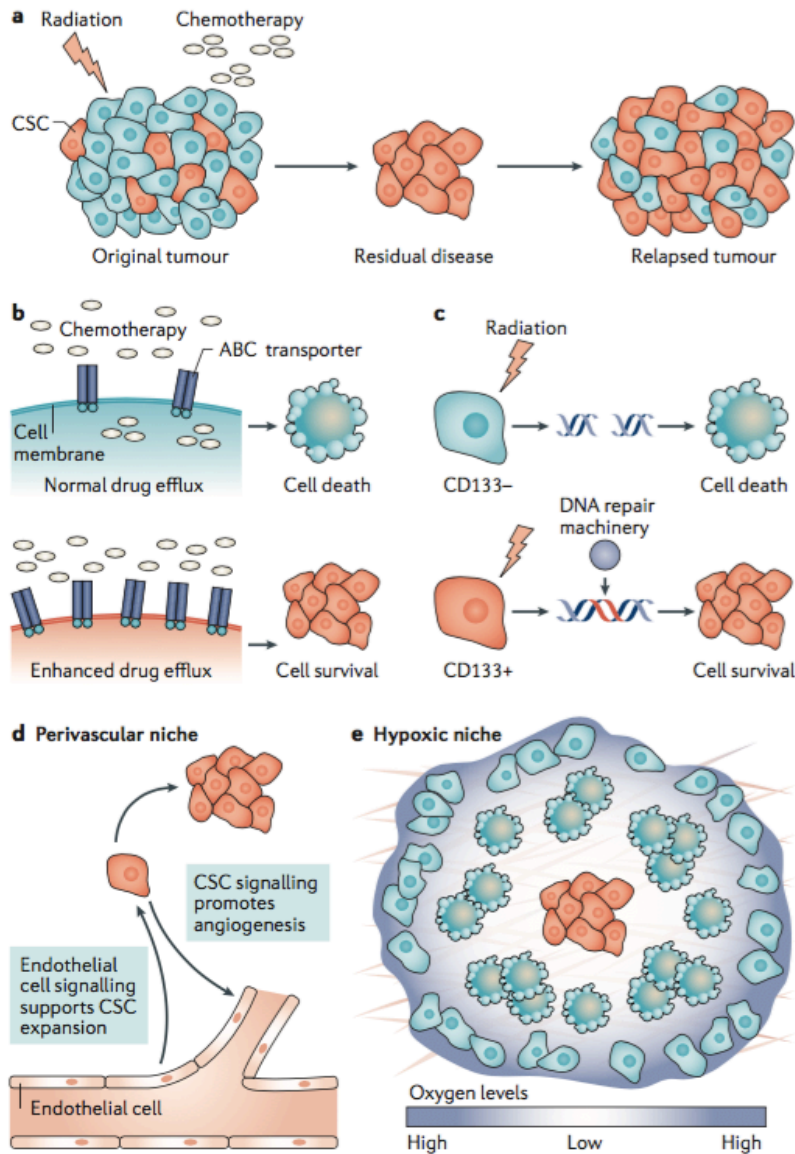


Figure 1.5. Therapy resistance in cancer stem cells

(A) Cytotoxic agents such as radiation and chemotherapy are commonly used to treat cancer, efficiently targeting bulk cancer (blue cells), but not cancer stem cells (CSCs, orange cells). The residual disease can be enriched in CSC populations that can drive a more aggressive disease, triggering recurrence. **(B)** Stem cell properties are commonly hijacked in cancer. One such property is enhanced drug efflux. Chemotherapeutic agents target bulk cancer cells with normal levels of drug efflux, resulting in cell death (top). In CSCs, higher expression of ABC transporters can enhance drug efflux capacity, increasing cell survival (bottom). **(C)** Enhanced DNA repair can also be hijacked in cancer. In glioblastoma, radiation generates unrepaired double strand breaks in CD133⁻ bulk cancer cells, leading to cell death (top). In CD133⁺ CSCs (bottom), the DNA damage checkpoint is activated allowing for repair which leads to enhanced cell survival. **(D)** CSCs utilize the tumor microenvironment for enhanced survival. In brain tumors, the endothelial cells of the perivascular niche promote the survival of CSCs. Endothelial cell signaling supports the stem cell properties of the cancer, which allows CSC expansion. CSCs can promote angiogenesis by secreting factors such as VEGF and SDF1. **(E)** Hypoxic environments can support CSCs. Although hypoxia (represented by the descending oxygen gradient shown in blue) induces some cell death within the tumor, it also promotes CSC expansion (red cells) and triggers expression of genes that promote therapy resistance.

STEM CELL STATES IN THERAPY RESISTANCE

A major challenge in cancer therapy is the fact that not all cells within a tumor are equivalently sensitive to or effectively targeted by most therapies (**Figure 1.5A**). In large part the cells that are not eliminated contribute to residual disease and are the key drivers of cancer relapse. Thus, understanding the basis of differential sensitivity to drugs is critical to more efficient therapies and control of tumor growth. While some cytotoxic therapies have been thought to directly induce mutations that can lead to acquired resistance¹¹⁰⁻¹¹², other studies have revealed pre-existing resistant clones within the tumor that drive tumor re-growth following therapy¹¹¹⁻¹¹⁵. Beyond genomic heterogeneity, it is becoming clear that epigenetic heterogeneity^{116,117} is a key driver of differential sensitivity of cancer cells to multiple therapies. Such epigenetically driven resistance often depends on hijacked properties of normal stem cells such as the expression of drug transporters¹¹⁸ (**Figure 1.5B**), heightened DNA damage repair capacity¹¹⁹ (**Figure 1.5C**), and recruitment of a protective niche¹²⁰.

Resistance to chemotherapy and radiotherapy

Cytotoxic drug efflux is frequently controlled by ABC transporters, including the efflux pumps P-glycoprotein (also known as ABCB1) and BCRP (also known as ABCG2), which are highly expressed on normal and malignant hematopoietic and neural stem cells¹²¹⁻¹²³. Since ABC transporters are generally promiscuous, they have the capacity to non-specifically clear a range of toxic agents. Thus, cytotoxic chemotherapies can relatively successfully eliminate “bulk” tumor cells but leave behind aggressive cancer stem cells that continue to express high levels of ABC transporters (**Figure 1.5B**). In primary neuroblastoma patient derived cell lines, ABCG2^{hi}/ABCA3^{hi} side population tumor cells are able to sustain long-term expansion *ex vivo* and rapidly clear the cytotoxic drug mitoxantrone¹²⁴. Interestingly, this population divides through asymmetric division to give rise to ABCG2^{hi}/ABCA3^{hi} stem cells and more differentiated ABCG2^{low}/ABCA3^{low} daughter cells, suggesting that drug pump expression may be specifically inherited asymmetrically by the self-renewing daughter cell.

Resistance to radiation has been well studied and its links to stem cell traits are perhaps best explored in glioblastoma where radiation is a standard of care. While radiotherapy improves overall survival and quality of life, the majority of patients relapse even following full remission¹²⁵. CD133+ cancer cells, a key population driving tumor growth in human disease¹²⁶, are highly enriched following radiation *in vitro* and

in patient xenografts¹²⁷. This enrichment appears to be driven by the preferential ability of the stem cell population to repair DNA-damage (**Figure 1.5C**) by activating the checkpoint kinases CHK1 and CHK2. While preclinical studies indicated that these stem cells could be radio-sensitized with CHK1 and CHK2 inhibitors¹²⁷, this therapeutic approach failed in trials due to high toxicity¹²⁸. Recent studies suggest that glioma stem cells also rely on PCNA-associated factor (PAF)-driven translesion DNA synthesis for preferential survival following radiation¹²⁹: pharmacologic inhibition of translesion DNA synthesis leads to radio-sensitization and depletion of glioma stem cells, and thus represents a novel therapeutic approach for glioblastoma patients. Efforts to identify new strategies to erode programs that enable enhanced DNA repair in stem cells remain critical to improving the durability of non-targeted as well as some targeted therapies.

Targeted and immuno-therapies

In the last few decades, the greatest strides in molecularly targeted therapies have been led by the discovery of imatinib, the first tyrosine kinase inhibitor. Imatinib effectively blocks BCR-ABL activity in CML and leads to remarkably effective prevention of CML progression¹³⁰. However, among CML patients with minimal evidence of disease, approximately half relapsed within the first year of imatinib withdrawal¹³¹. This relapse was found to be driven by residual disease comprised of leukemia stem cells¹³²⁻¹³⁴. Although imatinib is effective in blocking BCR-ABL in the stem cell fraction¹³⁵, CML stem cells are insensitive to Imatinib because they are not addicted to BCR-ABL. Instead, resistant leukemia stem cells activate several alternative signals to enable survival and renewal including B-catenin, Smoothed, and arachidonate 5-lipoxygenase (ALOX5)¹³⁶⁻¹³⁹. These broad patterns have also been observed in lung cancer, where therapies targeting EGFR mutations leads to enrichment of stem-like cells that are dependent on Notch^{3140,141}, and this resistance can be overcome by inhibiting Notch signaling¹⁴². This provided an early and important example of drug resistance without the evolution of any new mutations, and is one of the best examples of a disease in which the stem cell fraction is the key contributor to residual disease.

With the advent of new cancer therapies exploiting the immune system's innate ability to track and kill cancer cells¹⁴³⁻¹⁴⁶, understanding resistance to such therapies has become an increasing focus, and stem cell signals appear to be relevant in this context. A machine-learning algorithm used to identify epigenetic and transcriptomic signatures from normal stem and differentiated cells revealed that a stem-

high, undifferentiated landscape in tumors is associated with lower immune infiltrate and downregulated PD-L1 pathway¹⁴⁷, which is predictive of poor immunotherapy response^{148,149}. This link is supported by earlier data in melanoma where tumors with high T-cell infiltration responded to immune checkpoint inhibitors¹⁴⁹, and T-cell infiltration was found only in tumors with low Wnt/beta-catenin signaling¹⁵⁰. These data suggest that cancer stem cell signals can alter the tumor microenvironment by directly modulating tumor infiltrating lymphocytes. Bladder cancer stem cells also modulated tumor infiltrating lymphocytes by producing inflammatory mediators like IL-6 and IL-8, which led to infiltration of pro-tumorigenic myeloid cells¹⁵¹. In many ways these studies exemplify the interplay between stem cells and stem cell niche and highlight the importance of mapping the complex interactions tumor stem cells make in vivo that influences the rise of resistance.

The microenvironment in resistance

While intrinsic mechanisms of therapy resistance have been more frequently linked to enhanced survival of cancer stem cells, emerging studies suggest that the microenvironment may be equally critical. In brain tumors, endothelial cells have been shown to interact closely with stem-like cells and secrete factors that support maintenance of stem cell traits^{120,152-156} (**Figure 1.5D**). For example, endothelial cells can induce expression of stem cell programs in glioma cells by secreting nitric oxide to promote Notch signaling¹⁵⁵ or by secreting the CD44 ligand osteopontin¹⁵⁶. In contrast, endothelial cell inhibition through the use of the VEGF inhibitor bevacizumab¹⁵⁷ may also promote stem-like characteristics in non-stem cells through anti-VEGF triggered hypoxia, which can block cancer stem cell differentiation^{158,159} (**Figure 1.5E**). As an example, hypoxia triggers BLIMP1 expression in pancreatic cancer cells¹⁶⁰, which subsequently activates EMT genes associated with therapy resistance. These examples highlight the challenges of interpreting studies involving signals from the tumor microenvironment, as they can be pleiotropic and involve multiple cell types.

In addition to endothelial cells, recent studies have highlighted important roles for other niche components in therapy resistance. Non-stem cells help maintain a pool of cancer stem cells by secreting supportive signals such as WNT in lung adenocarcinoma¹⁶¹ and brain-derived neurotrophic factor (BDNF) in glioblastoma¹⁶². Analysis of cancer associated fibroblasts from breast cancer samples before and after chemotherapy revealed an enrichment of fibroblasts in therapy-resistant tumors¹⁶³. This population was not

only resistant to chemotherapy, but also created a therapy-resistant niche by closely interacting with cancer stem cells and secreting factors such as IL-6 and IL-8 that promoted cancer stem cell survival¹⁶³. Fibroblasts have also been shown to promote cancer stem cell survival and expansion in non-small cell lung cancer¹⁶⁴, basal cell carcinoma¹⁶⁵, and colorectal cancer¹⁶⁶.

Although the microenvironment is generally thought to be particularly important for therapy resistance in solid cancers, emerging evidence shows that leukemia cells generally considered to be highly motile may in fact share this dependency. For example, genetic loss of CD98, a hub for integrin signaling, triggers defects in interactions of AML stem cells with endothelial cells and leads to their depletion¹⁶⁷. Similarly tetraspanin 3 (TSPAN3) loss blocked AML localization to CXCL12-rich bone marrow regions and led to impaired leukemia and AML stem cell growth¹⁶⁸. In addition to myeloid leukemia, T-ALL initiating cells are dependent on CXCR4-mediated cell motility for survival, and microenvironmental-derived CXCL12 is essential for CXCR4 activation¹⁶⁹. In human BCP-ALL and T-ALL, long-term dormant cells are preferentially therapy resistant when associated with microenvironmental cells, suggesting the microenvironment can drive therapy resistance¹⁷⁰. These studies highlight the importance of niche signals for leukemia stem cell homing, proliferation, and survival.

NEW TECHNOLOGIES

The recent development of culture conditions that support long term expansion of normal and neoplastic organoids^{171,172} has provided a new platform for identifying drivers of therapy resistance and improving prediction of good responders. Importantly, patient-derived organoid cultures from colorectal cancer¹⁷³, pancreatic cancer^{174,175}, breast cancer¹⁷⁶, liver¹⁷⁷, and bladder cancer¹⁷⁸ have been shown to retain genetic mutations present in the parental tumor sample. As expected, colorectal cancer organoids with wild-type p53 responded well to nutlin-3a and those with activating mutations in the WNT pathway were sensitive to WNT inhibitors¹⁷³. Additionally, *in vitro* drug screens using patient derived organoids recapitulated *in vivo* xenograft drug response^{176,178}, which supports the robust nature of this system for accurately predicting therapy response. Interestingly, much of the variability in therapy response in tumor organoids can only marginally be explained by mutation burden^{173,178}, suggesting diverse mechanisms of therapy resistance that may reflect patient diversity. This was supported by unbiased longitudinal tracking

of patient and matched pancreatic cancer organoid response to common chemotherapies¹⁷⁵: organoids that were markedly responsive or resistant to specific chemotherapies coincided with patient outcome accordingly. Moreover, parallel transcriptome analysis led to the identification of transcriptional signatures that correlated with patient response¹⁷⁵. Since organoids are specifically derived from cancer stem cells in colon¹⁷³ and pancreas (Lytle, Rajbhandari and Reya, unpublished observations), the studies discussed above provide a unique platform for measuring drug responsiveness of a heterogeneous population that is sustained by stem cell programs. Thus “drug sensitive” organoid signatures provide unique insight into inter-tumoral stem cell heterogeneity and may allow us to better predict vulnerabilities.

PERSPECTIVES

The discussion above provides a view into how stem cell programs can enable cancer initiation, therapy resistance and metastasis. The compelling biology in this rapidly moving field has already led to the development of agents targeting stem cell signals that have emerged as an important new class of differentiation therapies. Among these, the Smoothed antagonists, which inhibit the Hedgehog pathway, are furthest along and are approved for use in the treatment of advanced basal cell carcinoma, and have been in trials for several cancers including medulloblastoma and lung cancer¹⁷⁹⁻¹⁸⁶ based on studies identifying its importance in driving these cancers^{139,187-189}. The Notch pathway has been inhibited using gamma-secretase inhibitors, which prevent cleavage of Notch though are not specific to Notch signaling³². More recently, anti-DLL4 monoclonal antibodies, which more specifically target the Notch pathway, have also been developed and are in trials for multiple advanced malignancies including metastatic colorectal cancer and ovarian cancer¹⁹⁰. The development of WNT inhibitors, while critical given its extensive mutations in colon cancer and activation in multiple other cancers, have been a more challenging undertaking¹⁹¹. However, the development of a CBP/ β -catenin antagonist (PRI-724), which interferes with the binding of β -catenin with CBP and not p300¹⁹², has allowed clinical testing of WNT pathway inhibition in advanced myeloid malignancies. Additional trials have tested the impact of inhibiting the WNT pathway at the level of WNT secretion or receptor binding using an anti-FZD7 receptor monoclonal antibody (vantictumab)¹⁹³; a WNT ligand antagonist (ipafriccept)¹⁹⁴, or a Porcupine inhibitor (LGK974) in cancers such as pancreatic cancer and breast cancer¹⁹⁵.

At a broader level, it is worth considering the fact that despite the intense focus on identifying key signaling events and targeting these as potential strategies for therapeutic intervention, the rate of failure at trials remains high. It is likely that many drugs could be very effective but inefficient delivery as well as trials in advanced stage disease likely reduces their impact on tumor growth. Improving methods of delivery through nanoparticle or lipid-mediated delivery, antibody-drug conjugate strategies as well as local delivery efforts are crucial areas to explore to improve outcomes. The issue of early intervention has significant ramifications for treatment outcomes in general. Among targeted therapies, imatinib is extraordinary in leading to remarkable long-term remissions that have allowed a majority to patients to live normal lives. Though usually considered a poster child of targeted therapies, the success of imatinib may have more to do with it being a true early intervention, since CML can be detected in the indolent and benign chronic phase, and imatinib is far less successful in controlling the disease as CML progresses into blast crisis¹⁹⁶. This highlights the need for a greater focus on early detection methods and raises the possibility that strategies to detect stem cell signatures could be useful as an indicator of disease progression. Combining the development of innovative early detection tools with an understanding of the signals that drive benign disease to a more malignant phase would enable effective early intervention and provide a more balanced approach to controlling cancer.

ACKNOWLEDGEMENTS

We are grateful to Marcie Kritzik for her input on the manuscript and figures. N.K.L received support from NIH grant T32 GM00752 and National Research Service Individual Award F31 CA206416. A.B. received support from NIH grant R01 DK099335-S1 and NIH grant T32 CA121938. T.R. was supported by NIH grant R35 CA197699 and Stand Up To Cancer–Cancer Research UK–Lustgarten Foundation Pancreatic Cancer Dream Team Research Grant (SU2C-AACR-DT-20-16).

AUTHOR CONTRIBUTION

N.K.L, A.B. and T.R. researched data for the article, wrote the article and reviewed or edited the manuscript before submission. N.K.L and T.R. made substantial contributions to the discussion of content.

DISSERTATION ACKNOWLEDGEMENTS

Chapter 1, in full, has been submitted for publication of the material as it may appear in *Nature Reviews Cancer*. Lytle NK, Barber A, Reya T. Stem cell fate in cancer growth, progression and therapy resistance. The dissertation author is the primary author of this work.

REFERENCES

- 1 Hunger, S. P., Winick, N. J., Sather, H. N. & Carroll, W. L. Therapy of low-risk subsets of childhood acute lymphoblastic leukemia: when do we say enough? *Pediatr Blood Cancer* **45**, 876-880, doi:10.1002/pbc.20501 (2005).
- 2 Hodgson, D. C., Hudson, M. M. & Constine, L. S. Pediatric hodgkin lymphoma: maximizing efficacy and minimizing toxicity. *Semin Radiat Oncol* **17**, 230-242, doi:10.1016/j.semradonc.2007.02.009 (2007).
- 3 Barker, N., Ridgway, R. A., van Es, J. H., van de Wetering, M., Begthel, H., van den Born, M., Danenberg, E., Clarke, A. R., Sansom, O. J. & Clevers, H. Crypt stem cells as the cells-of-origin of intestinal cancer. *Nature* **457**, 608-611, doi:10.1038/nature07602 (2009).
- 4 Gibson, P., Tong, Y., Robinson, G., Thompson, M. C., Currie, D. S., Eden, C., Kranenburg, T. A., Hogg, T., Poppleton, H., Martin, J., Finkelstein, D., Pounds, S., Weiss, A., Patay, Z., Scoggins, M., Ogg, R., Pei, Y., Yang, Z. J., Brun, S., Lee, Y., Zindy, F., Lindsey, J. C., Taketo, M. M., Boop, F. A., Sanford, R. A., Gajjar, A., Clifford, S. C., Roussel, M. F., McKinnon, P. J., Gutmann, D. H., Ellison, D. W., Wechsler-Reya, R. & Gilbertson, R. J. Subtypes of medulloblastoma have distinct developmental origins. *Nature* **468**, 1095-1099, doi:10.1038/nature09587 (2010).
- 5 Lapouge, G., Youssef, K. K., Vokaer, B., Achouri, Y., Michaux, C., Sotiropoulou, P. A. & Blanpain, C. Identifying the cellular origin of squamous skin tumors. *Proc Natl Acad Sci U S A* **108**, 7431-7436, doi:10.1073/pnas.1012720108 (2011).
- 6 Xu, X., Rock, J. R., Lu, Y., Futtner, C., Schwab, B., Guinney, J., Hogan, B. L. & Onaitis, M. W. Evidence for type II cells as cells of origin of K-Ras-induced distal lung adenocarcinoma. *Proc Natl Acad Sci U S A* **109**, 4910-4915, doi:10.1073/pnas.1112499109 (2012).
- 7 Reya, T., Morrison, S. J., Clarke, M. F. & Weissman, I. L. Stem cells, cancer, and cancer stem cells. *Nature* **414**, 105-111, doi:10.1038/35102167 (2001).
- 8 Daley, G. Q., Van Etten, R. A. & Baltimore, D. Induction of chronic myelogenous leukemia in mice by the P210bcr/abl gene of the Philadelphia chromosome. *Science* **247**, 824-830 (1990).
- 9 Whang, J., Frei, E., 3rd, Tjio, J. H., Carbone, P. P. & Brecher, G. The Distribution of the Philadelphia Chromosome in Patients with Chronic Myelogenous Leukemia. *Blood* **22**, 664-673 (1963).
- 10 Krivtsov, A. V., Figueroa, M. E., Sinha, A. U., Stubbs, M. C., Feng, Z., Valk, P. J., Delwel, R., Dohner, K., Bullinger, L., Kung, A. L., Melnick, A. M. & Armstrong, S. A. Cell of origin determines clinically relevant subtypes of MLL-rearranged AML. *Leukemia* **27**, 852-860, doi:10.1038/leu.2012.363 (2013).
- 11 Shlush, L. I., Zandi, S., Mitchell, A., Chen, W. C., Brandwein, J. M., Gupta, V., Kennedy, J. A., Schimmer, A. D., Schuh, A. C., Yee, K. W., McLeod, J. L., Doedens, M., Medeiros, J. J., Marke, R., Kim, H. J., Lee, K., McPherson, J. D., Hudson, T. J., Consortium, H. P.-L. G. P., Brown, A. M., Yousif, F., Trinh, Q. M., Stein, L. D., Minden, M. D., Wang, J. C. & Dick, J. E. Identification of pre-leukaemic haematopoietic stem cells in acute leukaemia. *Nature* **506**, 328-333, doi:10.1038/nature13038 (2014).
- 12 Blaas, L., Pucci, F., Messal, H. A., Andersson, A. B., Josue Ruiz, E., Gerling, M., Douagi, I., Spencer-Dene, B., Musch, A., Mitter, R., Bhaw, L., Stone, R., Bornhorst, D., Sesay, A. K., Jonkers, J., Stamp, G., Malanchi, I., Toftgard, R. & Behrens, A. Lgr6 labels a rare population of mammary

- gland progenitor cells that are able to originate luminal mammary tumours. *Nat Cell Biol* **18**, 1346-1356, doi:10.1038/ncb3434 (2016).
- 13 Zhao, C., Blum, J., Chen, A., Kwon, H. Y., Jung, S. H., Cook, J. M., Lagoo, A. & Reya, T. Loss of beta-catenin impairs the renewal of normal and CML stem cells in vivo. *Cancer Cell* **12**, 528-541, doi:10.1016/j.ccr.2007.11.003 (2007).
 - 14 Latil, M., Nassar, D., Beck, B., Boumahdi, S., Wang, L., Brisebarre, A., Dubois, C., Nkusi, E., Lenglez, S., Checinska, A., Vercauteren Drubbel, A., Devos, M., Declercq, W., Yi, R. & Blanpain, C. Cell-Type-Specific Chromatin States Differentially Prime Squamous Cell Carcinoma Tumor-Initiating Cells for Epithelial to Mesenchymal Transition. *Cell Stem Cell* **20**, 191-204 e195, doi:10.1016/j.stem.2016.10.018 (2017).
 - 15 Alcantara Llaguno, S. R., Wang, Z., Sun, D., Chen, J., Xu, J., Kim, E., Hatanpaa, K. J., Raisanen, J. M., Burns, D. K., Johnson, J. E. & Parada, L. F. Adult Lineage-Restricted CNS Progenitors Specify Distinct Glioblastoma Subtypes. *Cancer Cell* **28**, 429-440, doi:10.1016/j.ccell.2015.09.007 (2015).
 - 16 Alcantara Llaguno, S., Chen, J., Kwon, C. H., Jackson, E. L., Li, Y., Burns, D. K., Alvarez-Buylla, A. & Parada, L. F. Malignant astrocytomas originate from neural stem/progenitor cells in a somatic tumor suppressor mouse model. *Cancer Cell* **15**, 45-56, doi:10.1016/j.ccr.2008.12.006 (2009).
 - 17 Yang, Z. J., Ellis, T., Markant, S. L., Read, T. A., Kessler, J. D., Bourbonoulas, M., Schuller, U., Machold, R., Fishell, G., Rowitch, D. H., Wainwright, B. J. & Wechsler-Reya, R. J. Medulloblastoma can be initiated by deletion of Patched in lineage-restricted progenitors or stem cells. *Cancer Cell* **14**, 135-145, doi:10.1016/j.ccr.2008.07.003 (2008).
 - 18 Schuller, U., Heine, V. M., Mao, J., Kho, A. T., Dillon, A. K., Han, Y. G., Huillard, E., Sun, T., Ligon, A. H., Qian, Y., Ma, Q., Alvarez-Buylla, A., McMahon, A. P., Rowitch, D. H. & Ligon, K. L. Acquisition of granule neuron precursor identity is a critical determinant of progenitor cell competence to form Shh-induced medulloblastoma. *Cancer Cell* **14**, 123-134, doi:10.1016/j.ccr.2008.07.005 (2008).
 - 19 Xie, W., Kagiampakis, I., Pan, L., Zhang, Y. W., Murphy, L., Tao, Y., Kong, X., Kang, B., Xia, L., Carvalho, F. L. F., Sen, S., Chiu Yen, R. W., Zahnnow, C. A., Ahuja, N., Baylin, S. B. & Easwaran, H. DNA Methylation Patterns Separate Senescence from Transformation Potential and Indicate Cancer Risk. *Cancer Cell* **33**, 309-321 e305, doi:10.1016/j.ccell.2018.01.008 (2018).
 - 20 Yu, Y., Schleich, K., Yue, B., Ji, S., Lohneis, P., Kemper, K., Silvis, M. R., Qutob, N., van Rooijen, E., Werner-Klein, M., Li, L., Dhawan, D., Meierjohann, S., Reimann, M., Elkahlon, A., Treitschke, S., Dorken, B., Speck, C., Mallette, F. A., Zon, L. I., Holmen, S. L., Peeper, D. S., Samuels, Y., Schmitt, C. A. & Lee, S. Targeting the Senescence-Overriding Cooperative Activity of Structurally Unrelated H3K9 Demethylases in Melanoma. *Cancer Cell* **33**, 322-336 e328, doi:10.1016/j.ccell.2018.01.002 (2018).
 - 21 Kaufman, C. K., Mosimann, C., Fan, Z. P., Yang, S., Thomas, A. J., Ablain, J., Tan, J. L., Fogley, R. D., van Rooijen, E., Hagedorn, E. J., Ciarlo, C., White, R. M., Matos, D. A., Puller, A. C., Santoriello, C., Liao, E. C., Young, R. A. & Zon, L. I. A zebrafish melanoma model reveals emergence of neural crest identity during melanoma initiation. *Science* **351**, aad2197, doi:10.1126/science.aad2197 (2016).
 - 22 Gilbert, N., Boyle, S., Fiegler, H., Woodfine, K., Carter, N. P. & Bickmore, W. A. Chromatin architecture of the human genome: gene-rich domains are enriched in open chromatin fibers. *Cell* **118**, 555-566, doi:10.1016/j.cell.2004.08.011 (2004).

- 23 Hoadley, K. A., Yau, C., Hinoue, T., Wolf, D. M., Lazar, A. J., Drill, E., Shen, R., Taylor, A. M., Cherniack, A. D., Thorsson, V., Akbani, R., Bowlby, R., Wong, C. K., Wiznerowicz, M., Sanchez-Vega, F., Robertson, A. G., Schneider, B. G., Lawrence, M. S., Noushmehr, H., Malta, T. M., Cancer Genome Atlas, N., Stuart, J. M., Benz, C. C. & Laird, P. W. Cell-of-Origin Patterns Dominate the Molecular Classification of 10,000 Tumors from 33 Types of Cancer. *Cell* **173**, 291-304 e296, doi:10.1016/j.cell.2018.03.022 (2018).
- 24 Vaz, M., Hwang, S. Y., Kagiampakis, I., Phallen, J., Patil, A., O'Hagan, H. M., Murphy, L., Zahnow, C. A., Gabrielson, E., Velculescu, V. E., Easwaran, H. P. & Baylin, S. B. Chronic Cigarette Smoke-Induced Epigenomic Changes Precede Sensitization of Bronchial Epithelial Cells to Single-Step Transformation by KRAS Mutations. *Cancer Cell* **32**, 360-376 e366, doi:10.1016/j.ccell.2017.08.006 (2017).
- 25 Kinzler, K. W. & Vogelstein, B. Lessons from hereditary colorectal cancer. *Cell* **87**, 159-170 (1996).
- 26 Cho, Y. J., Tsherniak, A., Tamayo, P., Santagata, S., Ligon, A., Greulich, H., Berhoukim, R., Amani, V., Goumnerova, L., Eberhart, C. G., Lau, C. C., Olson, J. M., Gilbertson, R. J., Gajjar, A., Delattre, O., Kool, M., Ligon, K., Meyerson, M., Mesirov, J. P. & Pomeroy, S. L. Integrative genomic analysis of medulloblastoma identifies a molecular subgroup that drives poor clinical outcome. *J Clin Oncol* **29**, 1424-1430, doi:10.1200/JCO.2010.28.5148 (2011).
- 27 Hahn, H., Wicking, C., Zaphiropoulous, P. G., Gailani, M. R., Shanley, S., Chidambaram, A., Vorechovsky, I., Holmberg, E., Uden, A. B., Gillies, S., Negus, K., Smyth, I., Pressman, C., Leffell, D. J., Gerrard, B., Goldstein, A. M., Dean, M., Toftgard, R., Chenevix-Trench, G., Wainwright, B. & Bale, A. E. Mutations of the human homolog of Drosophila patched in the nevoid basal cell carcinoma syndrome. *Cell* **85**, 841-851 (1996).
- 28 Ellisen, L. W., Bird, J., West, D. C., Soreng, A. L., Reynolds, T. C., Smith, S. D. & Sklar, J. TAN-1, the human homolog of the Drosophila notch gene, is broken by chromosomal translocations in T lymphoblastic neoplasms. *Cell* **66**, 649-661 (1991).
- 29 Gonzalez, M. E., Moore, H. M., Li, X., Toy, K. A., Huang, W., Sabel, M. S., Kidwell, K. M. & Kleer, C. G. EZH2 expands breast stem cells through activation of NOTCH1 signaling. *Proc Natl Acad Sci U S A* **111**, 3098-3103, doi:10.1073/pnas.1308953111 (2014).
- 30 Miyamoto, Y., Maitra, A., Ghosh, B., Zechner, U., Argani, P., Iacobuzio-Donahue, C. A., Sriuranpong, V., Iso, T., Meszoely, I. M., Wolfe, M. S., Hruban, R. H., Ball, D. W., Schmid, R. M. & Leach, S. D. Notch mediates TGF alpha-induced changes in epithelial differentiation during pancreatic tumorigenesis. *Cancer Cell* **3**, 565-576 (2003).
- 31 Valencia, A., Roman-Gomez, J., Cervera, J., Such, E., Barragan, E., Bolufer, P., Moscardo, F., Sanz, G. F. & Sanz, M. A. Wnt signaling pathway is epigenetically regulated by methylation of Wnt antagonists in acute myeloid leukemia. *Leukemia* **23**, 1658-1666, doi:10.1038/leu.2009.86 (2009).
- 32 Yuan, X., Wu, H., Xu, H., Xiong, H., Chu, Q., Yu, S., Wu, G. S. & Wu, K. Notch signaling: an emerging therapeutic target for cancer treatment. *Cancer Lett* **369**, 20-27, doi:10.1016/j.canlet.2015.07.048 (2015).
- 33 Ashihara, E., Takada, T. & Maekawa, T. Targeting the canonical Wnt/beta-catenin pathway in hematological malignancies. *Cancer Sci* **106**, 665-671, doi:10.1111/cas.12655 (2015).

- 34 Di Giacomo, D., Pierini, V., Barba, G., Ceccarelli, V., Vecchini, A. & Mecucci, C. Blast crisis Ph+ chronic myeloid leukemia with NUP98/HOXA13 up-regulating MSI2. *Mol Cytogenet* **7**, 42, doi:10.1186/1755-8166-7-42 (2014).
- 35 Yamashita, Y., Yuan, J., Suetake, I., Suzuki, H., Ishikawa, Y., Choi, Y. L., Ueno, T., Soda, M., Hamada, T., Haruta, H., Takada, S., Miyazaki, Y., Kiyoi, H., Ito, E., Naoe, T., Tomonaga, M., Toyota, M., Tajima, S., Iwama, A. & Mano, H. Array-based genomic resequencing of human leukemia. *Oncogene* **29**, 3723-3731, doi:10.1038/onc.2010.117 (2010).
- 36 Ley, T. J., Ding, L., Walter, M. J., McLellan, M. D., Lamprecht, T., Larson, D. E., Kandoth, C., Payton, J. E., Baty, J., Welch, J., Harris, C. C., Lichti, C. F., Townsend, R. R., Fulton, R. S., Dooling, D. J., Koboldt, D. C., Schmidt, H., Zhang, Q., Osborne, J. R., Lin, L., O'Laughlin, M., McMichael, J. F., Delehaunty, K. D., McGrath, S. D., Fulton, L. A., Magrini, V. J., Vickery, T. L., Hundal, J., Cook, L. L., Conyers, J. J., Swift, G. W., Reed, J. P., Alldredge, P. A., Wylie, T., Walker, J., Kalicki, J., Watson, M. A., Heath, S., Shannon, W. D., Varghese, N., Nagarajan, R., Westervelt, P., Tomasson, M. H., Link, D. C., Graubert, T. A., DiPersio, J. F., Mardis, E. R. & Wilson, R. K. DNMT3A mutations in acute myeloid leukemia. *N Engl J Med* **363**, 2424-2433, doi:10.1056/NEJMoa1005143 (2010).
- 37 Challen, G. A., Sun, D., Jeong, M., Luo, M., Jelinek, J., Berg, J. S., Bock, C., Vasanthakumar, A., Gu, H., Xi, Y., Liang, S., Lu, Y., Darlington, G. J., Meissner, A., Issa, J. P., Godley, L. A., Li, W. & Goodell, M. A. Dnmt3a is essential for hematopoietic stem cell differentiation. *Nat Genet* **44**, 23-31, doi:10.1038/ng.1009 (2011).
- 38 Tadokoro, Y., Ema, H., Okano, M., Li, E. & Nakauchi, H. De novo DNA methyltransferase is essential for self-renewal, but not for differentiation, in hematopoietic stem cells. *J Exp Med* **204**, 715-722, doi:10.1084/jem.20060750 (2007).
- 39 Mayle, A., Yang, L., Rodriguez, B., Zhou, T., Chang, E., Curry, C. V., Challen, G. A., Li, W., Wheeler, D., Rebel, V. I. & Goodell, M. A. Dnmt3a loss predisposes murine hematopoietic stem cells to malignant transformation. *Blood* **125**, 629-638, doi:10.1182/blood-2014-08-594648 (2015).
- 40 Hajkova, H., Markova, J., Haskovec, C., Sarova, I., Fuchs, O., Kosticka, A., Cetkovsky, P., Michalova, K. & Schwarz, J. Decreased DNA methylation in acute myeloid leukemia patients with DNMT3A mutations and prognostic implications of DNA methylation. *Leuk Res* **36**, 1128-1133, doi:10.1016/j.leukres.2012.05.012 (2012).
- 41 Yan, X. J., Xu, J., Gu, Z. H., Pan, C. M., Lu, G., Shen, Y., Shi, J. Y., Zhu, Y. M., Tang, L., Zhang, X. W., Liang, W. X., Mi, J. Q., Song, H. D., Li, K. Q., Chen, Z. & Chen, S. J. Exome sequencing identifies somatic mutations of DNA methyltransferase gene DNMT3A in acute monocytic leukemia. *Nat Genet* **43**, 309-315, doi:10.1038/ng.788 (2011).
- 42 Kagara, N., Huynh, K. T., Kuo, C., Okano, H., Sim, M. S., Elashoff, D., Chong, K., Giuliano, A. E. & Hoon, D. S. Epigenetic regulation of cancer stem cell genes in triple-negative breast cancer. *Am J Pathol* **181**, 257-267, doi:10.1016/j.ajpath.2012.03.019 (2012).
- 43 Gopisetty, G., Xu, J., Sampath, D., Colman, H. & Pudevalli, V. K. Epigenetic regulation of CD133/PROM1 expression in glioma stem cells by Sp1/myc and promoter methylation. *Oncogene* **32**, 3119-3129, doi:10.1038/onc.2012.331 (2013).
- 44 Zhang, W. & Xu, J. DNA methyltransferases and their roles in tumorigenesis. *Biomark Res* **5**, 1, doi:10.1186/s40364-017-0081-z (2017).

- 45 Martin, M., Ancey, P. B., Cros, M. P., Durand, G., Le Calvez-Kelm, F., Hernandez-Vargas, H. & Herceg, Z. Dynamic imbalance between cancer cell subpopulations induced by transforming growth factor beta (TGF-beta) is associated with a DNA methylome switch. *BMC Genomics* **15**, 435, doi:10.1186/1471-2164-15-435 (2014).
- 46 Weis, B., Schmidt, J., Maamar, H., Raj, A., Lin, H., Toth, C., Riedmann, K., Raddatz, G., Seitz, H. K., Ho, A. D., Lyko, F. & Linhart, H. G. Inhibition of intestinal tumor formation by deletion of the DNA methyltransferase 3a. *Oncogene* **34**, 1822-1830, doi:10.1038/onc.2014.114 (2015).
- 47 Tsai, H. C., Li, H., Van Neste, L., Cai, Y., Robert, C., Rassool, F. V., Shin, J. J., Harbom, K. M., Beaty, R., Pappou, E., Harris, J., Yen, R. W., Ahuja, N., Brock, M. V., Stearns, V., Feller-Kopman, D., Yarmus, L. B., Lin, Y. C., Welm, A. L., Issa, J. P., Minn, I., Matsui, W., Jang, Y. Y., Sharkis, S. J., Baylin, S. B. & Zahnow, C. A. Transient low doses of DNA-demethylating agents exert durable antitumor effects on hematological and epithelial tumor cells. *Cancer Cell* **21**, 430-446, doi:10.1016/j.ccr.2011.12.029 (2012).
- 48 Kondo, Y. Targeting histone methyltransferase EZH2 as cancer treatment. *J Biochem* **156**, 249-257, doi:10.1093/jb/mvu054 (2014).
- 49 Zuber, J., Shi, J., Wang, E., Rappaport, A. R., Herrmann, H., Sison, E. A., Magoon, D., Qi, J., Blatt, K., Wunderlich, M., Taylor, M. J., Johns, C., Chicas, A., Mulloy, J. C., Kogan, S. C., Brown, P., Valent, P., Bradner, J. E., Lowe, S. W. & Vakoc, C. R. RNAi screen identifies Brd4 as a therapeutic target in acute myeloid leukaemia. *Nature* **478**, 524-528, doi:10.1038/nature10334 (2011).
- 50 Riggs, M. G., Whittaker, R. G., Neumann, J. R. & Ingram, V. M. n-Butyrate causes histone modification in HeLa and Friend erythroleukaemia cells. *Nature* **268**, 462-464 (1977).
- 51 Fiskus, W., Sharma, S., Qi, J., Valenta, J. A., Schaub, L. J., Shah, B., Peth, K., Portier, B. P., Rodriguez, M., Devaraj, S. G., Zhan, M., Sheng, J., Iyer, S. P., Bradner, J. E. & Bhalla, K. N. Highly active combination of BRD4 antagonist and histone deacetylase inhibitor against human acute myelogenous leukemia cells. *Mol Cancer Ther* **13**, 1142-1154, doi:10.1158/1535-7163.MCT-13-0770 (2014).
- 52 Pei, Y., Liu, K. W., Wang, J., Garancher, A., Tao, R., Esparza, L. A., Maier, D. L., Udaka, Y. T., Murad, N., Morrissy, S., Seker-Cin, H., Brabetz, S., Qi, L., Kogiso, M., Schubert, S., Olson, J. M., Cho, Y. J., Li, X. N., Crawford, J. R., Levy, M. L., Kool, M., Pfister, S. M., Taylor, M. D. & Wechsler-Reya, R. J. HDAC and PI3K Antagonists Cooperate to Inhibit Growth of MYC-Driven Medulloblastoma. *Cancer Cell* **29**, 311-323, doi:10.1016/j.ccell.2016.02.011 (2016).
- 53 Fox, R. G., Lytle, N. K., Jaquish, D. V., Park, F. D., Ito, T., Bajaj, J., Koechlein, C. S., Zimdahl, B., Yano, M., Kopp, J. L., Kritzik, M., Sicklick, J. K., Sander, M., Grandgenett, P. M., Hollingsworth, M. A., Shibata, S., Pizzo, D., Valasek, M. A., Sasik, R., Scadeng, M., Okano, H., Kim, Y., MacLeod, A. R., Lowy, A. M. & Reya, T. Image-based detection and targeting of therapy resistance in pancreatic adenocarcinoma. *Nature* **534**, 407-411, doi:10.1038/nature17988 (2016).
- 54 Mazur, P. K., Herner, A., Mello, S. S., Wirth, M., Hausmann, S., Sanchez-Rivera, F. J., Lofgren, S. M., Kuschma, T., Hahn, S. A., Vangala, D., Trajkovic-Arsic, M., Gupta, A., Heid, I., Noel, P. B., Braren, R., Erkan, M., Kleeff, J., Sipos, B., Sayles, L. C., Heikenwalder, M., Hessmann, E., Ellenrieder, V., Esposito, I., Jacks, T., Bradner, J. E., Khatri, P., Sweet-Cordero, E. A., Attardi, L. D., Schmid, R. M., Schneider, G., Sage, J. & Siveke, J. T. Combined inhibition of BET family proteins and histone deacetylases as a potential epigenetics-based therapy for pancreatic ductal adenocarcinoma. *Nat Med* **21**, 1163-1171, doi:10.1038/nm.3952 (2015).

- 55 Shu, S., Lin, C. Y., He, H. H., Witwicki, R. M., Tabassum, D. P., Roberts, J. M., Janiszewska, M., Huh, S. J., Liang, Y., Ryan, J., Doherty, E., Mohammed, H., Guo, H., Stover, D. G., Ekram, M. B., Peluffo, G., Brown, J., D'Santos, C., Krop, I. E., Dillon, D., McKeown, M., Ott, C., Qi, J., Ni, M., Rao, P. K., Duarte, M., Wu, S. Y., Chiang, C. M., Anders, L., Young, R. A., Winer, E. P., Letai, A., Barry, W. T., Carroll, J. S., Long, H. W., Brown, M., Liu, X. S., Meyer, C. A., Bradner, J. E. & Polyak, K. Response and resistance to BET bromodomain inhibitors in triple-negative breast cancer. *Nature* **529**, 413-417, doi:10.1038/nature16508 (2016).
- 56 Zhang, B., Strauss, A. C., Chu, S., Li, M., Ho, Y., Shiang, K. D., Snyder, D. S., Huettner, C. S., Shultz, L., Holyoake, T. & Bhatia, R. Effective targeting of quiescent chronic myelogenous leukemia stem cells by histone deacetylase inhibitors in combination with imatinib mesylate. *Cancer Cell* **17**, 427-442, doi:10.1016/j.ccr.2010.03.011 (2010).
- 57 Pathania, R., Ramachandran, S., Elangovan, S., Padia, R., Yang, P., Cinghu, S., Veeranan-Karmegam, R., Arjunan, P., Gnana-Prakasam, J. P., Sadanand, F., Pei, L., Chang, C. S., Choi, J. H., Shi, H., Manicassamy, S., Prasad, P. D., Sharma, S., Ganapathy, V., Jothi, R. & Thangaraju, M. DNMT1 is essential for mammary and cancer stem cell maintenance and tumorigenesis. *Nat Commun* **6**, 6910, doi:10.1038/ncomms7910 (2015).
- 58 Heidel, F. H., Bullinger, L., Arreba-Tutusa, P., Wang, Z., Gaebel, J., Hirt, C., Niederwieser, D., Lane, S. W., Dohner, K., Vasioukhin, V., Fischer, T. & Armstrong, S. A. The cell fate determinant *lgl1* influences HSC fitness and prognosis in AML. *J Exp Med* **210**, 15-22, doi:10.1084/jem.20120596 (2013).
- 59 He, L., He, X., Lim, L. P., de Stanchina, E., Xuan, Z., Liang, Y., Xue, W., Zender, L., Magnus, J., Ridzon, D., Jackson, A. L., Linsley, P. S., Chen, C., Lowe, S. W., Cleary, M. A. & Hannon, G. J. A microRNA component of the p53 tumour suppressor network. *Nature* **447**, 1130-1134, doi:10.1038/nature05939 (2007).
- 60 Bu, P., Chen, K. Y., Chen, J. H., Wang, L., Walters, J., Shin, Y. J., Goerger, J. P., Sun, J., Witherspoon, M., Rakhilin, N., Li, J., Yang, H., Milsom, J., Lee, S., Zipfel, W., Jin, M. M., Gumus, Z. H., Lipkin, S. M. & Shen, X. A microRNA miR-34a-regulated bimodal switch targets Notch in colon cancer stem cells. *Cell Stem Cell* **12**, 602-615, doi:10.1016/j.stem.2013.03.002 (2013).
- 61 Li, Y., Guessous, F., Zhang, Y., Dipierro, C., Kefas, B., Johnson, E., Marcinkiewicz, L., Jiang, J., Yang, Y., Schmittgen, T. D., Lopes, B., Schiff, D., Purow, B. & Abounader, R. MicroRNA-34a inhibits glioblastoma growth by targeting multiple oncogenes. *Cancer Res* **69**, 7569-7576, doi:10.1158/0008-5472.CAN-09-0529 (2009).
- 62 Hwang, W. L., Jiang, J. K., Yang, S. H., Huang, T. S., Lan, H. Y., Teng, H. W., Yang, C. Y., Tsai, Y. P., Lin, C. H., Wang, H. W. & Yang, M. H. MicroRNA-146a directs the symmetric division of Snail-dominant colorectal cancer stem cells. *Nat Cell Biol* **16**, 268-280, doi:10.1038/ncb2910 (2014).
- 63 Wang, L., Bu, P., Ai, Y., Srinivasan, T., Chen, H. J., Xiang, K., Lipkin, S. M. & Shen, X. A long non-coding RNA targets microRNA miR-34a to regulate colon cancer stem cell asymmetric division. *Elife* **5**, doi:10.7554/eLife.14620 (2016).
- 64 Chen, G., Kong, J., Tucker-Burden, C., Anand, M., Rong, Y., Rahman, F., Moreno, C. S., Van Meir, E. G., Hadjipanayis, C. G. & Brat, D. J. Human Brat ortholog TRIM3 is a tumor suppressor that regulates asymmetric cell division in glioblastoma. *Cancer Res* **74**, 4536-4548, doi:10.1158/0008-5472.CAN-13-3703 (2014).

- 65 Bello, B., Reichert, H. & Hirth, F. The brain tumor gene negatively regulates neural progenitor cell proliferation in the larval central brain of *Drosophila*. *Development* **133**, 2639-2648, doi:10.1242/dev.02429 (2006).
- 66 Gateff, E. Malignant neoplasms of genetic origin in *Drosophila melanogaster*. *Science* **200**, 1448-1459 (1978).
- 67 Betschinger, J., Mechtler, K. & Knoblich, J. A. Asymmetric segregation of the tumor suppressor *brat* regulates self-renewal in *Drosophila* neural stem cells. *Cell* **124**, 1241-1253, doi:10.1016/j.cell.2006.01.038 (2006).
- 68 Bowman, S. K., Neumuller, R. A., Novatchkova, M., Du, Q. & Knoblich, J. A. The *Drosophila* NuMA Homolog Mud regulates spindle orientation in asymmetric cell division. *Dev Cell* **10**, 731-742, doi:10.1016/j.devcel.2006.05.005 (2006).
- 69 Wu, M., Kwon, H. Y., Rattis, F., Blum, J., Zhao, C., Ashkenazi, R., Jackson, T. L., Gaiano, N., Oliver, T. & Reya, T. Imaging hematopoietic precursor division in real time. *Cell Stem Cell* **1**, 541-554, doi:10.1016/j.stem.2007.08.009 (2007).
- 70 Ito, T., Kwon, H. Y., Zimdahl, B., Congdon, K. L., Blum, J., Lento, W. E., Zhao, C., Lagoo, A., Gerrard, G., Foroni, L., Goldman, J., Goh, H., Kim, S. H., Kim, D. W., Chuah, C., Oehler, V. G., Radich, J. P., Jordan, C. T. & Reya, T. Regulation of myeloid leukaemia by the cell-fate determinant *Musashi*. *Nature* **466**, 765-768, doi:10.1038/nature09171 (2010).
- 71 Zimdahl, B., Ito, T., Blevins, A., Bajaj, J., Konuma, T., Weeks, J., Koechlein, C. S., Kwon, H. Y., Arami, O., Rizzieri, D., Broome, H. E., Chuah, C., Oehler, V. G., Sasik, R., Hardiman, G. & Reya, T. *Lis1* regulates asymmetric division in hematopoietic stem cells and in leukemia. *Nat Genet* **46**, 245-252, doi:10.1038/ng.2889 (2014).
- 72 Cicalese, A., Bonizzi, G., Pasi, C. E., Faretta, M., Ronzoni, S., Giulini, B., Brisken, C., Minucci, S., Di Fiore, P. P. & Pelicci, P. G. The tumor suppressor p53 regulates polarity of self-renewing divisions in mammary stem cells. *Cell* **138**, 1083-1095, doi:10.1016/j.cell.2009.06.048 (2009).
- 73 Sheng, W., Dong, M., Chen, C., Li, Y., Liu, Q. & Dong, Q. *Musashi2* promotes the development and progression of pancreatic cancer by down-regulating *Numb* protein. *Oncotarget* **8**, 14359-14373, doi:10.18632/oncotarget.8736 (2016).
- 74 Shen, Q., Zhong, W., Jan, Y. N. & Temple, S. Asymmetric *Numb* distribution is critical for asymmetric cell division of mouse cerebral cortical stem cells and neuroblasts. *Development* **129**, 4843-4853 (2002).
- 75 Sugiarto, S., Persson, A. I., Munoz, E. G., Waldhuber, M., Lamagna, C., Andor, N., Hanecker, P., Ayers-Ringler, J., Phillips, J., Siu, J., Lim, D. A., Vandenberg, S., Stallcup, W., Berger, M. S., Bergers, G., Weiss, W. A. & Petritsch, C. Asymmetry-defective oligodendrocyte progenitors are glioma precursors. *Cancer Cell* **20**, 328-340, doi:10.1016/j.ccr.2011.08.011 (2011).
- 76 Thiery, J. P. Epithelial-mesenchymal transitions in tumour progression. *Nat Rev Cancer* **2**, 442-454, doi:10.1038/nrc822 (2002).
- 77 Zheng, X., Carstens, J. L., Kim, J., Scheible, M., Kaye, J., Sugimoto, H., Wu, C. C., LeBleu, V. S. & Kalluri, R. Epithelial-to-mesenchymal transition is dispensable for metastasis but induces chemoresistance in pancreatic cancer. *Nature* **527**, 525-530, doi:10.1038/nature16064 (2015).

- 78 Fischer, K. R., Durrans, A., Lee, S., Sheng, J., Li, F., Wong, S. T., Choi, H., El Rayes, T., Ryu, S., Troeger, J., Schwabe, R. F., Vahdat, L. T., Altorki, N. K., Mittal, V. & Gao, D. Epithelial-to-mesenchymal transition is not required for lung metastasis but contributes to chemoresistance. *Nature* **527**, 472-476, doi:10.1038/nature15748 (2015).
- 79 Jolly, M. K., Ware, K. E., Gilja, S., Somarelli, J. A. & Levine, H. EMT and MET: necessary or permissive for metastasis? *Mol Oncol* **11**, 755-769, doi:10.1002/1878-0261.12083 (2017).
- 80 Aiello, N. M., Maddipati, R., Norgard, R. J., Balli, D., Li, J., Yuan, S., Yamazoe, T., Black, T., Sahmoud, A., Furth, E. E., Bar-Sagi, D. & Stanger, B. Z. EMT Subtype Influences Epithelial Plasticity and Mode of Cell Migration. *Dev Cell* **45**, 681-695 e684, doi:10.1016/j.devcel.2018.05.027 (2018).
- 81 Sampson, V. B., David, J. M., Puig, I., Patil, P. U., de Herreros, A. G., Thomas, G. V. & Rajasekaran, A. K. Wilms' tumor protein induces an epithelial-mesenchymal hybrid differentiation state in clear cell renal cell carcinoma. *PLoS One* **9**, e102041, doi:10.1371/journal.pone.0102041 (2014).
- 82 Schliekelman, M. J., Taguchi, A., Zhu, J., Dai, X., Rodriguez, J., Celiktas, M., Zhang, Q., Chin, A., Wong, C. H., Wang, H., McFerrin, L., Selamat, S. A., Yang, C., Kroh, E. M., Garg, K. S., Behrens, C., Gazdar, A. F., Laird-Offringa, I. A., Tewari, M., Wistuba, II, Thiery, J. P. & Hanash, S. M. Molecular portraits of epithelial, mesenchymal, and hybrid States in lung adenocarcinoma and their relevance to survival. *Cancer Res* **75**, 1789-1800, doi:10.1158/0008-5472.CAN-14-2535 (2015).
- 83 Grosse-Wilde, A., Fouquier d'Herouel, A., McIntosh, E., Ertaylan, G., Skupin, A., Kuestner, R. E., del Sol, A., Walters, K. A. & Huang, S. Stemness of the hybrid Epithelial/Mesenchymal State in Breast Cancer and Its Association with Poor Survival. *PLoS One* **10**, e0126522, doi:10.1371/journal.pone.0126522 (2015).
- 84 Ocana, O. H., Corcoles, R., Fabra, A., Moreno-Bueno, G., Acloque, H., Vega, S., Barrallo-Gimeno, A., Cano, A. & Nieto, M. A. Metastatic colonization requires the repression of the epithelial-mesenchymal transition inducer Prrx1. *Cancer Cell* **22**, 709-724, doi:10.1016/j.ccr.2012.10.012 (2012).
- 85 Tsai, J. H., Donaher, J. L., Murphy, D. A., Chau, S. & Yang, J. Spatiotemporal regulation of epithelial-mesenchymal transition is essential for squamous cell carcinoma metastasis. *Cancer Cell* **22**, 725-736, doi:10.1016/j.ccr.2012.09.022 (2012).
- 86 Balic, M., Lin, H., Young, L., Hawes, D., Giuliano, A., McNamara, G., Datar, R. H. & Cote, R. J. Most early disseminated cancer cells detected in bone marrow of breast cancer patients have a putative breast cancer stem cell phenotype. *Clin Cancer Res* **12**, 5615-5621, doi:10.1158/1078-0432.CCR-06-0169 (2006).
- 87 Grillet, F., Bayet, E., Villeronce, O., Zappia, L., Lagerqvist, E. L., Lunke, S., Charafe-Jauffret, E., Pham, K., Molck, C., Rolland, N., Bourgaux, J. F., Prudhomme, M., Philippe, C., Bravo, S., Boyer, J. C., Canterel-Thouennon, L., Taylor, G. R., Hsu, A., Pascussi, J. M., Hollande, F. & Pannequin, J. Circulating tumour cells from patients with colorectal cancer have cancer stem cell hallmarks in ex vivo culture. *Gut* **66**, 1802-1810, doi:10.1136/gutjnl-2016-311447 (2017).
- 88 Charafe-Jauffret, E., Ginestier, C., Iovino, F., Wicinski, J., Cervera, N., Finetti, P., Hur, M. H., Diebel, M. E., Monville, F., Dutcher, J., Brown, M., Viens, P., Xerri, L., Bertucci, F., Stassi, G., Dontu, G., Birnbaum, D. & Wicha, M. S. Breast cancer cell lines contain functional cancer stem cells with metastatic capacity and a distinct molecular signature. *Cancer Res* **69**, 1302-1313, doi:10.1158/0008-5472.CAN-08-2741 (2009).

- 89 Dieter, S. M., Ball, C. R., Hoffmann, C. M., Nowrouzi, A., Herbst, F., Zavidij, O., Abel, U., Arens, A., Weichert, W., Brand, K., Koch, M., Weitz, J., Schmidt, M., von Kalle, C. & Glimm, H. Distinct types of tumor-initiating cells form human colon cancer tumors and metastases. *Cell Stem Cell* **9**, 357-365, doi:10.1016/j.stem.2011.08.010 (2011).
- 90 Aktas, B., Tewes, M., Fehm, T., Hauch, S., Kimmig, R. & Kasimir-Bauer, S. Stem cell and epithelial-mesenchymal transition markers are frequently overexpressed in circulating tumor cells of metastatic breast cancer patients. *Breast Cancer Res* **11**, R46, doi:10.1186/bcr2333 (2009).
- 91 Baccelli, I., Schneeweiss, A., Riethdorf, S., Stenzinger, A., Schillert, A., Vogel, V., Klein, C., Saini, M., Bauerle, T., Wallwiener, M., Holland-Letz, T., Hofner, T., Sprick, M., Scharpf, M., Marme, F., Sinn, H. P., Pantel, K., Weichert, W. & Trumpp, A. Identification of a population of blood circulating tumor cells from breast cancer patients that initiates metastasis in a xenograft assay. *Nat Biotechnol* **31**, 539-544, doi:10.1038/nbt.2576 (2013).
- 92 Al-Hajj, M., Wicha, M. S., Benito-Hernandez, A., Morrison, S. J. & Clarke, M. F. Prospective identification of tumorigenic breast cancer cells. *Proc Natl Acad Sci U S A* **100**, 3983-3988, doi:10.1073/pnas.0530291100 (2003).
- 93 Polyak, K. & Weinberg, R. A. Transitions between epithelial and mesenchymal states: acquisition of malignant and stem cell traits. *Nat Rev Cancer* **9**, 265-273, doi:10.1038/nrc2620 (2009).
- 94 Raimondi, C., Gradilone, A., Naso, G., Vincenzi, B., Petracca, A., Nicolazzo, C., Palazzo, A., Saltarelli, R., Spremberg, F., Cortesi, E. & Gazzaniga, P. Epithelial-mesenchymal transition and stemness features in circulating tumor cells from breast cancer patients. *Breast Cancer Res Treat* **130**, 449-455, doi:10.1007/s10549-011-1373-x (2011).
- 95 Shipitsin, M., Campbell, L. L., Argani, P., Weremowicz, S., Bloushtain-Qimron, N., Yao, J., Nikolskaya, T., Serebryskaya, T., Beroukhim, R., Hu, M., Halushka, M. K., Sukumar, S., Parker, L. M., Anderson, K. S., Harris, L. N., Garber, J. E., Richardson, A. L., Schnitt, S. J., Nikolsky, Y., Gelman, R. S. & Polyak, K. Molecular definition of breast tumor heterogeneity. *Cancer Cell* **11**, 259-273, doi:10.1016/j.ccr.2007.01.013 (2007).
- 96 Beck, B., Lapouge, G., Rorive, S., Drogat, B., Desaedelaere, K., Delafaille, S., Dubois, C., Salmon, I., Willekens, K., Marine, J. C. & Blanpain, C. Different levels of Twist1 regulate skin tumor initiation, stemness, and progression. *Cell Stem Cell* **16**, 67-79, doi:10.1016/j.stem.2014.12.002 (2015).
- 97 Fan, F., Samuel, S., Evans, K. W., Lu, J., Xia, L., Zhou, Y., Sceusi, E., Tozzi, F., Ye, X. C., Mani, S. A. & Ellis, L. M. Overexpression of snail induces epithelial-mesenchymal transition and a cancer stem cell-like phenotype in human colorectal cancer cells. *Cancer Med* **1**, 5-16, doi:10.1002/cam4.4 (2012).
- 98 Kurrey, N. K., Jalgaonkar, S. P., Joglekar, A. V., Ghanate, A. D., Chaskar, P. D., Doiphode, R. Y. & Bapat, S. A. Snail and slug mediate radioresistance and chemoresistance by antagonizing p53-mediated apoptosis and acquiring a stem-like phenotype in ovarian cancer cells. *Stem Cells* **27**, 2059-2068, doi:10.1002/stem.154 (2009).
- 99 Burk, U., Schubert, J., Wellner, U., Schmalhofer, O., Vincan, E., Spaderna, S. & Brabletz, T. A reciprocal repression between ZEB1 and members of the miR-200 family promotes EMT and invasion in cancer cells. *EMBO Rep* **9**, 582-589, doi:10.1038/embor.2008.74 (2008).
- 100 Mani, S. A., Guo, W., Liao, M. J., Eaton, E. N., Ayyanan, A., Zhou, A. Y., Brooks, M., Reinhard, F., Zhang, C. C., Shipitsin, M., Campbell, L. L., Polyak, K., Brisken, C., Yang, J. & Weinberg, R. A.

- The epithelial-mesenchymal transition generates cells with properties of stem cells. *Cell* **133**, 704-715, doi:10.1016/j.cell.2008.03.027 (2008).
- 101 Morel, A. P., Lievre, M., Thomas, C., Hinkal, G., Ansieau, S. & Puisieux, A. Generation of breast cancer stem cells through epithelial-mesenchymal transition. *PLoS One* **3**, e2888, doi:10.1371/journal.pone.0002888 (2008).
- 102 Wellner, U., Schubert, J., Burk, U. C., Schmalhofer, O., Zhu, F., Sonntag, A., Waldvogel, B., Vannier, C., Darling, D., zur Hausen, A., Brunton, V. G., Morton, J., Sansom, O., Schuler, J., Stemmler, M. P., Herzberger, C., Hopt, U., Keck, T., Brabletz, S. & Brabletz, T. The EMT-activator ZEB1 promotes tumorigenicity by repressing stemness-inhibiting microRNAs. *Nat Cell Biol* **11**, 1487-1495, doi:10.1038/ncb1998 (2009).
- 103 Oskarsson, T., Batlle, E. & Massague, J. Metastatic stem cells: sources, niches, and vital pathways. *Cell Stem Cell* **14**, 306-321, doi:10.1016/j.stem.2014.02.002 (2014).
- 104 Hermann, P. C., Huber, S. L., Herrler, T., Aicher, A., Ellwart, J. W., Guba, M., Bruns, C. J. & Heeschen, C. Distinct populations of cancer stem cells determine tumor growth and metastatic activity in human pancreatic cancer. *Cell Stem Cell* **1**, 313-323, doi:10.1016/j.stem.2007.06.002 (2007).
- 105 Pang, R., Law, W. L., Chu, A. C., Poon, J. T., Lam, C. S., Chow, A. K., Ng, L., Cheung, L. W., Lan, X. R., Lan, H. Y., Tan, V. P., Yau, T. C., Poon, R. T. & Wong, B. C. A subpopulation of CD26+ cancer stem cells with metastatic capacity in human colorectal cancer. *Cell Stem Cell* **6**, 603-615, doi:10.1016/j.stem.2010.04.001 (2010).
- 106 Patel, A. P., Tirosh, I., Trombetta, J. J., Shalek, A. K., Gillespie, S. M., Wakimoto, H., Cahill, D. P., Nahed, B. V., Curry, W. T., Martuza, R. L., Louis, D. N., Rozenblatt-Rosen, O., Suva, M. L., Regev, A. & Bernstein, B. E. Single-cell RNA-seq highlights intratumoral heterogeneity in primary glioblastoma. *Science* **344**, 1396-1401, doi:10.1126/science.1254257 (2014).
- 107 Tirosh, I., Venteicher, A. S., Hebert, C., Escalante, L. E., Patel, A. P., Yizhak, K., Fisher, J. M., Rodman, C., Mount, C., Filbin, M. G., Neftel, C., Desai, N., Nyman, J., Izar, B., Luo, C. C., Francis, J. M., Patel, A. A., Onozato, M. L., Riggi, N., Livak, K. J., Gennert, D., Satija, R., Nahed, B. V., Curry, W. T., Martuza, R. L., Mylvaganam, R., Iafraite, A. J., Frosch, M. P., Golub, T. R., Rivera, M. N., Getz, G., Rozenblatt-Rosen, O., Cahill, D. P., Monje, M., Bernstein, B. E., Louis, D. N., Regev, A. & Suva, M. L. Single-cell RNA-seq supports a developmental hierarchy in human oligodendroglioma. *Nature* **539**, 309-313, doi:10.1038/nature20123 (2016).
- 108 Bakker, B., Taudt, A., Belderbos, M. E., Porubsky, D., Spierings, D. C., de Jong, T. V., Halsema, N., Kazemier, H. G., Hoekstra-Wakker, K., Bradley, A., de Bont, E. S., van den Berg, A., Guryev, V., Lansdorp, P. M., Colome-Tatche, M. & Foijer, F. Single-cell sequencing reveals karyotype heterogeneity in murine and human malignancies. *Genome Biol* **17**, 115, doi:10.1186/s13059-016-0971-7 (2016).
- 109 Turner, K. M., Deshpande, V., Beyter, D., Koga, T., Rusert, J., Lee, C., Li, B., Arden, K., Ren, B., Nathanson, D. A., Kornblum, H. I., Taylor, M. D., Kaushal, S., Cavenee, W. K., Wechsler-Reya, R., Furnari, F. B., Vandenberg, S. R., Rao, P. N., Wahl, G. M., Bafna, V. & Mischel, P. S. Extrachromosomal oncogene amplification drives tumour evolution and genetic heterogeneity. *Nature* **543**, 122-125, doi:10.1038/nature21356 (2017).
- 110 Pao, W., Miller, V. A., Politi, K. A., Riely, G. J., Somwar, R., Zakowski, M. F., Kris, M. G. & Varmus, H. Acquired resistance of lung adenocarcinomas to gefitinib or erlotinib is associated with a second

- mutation in the EGFR kinase domain. *PLoS Med* **2**, e73, doi:10.1371/journal.pmed.0020073 (2005).
- 111 Ding, L., Ley, T. J., Larson, D. E., Miller, C. A., Koboldt, D. C., Welch, J. S., Ritchey, J. K., Young, M. A., Lamprecht, T., McLellan, M. D., McMichael, J. F., Wallis, J. W., Lu, C., Shen, D., Harris, C. C., Dooling, D. J., Fulton, R. S., Fulton, L. L., Chen, K., Schmidt, H., Kalicki-Veizer, J., Magrini, V. J., Cook, L., McGrath, S. D., Vickery, T. L., Wendl, M. C., Heath, S., Watson, M. A., Link, D. C., Tomasson, M. H., Shannon, W. D., Payton, J. E., Kulkarni, S., Westervelt, P., Walter, M. J., Graubert, T. A., Mardis, E. R., Wilson, R. K. & DiPersio, J. F. Clonal evolution in relapsed acute myeloid leukaemia revealed by whole-genome sequencing. *Nature* **481**, 506-510, doi:10.1038/nature10738 (2012).
- 112 Patch, A. M., Christie, E. L., Etemadmoghadam, D., Garsed, D. W., George, J., Fereday, S., Nones, K., Cowin, P., Alsop, K., Bailey, P. J., Kassahn, K. S., Newell, F., Quinn, M. C., Kazakoff, S., Quek, K., Wilhelm-Benartzi, C., Curry, E., Leong, H. S., Australian Ovarian Cancer Study, G., Hamilton, A., Mileskin, L., Au-Yeung, G., Kennedy, C., Hung, J., Chiew, Y. E., Harnett, P., Friedlander, M., Quinn, M., Pyman, J., Cordner, S., O'Brien, P., Leditschke, J., Young, G., Strachan, K., Waring, P., Azar, W., Mitchell, C., Traficante, N., Hendley, J., Thorne, H., Shackleton, M., Miller, D. K., Arnau, G. M., Tothill, R. W., Holloway, T. P., Semple, T., Harliwong, I., Nourse, C., Nourbakhsh, E., Manning, S., Idrisoglu, S., Bruxner, T. J., Christ, A. N., Poudel, B., Holmes, O., Anderson, M., Leonard, C., Lonie, A., Hall, N., Wood, S., Taylor, D. F., Xu, Q., Fink, J. L., Waddell, N., Drapkin, R., Stronach, E., Gabra, H., Brown, R., Jewell, A., Nagaraj, S. H., Markham, E., Wilson, P. J., Ellul, J., McNally, O., Doyle, M. A., Vedururu, R., Stewart, C., Lengyel, E., Pearson, J. V., Waddell, N., deFazio, A., Grimmond, S. M. & Bowtell, D. D. Whole-genome characterization of chemoresistant ovarian cancer. *Nature* **521**, 489-494, doi:10.1038/nature14410 (2015).
- 113 Lee, M. C., Lopez-Diaz, F. J., Khan, S. Y., Tariq, M. A., Dayn, Y., Vaske, C. J., Radenbaugh, A. J., Kim, H. J., Emerson, B. M. & Pourmand, N. Single-cell analyses of transcriptional heterogeneity during drug tolerance transition in cancer cells by RNA sequencing. *Proc Natl Acad Sci U S A* **111**, E4726-4735, doi:10.1073/pnas.1404656111 (2014).
- 114 Kurtova, A. V., Xiao, J., Mo, Q., Pazhanisamy, S., Krasnow, R., Lerner, S. P., Chen, F., Roh, T. T., Lay, E., Ho, P. L. & Chan, K. S. Blocking PGE2-induced tumour repopulation abrogates bladder cancer chemoresistance. *Nature* **517**, 209-213, doi:10.1038/nature14034 (2015).
- 115 Kim, C., Gao, R., Sei, E., Brandt, R., Hartman, J., Hatschek, T., Crosetto, N., Foukakis, T. & Navin, N. E. Chemoresistance Evolution in Triple-Negative Breast Cancer Delineated by Single-Cell Sequencing. *Cell* **173**, 879-893 e813, doi:10.1016/j.cell.2018.03.041 (2018).
- 116 Sharma, S. V., Lee, D. Y., Li, B., Quinlan, M. P., Takahashi, F., Maheswaran, S., McDermott, U., Azizian, N., Zou, L., Fischbach, M. A., Wong, K. K., Brandstetter, K., Wittner, B., Ramaswamy, S., Classon, M. & Settleman, J. A chromatin-mediated reversible drug-tolerant state in cancer cell subpopulations. *Cell* **141**, 69-80, doi:10.1016/j.cell.2010.02.027 (2010).
- 117 Hata, A. N., Niederst, M. J., Archibald, H. L., Gomez-Caraballo, M., Siddiqui, F. M., Mulvey, H. E., Maruvka, Y. E., Ji, F., Bhang, H. E., Krishnamurthy Radhakrishna, V., Siravegna, G., Hu, H., Raof, S., Lockerman, E., Kalsy, A., Lee, D., Keating, C. L., Ruddy, D. A., Damon, L. J., Crystal, A. S., Costa, C., Piotrowska, Z., Bardelli, A., Iafrate, A. J., Sadreyev, R. I., Stegmeier, F., Getz, G., Sequist, L. V., Faber, A. C. & Engelman, J. A. Tumor cells can follow distinct evolutionary paths to become resistant to epidermal growth factor receptor inhibition. *Nat Med* **22**, 262-269, doi:10.1038/nm.4040 (2016).
- 118 Dean, M. Cancer stem cells: Implications for cancer causation and therapy resistance. *Discov Med* **5**, 278-282 (2005).

- 119 Blanpain, C., Mohrin, M., Sotiropoulou, P. A. & Passegue, E. DNA-damage response in tissue-specific and cancer stem cells. *Cell Stem Cell* **8**, 16-29, doi:10.1016/j.stem.2010.12.012 (2011).
- 120 Hovinga, K. E., Shimizu, F., Wang, R., Panagiotakos, G., Van Der Heijden, M., Moayedpardazi, H., Correia, A. S., Soulet, D., Major, T., Menon, J. & Tabar, V. Inhibition of notch signaling in glioblastoma targets cancer stem cells via an endothelial cell intermediate. *Stem Cells* **28**, 1019-1029, doi:10.1002/stem.429 (2010).
- 121 Chaudhary, P. M. & Roninson, I. B. Expression and activity of P-glycoprotein, a multidrug efflux pump, in human hematopoietic stem cells. *Cell* **66**, 85-94 (1991).
- 122 Zhou, S., Schuetz, J. D., Bunting, K. D., Colapietro, A. M., Sampath, J., Morris, J. J., Lagutina, I., Grosveld, G. C., Osawa, M., Nakauchi, H. & Sorrentino, B. P. The ABC transporter Bcrp1/ABCG2 is expressed in a wide variety of stem cells and is a molecular determinant of the side-population phenotype. *Nat Med* **7**, 1028-1034, doi:10.1038/nm0901-1028 (2001).
- 123 Lin, T., Islam, O. & Heese, K. ABC transporters, neural stem cells and neurogenesis--a different perspective. *Cell Res* **16**, 857-871, doi:10.1038/sj.cr.7310107 (2006).
- 124 Hirschmann-Jax, C., Foster, A. E., Wulf, G. G., Nuchtern, J. G., Jax, T. W., Gobel, U., Goodell, M. A. & Brenner, M. K. A distinct "side population" of cells with high drug efflux capacity in human tumor cells. *Proc Natl Acad Sci U S A* **101**, 14228-14233, doi:10.1073/pnas.0400067101 (2004).
- 125 Stupp, R., Hegi, M. E., Mason, W. P., van den Bent, M. J., Taphoorn, M. J., Janzer, R. C., Ludwin, S. K., Allgeier, A., Fisher, B., Belanger, K., Hau, P., Brandes, A. A., Gijtenbeek, J., Marosi, C., Vecht, C. J., Mokhtari, K., Wesseling, P., Villa, S., Eisenhauer, E., Gorlia, T., Weller, M., Lacombe, D., Cairncross, J. G., Mirimanoff, R. O., European Organisation for, R., Treatment of Cancer Brain, T., Radiation Oncology, G. & National Cancer Institute of Canada Clinical Trials, G. Effects of radiotherapy with concomitant and adjuvant temozolomide versus radiotherapy alone on survival in glioblastoma in a randomised phase III study: 5-year analysis of the EORTC-NCIC trial. *Lancet Oncol* **10**, 459-466, doi:10.1016/S1470-2045(09)70025-7 (2009).
- 126 Singh, S. K., Clarke, I. D., Terasaki, M., Bonn, V. E., Hawkins, C., Squire, J. & Dirks, P. B. Identification of a cancer stem cell in human brain tumors. *Cancer Res* **63**, 5821-5828 (2003).
- 127 Bao, S., Wu, Q., McLendon, R. E., Hao, Y., Shi, Q., Hjelmeland, A. B., Dewhirst, M. W., Bigner, D. D. & Rich, J. N. Glioma stem cells promote radioresistance by preferential activation of the DNA damage response. *Nature* **444**, 756-760, doi:10.1038/nature05236 (2006).
- 128 Dent, P., Tang, Y., Yacoub, A., Dai, Y., Fisher, P. B. & Grant, S. CHK1 inhibitors in combination chemotherapy: thinking beyond the cell cycle. *Mol Interv* **11**, 133-140, doi:10.1124/mi.11.2.11 (2011).
- 129 Ong, D. S. T., Hu, B., Ho, Y. W., Sauve, C. G., Bristow, C. A., Wang, Q., Multani, A. S., Chen, P., Nezi, L., Jiang, S., Gorman, C. E., Monasterio, M. M., Koul, D., Marchesini, M., Colla, S., Jin, E. J., Sulman, E. P., Spring, D. J., Yung, W. A., Verhaak, R. G. W., Chin, L., Wang, Y. A. & DePinho, R. A. PAF promotes stemness and radioresistance of glioma stem cells. *Proc Natl Acad Sci U S A* **114**, E9086-E9095, doi:10.1073/pnas.1708122114 (2017).
- 130 Druker, B. J., Tamura, S., Buchdunger, E., Ohno, S., Segal, G. M., Fanning, S., Zimmermann, J. & Lydon, N. B. Effects of a selective inhibitor of the Abl tyrosine kinase on the growth of Bcr-Abl positive cells. *Nat Med* **2**, 561-566 (1996).

- 131 Kimura, S. Current status of ABL tyrosine kinase inhibitors stop studies for chronic myeloid leukemia. *Stem Cell Investig* **3**, 36, doi:10.21037/sci.2016.07.08 (2016).
- 132 Bhatia, R., Holtz, M., Niu, N., Gray, R., Snyder, D. S., Sawyers, C. L., Arber, D. A., Slovak, M. L. & Forman, S. J. Persistence of malignant hematopoietic progenitors in chronic myelogenous leukemia patients in complete cytogenetic remission following imatinib mesylate treatment. *Blood* **101**, 4701-4707, doi:10.1182/blood-2002-09-2780 (2003).
- 133 Chomel, J. C., Bonnet, M. L., Sorel, N., Bertrand, A., Meunier, M. C., Fichelson, S., Melkus, M., Bennaceur-Griscelli, A., Guilhot, F. & Turhan, A. G. Leukemic stem cell persistence in chronic myeloid leukemia patients with sustained undetectable molecular residual disease. *Blood* **118**, 3657-3660, doi:10.1182/blood-2011-02-335497 (2011).
- 134 Graham, S. M., Jorgensen, H. G., Allan, E., Pearson, C., Alcorn, M. J., Richmond, L. & Holyoake, T. L. Primitive, quiescent, Philadelphia-positive stem cells from patients with chronic myeloid leukemia are insensitive to STI571 in vitro. *Blood* **99**, 319-325 (2002).
- 135 Corbin, A. S., Agarwal, A., Loriaux, M., Cortes, J., Deininger, M. W. & Druker, B. J. Human chronic myeloid leukemia stem cells are insensitive to imatinib despite inhibition of BCR-ABL activity. *J Clin Invest* **121**, 396-409, doi:10.1172/JCI35721 (2011).
- 136 Jabbour, E. J., Cortes, J. E. & Kantarjian, H. M. Tyrosine kinase inhibition: a therapeutic target for the management of chronic-phase chronic myeloid leukemia. *Expert Rev Anticancer Ther* **13**, 1433-1452, doi:10.1586/14737140.2013.859074 (2013).
- 137 Chen, Y., Hu, Y., Zhang, H., Peng, C. & Li, S. Loss of the Alox5 gene impairs leukemia stem cells and prevents chronic myeloid leukemia. *Nat Genet* **41**, 783-792, doi:10.1038/ng.389 (2009).
- 138 Hu, Y., Chen, Y., Douglas, L. & Li, S. beta-Catenin is essential for survival of leukemic stem cells insensitive to kinase inhibition in mice with BCR-ABL-induced chronic myeloid leukemia. *Leukemia* **23**, 109-116, doi:10.1038/leu.2008.262 (2009).
- 139 Zhao, C., Chen, A., Jamieson, C. H., Fereshteh, M., Abrahamsson, A., Blum, J., Kwon, H. Y., Kim, J., Chute, J. P., Rizzieri, D., Munchhof, M., VanArsdale, T., Beachy, P. A. & Reya, T. Hedgehog signalling is essential for maintenance of cancer stem cells in myeloid leukaemia. *Nature* **458**, 776-779, doi:10.1038/nature07737 (2009).
- 140 Shien, K., Toyooka, S., Yamamoto, H., Soh, J., Jida, M., Thu, K. L., Hashida, S., Maki, Y., Ichihara, E., Asano, H., Tsukuda, K., Takigawa, N., Kiura, K., Gazdar, A. F., Lam, W. L. & Miyoshi, S. Acquired resistance to EGFR inhibitors is associated with a manifestation of stem cell-like properties in cancer cells. *Cancer Res* **73**, 3051-3061, doi:10.1158/0008-5472.CAN-12-4136 (2013).
- 141 Arasada, R. R., Amann, J. M., Rahman, M. A., Huppert, S. S. & Carbone, D. P. EGFR blockade enriches for lung cancer stem-like cells through Notch3-dependent signaling. *Cancer Res* **74**, 5572-5584, doi:10.1158/0008-5472.CAN-13-3724 (2014).
- 142 Hu, S., Fu, W., Li, T., Yuan, Q., Wang, F., Lv, G., Lv, Y., Fan, X., Shen, Y., Lin, F., Tang, Y., Ye, X., Yang, Y. & Lei, C. Antagonism of EGFR and Notch limits resistance to EGFR inhibitors and radiation by decreasing tumor-initiating cell frequency. *Sci Transl Med* **9**, doi:10.1126/scitranslmed.aag0339 (2017).

- 143 Brahmer, J. R., Tykodi, S. S., Chow, L. Q., Hwu, W. J., Topalian, S. L., Hwu, P., Drake, C. G., Camacho, L. H., Kauh, J., Odunsi, K., Pitot, H. C., Hamid, O., Bhatia, S., Martins, R., Eaton, K., Chen, S., Salay, T. M., Alaparthi, S., Grosso, J. F., Korman, A. J., Parker, S. M., Agrawal, S., Goldberg, S. M., Pardoll, D. M., Gupta, A. & Wigginton, J. M. Safety and activity of anti-PD-L1 antibody in patients with advanced cancer. *N Engl J Med* **366**, 2455-2465, doi:10.1056/NEJMoa1200694 (2012).
- 144 Iwai, Y., Ishida, M., Tanaka, Y., Okazaki, T., Honjo, T. & Minato, N. Involvement of PD-L1 on tumor cells in the escape from host immune system and tumor immunotherapy by PD-L1 blockade. *Proc Natl Acad Sci U S A* **99**, 12293-12297, doi:10.1073/pnas.192461099 (2002).
- 145 Leach, D. R., Krummel, M. F. & Allison, J. P. Enhancement of antitumor immunity by CTLA-4 blockade. *Science* **271**, 1734-1736 (1996).
- 146 Ribas, A. & Wolchok, J. D. Cancer immunotherapy using checkpoint blockade. *Science* **359**, 1350-1355, doi:10.1126/science.aar4060 (2018).
- 147 Malta, T. M., Sokolov, A., Gentles, A. J., Burzykowski, T., Poisson, L., Weinstein, J. N., Kaminska, B., Huelsken, J., Omberg, L., Gevaert, O., Colaprico, A., Czerwinska, P., Mazurek, S., Mishra, L., Heyn, H., Krasnitz, A., Godwin, A. K., Lazar, A. J., Cancer Genome Atlas Research, N., Stuart, J. M., Hoadley, K. A., Laird, P. W., Noushmehr, H. & Wiznerowicz, M. Machine Learning Identifies Stemness Features Associated with Oncogenic Dedifferentiation. *Cell* **173**, 338-354 e315, doi:10.1016/j.cell.2018.03.034 (2018).
- 148 Zaretsky, J. M., Garcia-Diaz, A., Shin, D. S., Escuin-Ordinas, H., Hugo, W., Hu-Lieskovan, S., Torrejon, D. Y., Abril-Rodriguez, G., Sandoval, S., Barthly, L., Saco, J., Homet Moreno, B., Mezzadra, R., Chmielowski, B., Ruchalski, K., Shintaku, I. P., Sanchez, P. J., Puig-Saus, C., Cherry, G., Seja, E., Kong, X., Pang, J., Berent-Maoz, B., Comin-Anduix, B., Graeber, T. G., Tume, P. C., Schumacher, T. N., Lo, R. S. & Ribas, A. Mutations Associated with Acquired Resistance to PD-1 Blockade in Melanoma. *N Engl J Med* **375**, 819-829, doi:10.1056/NEJMoa1604958 (2016).
- 149 Ji, R. R., Chasalow, S. D., Wang, L., Hamid, O., Schmidt, H., Cogswell, J., Alaparthi, S., Berman, D., Jure-Kunkel, M., Siemers, N. O., Jackson, J. R. & Shahabi, V. An immune-active tumor microenvironment favors clinical response to ipilimumab. *Cancer Immunol Immunother* **61**, 1019-1031, doi:10.1007/s00262-011-1172-6 (2012).
- 150 Spranger, S., Bao, R. & Gajewski, T. F. Melanoma-intrinsic beta-catenin signalling prevents anti-tumour immunity. *Nature* **523**, 231-235, doi:10.1038/nature14404 (2015).
- 151 Cheah, M. T., Chen, J. Y., Sahoo, D., Contreras-Trujillo, H., Volkmer, A. K., Scheeren, F. A., Volkmer, J. P. & Weissman, I. L. CD14-expressing cancer cells establish the inflammatory and proliferative tumor microenvironment in bladder cancer. *Proc Natl Acad Sci U S A* **112**, 4725-4730, doi:10.1073/pnas.1424795112 (2015).
- 152 Calabrese, C., Poppleton, H., Kocak, M., Hogg, T. L., Fuller, C., Hamner, B., Oh, E. Y., Gaber, M. W., Finklestein, D., Allen, M., Frank, A., Bayazitov, I. T., Zakharenko, S. S., Gajjar, A., Davidoff, A. & Gilbertson, R. J. A perivascular niche for brain tumor stem cells. *Cancer Cell* **11**, 69-82, doi:10.1016/j.ccr.2006.11.020 (2007).
- 153 Bao, S., Wu, Q., Sathornsumetee, S., Hao, Y., Li, Z., Hjelmeland, A. B., Shi, Q., McLendon, R. E., Bigner, D. D. & Rich, J. N. Stem cell-like glioma cells promote tumor angiogenesis through vascular

- endothelial growth factor. *Cancer Res* **66**, 7843-7848, doi:10.1158/0008-5472.CAN-06-1010 (2006).
- 154 Folkins, C., Shaked, Y., Man, S., Tang, T., Lee, C. R., Zhu, Z., Hoffman, R. M. & Kerbel, R. S. Glioma tumor stem-like cells promote tumor angiogenesis and vasculogenesis via vascular endothelial growth factor and stromal-derived factor 1. *Cancer Res* **69**, 7243-7251, doi:10.1158/0008-5472.CAN-09-0167 (2009).
- 155 Charles, N., Ozawa, T., Squatrito, M., Bleau, A. M., Brennan, C. W., Hambardzumyan, D. & Holland, E. C. Perivascular nitric oxide activates notch signaling and promotes stem-like character in PDGF-induced glioma cells. *Cell Stem Cell* **6**, 141-152, doi:10.1016/j.stem.2010.01.001 (2010).
- 156 Pietras, A., Katz, A. M., Ekstrom, E. J., Wee, B., Halliday, J. J., Pitter, K. L., Werbeck, J. L., Amankulor, N. M., Huse, J. T. & Holland, E. C. Osteopontin-CD44 signaling in the glioma perivascular niche enhances cancer stem cell phenotypes and promotes aggressive tumor growth. *Cell Stem Cell* **14**, 357-369, doi:10.1016/j.stem.2014.01.005 (2014).
- 157 Vredenburgh, J. J., Desjardins, A., Herndon, J. E., 2nd, Dowell, J. M., Reardon, D. A., Quinn, J. A., Rich, J. N., Sathornsumetee, S., Gururangan, S., Wagner, M., Bigner, D. D., Friedman, A. H. & Friedman, H. S. Phase II trial of bevacizumab and irinotecan in recurrent malignant glioma. *Clin Cancer Res* **13**, 1253-1259, doi:10.1158/1078-0432.CCR-06-2309 (2007).
- 158 Das, B., Tsuchida, R., Malkin, D., Koren, G., Baruchel, S. & Yeger, H. Hypoxia enhances tumor stemness by increasing the invasive and tumorigenic side population fraction. *Stem Cells* **26**, 1818-1830, doi:10.1634/stemcells.2007-0724 (2008).
- 159 Heddleston, J. M., Li, Z., McLendon, R. E., Hjelmeland, A. B. & Rich, J. N. The hypoxic microenvironment maintains glioblastoma stem cells and promotes reprogramming towards a cancer stem cell phenotype. *Cell Cycle* **8**, 3274-3284, doi:10.4161/cc.8.20.9701 (2009).
- 160 Chiou, S. H., Risca, V. I., Wang, G. X., Yang, D., Gruner, B. M., Kathiria, A. S., Ma, R. K., Vaka, D., Chu, P., Kozak, M., Castellini, L., Graves, E. E., Kim, G. E., Mourrain, P., Koong, A. C., Giaccia, A. J. & Winslow, M. M. BLIMP1 Induces Transient Metastatic Heterogeneity in Pancreatic Cancer. *Cancer Discov* **7**, 1184-1199, doi:10.1158/2159-8290.CD-17-0250 (2017).
- 161 Tammela, T., Sanchez-Rivera, F. J., Cetinbas, N. M., Wu, K., Joshi, N. S., Helenius, K., Park, Y., Azimi, R., Kerper, N. R., Wesselhoeft, R. A., Gu, X., Schmidt, L., Cornwall-Brady, M., Yilmaz, O. H., Xue, W., Katajisto, P., Bhutkar, A. & Jacks, T. A Wnt-producing niche drives proliferative potential and progression in lung adenocarcinoma. *Nature* **545**, 355-359, doi:10.1038/nature22334 (2017).
- 162 Wang, X., Prager, B. C., Wu, Q., Kim, L. J. Y., Gimple, R. C., Shi, Y., Yang, K., Morton, A. R., Zhou, W., Zhu, Z., Obara, E. A. A., Miller, T. E., Song, A., Lai, S., Hubert, C. G., Jin, X., Huang, Z., Fang, X., Dixit, D., Tao, W., Zhai, K., Chen, C., Dong, Z., Zhang, G., Dombrowski, S. M., Hamerlik, P., Mack, S. C., Bao, S. & Rich, J. N. Reciprocal Signaling between Glioblastoma Stem Cells and Differentiated Tumor Cells Promotes Malignant Progression. *Cell Stem Cell* **22**, 514-528 e515, doi:10.1016/j.stem.2018.03.011 (2018).
- 163 Su, S., Chen, J., Yao, H., Liu, J., Yu, S., Lao, L., Wang, M., Luo, M., Xing, Y., Chen, F., Huang, D., Zhao, J., Yang, L., Liao, D., Su, F., Li, M., Liu, Q. & Song, E. CD10(+)GPR77(+) Cancer-Associated Fibroblasts Promote Cancer Formation and Chemoresistance by Sustaining Cancer Stemness. *Cell* **172**, 841-856 e816, doi:10.1016/j.cell.2018.01.009 (2018).

- 164 Chen, W. J., Ho, C. C., Chang, Y. L., Chen, H. Y., Lin, C. A., Ling, T. Y., Yu, S. L., Yuan, S. S., Chen, Y. J., Lin, C. Y., Pan, S. H., Chou, H. Y., Chen, Y. J., Chang, G. C., Chu, W. C., Lee, Y. M., Lee, J. Y., Lee, P. J., Li, K. C., Chen, H. W. & Yang, P. C. Cancer-associated fibroblasts regulate the plasticity of lung cancer stemness via paracrine signalling. *Nat Commun* **5**, 3472, doi:10.1038/ncomms4472 (2014).
- 165 Sneddon, J. B., Zhen, H. H., Montgomery, K., van de Rijn, M., Tward, A. D., West, R., Gladstone, H., Chang, H. Y., Morganroth, G. S., Oro, A. E. & Brown, P. O. Bone morphogenetic protein antagonist gremlin 1 is widely expressed by cancer-associated stromal cells and can promote tumor cell proliferation. *Proc Natl Acad Sci U S A* **103**, 14842-14847, doi:10.1073/pnas.0606857103 (2006).
- 166 Vermeulen, L., De Sousa, E. M. F., van der Heijden, M., Cameron, K., de Jong, J. H., Borovski, T., Tuynman, J. B., Todaro, M., Merz, C., Rodermond, H., Sprick, M. R., Kemper, K., Richel, D. J., Stassi, G. & Medema, J. P. Wnt activity defines colon cancer stem cells and is regulated by the microenvironment. *Nat Cell Biol* **12**, 468-476, doi:10.1038/ncb2048 (2010).
- 167 Bajaj, J., Konuma, T., Lytle, N. K., Kwon, H. Y., Ablack, J. N., Cantor, J. M., Rizzieri, D., Chuah, C., Oehler, V. G., Broome, E. H., Ball, E. D., van der Horst, E. H., Ginsberg, M. H. & Reya, T. CD98-Mediated Adhesive Signaling Enables the Establishment and Propagation of Acute Myelogenous Leukemia. *Cancer Cell* **30**, 792-805, doi:10.1016/j.ccell.2016.10.003 (2016).
- 168 Kwon, H. Y., Bajaj, J., Ito, T., Blevins, A., Konuma, T., Weeks, J., Lytle, N. K., Koechlein, C. S., Rizzieri, D., Chuah, C., Oehler, V. G., Sasik, R., Hardiman, G. & Reya, T. Tetraspanin 3 Is Required for the Development and Propagation of Acute Myelogenous Leukemia. *Cell Stem Cell* **17**, 152-164, doi:10.1016/j.stem.2015.06.006 (2015).
- 169 Passaro, D., Irigoyen, M., Catherinet, C., Gachet, S., Da Costa De Jesus, C., Lasgi, C., Tran Quang, C. & Ghysdael, J. CXCR4 Is Required for Leukemia-Initiating Cell Activity in T Cell Acute Lymphoblastic Leukemia. *Cancer Cell* **27**, 769-779, doi:10.1016/j.ccell.2015.05.003 (2015).
- 170 Ebinger, S., Ozdemir, E. Z., Ziegenhain, C., Tiedt, S., Castro Alves, C., Grunert, M., Dworzak, M., Lutz, C., Turati, V. A., Enver, T., Horny, H. P., Sotlar, K., Parekh, S., Spiekermann, K., Hiddemann, W., Schepers, A., Polzer, B., Kirsch, S., Hoffmann, M., Knapp, B., Hasenauer, J., Pfeifer, H., Panzer-Grumayer, R., Enard, W., Gires, O. & Jeremias, I. Characterization of Rare, Dormant, and Therapy-Resistant Cells in Acute Lymphoblastic Leukemia. *Cancer Cell* **30**, 849-862, doi:10.1016/j.ccell.2016.11.002 (2016).
- 171 Sato, T., Vries, R. G., Snippert, H. J., van de Wetering, M., Barker, N., Stange, D. E., van Es, J. H., Abo, A., Kujala, P., Peters, P. J. & Clevers, H. Single Lgr5 stem cells build crypt-villus structures in vitro without a mesenchymal niche. *Nature* **459**, 262-265, doi:10.1038/nature07935 (2009).
- 172 Drost, J. & Clevers, H. Organoids in cancer research. *Nat Rev Cancer* **18**, 407-418, doi:10.1038/s41568-018-0007-6 (2018).
- 173 Roerink, S. F., Sasaki, N., Lee-Six, H., Young, M. D., Alexandrov, L. B., Behjati, S., Mitchell, T. J., Grossmann, S., Lightfoot, H., Egan, D. A., Pronk, A., Smakman, N., van Gorp, J., Anderson, E., Gamble, S. J., Alder, C., van de Wetering, M., Campbell, P. J., Stratton, M. R. & Clevers, H. Intra-tumour diversification in colorectal cancer at the single-cell level. *Nature* **556**, 457-462, doi:10.1038/s41586-018-0024-3 (2018).
- 174 Boj, S. F., Hwang, C. I., Baker, L. A., Chio, I., Engle, D. D., Corbo, V., Jager, M., Ponz-Sarvisé, M., Tiriác, H., Spector, M. S., Gračanin, A., Oni, T., Yu, K. H., van Boxtel, R., Huch, M., Rivera, K. D.,

- Wilson, J. P., Feigin, M. E., Ohlund, D., Handly-Santana, A., Ardito-Abraham, C. M., Ludwig, M., Elyada, E., Alagesan, B., Biffi, G., Yordanov, G. N., Delcuze, B., Creighton, B., Wright, K., Park, Y., Morsink, F. H., Molenaar, I. Q., Borel Rinkes, I. H., Cuppen, E., Hao, Y., Jin, Y., Nijman, I. J., Iacobuzio-Donahue, C., Leach, S. D., Pappin, D. J., Hammell, M., Klimstra, D. S., Basturk, O., Hruban, R. H., Offerhaus, G. J., Vries, R. G., Clevers, H. & Tuveson, D. A. Organoid models of human and mouse ductal pancreatic cancer. *Cell* **160**, 324-338, doi:10.1016/j.cell.2014.12.021 (2015).
- 175 Tiriac, H., Belleau, P., Engle, D. D., Plenker, D., Deschenes, A., Somerville, T., Froeling, F. E. M., Burkhart, R. A., Denroche, R. E., Jang, G. H., Miyabayashi, K., Young, C. M., Patel, H., Ma, M., LaComb, J. F., Palmaira, R. L. D., Javed, A. A., Huynh, J. A., Johnson, M., Arora, K., Robine, N., Shah, M., Sanghvi, R., Goetz, A. B., Lowder, C. Y., Martello, L., Driehuis, E., Lecomte, N., Askan, G., Iacobuzio-Donahue, C. A., Clevers, H., Wood, L. D., Hruban, R. H., Thompson, E. D., Aguirre, A. J., Wolpin, B. M., Sasson, A., Kim, J., Wu, M., Bucobo, J. C., Allen, P. J., Sejpal, D. V., Nealon, W., Sullivan, J. D., Winter, J. M., Gimotty, P. A., Grem, J. L., DiMaio, D. J., Buscaglia, J. M., Grandgenett, P. M., Brody, J. R., Hollingsworth, M. A., O'Kane, G. M., Notta, F., Kim, E. J., Crawford, J. M., Devoe, C. E., Ocean, A., Wolfgang, C. L., Yu, K. H., Li, E., Vakoc, C. R., Hubert, B., Fischer, S. E., Wilson, J. M., Moffitt, R. A., Knox, J. J., Krasnitz, A., Gallinger, S. & Tuveson, D. A. Organoid profiling identifies common responders to chemotherapy in pancreatic cancer. *Cancer Discov*, doi:10.1158/2159-8290.CD-18-0349 (2018).
- 176 Sachs, N., de Ligt, J., Kopper, O., Gogola, E., Bounova, G., Weeber, F., Balgobind, A. V., Wind, K., Gracanin, A., Begthel, H., Korving, J., van Boxtel, R., Duarte, A. A., Lelieveld, D., van Hoeck, A., Ernst, R. F., Blokzijl, F., Nijman, I. J., Hoogstraat, M., van de Ven, M., Egan, D. A., Zinzalla, V., Moll, J., Boj, S. F., Voest, E. E., Wessels, L., van Diest, P. J., Rottenberg, S., Vries, R. G. J., Cuppen, E. & Clevers, H. A Living Biobank of Breast Cancer Organoids Captures Disease Heterogeneity. *Cell* **172**, 373-386 e310, doi:10.1016/j.cell.2017.11.010 (2018).
- 177 Broutier, L., Mastrogiovanni, G., Verstegen, M. M., Francies, H. E., Gavarro, L. M., Bradshaw, C. R., Allen, G. E., Arnes-Benito, R., Sidorova, O., Gaspersz, M. P., Georgakopoulos, N., Koo, B. K., Dietmann, S., Davies, S. E., Praseedom, R. K., Lieshout, R., JNM, I. J., Wigmore, S. J., Saeb-Parsy, K., Garnett, M. J., van der Laan, L. J. & Huch, M. Human primary liver cancer-derived organoid cultures for disease modeling and drug screening. *Nat Med* **23**, 1424-1435, doi:10.1038/nm.4438 (2017).
- 178 Lee, S. H., Hu, W., Matulay, J. T., Silva, M. V., Owczarek, T. B., Kim, K., Chua, C. W., Barlow, L. J., Kandoth, C., Williams, A. B., Bergren, S. K., Pietzak, E. J., Anderson, C. B., Benson, M. C., Coleman, J. A., Taylor, B. S., Abate-Shen, C., McKiernan, J. M., Al-Ahmadie, H., Solit, D. B. & Shen, M. M. Tumor Evolution and Drug Response in Patient-Derived Organoid Models of Bladder Cancer. *Cell* **173**, 515-528 e517, doi:10.1016/j.cell.2018.03.017 (2018).
- 179 Danial, C., Sarin, K. Y., Oro, A. E. & Chang, A. L. An Investigator-Initiated Open-Label Trial of Sonidegib in Advanced Basal Cell Carcinoma Patients Resistant to Vismodegib. *Clin Cancer Res* **22**, 1325-1329, doi:10.1158/1078-0432.CCR-15-1588 (2016).
- 180 Sekulic, A., Migden, M. R., Basset-Seguín, N., Garbe, C., Gesierich, A., Lao, C. D., Miller, C., Mortier, L., Murrell, D. F., Hamid, O., Quevedo, J. F., Hou, J., McKenna, E., Dimier, N., Williams, S., Schadendorf, D., Hauschild, A. & Investigators, E. B. Long-term safety and efficacy of vismodegib in patients with advanced basal cell carcinoma: final update of the pivotal ERIVANCE BCC study. *BMC Cancer* **17**, 332, doi:10.1186/s12885-017-3286-5 (2017).
- 181 Chang, A. L., Arron, S. T., Migden, M. R., Solomon, J. A., Yoo, S., Day, B. M., McKenna, E. F. & Sekulic, A. Safety and efficacy of vismodegib in patients with basal cell carcinoma nevus syndrome: pooled analysis of two trials. *Orphanet J Rare Dis* **11**, 120, doi:10.1186/s13023-016-0506-z (2016).

- 182 Sekulic, A., Migden, M. R., Oro, A. E., Dirix, L., Lewis, K. D., Hainsworth, J. D., Solomon, J. A., Yoo, S., Arron, S. T., Friedlander, P. A., Marmur, E., Rudin, C. M., Chang, A. L., Low, J. A., Mackey, H. M., Yauch, R. L., Graham, R. A., Reddy, J. C. & Hauschild, A. Efficacy and safety of vismodegib in advanced basal-cell carcinoma. *N Engl J Med* **366**, 2171-2179, doi:10.1056/NEJMoa1113713 (2012).
- 183 Robinson, G. W., Orr, B. A., Wu, G., Gururangan, S., Lin, T., Qaddoumi, I., Packer, R. J., Goldman, S., Prados, M. D., Desjardins, A., Chintagumpala, M., Takebe, N., Kaste, S. C., Rusch, M., Allen, S. J., Onar-Thomas, A., Stewart, C. F., Fouladi, M., Boyett, J. M., Gilbertson, R. J., Curran, T., Ellison, D. W. & Gajjar, A. Vismodegib Exerts Targeted Efficacy Against Recurrent Sonic Hedgehog-Subgroup Medulloblastoma: Results From Phase II Pediatric Brain Tumor Consortium Studies PBTC-025B and PBTC-032. *J Clin Oncol* **33**, 2646-2654, doi:10.1200/JCO.2014.60.1591 (2015).
- 184 Belani, C. P., Dahlberg, S. E., Rudin, C. M., Fleisher, M., Chen, H. X., Takebe, N., Velasco, M. R., Jr., Tester, W. J., Sturtz, K., Hann, C. L., Shanks, J. C., Monga, M., Ramalingam, S. S. & Schiller, J. H. Vismodegib or cixutumumab in combination with standard chemotherapy for patients with extensive-stage small cell lung cancer: A trial of the ECOG-ACRIN Cancer Research Group (E1508). *Cancer* **122**, 2371-2378, doi:10.1002/cncr.30062 (2016).
- 185 *US National Library of Medicine*, <<https://clinicaltrials.gov/ct2/show/NCT00833417>> (2015).
- 186 *US National Library of Medicine*, <<https://clinicaltrials.gov/ct2/show/NCT01529450>> (2017).
- 187 Taipale, J., Chen, J. K., Cooper, M. K., Wang, B., Mann, R. K., Milenkovic, L., Scott, M. P. & Beachy, P. A. Effects of oncogenic mutations in Smoothed and Patched can be reversed by cyclopamine. *Nature* **406**, 1005-1009, doi:10.1038/35023008 (2000).
- 188 Atwood, S. X., Li, M., Lee, A., Tang, J. Y. & Oro, A. E. GLI activation by atypical protein kinase C iota/lambda regulates the growth of basal cell carcinomas. *Nature* **494**, 484-488, doi:10.1038/nature11889 (2013).
- 189 Rimkus, T. K., Carpenter, R. L., Qasem, S., Chan, M. & Lo, H. W. Targeting the Sonic Hedgehog Signaling Pathway: Review of Smoothed and GLI Inhibitors. *Cancers (Basel)* **8**, doi:10.3390/cancers8020022 (2016).
- 190 *US National Library of Medicine*, <<https://clinicaltrials.gov/ct2/show/NCT03035253>> (2018).
- 191 Lyou, Y., Habowski, A. N., Chen, G. T. & Waterman, M. L. Inhibition of nuclear Wnt signalling: challenges of an elusive target for cancer therapy. *Br J Pharmacol*, doi:10.1111/bph.13963 (2017).
- 192 *US National Library of Medicine*, <<https://clinicaltrials.gov/ct2/show/NCT01606579>> (2017).
- 193 *US National Library of Medicine*, <<https://clinicaltrials.gov/ct2/show/NCT01345201>> (2016).
- 194 Jimeno, A., Gordon, M. S., Chugh, R., Messersmith, W., Mendelson, D. S., Dupont, J., Stagg, R. J., Kapoun, A. M., Xu, L., Uttamsingh, S., Brachmann, R. & Smith, D. C. A first-in-human Phase 1 study of the anti-cancer stem cell agent ipafricept (OMP-54F28), a decoy receptor for Wnt ligands, in patients with advanced solid tumors. *Clin Cancer Res*, doi:10.1158/1078-0432.CCR-17-2157 (2017).
- 195 *US National Library of Medicine*, <<https://clinicaltrials.gov/ct2/show/NCT01351103>> (2018).

- 196 Jain, P., Kantarjian, H. M., Ghorab, A., Sasaki, K., Jabbour, E. J., Noguera Gonzalez, G., Kanagal-Shamanna, R., Issa, G. C., Garcia-Manero, G., Kc, D., Deltasala, S., Pierce, S., Konopleva, M., Wierda, W. G., Verstovsek, S., Daver, N. G., Kadia, T. M., Borthakur, G., O'Brien, S., Estrov, Z., Ravandi, F. & Cortes, J. E. Prognostic factors and survival outcomes in patients with chronic myeloid leukemia in blast phase in the tyrosine kinase inhibitor era: Cohort study of 477 patients. *Cancer* **123**, 4391-4402, doi:10.1002/cncr.30864 (2017).

CHAPTER 2

Image based detection and targeting of therapy resistance in pancreatic adenocarcinoma

Raymond G. Fox^{#,1,2,3}, Nikki K. Lytle^{#,1,2,3}, Dawn V. Jaquish^{3,4}, Frederick D. Park^{1,2,3,5}, Takahiro Ito^{1,2,3}, Jeevisha Bajaj^{1,2,3}, Claire S. Koechlein^{1,2,3}, Bryan Zimdahl^{1,2,3}, Masato Yano⁶, Janel Kopp^{2,7}, Marcie Kritzik^{1,2,3}, Jason Sicklick^{3,4}, Maïke Sander^{2,7}, Paul M. Grandgenett⁸, Michael A. Hollingsworth⁸, Shinsuke Shibata⁶, Donald Pizzo⁹, Mark Valasek⁹, Roman Sasik¹⁰, Miriam Scadeng¹¹, Hideyuki Okano⁶, Youngsoo Kim¹², A. Robert MacLeod¹², Andrew M. Lowy^{3,4}, and Tannishtha Reya^{1,2,3}

These authors contributed equally to this work

¹Departments of Pharmacology and Medicine, University of California San Diego School of Medicine

²Sanford Consortium for Regenerative Medicine, La Jolla, CA

³Moore's Cancer Center, La Jolla, CA

⁴Department of Surgery, Division of Surgical Oncology, University of California San Diego, La Jolla, CA

⁵Department of Medicine, Division of Gastroenterology, University of California San Diego, La Jolla, CA

⁶Department of Physiology, Graduate School of Medicine, Keio University, Japan

⁷Department of Cellular and Molecular Medicine, University of California San Diego, La Jolla, CA

⁸Eppley Institute for Research in Cancer and Allied Diseases, Department of Pathology, University of Nebraska Medical Center, Omaha, NE

⁹Department of Pathology, University of California San Diego School of Medicine, La Jolla, CA

¹⁰Center for Computational Biology and Bioinformatics, University of California San Diego, La Jolla, CA

¹¹Department of Radiology, University of California San Diego School of Medicine, La Jolla, CA

¹²Department of Oncology Drug Discovery, Ionis Pharmaceuticals, Carlsbad, CA

Published in *Nature*

June 2016

PREFACE TO CHAPTER 2:

Chapter 2, in full, is an article published in *Nature* entitled “Image based detection and targeting of therapy resistance in pancreatic adenocarcinoma.” Soon after joining the Reya lab, I began working on this project alongside Dr. Raymond Fox, who was a co-first author on the manuscript. I am immensely grateful for his mentorship and his willingness to work together to uncover this exciting story. The manuscript presented here identified the stem cell fate determinant Musashi as a potent driver of pancreatic cancer progression and therapy resistance. We utilized multiple novel genetic mouse models to track pancreatic cancer stem cells in an autochthonous tumor setting to achieve a deeper understanding of the potent role of stem cell signals in pancreatic cancer. Finally, we developed a novel inhibitor of Musashi by harnessing anti-sense oligonucleotide (ASO) technology, which represents an exciting new therapeutic approach for PDAC patients.

ABSTRACT

Pancreatic intraepithelial neoplasia (PanIN) is a premalignant lesion that can progress to pancreatic ductal adenocarcinoma, a highly lethal malignancy marked by its late stage at clinical presentation and profound drug resistance¹. The genomic alterations that commonly occur in pancreatic cancer include activation of KRAS2 and inactivation of p53, and SMAD4²⁻⁴. To date, however, it has been challenging to target these pathways therapeutically; thus the search for other key mediators of pancreatic cancer growth remains an important endeavor. Here we show that the stem cell determinant Musashi (Msi) is a critical element of pancreatic cancer progression in both genetic models and patient derived xenografts. Specifically, we developed Msi reporter mice that allowed image based tracking of stem cell signals within cancers, revealing that Msi expression rises as PanIN progresses to adenocarcinoma, and that Msi-expressing cells are key drivers of pancreatic cancer: they preferentially harbor the capacity to propagate adenocarcinoma, are enriched in circulating tumor cells, and are markedly drug resistant. This population could be effectively targeted by deletion of either Msi1 or Msi2, which led to a striking defect in PanIN progression to adenocarcinoma and an improvement in overall survival. Msi inhibition also blocked the growth of primary patient-derived tumors, suggesting that this signal is required for human disease. To define the translational potential of this work we developed antisense oligonucleotides against Msi; these showed reliable tumor penetration, uptake and target inhibition, and effectively blocked pancreatic cancer growth. Collectively, these studies highlight Msi reporters as a unique tool to identify therapy resistance, and define Msi signaling as a central regulator of pancreatic cancer.

KEYWORDS

Cancer stem cells, stem cell signals, Musashi, tumor heterogeneity, therapy resistance, circulating tumor cells, pancreatic cancer, intravital imaging

RESULTS

To understand the mechanisms that underlie pancreatic cancer development and progression, we investigated signals that control self-renewal, a key stem cell property often hijacked in cancer. In particular, we focused on the role of Musashi (Msi), a highly conserved RNA binding protein originally identified in *Drosophila*⁵. While Msi has long been used as a marker of stem/progenitor cells⁶, the breadth of its functional impact is only beginning to emerge: genetic loss-of-function models have shown that Msi signaling is important for maintaining stem cells in the mammalian nervous system⁷, and more recently in normal and malignant hematopoiesis⁸⁻¹². However, the role of Msi in pancreatic cancer biology and whether it may be a viable therapeutic target remains unknown.

To address these questions, we first analyzed MSI expression in human pancreatic cancers. MSI1 and MSI2 were expressed in all primary tumor samples analyzed, with expression increasing during progression (**Figure Supplement 2.1**). To track the function of Msi-expressing cells, we developed Msi knock-in reporters (Reporter for Musashi, REM) in which fluorescent signals reflected endogenous Msi expression (**Figure 2.1A-B; Figure Supplement 2.2A-C**). To define if Msi-expressing cells contribute to pancreatic cancer, we crossed REM mice to the $Kras^{LSL-G12D/+};p53^{ff};Ptf1a^{CRE/+}$ model¹³⁻¹⁵ (**Figure Supplement 2.2D-H**). *In vivo* imaging of living tumors revealed clear Msi1 and Msi2 reporter activity within remarkable spatially restricted domains frequently surrounded by blood vessels (**Figure 2.1C-D; Figure Supplement 2.2I**). Cells with high levels of Msi reporter expression were rare, and detected in 1.18% and 9.7% of REM1 and REM2 cancers (**Figure 2.1E-F**). Because cancer stem cells can be similarly rare^{16,17}, we tested if Msi-expressing cells have preferential capacity for tumor propagation¹⁸. Consistent with this possibility, Msi⁺ cells expressed ALDH¹⁹, and were dramatically more tumorigenic *in vitro* and *in vivo* (**Figure 2.1G-I; Figure Supplement 2.3A-G**). Most importantly, Msi2⁺ cells were highly lethal: while 100% of mice orthotopically transplanted with Msi2⁺ cells developed invasive tumors and died, none of the mice receiving Msi2⁻ cells showed signs of disease (**Figure 2.1J, Figure Supplement 2.3H**). Given the suggestion that certain markers may not consistently enrich for tumor propagating ability²⁰, our findings indicate that Msi-expression can identify cancer stem cells at least in some contexts, and that Msi2⁺ cells preferentially drive pancreatic cancer growth, invasion and lethality.

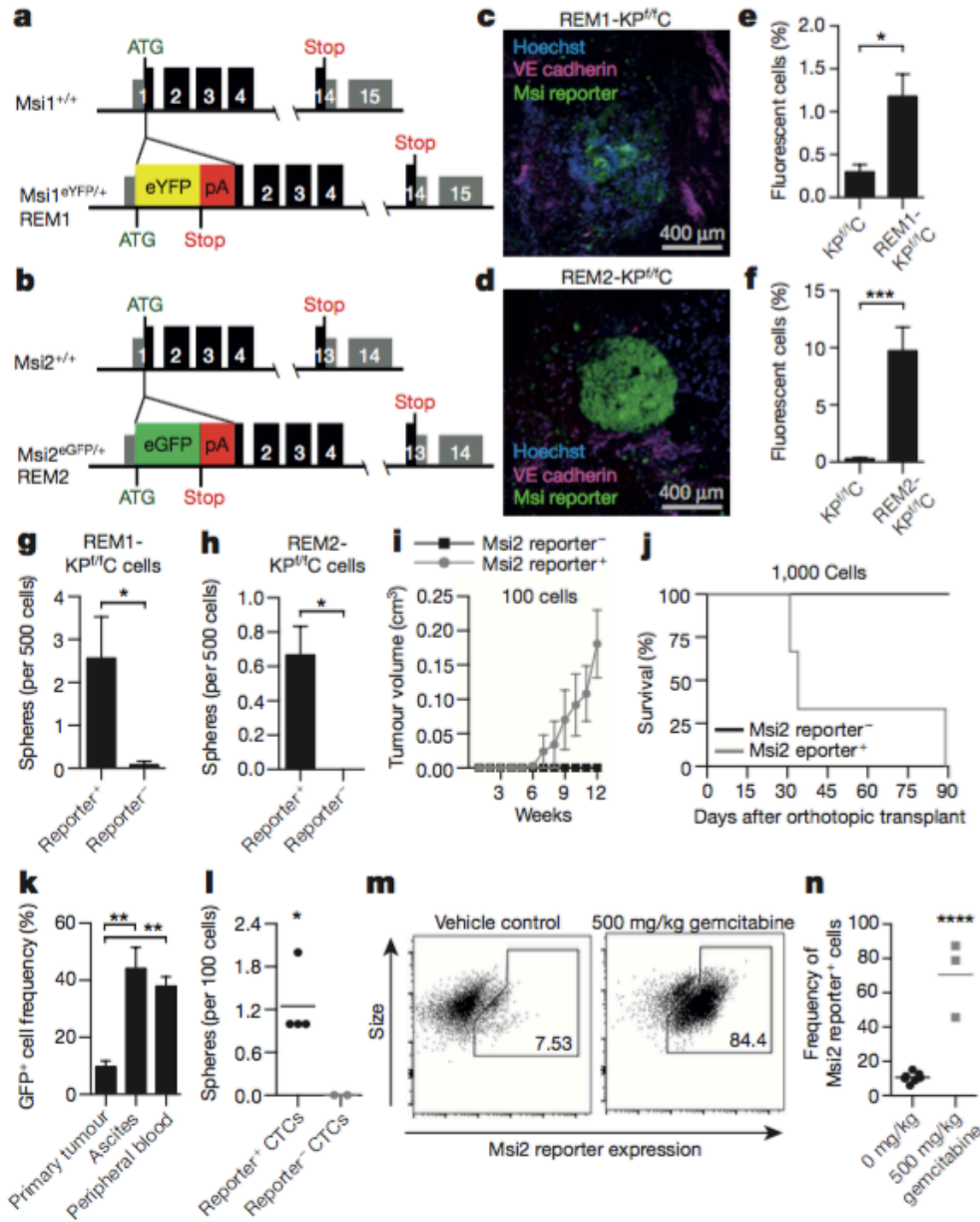


Figure 2.1. Msi reporter positive pancreatic cancer cells are enriched for tumor initiating capacity.

(A-B) Design of Msi reporter constructs (REM1, *Msi1*^{eYFP/+}; REM2, *Msi2*^{eGFP/+}). (C-D) Live images of Msi reporter cells in (C) REM1-KP^{fl/C} and (D) REM2-KP^{fl/C} tumors; VE-cadherin (magenta), Hoechst (blue), Msi reporter (green). (E-F) Msi1 and Msi2 reporter expression in dissociated tumors (n=6). (G-H) Sphere-forming ability of Msi-reporter⁺ and reporter⁻ cells (g, n=8; h, n=6). (I) *In vivo* growth of Msi2 reporter⁺ tumor cells (n=8). (J) Survival of mice orthotopically transplanted with Msi2 reporter⁺ and reporter⁻ KP^{fl/C} tumor cells (n=6). Log-rank (Mantel-Cox) survival analysis (p<0.05). (K) Reporter frequency in primary tumors (n=3), and CTCs from ascites (n=3) or peripheral blood (n=4). (L) Average frequency of tumor-spheres from Msi2 reporter⁺ and reporter⁻ CTCs (n=3 technical replicates). (M-N) Reporter frequency in REM2-KP^{fl/C} mice treated with vehicle or 500mg/kg Gemcitabine (n=6). Data are represented as mean ± SEM. * P < 0.05, ** P < 0.01, *** P < 0.001, **** P < 0.0001 by Student's t-test or One-way ANOVA. Source Data for all panels are available online.

Msi2+ cells also represented a high proportion of circulating tumor cells, and were more tumorigenic than Msi2- CTCs (**Figure 2.1K-L**). While this suggests that Msi2+ CTCs may pose a greater risk for tumor dissemination²¹, the fact that Msi was not consistently elevated in metastatic patient-samples analyzed leaves the question of Msi's role in metastasis open. The Msi reporter also provided an opportunity to define if it could be used to identify therapy resistance. Exposure to gemcitabine led to preferential survival of Msi2+ cells even at high doses (**Figure 2.1M-N; Figure Supplement 2.3I-K**). These experiments show that Msi2+ cells are a predominant gemcitabine-resistant population, and suggest Msi reporters could serve as a tool to visualize drug resistant cells, and identify therapies to target them.

Because Msi expression rose during progression (**Figure Supplement 2.1F-K, Figure Supplement 2.4A**), and marked therapy resistant cells, we tested if genetic or pharmacologic targeting of Msi could eradicate this 'high risk' population. Deletion of Msi1 led to a 5-fold reduction in tumor volume by MRI (**Figure 2.2A-B, Figure Supplement 2.4B**). Histologically, adenocarcinoma areas comprised 67% of WT-KP^{fl}C but less than 10% of Msi1^{-/-}-KP^{fl}C pancreata; further while Msi1 loss allowed low grade PanINs to form, it largely blocked progression to adenocarcinoma (**Figure 2.2C-F, Figure Supplement 2.4C-D**). Finally, Msi1 deletion improved survival in orthotopic grafts: median survival for WT-KP^{fl}C graft recipients was 28.5 days, and for Msi1^{-/-}-KP^{fl}C grafts was 70.5 days, representing a 2.5-fold increase in survival time and a 23-fold decrease in risk of death (**Figure 2.2G**).

Because both Msi1 and Msi2 are expressed in pancreatic cancer, we also analyzed the impact of deleting Msi2⁹. MRI showed no detectable tumor mass in most Msi2^{-/-}-KP^{fl}C mice (**Figure 2.2H-I; Figure Supplement 2.4E**). Histologically, KP^{fl}C pancreata were mostly replaced by adenocarcinoma, often accompanied by extracapsular invasion into surrounding structures; in contrast, Msi2^{-/-}-KP^{fl}C pancreata contained low-grade PanIN with rare high-grade PanIN and microscopic foci of adenocarcinoma within predominantly normal tissue (**Figure 2.2J-O**). Median survival, tracked in the autochthonous model, was 122 days for Msi2^{-/-}-KP^{fl}C vs. 87 days for WT-KP^{fl}C mice (**Figure 2.2P**), representing a 4-fold decreased risk of death. Collectively, our data show that Msi inhibition significantly improves disease trajectory, leading to an approximate doubling of survival. The fact that the mice ultimately succumbed to disease is likely due to the strong selection for escaper cells in Msi1 and Msi2 single, or double knockout mice (**Figure**

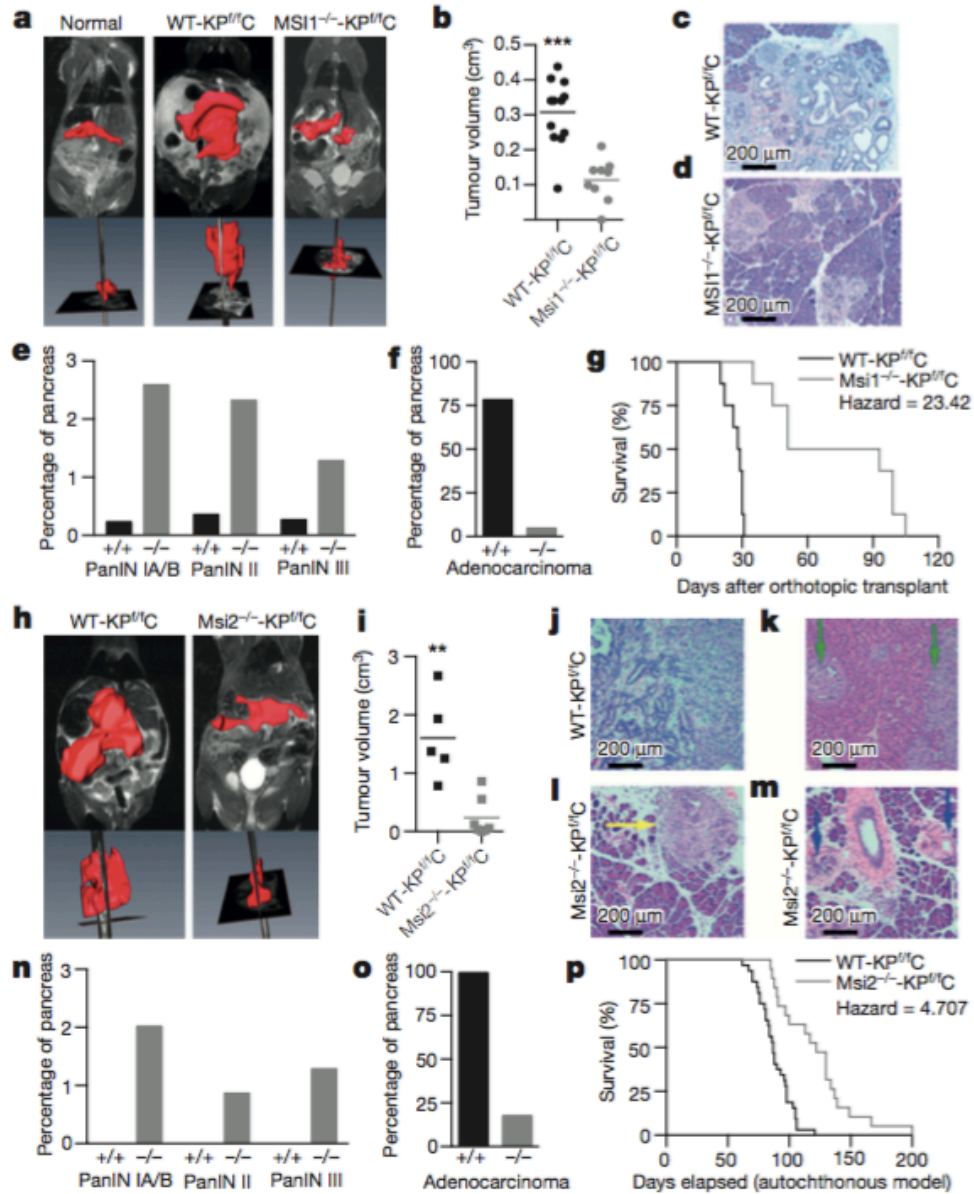


Figure 2.2. Loss of *Msi* impairs tumor initiation and progression in a mouse model of PDAC.

(A) Coronal and sagittal MRI images of normal, WT-KP^{fl/C} and Msi1^{-/-}-KP^{fl/C} mice with 3-dimensional volume rendering of tumor mass (red). (B) Average volumes of isolated WT-KP^{fl/C} (n=13) and Msi1^{-/-}-KP^{fl/C} tumors (n=9). (C-D) Histology and (E-F) quantification of PanIN and/or adenocarcinoma areas in WT-KP^{fl/C} and Msi1^{-/-}-KP^{fl/C} tumors. (G) Survival of mice orthotopically grafted with Msi1^{-/-}-KP^{fl/C} or WT-KP^{fl/C} tumors (n=16). Analysis of Msi2^{-/-}-KP^{fl/C} tumors (H) by MRI and (I) after isolation, WT-KP^{fl/C} (n=5), Msi2^{-/-}-KP^{fl/C} (n=7). (J-M) Histology of WT-KP^{fl/C} and Msi2^{-/-}-KP^{fl/C} pancreatic tumors (40x magnification); (K) Adenocarcinoma, liver invasion (green arrows), (L) adenocarcinoma (yellow arrows), (M) PanINs (blue arrows). (N-O) quantification of PanIN and/or adenocarcinoma areas in WT-KP^{fl/C} and Msi2^{-/-}-KP^{fl/C} tumors (n=6). (P) Survival of autochthonous Msi2^{-/-}-KP^{fl/C} (n=19) or WT-KP^{fl/C} (n=32) mice. Log-rank (Mantel-Cox) survival analysis (p<0.0001). Data represented as mean ± SEM. ** P < 0.01, *** P < 0.001 by Student's t-test. Source Data for all panels are available online.

Supplement 2.5). Additionally, some redundancy between Msi1 and Msi2, as well as a partial gene fragment present in Msi1^{-/-} mice (data not shown) may also exert compensatory activity.

To understand the molecular basis of the effects of Msi loss, we genomically profiled Msi deficient tumor cells (**Figure Supplement 2.6, Figure Supplement 2.7A-D**). Msi loss led to down-regulation of many key genes, including regulators of stem cell function (Wnt7a, Aldh, Lin28), proto-oncogenes (c-Met, Fos, Fyn) and Regenerating (Reg) family genes, linked to gastrointestinal cancers. Among these, analysis of 3'UTRs for Msi binding-sites and RIP-PCR identified BRD4, c-MET and HMGA2 as potential direct targets (**Figure 2.3A, Figure Supplement 2.7E**). We focused on c-MET²², which was diminished in Msi null pancreatic cancer and also bound MSI1 in CLIP-seq experiments (**Figure 2.3B-D, Figure Supplement 2.7F-G**). c-Met could not only be activated molecularly by MSI but also effectively complemented MSI loss (**Figure 2.3E-F; Figure Supplement 2.7H**). While these suggest that c-Met is a direct functional target of Msi, it is almost certainly one of many. In fact, Msi's powerful impact on cancer is probably because of its ability to control a broad range of programs (**Figure Supplement 2.6**). In this context, BRD4 and HMGA2 may be particularly attractive targets^{23,24}, as they could act at an epigenetic level with c-Met to collectively mediate Msi function. Underscoring such a potential convergence of epigenetic and oncogenic pathways, inhibitors of both Brd4 and c-Met effectively targeted gemcitabine-resistant Msi2+ cells (**Figure 2.3G-H**).

To complement the mouse models, we tested the impact of MSI inhibition on primary patient samples, which harbor more complex mutations, and are uniformly drug resistant. Primary pancreatic cancer cells were infected with MSI shRNAs and xenografted (**Figure Supplement 2.8A**). While shMSI cells were equivalently present at time of transplant, their ability to contribute to the tumor mass *in vivo* was reduced by 4.9-6.5 fold (**Figure 2.4A-B, Figure Supplement 2.8B-C**), demonstrating that inhibition of either MSI1 or MSI2 results in marked suppression of primary human pancreatic cancer growth. Interestingly, MSI2 expression was more homogeneous in patients than in mouse models (**Figure Supplement 2.1A-B, Figure Supplement 2.2D-E**). This could be a consequence of selection due to treatment and end-stage disease in patients, or because MSI2 patterns differ between mouse models and human disease. However, regardless of the level of heterogeneity, our loss-of-function studies indicate that the mouse and human disease are both highly dependent on Msi signaling.

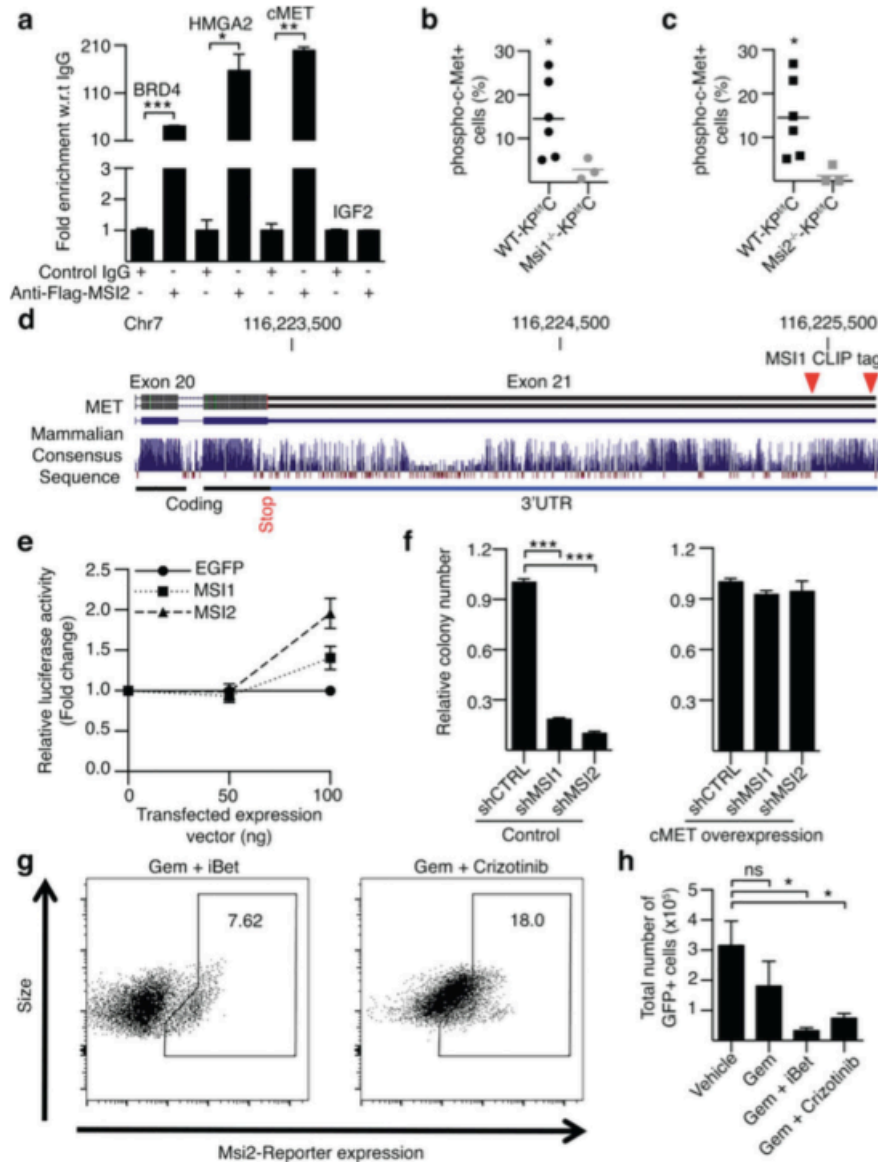


Figure 2.3. Msi controls expression of key oncogenic and epigenetic signals

(A) Msi RIP-PCR for indicated transcripts. (B-C) Frequency of phospho-c-Met⁺ cells in WT-KP^{fl}C, Msi1^{-/-}-KP^{fl}C, and Msi2^{-/-}-KP^{fl}C mice, (b, n=8; c, n=6). (D) Schematic of c-MET exons and 3'UTR. CLIP tags (red triangles) indicate MSI1 binding in 3'UTR. (E) c-MET 3'UTR luciferase reporter activity in the presence or absence of MSI1 or MSI2 (n=3 independent experiments). (F) Colony formation of MSI1 or MSI2 knockdown cells with or without c-MET (n=4 independent experiments). (G-H) FACS analysis of tumors from Gemcitabine-treated REM2-KP^{fl}C mice, in the presence or absence of Crizotinib and iBet762; Vehicle (n=7), Gemcitabine (n=3), Gemcitabine+iBet762 (n=3), Gemcitabine+Crizotinib (n=3). Data represented as mean ± SEM. * P < 0.05, ** P < 0.01, *** P < 0.001 by Student's t-test or One-way ANOVA. ns, not significant. Source Data for all panels are available online.

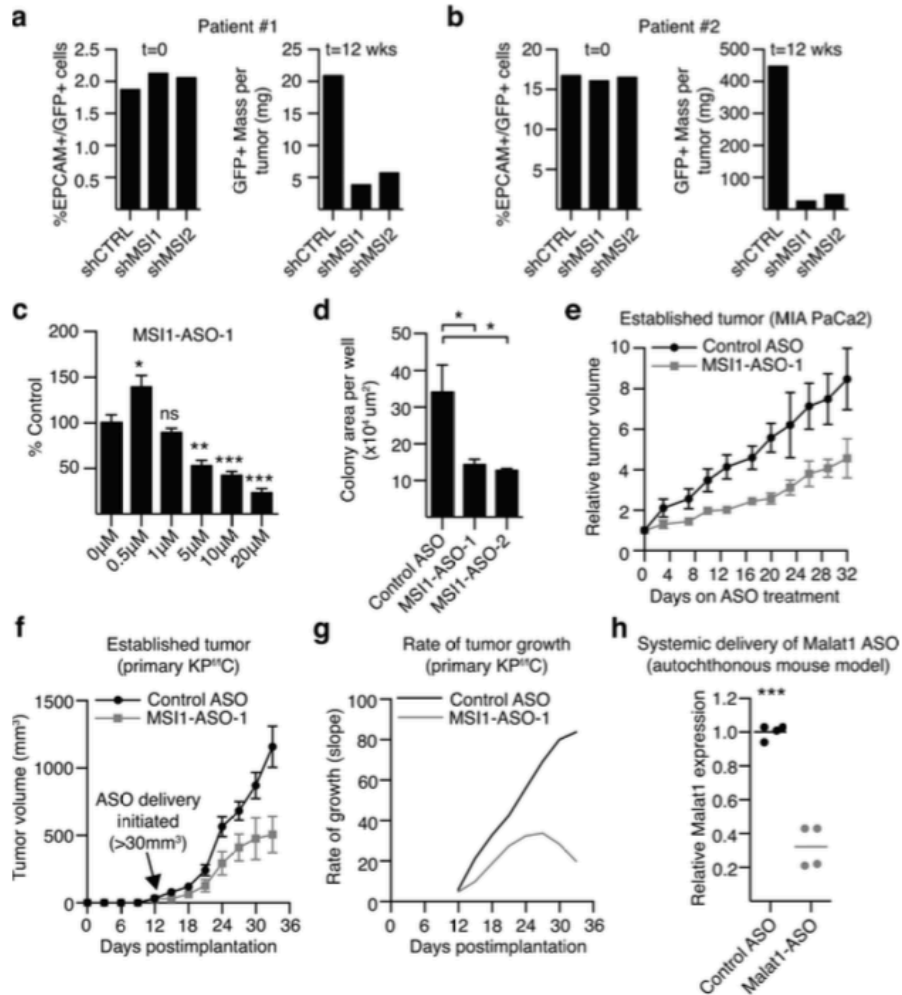


Figure 2.4. Targeting MSI inhibits pancreatic cancer growth in patient-derived xenografts

(A-B) Frequency of GFP+ tumor cells before and after transplantation. (C) MSI1 expression following MS11-ASO free uptake in human pancreatic cancer line (n=3 independent experiments/dose). (D) Colony formation of control or MS11-ASO treated human pancreatic cancer line (n=3 independent experiments). (E) *In vivo* growth of human cell line-derived tumors in control or MS11-ASO treated mice (n=10). (F) Relative tumor volume and (G) rate of growth of KP^{fl}C-derived tumors in control or MS11-ASO treated mice (n=8). (H) Malat1 expression in autochthonous KP^{fl}C tumors following systemic delivery of lead-optimized control or Malat1-ASO (n=6). Data represented as mean ± SEM. * *P* < 0.05, ** *P* < 0.01, *** *P* < 0.001 by One-way ANOVA. ns, not significant. Source Data for all panels are available online.

Given that inhibition of Msi has profound effects on pancreatic cancer progression, we explored its potential as a therapeutic target by developing antisense oligonucleotides (ASOs)^{25,26} specific for MSI1. Because ASO inhibitors are designed based on target RNA sequences, they can be a powerful approach for inhibiting proteins like Msi, considered “undruggable” by traditional approaches²⁷. Of 400 candidate MSI1-ASOs screened, the two most potent markedly reduced colony formation, as well as human cell line and KP^{ff}C derived tumor growth *in vivo* (**Figure 2.4C-G, Figure Supplement 2.8D-E**). The MSI1-ASOs have not yet been lead-optimized, a longer-term process designed to maximize therapeutic level efficacy with systemic delivery. To test if a lead-optimized ASO can penetrate the tumor microenvironment, a lead-optimized ASO against Malat1 was delivered intraperitoneally and was effective in knocking down its target in both stem and non-stem cell fractions (**Figure 2.4H; Figure Supplement 2.8F-J**). These studies provide proof-of-principle that deliverable Msi inhibitors can antagonize pancreatic cancer growth *in vivo*, and suggest that ASOs should be explored further as a new class of therapeutics in this disease.

The Msi reporters we describe here may be broadly applicable for cancer diagnostic and therapeutic studies. Because Msi reporter activity can be visualized through live imaging, these mice can be used to track cancer stem cells *in vivo*, and provide a dynamic view of cancer growth and dissemination within the native microenvironment. The fact that reporter-positive cells are gemcitabine-resistant raises the exciting possibility that this could serve as a platform to visualize resistance *in vivo*. Integration of such reporters during drug development may provide a powerful complement to conventional screens, and allow identification of therapies that can better target therapy-resistant disease. Further, the spatially restricted distribution of Msi+ cells could have important implications for designing strategies to loco-regionally target cells that drive residual disease and relapse.

One of the biggest disappointments in pancreatic cancer therapy has been the failure of targeted agents to make a meaningful impact. Our data demonstrate that Msi function is critical for growth and progression of pancreatic cancer, and Msi therefore represents an attractive therapeutic target. Here we show that cell-penetrating antisense oligonucleotides are able to antagonize Msi and inhibit growth of pancreatic cancer. These findings highlight the value of targeting Msi, and suggest that ASOs²⁷⁻³⁰ and other antagonists should be developed for pancreatic and other cancers marked by high Msi expression. Finally, the rise of Msi in pancreatitis (**Figure Supplement 2.9**) raises the possibility that Msi inhibition could serve

as a strategy to decrease the risk of developing pancreatic cancer. In the long term, blocking Msi signaling could provide a new approach to controlling cancer establishment, progression, and therapy resistance.

METHODS

Mice. REM1 (*Msi1^{eYFP/+}*) and REM2 (*Msi2^{eGFP/+}*) reporter mice were generated by conventional gene targeting (Genoway, France; Fig. 1); all of the reporter mice used in experiments were heterozygous for the corresponding Msi allele. The Msi1^{flf} (*Msi1^{flox/flox}*) mice were generated by conventional gene targeting by inserting LoxP sites around Exons 1-4 (Genoway, France). The Msi2 mutant mouse, B6; CB-*Msi2^{Gt(pU-21T)2Imeg}* (*Msi2^{-/-}*) was established by gene trap mutagenesis as previously described⁹. Dr. Hideyuki Okano provided the Msi1^{-/-} mice as previously described⁷. The LSL-Kras G12D mouse, B6.129S4-*Kras^{tm4Tyj}*/J (Stock No: 008179) and the p53flox/flox mouse, B6.129P2-*Trp53^{tm1Brn}*/J (Stock No: 008462), were purchased from The Jackson Laboratory. Dr. Maïke Sander provided Ptf1a-Cre mice as previously described¹⁴. Dr. Andrew Lowy provided Pdx1-Cre mice as previously described¹³. Mice were bred and maintained in the animal care facilities at the University of California San Diego. All animal experiments were performed according to protocols approved by the University of California San Diego Institutional Animal Care and Use Committee. No sexual dimorphism was noted in all mouse models. Therefore males and females were equally used for experimental purposes and both sexes are represented in all data sets.

Tissue dissociation and cell isolation. (A) Mouse pancreatic tumors were washed in RPMI 1640 (Gibco, Life Technologies) and cut into 2-4 mm pieces immediately following resection. Dissociation into a single cell suspension was performed using the Miltenyi Biotec Mouse Tumor Dissociation Kit (130-096-730). Briefly, tumor pieces were collected into gentleMACS C tubes containing RPMI 1640 dissociation enzymes, and further homogenized using the gentleMACS Dissociator. Samples were incubated for 40 minutes at 37°C under continuous rotation, then passaged through a 70 µm nylon mesh (Corning). Red blood cells were lysed using RBC Lysis Buffer (eBioscience), and the remaining tumor cells were used for FACS analysis and cell sorting. (B) Freshly resected mouse brains were rinsed in PBS, placed in accutase (Life Technologies), and cut into <2 mm pieces. Samples were incubated 15 minutes at 37°C, then passaged through a 70 µm nylon mesh (Corning). Red blood cells were lysed as above prior to FACS analysis and sorting of brain cells. (C) Bone marrow cells were suspended in HBSS (Gibco, Life Technologies) containing 5% FBS and 2 mM EDTA and were prepared for FACS analysis and sorting as previously described³¹.

Analysis and cell sorting were carried out on a FACSAria III machine (Becton Dickinson), and data were analyzed with FlowJo software (Tree Star).

Immunofluorescence and immunohistochemical staining. (A) Human primary pancreatic cancer tissues were fixed in 10% neutral buffered formalin and paraffin embedded at the Moores Cancer Center at UCSD according to standard protocols. 7 μm sections were obtained and deparaffinized in xylene. The UNMC Rapid Autopsy Pancreas (RAP) Program provided a second cohort of human primary pancreatic cancer tissues and matched liver metastases. Pancreatic cancer tissue from KP^{fl}C mice were fixed in 4% paraformaldehyde and paraffin embedded at the UCSD Histology and Immunohistochemistry Core at The Sanford Consortium for Regenerative Medicine according to standard protocols. 5 μm sections were obtained and deparaffinized in xylene. Antigen retrieval was performed for 20-40 minutes in 95-100°C 1x Citrate Buffer, pH 6.0 (eBioscience). Sections were blocked in TBS or PBS containing 0.1% Triton X100 (Sigma-Aldrich), 10% Goat or Donkey Serum (Sigma Aldrich), and 5% bovine serum albumin. (B) Single cell suspensions from mouse pancreatic tumors and brain. Cells isolated by FACS were suspended in DMEM (Gibco, Life Technologies) supplemented with 50% FBS and adhered to slides by centrifugation at 500rpm. 24 hours later, cells were fixed with 4% paraformaldehyde (USB Corporation), washed in PBS containing 0.1% Tween-20 (Sigma-Aldrich), and blocked with PBS containing 0.1% Triton X-100 (Sigma-Aldrich), 10% Goat serum (Invitrogen), and 5% bovine serum albumin (Invitrogen). (C) Single cell suspensions from mouse bone marrow. Cells were allowed to settle onto chambered cover glass (LabTek) coated with poly-L-lysine (Sigma) at 37°C, fixed with 4% paraformaldehyde (USB Corporation), washed in 1x Dako wash buffer (Dako), and blocked with Dako wash buffer containing 10% Goat serum (Invitrogen). All incubations with primary antibodies were carried out overnight at 4 °C. For immunofluorescent staining, incubation with Alexafluor-conjugated secondary antibodies (Molecular Probes) was performed for 1 hour at room temperature. DAPI (Molecular Probes) was used to detect DNA and images were obtained with a Confocal Leica TCS SP5 II (Leica Microsystems) or with a Nikon Eclipse E600 fluorescent microscope. For immunohistochemical staining, endogenous peroxidase was blocked by incubating slides in 3% H₂O₂ for 15 minutes prior to primary antibody. Incubation with Biotinylated secondary antibodies (Vector Laboratories) was performed for 45 minutes at room temperature. ImmPACT NovaRED Kit (Vector

Laboratories) was used per manufacturer's protocol. Sections were counterstained with hematoxylin. The following primary antibodies were used for human tissue sections: rabbit anti-Msi1 (Abcam, ab52865) 4 µg/ml; rabbit anti-Msi2 (Abcam, ab76148) 1 µg/ml; and mouse anti-Keratin (Abcam, ab8068) 1:20. The following primary antibodies were used to stain mouse tissues: rabbit anti-ALDH1 (Abcam, ab24343) 1:200; rabbit anti-cMet (Abcam, ab5662) 1:250; chicken anti-GFP (Abcam, ab13970) 1:250 (for pancreatic tumors and brain) or 1:200 (for bone marrow); rabbit anti-Msi2 (Abcam, ab76148) 1:500 (for pancreatic tumors and brain) or 1:200 (for bone marrow); rat anti-Ki67 (eBioscience, 14-5698) 1:1000; rat anti-Msi1 (eBioscience, 14-9896-82) 1:500; mouse anti-Keratin (Abcam, ab8068) 1:10; and biotinylated DBA (Vector Laboratories, B-1035) 1:1000.

Pancreatic tumorsphere formation assay. (A) Pancreatic tumorsphere formation assays were performed on freshly isolated mouse pancreatic tumor cells or circulating tumor cells from peripheral blood modified from Rovira, et al³². Briefly, pancreatic tumors from 10-13 week old REM1-KP^{ff}C or REM2-KP^{ff}C mice were dissociated and FACS sorted for YFP+ and YFP- or EpCAM+/GFP+ and EpCAM+/GFP- cells, respectively. 100-500 cells were suspended in 100 µl DMEM F-12 (Gibco, Life Technologies) containing 1x B-27 supplement (Gibco, Life Technologies), 3% FBS, 100mM B-mercaptoethanol (Gibco, Life Technologies), 1x non-essential amino acids (Gibco, Life Technologies), 1x N2 supplement (Gibco, Life Technologies), 20 ng/ml EGF (Gibco, Life Technologies), 20 ng/ml FGF₂ (Gibco, Life Technologies), and 10 ng/ml ESGRO mLIF (Millipore). Culture media for circulating tumor cells also contained 20 ng/ml mHGF (R&D Systems). Cells in media were plated in 96-well ultra-low adhesion culture plates (Costar) and incubated at 37°C for 7 days. Sphere images were obtained with a Nikon80i. Sphere size was measured using ImageJ 1.47v software.

Lentiviral constructs and production. Short hairpin RNA (shRNA) constructs were designed and cloned into plenti-hU6BX vector with a GFP tag by Cellogenetics. The target sequences are 5'-CCCAGATAGCCTTAGAGACTAT-3' for MSI1, 5'-CCCAGATAGCCTTAGAGACTAT-3' for MSI2 and 5'-CTGTGCCAGAGTCCTTCGATAG-3' for the control scrambled sequence. Additional (shRNA) target sequences were cloned into a plenty-FG12 vector with a Tomato Red tag. These target sequences are 5'-

ATGAGTTAGATTCCAAGACGAT-3' for MSI2 and 5'-AGGATTCCAATTCAGCGGGAGC-3' for control scrambled sequence. Virus was produced in 293T cells transfected with plenti-shRNA constructs along with pRSV/REV, pMDLg/pRRE, and pHCMVG constructs. Viral supernatants were collected for three days followed by ultracentrifugal concentration at 50,000xg for 2h.

Agarose colony formation assays. MIA PaCa-2, Panc-1, Capan-2, and HPAC human pancreatic cancer cell lines were purchased from ATCC, and cultured in the appropriate growth media as recommended by ATCC. ASPC1, FG, and AA0779E human pancreatic cancer cell lines were provided by Dr. Andrew Lowy, and grown in DMEM containing 10% FBS, 1x Glutamax, and 1x PS (pen/strep). Human pancreatic cancer cell lines were infected with GFP-tagged or TomatoRed-tagged lentiviral particles containing shRNAs for MSI1, MSI2, and a scrambled control. Positively infected cells were sorted 72 hours after transduction. For colony assays, 24-well plates were first coated with 0.6% agarose in DMEM without supplements. Cells were plated at a density of 2000 cells per well in 0.3% agarose containing DMEM, 10% FBS, NEAA, PS, and Glutamax. Growth medium was placed over the solidified agarose layers and was supplemented every three days. Colonies were counted 14 days after plating.

MRI. Magnetic resonance imaging was used to determine the pancreatic volumes of the mice *in vivo*. Mice were anesthetized using 1.5% isoflurane and imaged in a 7.0 Tesla small animal scanner (Bruker-Biospin, Ettlingen, Germany). Contiguous coronal slices were acquired using a multi-slice, RARE sequence: repetition time/echo time = 4826 ms/33 ms, Field of View = 6x3 cm, and Matrix = 126 x128 with up to 44 slices with a thickness of 0.5mm. Segmentation and volume rendering were performed using Amira software (FEI Visualization Sciences Group, Burlington, MA).

Histological analysis/Quantification of PanIN and PDAC. Mouse tumors from 4.5-13 week old *Msi1^{-/-}-KP^{fl/c}*, *Msi2^{-/-}-KP^{fl/c}* mice, and WT-KP^{fl/c} littermates were isolated, fixed in 4% paraformaldehyde, and paraffin embedded according to standard protocols. 5 μ m sections were obtained for hematoxylin and eosin and periodic acid-Schiff/Alcian Blue staining. To quantify tumor areas, each slide was digitally scanned with

an Aperio slide scanner. Imagescope software was used to measure PDAC area, PanIN area, and normal pancreas area.

Gene expression microarray, RNA-Seq, and data analysis. (A) WT-KP^{fl/c} or Msi1^{-/-}-KP^{fl/c} mice were euthanized at 11 weeks of age. Tumors were harvested and total cellular RNAs were purified, labeled and hybridized onto Affymetrix GeneChip Mouse Genome 430 2.0 Arrays and raw hybridization data were collected (VA/VMRF Microarray & NGS Core, UCSD). Expression level data were extracted using *R* package *gcrma*¹⁴, and normalized using a multiple-loess algorithm as previously described^{33,34}. Probes whose expression levels exceed a threshold value in at least one sample were considered detected. The threshold value is found by inspection from the distribution plots of log₂ expression levels. Detected probes were sorted according to their *q*-value, which is the smallest false discovery rate (FDR) at which a probe is called significant^{13,35}. An FDR value of α is the expected fraction of false positives among all genes with $q \leq \alpha$. FDR was evaluated using Significance Analysis of Microarrays (SAM) and its implementation in the official statistical package *samr*^{36,37}. The samples were treated as "Two class paired" according to the date of RNA extraction. No genes reached a significance level of $\alpha=0.1$. A heat map of selected genes was created using in-house software. (B) MIA PaCa2 cells were infected with GFP-tagged or TomatoRed-tagged lentiviral particles containing shRNAs for MSI1, MSI2, MSI1+MSI2, and a scrambled control. At 72 hours post-infection, positively infected cells were sorted and total cellular RNAs were isolated using a Qiagen RNeasy mini kit. RNA-seq fastq files were processed into transcript-level summaries using *kallisto*, an ultrafast pseudo-alignment algorithm with expectation maximization. Transcript-level summaries were processed into gene-level summaries by adding all transcript counts from the same gene. Gene counts were normalized across samples using DESeq normalization³⁸, and the gene list was filtered based on mean abundance, which left 13,684 "detected" genes for further analysis. Differential expression was assessed with an *R* package *limma*³⁹ applied to log₂-transformed counts. Statistical significance of each test was expressed in terms of posterior error probability p^E using the *limma* function *eBayes*^{40,41}. Posterior error probability, also called local false discovery rate, is the probability that a particular gene is not differentially expressed, given the prior probabilities of the model. The list of genes sorted by p^E (in ascending order) were analyzed for over-represented biological processes and pathways using a non-

parametric version of Gene Set Enrichment Analysis^{42,43}. Denoting $p^E(1)$ the probability that a gene is not differentially expressed in the Msi1 knockdown and $p^E(2)$ the probability that a gene is not differentially expressed in the Msi2 knockdown, the probability that a gene is differentially expressed in both samples was estimated as $[1-p^E(1)][1-p^E(2)]$. By the same token, the probability that a gene is differentially expressed in the Msi1 knockdown but not in the Msi2 knockdown was estimated as $[1-p^E(1)]p^E(2)$; likewise with indices 1 and 2 switched.

RT-PCR analysis. RNA was isolated using RNeasy Micro and Mini kits (Qiagen) and converted to cDNA using Superscript III (Invitrogen). Quantitative real-time PCR was performed using an iCycler (BioRad) by mixing cDNAs, iQ SYBR Green Supermix (BioRad) and gene specific primers. Primer sequences are available upon request. All real time data was normalized to actin or Gapdh.

***In vivo* transplantation assay and analysis.** *In vivo* we focused on the tumorigenic potential of Msi2 reporter cells since Msi1⁺ cells were unable to form tumors in small numbers (100, 1000), possibly because they are less tumorigenic or more quiescent (data not shown). Pancreatic tumors from 10-13 week-old REM2-KP^{fl}C mice were dissociated and FACS sorted for EpCAM⁺/reporter⁺ (GFP⁺) and EpCAM⁺/reporter⁻ (GFP⁻) cells. 100, 500, 1000, or 5000 GFP⁺ and GFP⁻ cells were suspended in DMEM (Gibco, Life Technologies) containing 10% FBS, then mixed 1:1 with matrigel (BD Biosciences). Cells were injected subcutaneously into the left or right flank or orthotopically into the tail of the pancreas of 5-8 week-old NOD/SCID *Il2ry*^{-/-} (NSG) recipient mice. Subcutaneous tumor dimensions were measured with calipers every 7 days for 8-12 weeks. Tumor volume was calculated using the standard modified ellipsoid formula, $\frac{1}{2}(\text{Length} \times \text{Width}^2)$. At endpoint, flank tumors were removed and dissociated as described above. Tumor cells were stained with anti-mouse EpCAM antibody (eBiosciences) then analyzed for GFP expression by flow cytometry on a FACSAria III machine (Becton Dickinson), and data analyzed with FlowJo software (Tree Star). Subcutaneous tumors did not exceed 2cm in diameter as per the University of California San Diego Institutional Animal Care and Use Committee Policy on Experimental Neoplasia.

Patient-derived xenograft infection and *in vivo* transplant. Patient samples were obtained from Moores UCSD Cancer Center from Institutional Review Board-approved protocols with written informed consent in accordance with the Declaration of Helsinki. All knockdown experiments were conducted with the construct shCTRL (scrambled), shMSI1, and shMSI2. Briefly, freshly dissociated (GentleMACS Dissociator, Miltenyi) patient-derived xenograft cells were plated in RPMI-1640 with 20% FBS, 1x glutamax, 1x non-essential amino acids, 100 IU/ml penicillin, and 100 µg/ml streptomycin. Cells were transduced with GFP-tagged lentiviral shRNAs, and FACS analysis was performed after 24 hours on a portion of the cells; the remaining cells were transplanted into the flank of 5-8 week-old NSG recipient mice. Tumor size was monitored by caliper measurement, and mice were euthanized when tumors reached 2 cm in diameter. Subcutaneous tumors did not exceed 2cm in diameter as per the University of California San Diego Institutional Animal Care and Use Committee Policy on Experimental Neoplasia. Tumors were harvested, dissociated, and analyzed by FACS.

RIP-qPCR. HEK 293T cells were transfected with MSCV-Flag-Msi2-IRES-tNGFR and lysed 72 hours post-transfection. RNA-immunoprecipitation was carried out with anti-Flag antibody (Sigma-Aldrich) or control IgG using the EZ-Magna RIP kit as per the manufacturers' protocol (Millipore). Immunoprecipitated RNA was converted to cDNA and analyzed for the expression of indicated genes by real-time PCR.

CLIP SEQ. Briefly, MIA PaCa-2 cells were UV cross-linked with a Stratalinker (Model 2400, Stratagene). Cells were lysed and supernatant added to Dynabeads conjugated to MSI1 antibody (clone 14H1, eBiosciences). CLIP library preparation and sequencing, as well as sample preparation and sequencing, were performed as previously described⁴⁴. 73,329 unique tags were obtained from MSI1-bound targets including tags with the binding core sequence "rUAG" site, as reported previously⁴⁵.

MET rescue Assay. Using gateway technology, pENTR-Human c-MET was engineered into the pLENTI-PGK-PURO DEST vector. MIA PaCa-2 cells were infected with pLENTI PGK-MET or pLENTI PGK-EMPTY virus. Following the establishment of the stable cell line over expressing c-MET; lentiviruses containing

shRNAs for Control, MSI1, or MSI2 were delivered. Cells were sorted for GFP expression and plated into a soft agar colony assay. Colonies were counted 14 days after plating.

in vivo and in vitro drug therapy. 9-10 week old REM2-KP^{fl/c} mice were treated with Gemcitabine alone or in combination with Crizotinib or iBet762 for 6 days. On day 6, tumors were removed, dissociated (as described above), counted for total cellular content, stained with anti-mouse EpCAM antibody and analyzed for reporter expression by flow cytometry. Gemcitabine (Sigma, G6423) was resuspended in H₂O at 20mg/ml and delivered at 200 mg/kg or 500 mg/kg by IP injection twice over 6 days (on day 0 and 3). Crizotinib (Selleckchem PF-02341066) was resuspended in DMSO at 50 mg/ml, diluted 1:10 in H₂O, and delivered at 100 mg/kg/day for 6 days by oral gavage. iBet762 (Selleckchem S7189) was resuspended in DMSO at 50 mg/ml, diluted 1:10 in H₂O, and delivered at 30 mg/kg/day by IP injection for 6 days. For *in vitro* drug assay, low passage Msi2 Reporter KP^{fl/c} cells loaded with 2 μ M Dil and imaged continuously for up to 48 hours while receiving 10 μ M gemcitabine treatment.

ASO inhibitors. To identify human Msi ASO inhibitors, rapid throughput screens were performed to identify effective ASOs as previously described^{46,47}. ASOs were tested in full dose-response experiments to determine potency. The top 2 most effective ASOs were chosen to test free uptake and verify target knockdown in MIA PaCa-2 cells. The sequences of Gen 2.5 MSI1 ASOs used for the study were ASO-1, 5'- ATATGATACAGGACGG -3', and ASO-2, 5'- TTACATATGATACAGG -3', with underlined letters indicating cEt modified bases. The sequence of Gen 2.5 scrambled (5'- GGCTACTACGCCGTCA -3') ASO with no perfect match for any known transcript was included as a negative control. (A) *In Vitro*: MIA PaCa-2 cells were treated with 0.5-20 μ M of antisense compound for 24 hours, after which cells were lysed and RNA isolated. Gene expression was assessed with Taqman probes for MSI1 and MSI2. Actin was used to normalize all real time data. For functional testing, MIA PaCa-2 cells were plated in the colony assay as previously described. The growth medium was supplemented with 0.25-10 μ M of ASO. Cells were supplemented weekly with fresh antisense compound. Colonies were counted 21 days after the first ASO treatment. (B) *In Vivo*: 5x10⁵ MIA PaCa-2 cells were transplanted into the flank of 5-8 week-old NSG recipient mice. Once tumors were measurable at 2 weeks post transplant, 50 μ g of either Control ASO or

MSI1 ASO-1 in PBS was administered intratumorally. ASOs were delivered daily over the course of the study. Tumor measurements were recorded every 3 days. Subcutaneous tumors did not exceed 2 cm in diameter as per the University of California San Diego Institutional Animal Care and Use Committee Policy on Experimental Neoplasia. (C) *In Vivo*: In 8 week-old WT-KP^{ff}/C mice, either Control ASO or Malat1 ASO was delivered by intraperitoneal injection at a dose of 50 mg/kg. ASOs were delivered daily for 14 days. On day 15, mice were sacrificed and the tumor removed. Tumors were harvested and used as follows: (1) flash frozen for RNA isolation and qPCR analysis for Malat1; (2) placed into 4% paraformaldehyde for paraffin embedding, sectioning, and in situ hybridization analysis for Malat1; and (3) dissociated and sorted for RNA isolation to compare Malat1 expression in EpCAM⁺/ALDH⁺ and EpCAM⁺/ALDH⁻ populations.

Tumor imaging. 11-12 week old REM-KP^{ff}/C mice were anesthetized by intraperitoneal injection of ketamine and xylazine (100/20 mg/kg). In order to visualize blood vessels and nuclei, mice were injected retro-orbitally with AlexaFluor 647 anti-mouse CD144 (VE-cadherin) antibody and Hoechst 33342 immediately following anesthesia induction. Pancreatic tumors were removed and placed in HBSS containing 5% FBS and 2mM EDTA. 80-100 micron images in 1024 x 1024 format were acquired with an HCX APO L20x objective on an upright Leica SP5 confocal system using Leica LAS AF 1.8.2 software. Videos were generated using Volocity 3D Image Analysis Software and compressed using Microsoft Video 1 compression.

Circulating tumor cell analysis. 10-13 week old REM2-KP^{ff}/C mice were anesthetized and approximately 100 μ l of peripheral blood and ascites was collected in PBS containing 5mM EDTA and 2% Dextran. Samples were incubated at 37°C and red blood cells were lysed using RBC lysis buffer (eBiosciences). Remaining cells were stained with anti-mouse EpCAM-PE (eBiosciences) and anti-mouse CD45-PE-Cy7 (eBiosciences) antibodies. Analysis was carried out on a FACSAria III machine (Becton Dickinson) and data analyzed with FlowJo software (Tree Star).

In situ hybridization. Msi1 and Msi2 mRNA were detected in tumor samples using RNAscope, an RNA *in situ* hybridization method that permits signal amplification and background suppression. Human tissue was

drop-fixed in neutral-buffered formalin and processed and embedded in paraffin. 4 μ m tissue sections were collected in RNase-free manner and dried at room temperature overnight. Staining was initiated by baking the slides for 32 min at 60 degrees, then they were deparaffinized, subjected to antigen retrieval and treated with protease (two sequential incubations at 65 and 75 degrees for 12 min each) to enhance probe penetration, as described by the manufacturer (Advanced Cell Diagnostics). Msi1-specific and Msi2-specific RNA target probe sets were generated and supplied by the manufacturer (Advanced Cell Diagnostics). Sequential amplification steps result in a large number of horseradish peroxidase molecules per mRNA. The probe was visualized by incubation with 3,3' diaminobenzidine (DAB). Sections were counterstained with hematoxylin. All steps of this procedure were performed using a Ventana Discovery Ultra (Roche). Slides were analyzed by conventional light microscopy.

Msi1^{-/-}KP^{fl/c} Survival Curve. For the Msi1^{-/-}KP^{fl/c} mice, tracking survival was complicated by the incidence of hydrocephaly observed in the knockout mice reported previously⁷. To avoid confounding the data with deaths due to non-tumorigenic events, we carried out orthotopic transplants. Briefly, Msi1^{-/-}KP^{fl/c} and WT KP^{fl/c} mice at 8 weeks of age were sacrificed and tumors collected. Tumors were divided into four equal chunks, and then surgically transplanted into the pancreas of 8-week-old NSG mice. After surgery, the orthotopically transplanted mice were tracked for survival.

Luciferase assay. A Lightswitch Luciferase Assay System (Active Motif, Inc) was used for the assessment of MSI1 regulation of cMET. Briefly, 1x10⁴ MIA PaCa-2 cells were plated into 96 well plates and cultured for 24 hours. 50 ng of cMET 3'UTR GoClone (S811259, Active Motif, Inc) plasmid DNA and increasing concentrations (0 ng, 50 ng, and 100 ng) of either PGK-GFP or PGK-MSI1 plasmid vector DNA were co-transfected into MIA PaCa-2 cells. After 24 hours, cells were lysed using the Lightswitch Luciferase Assay Reagent (LS100, Active Motif, Inc) and luciferase activity measured using a plate scanner (Infinite 200, Tecan).

Caerulein-induced pancreatitis. 4-week-old C57BL/6 mice received 8 injections of 50 μ g/kg caerulein (Sigma-Aldrich) or PBS hourly each day for two consecutive days (for a total of 16 injections). Pancreata

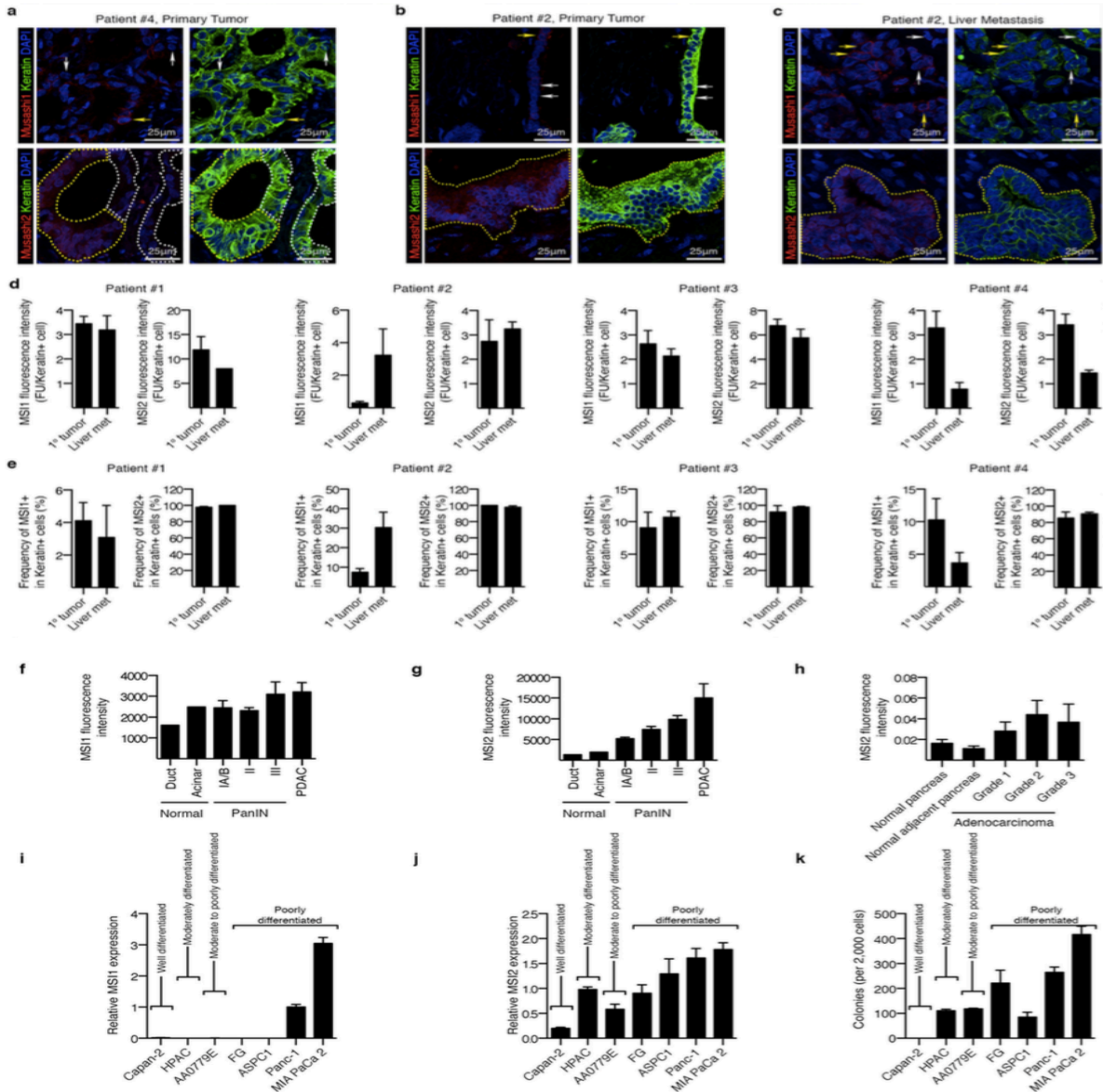
were isolated 2 days after the last injection, fixed in 4% paraformaldehyde and paraffin embedded according to standard protocols. 7 μ m sections were obtained, deparaffinized in xylene, and stained as described above.

Statistical analysis. Statistical analyses were carried out using GraphPad Prism software version 6.0d (GraphPad Software Inc.). Sample sizes were determined based on the variability of pancreatic tumor models used. Tumor bearing animals within each group were randomly assigned to treatment groups. Data are shown as the mean \pm SEM. Two-tailed unpaired Student's *t*-tests with Welch's correction or One-way analysis of variance (ANOVA) for multiple comparisons when appropriate were used to determine statistical significance (* P <0.05, ** P <0.01, *** P <0.001, **** P <0.0001).

Accession codes. Microarray and RNA-seq data reported here have been deposited in the Gene Expression Omnibus (accession GSE73312 and GSE75797).

Figure Supplement 2.1. The Musashi genes *MSI1* and *MSI2* are expressed in human PDAC.

(A, top row) Representative images of a primary patient pancreatic adenocarcinoma sample stained with anti-keratin (green), DAPI (blue), and anti-MSI1 (red) antibodies. White arrows indicate MSI1 negative cells; yellow arrow indicates a MSI1 positive cell. **(A, bottom row)** Representative images of a primary patient pancreatic adenocarcinoma sample stained with anti-keratin (green), DAPI (blue), and anti-MSI2 (red) antibodies. White dotted regions indicate MSI2 negative cells while yellow dotted regions indicate MSI2 positive cells. **(B, top row)** Representative images of a primary patient pancreatic adenocarcinoma sample stained with anti-keratin (green), DAPI (blue), and anti-MSI1 (red) antibodies. White arrows indicate MSI1 negative cells; yellow arrow indicates a MSI1 positive cell. **(B, bottom row)** Representative images of a primary patient pancreatic adenocarcinoma sample stained with anti-keratin (green), DAPI (blue), and anti-MSI2 (red) antibodies. Yellow dotted region indicates MSI2 positive cells. **(C, top row)** Representative images of a matched liver metastasis from a patient with pancreatic adenocarcinoma stained with anti-keratin (green), DAPI (blue), and anti-MSI1 (red) antibodies. White arrows indicate MSI1 negative cells; yellow arrows indicate MSI1 positive cells. **(C, bottom row)** Representative images of a matched liver metastasis from a patient with pancreatic adenocarcinoma stained with anti-keratin (green), DAPI (blue), and anti-MSI2 (red) antibodies. Yellow dotted region indicates MSI2 positive cells. **(D)** Quantification of MSI1 and MSI2 expression in four patients comparing primary pancreatic adenocarcinoma to the patient matched liver metastasis; 4 images analyzed per patient. **(E)** Quantification of the frequency of MSI1 and MSI2 positive cells in four patients comparing primary pancreatic adenocarcinoma to the patient matched liver metastasis; 4 images analyzed per patient. **(F)** MSI1 and **(G)** MSI2 expression in normal pancreas (n=1), PanIN (n=9), and pancreatic adenocarcinoma samples (n=9). **(H)** Quantification of MSI2 expression from a human tissue array comparing Grade 1 (well-differentiated, n=9), Grade 2 (moderately differentiated, n=12), and Grade 3 (poorly differentiated, n=16) adenocarcinoma relative to normal pancreas (n=14) and normal adjacent pancreas (n=16). **(I)** *MSI1* and **(J)** *MSI2* expression in well-differentiated, moderately differentiated, and poorly differentiated human pancreatic cancer cell lines (n=3 independent experiments). **(K)** Colony formation of well-differentiated, moderately differentiated, and poorly differentiated human pancreatic cancer cell lines (n=3 independent experiments). Data are represented as mean \pm SEM. Total Magnification 200x A-B. Source Data for all panels are available online.



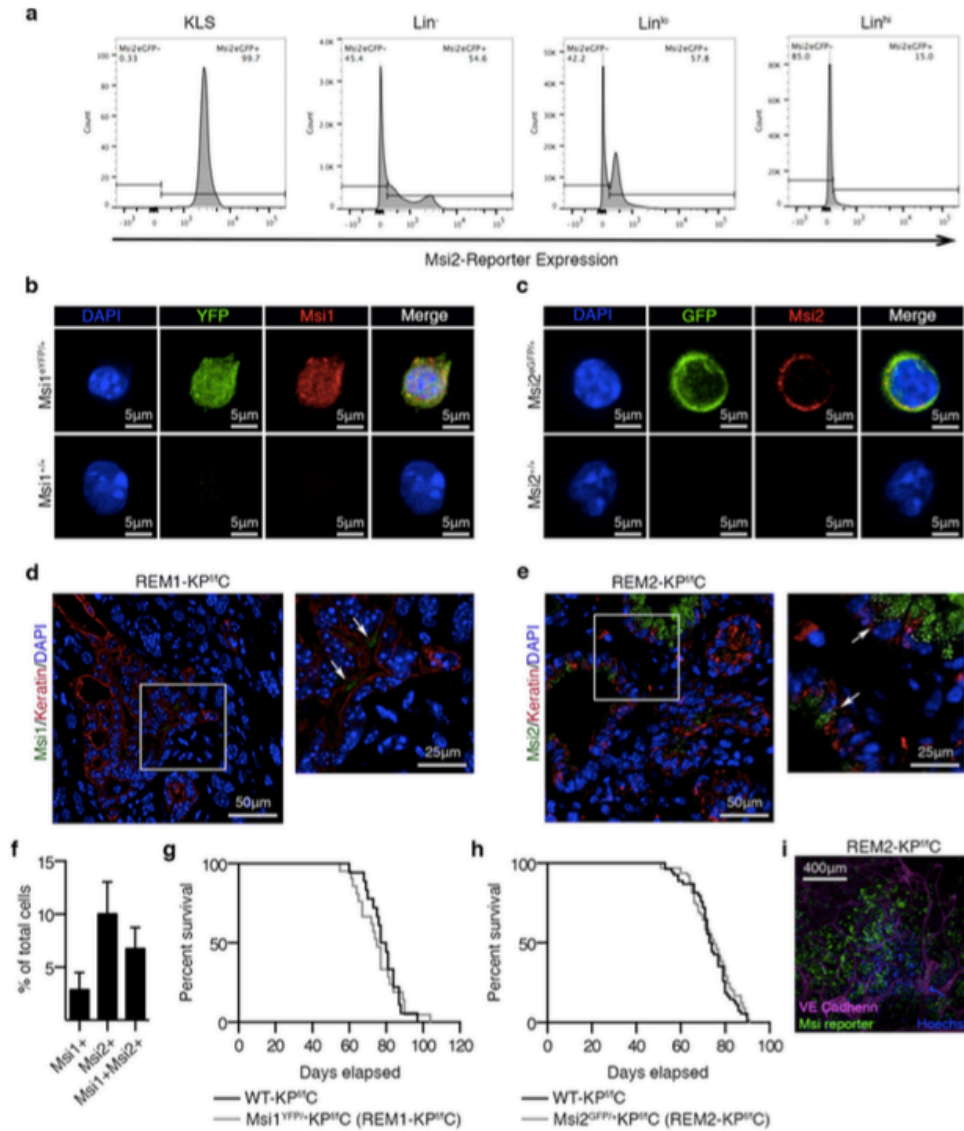


Figure Supplement 2.2. Validation of Msi1 and Msi2 reporter mice.

(A) FACS analysis of Msi2 reporter expression in hematopoietic stem cells, progenitors and lineage-positive differentiated cells. (B) Representative image of Msi1 expression in FACS sorted YFP⁺ neuronal cells; YFP (green), Msi1 (red), and DAPI (blue). (C) Representative image of Msi2 expression in FACS sorted GFP⁺ hematopoietic cells; GFP (green), Msi1 (red), and DAPI (blue). (D-E) Msi-expression in keratin⁺ cells. (D) Msi1-YFP reporter (green, white arrows) and keratin (red) staining was performed on tissue sections of REM1-KP^{fl/c} mice; (E) Msi2-GFP reporter (green, white arrows) and keratin (red) staining was performed on tissue sections of REM2-KP^{fl/c} mice. DAPI staining is shown in blue. Rare cells (<5%) were found to be keratin-negative (possibly mesenchymal population). (F) Immunofluorescence analysis of Msi1 and Msi2 expression overlap in isolated EpCAM⁺ KP^{fl/c} cells (n=3, 1000 total cells analyzed from 3 independent experiments). Data are represented as mean ± SEM. (G) Survival of Msi reporter-KP^{fl/c} and WT-KP^{fl/c} mice. Survival curves of (g) Msi1^{YFP/+}-KP^{fl/c} (REM1-KP^{fl/c}, n=21) or WT-KP^{fl/c} (n=18) mice, and (h) Msi2^{GFP/+}-KP^{fl/c} (REM2-KP^{fl/c}, n=65) or WT-KP^{fl/c} (n=54) mice. (i) Live image of Msi2 reporter cells in REM2-KP^{fl/c} tumor; VE-cadherin (magenta), Hoescht (blue), Msi reporter (green). See also Figure 1c-d. Source Data for all panels are available online.

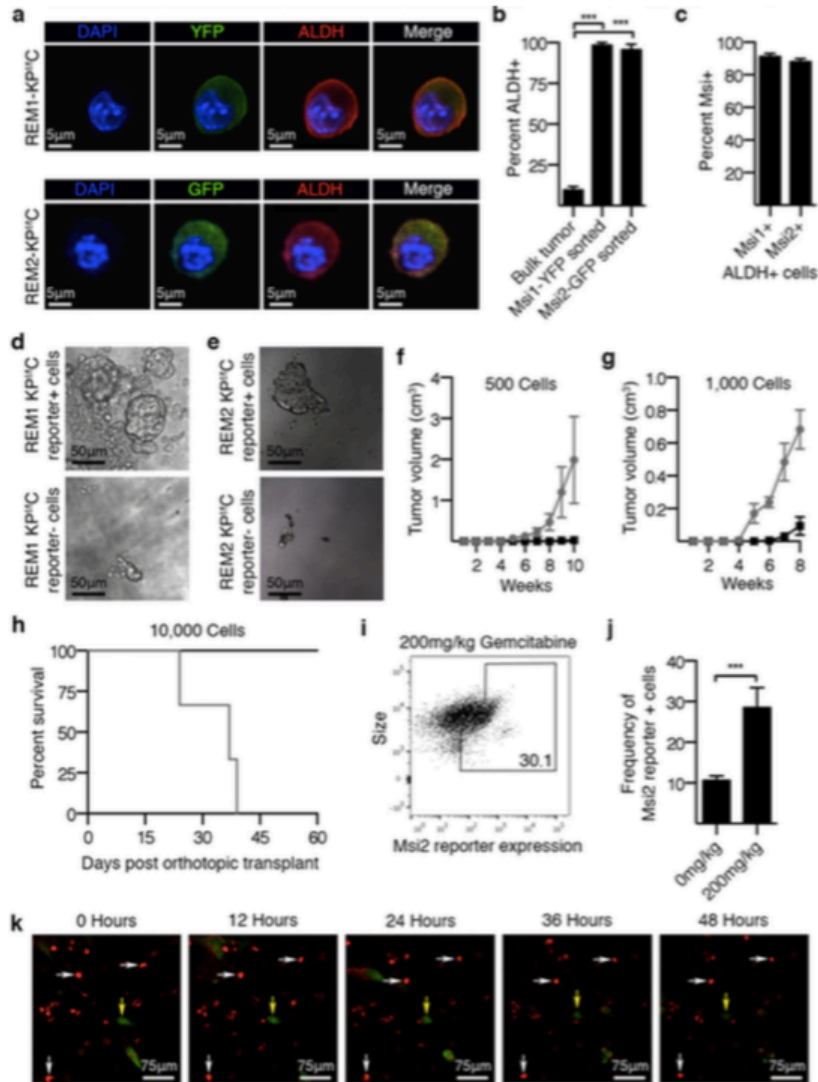


Figure Supplement 2.3. Analysis of stem cell traits in *Msi1* and *Msi2* reporter+ *KP^{ffC}* populations. (A) ALDH expression in reporter positive tumor cells sorted from REM1-*KP^{ffC}* (top row) and REM2-*KP^{ffC}* (bottom row) mice; ALDH1 (red), DAPI (blue) and GFP or YFP (green). (B) Average ALDH expression in bulk or *Msi1* and *Msi2* reporter positive tumor cells ($n=3$ each; 90 total cells analyzed from 3 REM1-*KP^{ffC}* and 150 total cells analyzed from 3 REM2-*KP^{ffC}*). (C) Average *Msi* expression in ALDH+ cells from REM1-*KP^{ffC}* and REM2-*KP^{ffC}* tumors ($n=3$ independent experiments for each genotype). (D-E) Representative images of spheres formed from (D) *Msi1* and (E) *Msi2* reporter+ and reporter- tumor cells. See also Figure 1g-h. (F-G) *In vivo* tumor growth of *Msi2* reporter+ or *Msi* reporter- *KP^{ffC}* cells at (F) 500 or (G) 1000 cells ($n=16$). See also Figure 1i. (H) Survival of mice orthotopically transplanted with 10,000 *Msi2* reporter+ and reporter- *KP^{ffC}* tumor cells ($n=6$). See also Figure 1j. Log-rank (Mantel-Cox) survival analysis ($p<0.05$). (I-J) Reporter frequency in REM2-*KP^{ffC}* mice treated with vehicle or 200mg/kg Gemcitabine ($n=3$ each). See also Figure 1m-n for high dose (500mg/kg) Gemcitabine. Data are represented as mean \pm SEM. *** $P < 0.001$ by Student's t-test or One-way ANOVA. (K) *Msi2* reporter-negative *KP^{ffC}* cells do not turn on *Msi2* expression following *in vitro* gemcitabine treatment, suggesting that *Msi*-reporter+ cells are differentially resistant to Gemcitabine. Low passage *Msi2* reporter *KP^{ffC}* cells loaded with Dil were live-imaged continuously for up to 48 hours. Representative series of images from 10 μ M gemcitabine treatment. Reporter-negative cells (red); GFP reporter-positive cells (green); tracking of *Msi2* reporter-negative cells (white arrows); tracking of *Msi2* reporter-positive cells (yellow arrows) ($n=3$ independent experiments). Source Data for all panels are available online.

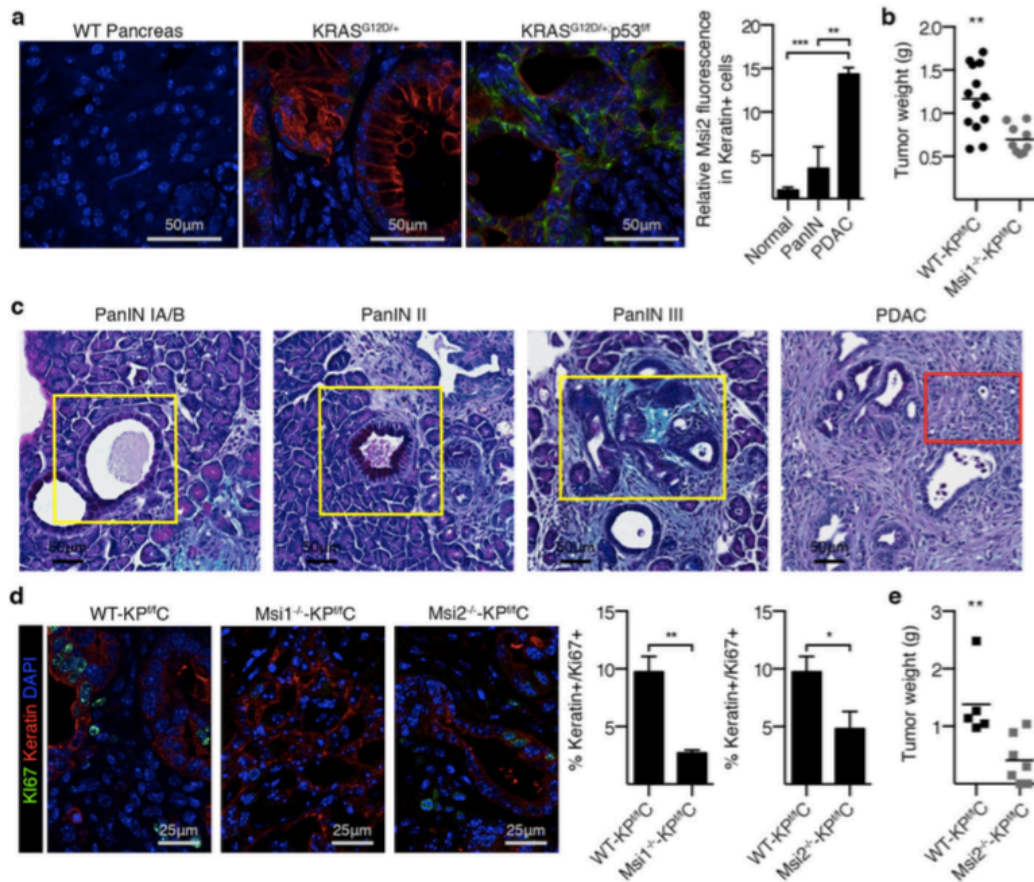


Figure Supplement 2.4. Analysis of tumors from Msi null KP^{ff}C mice

(A) Msi2 (green) and Keratin (red) immunofluorescent staining was performed on tissue sections from WT pancreas (Normal, n=3 samples), KRAS^{G12D/+};Ptf1a^{Cre/+} (PanIN, n=2 samples), and KRAS^{G12D/+};p53^{ff};Ptf1a^{Cre/+} (PDAC, n=3 samples) mice with quantification of Msi2 fluorescence in Keratin positive cells. (B) Average weights of WT-KP^{ff}C (n=13) and Msi1^{-/-}-KP^{ff}C tumors (n=9). See also Figure 2h-i. for tumor volume analysis (C) PAS and Alcian Blue stained sections of pancreata isolated from WT-KP^{ff}C represent areas used to identify the stages of PanINs (yellow boxes) and adenocarcinoma (red box). (D) Tumors from 11-13 week old WT-KP^{ff}C (n=6), Msi1^{-/-}-KP^{ff}C (n=3), and Msi2^{-/-}-KP^{ff}C (n=3) mice were stained and quantified for percent of Keratin+ tumor cells (red) expressing Ki67 (green); DAPI staining is shown in blue. (E) Average weights of WT-KP^{ff}C (n=5) and Msi2^{-/-}-KP^{ff}C tumors (n=7). See also Figure 2h-l for tumor volume analysis. Data are represented as mean ± SEM. * P < 0.05, ** P < 0.01, *** P < 0.001 by Student's t-test or One-way ANOVA. Source Data for all panels are available online.

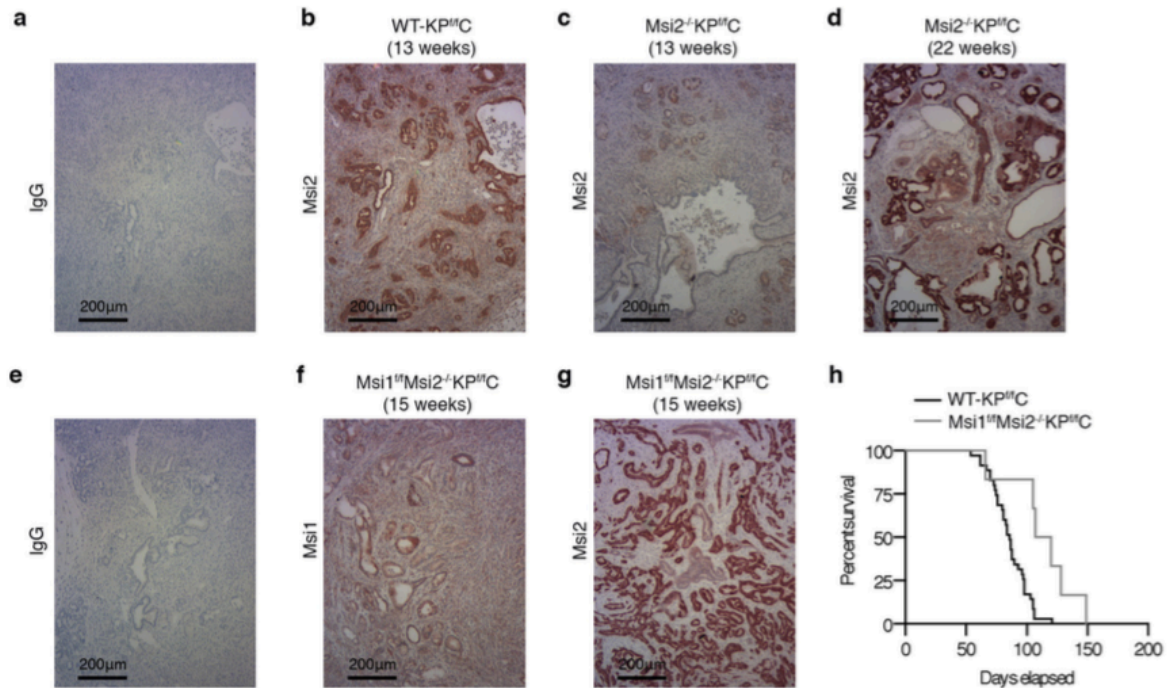


Figure Supplement 2.5. Selection for escaper Msi expressing cells in Msi knockout KP^{ff}C mice
(A-C) Immunohistochemical staining for **(A)** IgG control (n=4), or **(B-C)**, red) Msi2 in 13 week old WT-KP^{ff}C (n=4) and Msi2^{-/-}KP^{ff}C (n=4) mice. **(D)** Immunohistochemical staining for Msi2 (red) in 22 week old Msi2^{-/-}KP^{ff}C mouse (n=1). **(E-G)** Immunohistochemical staining for **(E)** IgG control, **(F)**, red) Msi1 and **(G)**, red) Msi2 in 15-week-old Msi1^{ff}Msi2^{-/-} double knockout KP^{ff}C mouse (n=1). **(H)** Survival curves of Msi1^{ff}Msi2^{-/-}-KP^{ff}C (n=6) or WT-KP^{ff}C tumors (n=35). Source Data for all panels are available online.

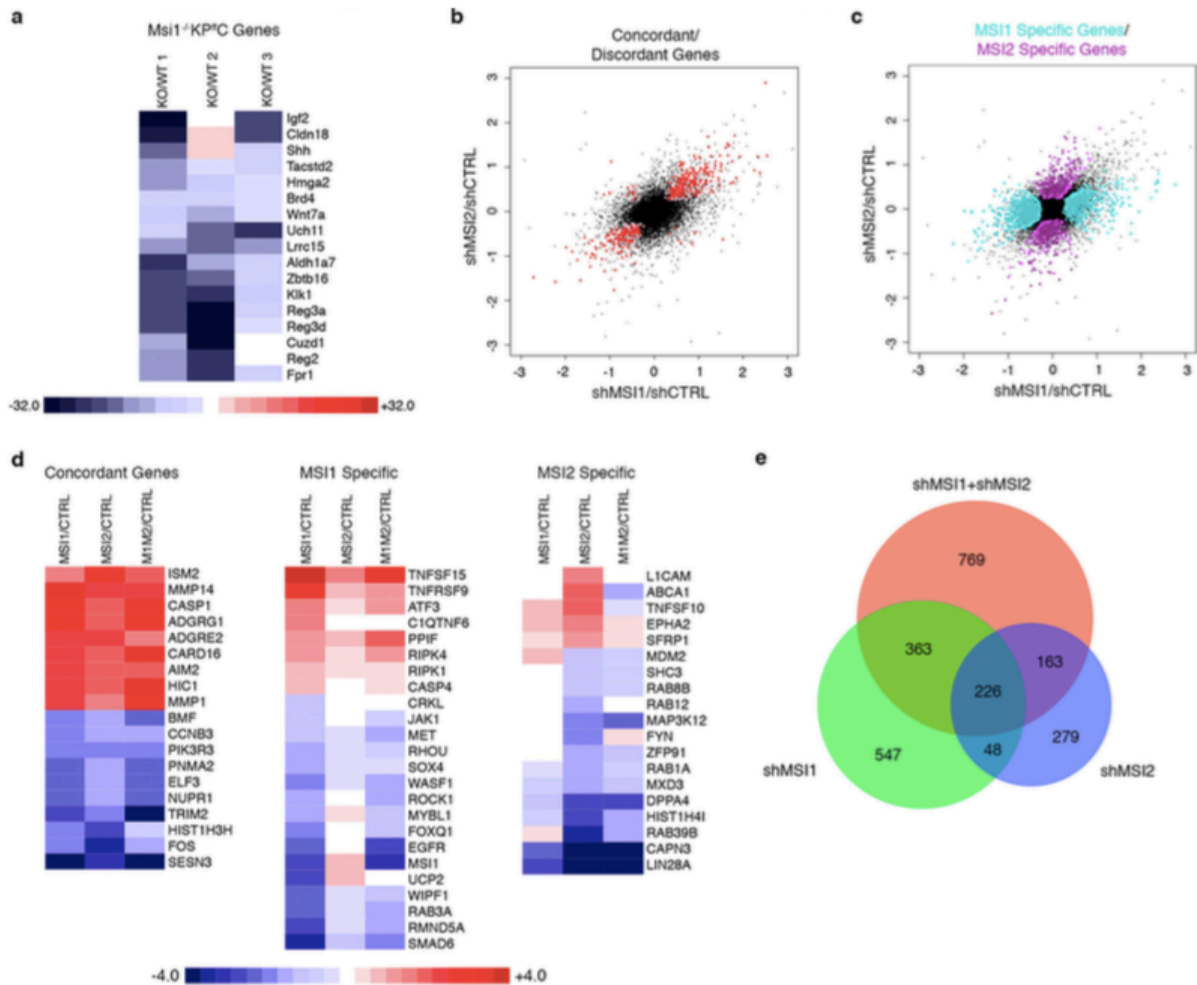


Figure Supplement 2.6. Genome wide analysis of Msi controlled programs in pancreatic cancer

(A) Genome wide expression analysis of dissociated pancreatic tumors. Microarray analysis was performed on RNA from 3 pairs of WT-KP^{flC} and Msi1^{-/-}-KP^{flC} matched littermates. Heat map shows differential expression of selected mRNAs identified as part of a stem cell associated gene signature. (B) Concordantly (upper right and lower left quadrants) and discordantly (upper left and lower right quadrants) regulated genes (red) in MSI1-knockdown and MSI2-knockdown MIA PaCa2 cells. (C) Gene changes specific to MSI1-knockdown (turquoise) or MSI2-knockdown (purple) in MIA PaCa2 cells. (D) Heat maps indicating concordant, MSI1 specific, and MSI2 specific genes. (E) Venn diagram displaying the intersection of probe sets that are differentially regulated in MSI1-knockdown, MSI2-knockdown and double knockdown of MSI1 and MSI2 in MIA PaCa2 cells. Within scatterplots, lighter color corresponds to a probability >0.5 and the darker color corresponds to a probability >0.75. Source Data for all panels are available online.

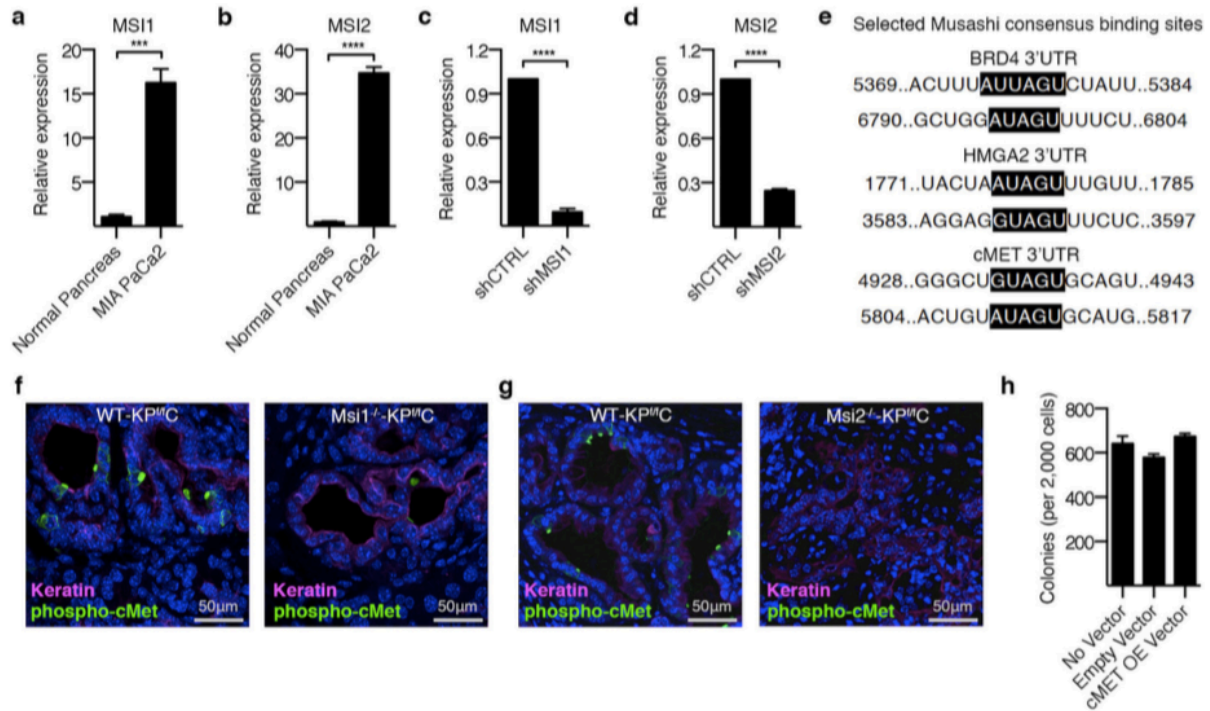


Figure Supplement 2.7. Molecular targets of Msi signaling

(A-B) Real-time PCR analysis of (A) Msi1 and (B) Msi2 expression in MIA PaCa-2 human pancreatic cancer cells relative to normal pancreas (n=3 independent experiments). (C-D) Analysis of shRNA knockdown efficiency in GFP+ sorted MIA PaCa-2 cells infected with GFP tagged lentiviral shRNA against scrambled control sequences, (C) MSI1 or (D) MSI2 (n=3 independent experiments). Analysis of direct Msi targets (E) Msi consensus binding sites in 3'UTR of Brd4, Hmga2 and c-Met transcripts. (F-G) Phospho-c-Met staining in WT-KP^{fl/c} and (F) Msi1^{-/-}-KP^{fl/c}, (G) Msi2^{-/-}-KP^{fl/c} mice; Keratin (magenta), phospho-c-Met (green), DAPI (blue). See Figure 3b-c for quantified data. (H) Colony formation of MIA PaCa-2 cells infected with empty vector or c-MET overexpression vector (3 independent experiments) shows no impact of overexpressed c-Met on control MIA PaCa-2 (control for c-Met mediated rescue of MSI knockdown in Figure 3f). Data are represented as mean ± SEM. *** $P < 0.001$, **** $P < 0.0001$ by Student's t-test. Source Data for all panels are available online.

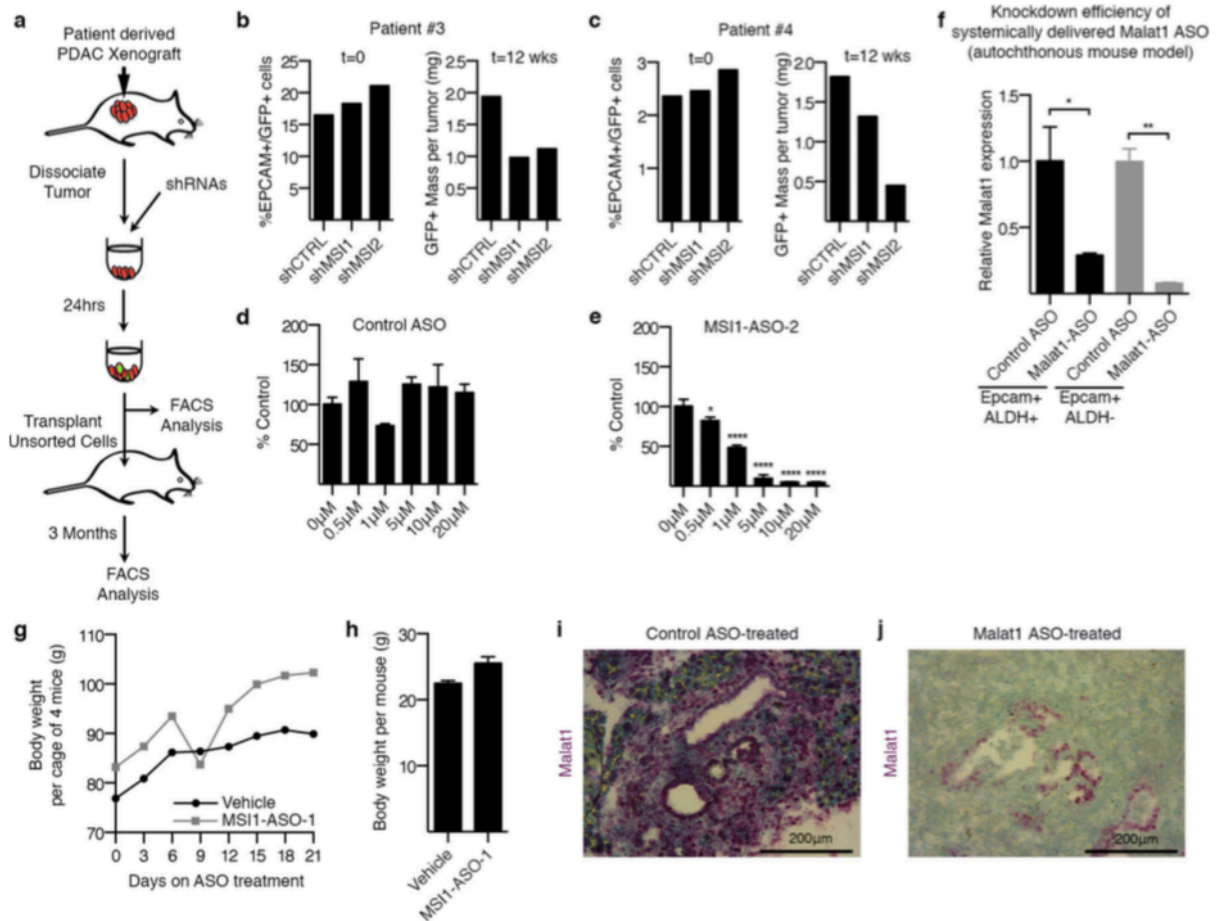


Figure Supplement 2.8. Analysis of impaired pancreatic cancer growth with shMSI and MSI1-ASOs

(A) Schematic for inhibiting MSI in primary patient-derived xenografts. (B-C) Frequency of GFP+ patient tumor cells before and after transplantation. See also Figure 4a-b for Patient#1, #2. ASO delivery *in vivo* (D-E) MSI1 expression following free uptake of (D) control ASO or (E) MSI1-ASO2 in human pancreatic cancer line (n=3 per condition). See also Figure 4c for impact of MSI1-ASO1. Target knockdown efficacy of lead optimized ASO in KP^{fl/c} stem cells (F) Malat1 expression in EpcAM+/ALDH+ and EpcAM+/ALDH- cells following systemic delivery of lead-optimized control ASO or Malat1-ASO in autochthonous KP^{fl/c} model (n=3 independent experiments) See also Figure 4h for target knockdown in unfractionated Epcam+ cells. Analysis of potential toxicity of MSI-ASO (G) Cage weight of mice receiving daily treatment of MSI1 ASO-1 (50mg/kg) or vehicle by IP injection; 4 mice per cage; cage weight was measured every 3 days. (H) Average body weight of mice following 3 weeks of daily treatment with MSI1 ASO-1 (50mg/kg) or vehicle by IP injection (n=4 mice/cohort). *In vivo* delivery of MSI1 ASOs (50mg/kg) had no deleterious impact on body weight and maintained plasma chemistry markers (AST, ALT, BUN, T.Bil) within 3x ULN (upper limit of normal). (I-J) Representative images of *in situ* hybridization for Malat1 (purple) in pancreatic tumors isolated from KP^{fl/c} mice treated by daily IP injection with (I) control ASO (50mg/kg) or (J) Malat1-ASO (50mg/kg) for 14 days. Source Data for all panels are available online.

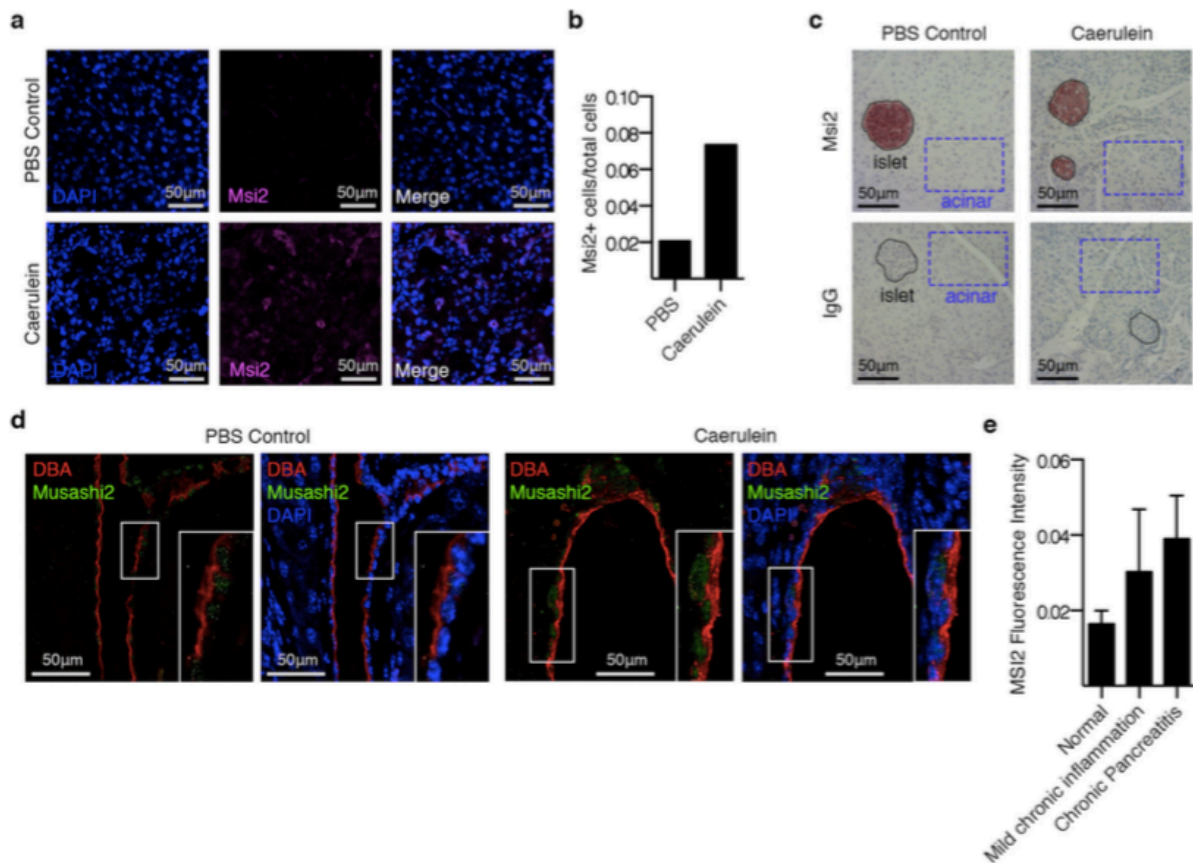


Figure Supplement 2.9. Elevated expression of Msi in pancreatitis

Msi2 expression in a caerulein-induced mouse model of pancreatitis, and in human pancreatitis. **(A)** Msi2 staining and **(B)** quantification of 10 images per group in pancreas from PBS-treated (**A**, top panels, n=1) and caerulein-treated mice (**A**, bottom panels, n=1). **(C)** Msi2 immunohistochemical staining in islets (purple circles) and acinar cells (blue squares) in caerulein or PBS treated mice (n=1 for each group). **(D)** Immunofluorescent staining of Msi2 (green) in DBA+ ductal cells (red) treated with PBS (left panels) or caerulein (right panels) (n=1 for each group); DAPI is shown in blue. **(E)** Msi2 expression in human tissue arrays from patients presenting with mild chronic inflammation (n=4) and chronic pancreatitis (n=6) compared to normal pancreas (n=14). Data are represented as mean \pm SEM. **** $P < 0.0001$ by Student's t-test. Source Data for all panels are available online.

ACKNOWLEDGEMENTS

We are grateful to Inder Verma, Michael Karin, and David Cheresh for advice and comments on the manuscript, Annette Luo for technical support, Gene Yeo for advice on Msi targeting, Keith Jenne for advice on MRI imaging, Nisha Patel and Paul Mischel for reagents and experimental advice, and Eric O'Conner and Karl Marquez for cell sorting. R.F. is a recipient of a California Institute for Regenerative Medicine interdisciplinary stem cell training program fellowship and also received support from T32 HL086344 and T32 CA009523, N.L. and C.K. received support from T32 GM007752, B.Z. received support from T32 GM007184-33 (Duke University). F.P. is a recipient of a California Institute for Regenerative Medicine interdisciplinary stem cell training program fellowship and the UCSD Clinical and Translational Research Institute KL2 Award. T.I. is the recipient of a California Institute for Regenerative Medicine interdisciplinary stem cell training program fellowship, J.B. is supported by a postdoctoral fellowship from National Cancer Center, and T.R. was supported in part by the Leukemia and Lymphoma Society Scholar Award. P.M.G. and M.A.H. are supported by a SPORE in Pancreatic Cancer, CA127297, a TMEN Tumor Microenvironment Network U54, an NCI Cancer Center Support Grant P30 CA36727 and an EDNRN U01 CA111294. A.M.L. was generously supported by donations from Ride The Point. This work was also supported by CA155620 to A.M.L., DK63031, HL097767, DP1 CA174422 and R35 CA197699 to T.R., and CA186043 to A.M.L. and T.R.

AUTHOR CONTRIBUTIONS

R.F. designed and performed all experiments related to Msi expression and deletion, whole genome and target analysis and ASO delivery in pancreatic cancer; N.K.L. designed and performed all live imaging of Msi reporter pancreatic tumors, and provided functional analysis of cancer stem cells, circulating tumor cells and therapy resistance; R.F., N.K.L. and M.K. helped write the paper; D.V.J. performed histological analysis, and provided mouse and xenograft models; F.P., T.I., J.B., C.K. and B.Z. provided experimental data and advice; R.S. performed all bioinformatics analysis; M.Y., S.S. and H.O. provided Msi^{1-/-} mice and CLIP-Seq analysis; M.V. and D.P. performed pathology/ ISH analysis; M. S. (Scadeng) performed MRI analysis; J.K. and M. S. (Sander) provided experimental advice, tumor samples and mouse models; J.S., A.M.L., M.V., P.A.G. and M.A.H. provided patient samples; Y.K. and R.M. designed,

synthesized and screened MSI ASOs, and provided advice on ASO related experiments. A.M.L and T.R. conceived of the project, planned and guided the research, and wrote the paper.

DISSERTATION ACKNOWLEDGEMENTS

Chapter 2, in full, is a reprint of the material as it appears in *Nature*. Fox RG*, Lytle NK*, Jaquish DV, Park FD, Ito T, Bajaj J, Koechlein CS, Zimdahl B, Yano M, Kopp J, Kritzik M, Sicklick J, Sander M, Gradgenett PM, Hollingsworth MA, Shibata S, Pizzo D, Valasek M, Sasik R, Scadeng M, Okano H, Kim Y, MacLeod AR, Lowy AM, Reya T. Image-based detection and targeting of therapy resistance in pancreatic adenocarcinoma. *Nature*. 2016 June 16;534(7607):407-411. The dissertation author was a co-primary author of this paper.

REFERENCES

- 1 Yachida, S. & Iacobuzio-Donahue, C. A. The pathology and genetics of metastatic pancreatic cancer. *Arch Pathol Lab Med* **133**, 413-422, doi:10.1043/1543-2165-133.3.413 (2009).
- 2 Almoguera, C., Shibata, D., Forrester, K., Martin, J., Arnheim, N. & Perucho, M. Most human carcinomas of the exocrine pancreas contain mutant c-K-ras genes. *Cell* **53**, 549-554 (1988).
- 3 Hahn, S. A., Schutte, M., Hoque, A. T., Moskaluk, C. A., da Costa, L. T., Rozenblum, E., Weinstein, C. L., Fischer, A., Yeo, C. J., Hruban, R. H. & Kern, S. E. DPC4, a candidate tumor suppressor gene at human chromosome 18q21.1. *Science* **271**, 350-353 (1996).
- 4 Redston, M. S., Caldas, C., Seymour, A. B., Hruban, R. H., da Costa, L., Yeo, C. J. & Kern, S. E. p53 mutations in pancreatic carcinoma and evidence of common involvement of homocopolymer tracts in DNA microdeletions. *Cancer Res* **54**, 3025-3033 (1994).
- 5 Nakamura, M., Okano, H., Blendy, J. A. & Montell, C. Musashi, a neural RNA-binding protein required for *Drosophila* adult external sensory organ development. *Neuron* **13**, 67-81 (1994).
- 6 Okano, H., Imai, T. & Okabe, M. Musashi: a translational regulator of cell fate. *J Cell Sci* **115**, 1355-1359 (2002).
- 7 Sakakibara, S., Nakamura, Y., Yoshida, T., Shibata, S., Koike, M., Takano, H., Ueda, S., Uchiyama, Y., Noda, T. & Okano, H. RNA-binding protein Musashi family: roles for CNS stem cells and a subpopulation of ependymal cells revealed by targeted disruption and antisense ablation. *Proc Natl Acad Sci U S A* **99**, 15194-15199, doi:10.1073/pnas.232087499 (2002).
- 8 Hope, K. J., Cellot, S., Ting, S. B., MacRae, T., Mayotte, N., Iscove, N. N. & Sauvageau, G. An RNAi screen identifies Msi2 and Prox1 as having opposite roles in the regulation of hematopoietic stem cell activity. *Cell Stem Cell* **7**, 101-113, doi:10.1016/j.stem.2010.06.007 (2010).
- 9 Ito, T., Kwon, H. Y., Zimdahl, B., Congdon, K. L., Blum, J., Lento, W. E., Zhao, C., Lagoo, A., Gerrard, G., Feroni, L., Goldman, J., Goh, H., Kim, S. H., Kim, D. W., Chuah, C., Oehler, V. G., Radich, J. P., Jordan, C. T. & Reya, T. Regulation of myeloid leukaemia by the cell-fate determinant Musashi. *Nature* **466**, 765-768, doi:10.1038/nature09171 (2010).
- 10 Kharas, M. G., Lengner, C. J., Al-Shahrour, F., Bullinger, L., Ball, B., Zaidi, S., Morgan, K., Tam, W., Paktinat, M., Okabe, R., Gozo, M., Einhorn, W., Lane, S. W., Scholl, C., Frohling, S., Fleming, M., Ebert, B. L., Gilliland, D. G., Jaenisch, R. & Daley, G. Q. Musashi-2 regulates normal hematopoiesis and promotes aggressive myeloid leukemia. *Nat Med* **16**, 903-908, doi:10.1038/nm.2187 (2010).
- 11 Kwon, H. Y., Bajaj, J., Ito, T., Blevins, A., Konuma, T., Weeks, J., Lytle, N. K., Koehlein, C. S., Rizzieri, D., Chuah, C., Oehler, V. G., Sasik, R., Hardiman, G. & Reya, T. Tetraspanin 3 Is Required for the Development and Propagation of Acute Myelogenous Leukemia. *Cell Stem Cell* **17**, 152-164, doi:10.1016/j.stem.2015.06.006 (2015).
- 12 de Andres-Aguayo, L., Varas, F., Kallin, E. M., Infante, J. F., Wurst, W., Floss, T. & Graf, T. Musashi 2 is a regulator of the HSC compartment identified by a retroviral insertion screen and knockout mice. *Blood* **118**, 554-564, doi:10.1182/blood-2010-12-322081 (2011).
- 13 Hingorani, S. R., Petricoin, E. F., Maitra, A., Rajapakse, V., King, C., Jacobetz, M. A., Ross, S., Conrads, T. P., Veenstra, T. D., Hitt, B. A., Kawaguchi, Y., Johann, D., Liotta, L. A., Crawford, H.

- C., Putt, M. E., Jacks, T., Wright, C. V., Hruban, R. H., Lowy, A. M. & Tuveson, D. A. Preinvasive and invasive ductal pancreatic cancer and its early detection in the mouse. *Cancer Cell* **4**, 437-450 (2003).
- 14 Kawaguchi, Y., Cooper, B., Gannon, M., Ray, M., MacDonald, R. J. & Wright, C. V. The role of the transcriptional regulator Ptf1a in converting intestinal to pancreatic progenitors. *Nat Genet* **32**, 128-134, doi:10.1038/ng959 (2002).
- 15 Tuveson, D. A., Shaw, A. T., Willis, N. A., Silver, D. P., Jackson, E. L., Chang, S., Mercer, K. L., Grochow, R., Hock, H., Crowley, D., Hingorani, S. R., Zaks, T., King, C., Jacobetz, M. A., Wang, L., Bronson, R. T., Orkin, S. H., DePinho, R. A. & Jacks, T. Endogenous oncogenic K-ras(G12D) stimulates proliferation and widespread neoplastic and developmental defects. *Cancer Cell* **5**, 375-387 (2004).
- 16 Reya, T., Morrison, S. J., Clarke, M. F. & Weissman, I. L. Stem cells, cancer, and cancer stem cells. *Nature* **414**, 105-111, doi:10.1038/35102167 (2001).
- 17 Wang, J. C. & Dick, J. E. Cancer stem cells: lessons from leukemia. *Trends Cell Biol* **15**, 494-501, doi:10.1016/j.tcb.2005.07.004 (2005).
- 18 Hermann, P. C., Huber, S. L., Herrler, T., Aicher, A., Ellwart, J. W., Guba, M., Bruns, C. J. & Heeschen, C. Distinct populations of cancer stem cells determine tumor growth and metastatic activity in human pancreatic cancer. *Cell Stem Cell* **1**, 313-323, doi:10.1016/j.stem.2007.06.002 (2007).
- 19 Kim, M. P., Fleming, J. B., Wang, H., Abbruzzese, J. L., Choi, W., Kopetz, S., McConkey, D. J., Evans, D. B. & Gallick, G. E. ALDH activity selectively defines an enhanced tumor-initiating cell population relative to CD133 expression in human pancreatic adenocarcinoma. *PLoS One* **6**, e20636, doi:10.1371/journal.pone.0020636 (2011).
- 20 Dosch, J. S., Ziemke, E. K., Shettigar, A., Rehemtulla, A. & Sebolt-Leopold, J. S. Cancer stem cell marker phenotypes are reversible and functionally homogeneous in a preclinical model of pancreatic cancer. *Cancer Res* **75**, 4582-4592, doi:10.1158/0008-5472.CAN-14-2793 (2015).
- 21 Rhim, A. D., Mirek, E. T., Aiello, N. M., Maitra, A., Bailey, J. M., McAllister, F., Reichert, M., Beatty, G. L., Rustgi, A. K., Vonderheide, R. H., Leach, S. D. & Stanger, B. Z. EMT and dissemination precede pancreatic tumor formation. *Cell* **148**, 349-361, doi:10.1016/j.cell.2011.11.025 (2012).
- 22 Li, C., Wu, J. J., Hynes, M., Dosch, J., Sarkar, B., Welling, T. H., Pasca di Magliano, M. & Simeone, D. M. c-Met is a marker of pancreatic cancer stem cells and therapeutic target. *Gastroenterology* **141**, 2218-2227 e2215, doi:10.1053/j.gastro.2011.08.009 (2011).
- 23 Belkina, A. C. & Denis, G. V. BET domain co-regulators in obesity, inflammation and cancer. *Nat Rev Cancer* **12**, 465-477, doi:10.1038/nrc3256 (2012).
- 24 Cleynen, I. & Van de Ven, W. J. The HMGA proteins: a myriad of functions (Review). *Int J Oncol* **32**, 289-305 (2008).
- 25 Hung, G., Xiao, X., Peralta, R., Bhattacharjee, G., Murray, S., Norris, D., Guo, S. & Monia, B. P. Characterization of target mRNA reduction through in situ RNA hybridization in multiple organ systems following systemic antisense treatment in animals. *Nucleic Acid Ther* **23**, 369-378, doi:10.1089/nat.2013.0443 (2013).

- 26 Seth, P. P., Siwkowski, A., Allerson, C. R., Vasquez, G., Lee, S., Prakash, T. P., Wancewicz, E. V., Witchell, D. & Swayze, E. E. Short antisense oligonucleotides with novel 2'-4' conformationally restricted nucleoside analogues show improved potency without increased toxicity in animals. *J Med Chem* **52**, 10-13, doi:10.1021/jm801294h (2009).
- 27 Li, N., Li, Q., Tian, X. Q., Qian, H. Y. & Yang, Y. J. Mipomersen is a promising therapy in the management of hypercholesterolemia: a meta-analysis of randomized controlled trials. *Am J Cardiovasc Drugs* **14**, 367-376, doi:10.1007/s40256-014-0077-0 (2014).
- 28 Hong, D., Kurzrock, R., Kim, Y., Woessner, R., Younes, A., Nemunaitis, J., Fowler, N., Zhou, T., Schmidt, J., Jo, M., Lee, S. J., Yamashita, M., Hughes, S. G., Fayad, L., Piha-Paul, S., Nadella, M. V., Mohseni, M., Lawson, D., Reimer, C., Blakey, D. C., Xiao, X., Hsu, J., Revenko, A., Monia, B. P. & MacLeod, A. R. AZD9150, a next-generation antisense oligonucleotide inhibitor of STAT3 with early evidence of clinical activity in lymphoma and lung cancer. *Sci Transl Med* **7**, 314ra185, doi:10.1126/scitranslmed.aac5272 (2015).
- 29 Lee, R. G., Crosby, J., Baker, B. F., Graham, M. J. & Crooke, R. M. Antisense technology: an emerging platform for cardiovascular disease therapeutics. *J Cardiovasc Transl Res* **6**, 969-980, doi:10.1007/s12265-013-9495-7 (2013).
- 30 Saad, F., Hotte, S., North, S., Eigl, B., Chi, K., Czaykowski, P., Wood, L., Pollak, M., Berry, S., Lattouf, J. B., Mukherjee, S. D., Gleave, M., Winkquist, E. & Canadian Uro-Oncology, G. Randomized phase II trial of Custirsen (OGX-011) in combination with docetaxel or mitoxantrone as second-line therapy in patients with metastatic castrate-resistant prostate cancer progressing after first-line docetaxel: CUOG trial P-06c. *Clin Cancer Res* **17**, 5765-5773, doi:10.1158/1078-0432.CCR-11-0859 (2011).
- 31 Domen, J., Cheshier, S. H. & Weissman, I. L. The role of apoptosis in the regulation of hematopoietic stem cells: Overexpression of Bcl-2 increases both their number and repopulation potential. *J Exp Med* **191**, 253-264 (2000).
- 32 Rovira, M., Scott, S. G., Liss, A. S., Jensen, J., Thayer, S. P. & Leach, S. D. Isolation and characterization of centroacinar/terminal ductal progenitor cells in adult mouse pancreas. *Proc Natl Acad Sci U S A* **107**, 75-80, doi:10.1073/pnas.0912589107 (2010).
- 33 Marino, S., Vooijs, M., van Der Gulden, H., Jonkers, J. & Berns, A. Induction of medulloblastomas in p53-null mutant mice by somatic inactivation of Rb in the external granular layer cells of the cerebellum. *Genes Dev* **14**, 994-1004 (2000).
- 34 Sasik, R., Woelk, C. H. & Corbeil, J. Microarray truths and consequences. *J Mol Endocrinol* **33**, 1-9 (2004).
- 35 Benjamini, Y. & Hochberg, Y. Controlling the False Discovery Rate - a Practical and Powerful Approach to Multiple Testing. *J Roy Stat Soc B Met* **57**, 289-300 (1995).
- 36 Bardeesy, N., Aguirre, A. J., Chu, G. C., Cheng, K. H., Lopez, L. V., Hezel, A. F., Feng, B., Brennan, C., Weissleder, R., Mahmood, U., Hanahan, D., Redston, M. S., Chin, L. & Depinho, R. A. Both p16(Ink4a) and the p19(Arf)-p53 pathway constrain progression of pancreatic adenocarcinoma in the mouse. *Proc Natl Acad Sci U S A* **103**, 5947-5952, doi:10.1073/pnas.0601273103 (2006).
- 37 Tusher, V. G., Tibshirani, R. & Chu, G. Significance analysis of microarrays applied to the ionizing radiation response. *Proc Natl Acad Sci U S A* **98**, 5116-5121, doi:10.1073/pnas.091062498 (2001).

- 38 Anders, S. & Huber, W. Differential expression analysis for sequence count data. *Genome Biol* **11**, R106, doi:10.1186/gb-2010-11-10-r106 (2010).
- 39 Ritchie, M. E., Phipson, B., Wu, D., Hu, Y., Law, C. W., Shi, W. & Smyth, G. K. limma powers differential expression analyses for RNA-sequencing and microarray studies. *Nucleic Acids Res* **43**, e47, doi:10.1093/nar/gkv007 (2015).
- 40 Efron, B. Microarrays, empirical Bayes and the two-groups model. *Stat Sci* **23**, 1-22, doi:10.1214/07-Sts236 (2008).
- 41 Lonnstedt, I. & Speed, T. Replicated microarray data. *Stat Sinica* **12**, 31-46 (2002).
- 42 Mootha, V. K., Lindgren, C. M., Eriksson, K. F., Subramanian, A., Sihag, S., Lehar, J., Puigserver, P., Carlsson, E., Ridderstrale, M., Laurila, E., Houstis, N., Daly, M. J., Patterson, N., Mesirov, J. P., Golub, T. R., Tamayo, P., Spiegelman, B., Lander, E. S., Hirschhorn, J. N., Altshuler, D. & Groop, L. C. PGC-1alpha-responsive genes involved in oxidative phosphorylation are coordinately downregulated in human diabetes. *Nat Genet* **34**, 267-273, doi:10.1038/ng1180 (2003).
- 43 Zimdahl, B., Ito, T., Blevins, A., Bajaj, J., Konuma, T., Weeks, J., Koechlein, C. S., Kwon, H. Y., Arami, O., Rizzieri, D., Broome, H. E., Chuah, C., Oehler, V. G., Sasik, R., Hardiman, G. & Reya, T. Lis1 regulates asymmetric division in hematopoietic stem cells and in leukemia. *Nat Genet* **46**, 245-252, doi:10.1038/ng.2889 (2014).
- 44 Licatalosi, D. D., Mele, A., Fak, J. J., Ule, J., Kayikci, M., Chi, S. W., Clark, T. A., Schweitzer, A. C., Blume, J. E., Wang, X., Darnell, J. C. & Darnell, R. B. HITS-CLIP yields genome-wide insights into brain alternative RNA processing. *Nature* **456**, 464-469, doi:10.1038/nature07488 (2008).
- 45 Ohyama, T., Nagata, T., Tsuda, K., Kobayashi, N., Imai, T., Okano, H., Yamazaki, T. & Katahira, M. Structure of Musashi1 in a complex with target RNA: the role of aromatic stacking interactions. *Nucleic Acids Res* **40**, 3218-3231, doi:10.1093/nar/gkr1139 (2012).
- 46 Carroll, J. B., Warby, S. C., Southwell, A. L., Doty, C. N., Greenlee, S., Skotte, N., Hung, G., Bennett, C. F., Freier, S. M. & Hayden, M. R. Potent and selective antisense oligonucleotides targeting single-nucleotide polymorphisms in the Huntington disease gene / allele-specific silencing of mutant huntingtin. *Mol Ther* **19**, 2178-2185, doi:10.1038/mt.2011.201 (2011).
- 47 Samuel, V. T., Choi, C. S., Phillips, T. G., Romanelli, A. J., Geisler, J. G., Bhanot, S., McKay, R., Monia, B., Shutter, J. R., Lindberg, R. A., Shulman, G. I. & Veniant, M. M. Targeting foxo1 in mice using antisense oligonucleotide improves hepatic and peripheral insulin action. *Diabetes* **55**, 2042-2050, doi:10.2337/db05-0705 (2006).

CHAPTER 3

A multiscale map of the stem cell state in pancreatic adenocarcinoma

Nikki K. Lytle^{1,2}, L. Paige Ferguson^{1,2}, Raymond G. Fox^{1,2}, Kathryn Gilroy³, Neil Robertson³, Anagha Deshpande⁴, Nirakar Rajbhandari^{1,2}, Tami Gilderman^{1,2}, Lourdes Adriana Esparza^{1,2}, Marcie Kritzik^{1,2}, Yutaka Shima^{1,2}, Philipp Spahn⁵, Randall French⁶, Wei Lin⁷, Pawan Noel⁷, Haiyong Han⁷, Daniel Von Hoff⁷, Nathan Lewis⁵, Kathleen M. Fisch⁸, Roman Sasik⁸, Sara Brin Rosenthal⁸, Trey Ideker^{6,9}, Aniruddha L. Deshpande⁴, Andrew M. Lowy^{6,10}, Peter Adams⁴, and Tannishtha Reya^{1,2,6,9}.

¹Departments of Pharmacology and Medicine, University of California San Diego School of Medicine

²Sanford Consortium for Regenerative Medicine, La Jolla, CA

³Institute of Cancer Sciences, College of Medical, Veterinary and Life Sciences; University of Glasgow; Glasgow G61 1BD; UK

⁴Tumor Initiation and Maintenance Program, NCI-designated Cancer Center, Sanford Burnham Prebys Medical Discovery Institute, La Jolla, CA

⁵Department of Pediatrics, University of California San Diego School of Medicine La Jolla, CA,

⁶Moore's Cancer Center, La Jolla, CA

⁷Molecular Medicine Division, The Translational Genomics Research Institute, Phoenix, Arizona

⁸Center for Computational Biology and Bioinformatics, University of California San Diego, La Jolla, CA

⁹Department of Medicine, University of California San Diego School of Medicine La Jolla, CA,

¹⁰Department of Surgery, Division of Surgical Oncology, University of California San Diego School of Medicine, La Jolla, CA

Submitted, in part, for publication

August 2018

PREFACE TO CHAPTER 3:

Chapter 3, in full, was submitted for publication entitled “A multiscale map of the stem cell state in pancreatic adenocarcinoma.” The goal of this project was to identify what drives and maintains the unique characteristics and functional dependencies of pancreatic cancer stem cells. We did this by first defining the transcriptomic and epigenetic signature in primary pancreatic stem and non-stem tumor cells, then crossed that data to an unbiased dropout screen designed to identify genes that are required for stem cell maintenance. These studies led us to discover a novel and exciting role for the retinoic acid orphan receptor, ROR γ , in promoting a stem like state in pancreatic cancer. As luck would have it, there are clinically-approved inhibitors of ROR γ that we show effectively deplete cancer stem cells *in vivo* by disrupting critical pro-tumorigenic signals. This results in a delay in tumor progression and improved overall survival in a mouse model of pancreatic cancer. Thus, the work described in this chapter illuminates a promising new therapeutic approach for pancreatic cancer patients.

ABSTRACT

Therapy resistance and resultant relapse remain key challenges in pancreatic cancer, and are in part driven by the inherent heterogeneity of the tumor that prevents effective targeting of all malignant cells. To better understand the pathways that allow some cells to be more aggressive and drug resistant, we utilized a combination of RNA-seq, ChIP-seq and genome-wide CRISPR screening to systematically map molecular dependencies of pancreatic cancer stem cells, highly drug resistant cells that are also enriched in the capacity to drive tumor progression¹⁻⁴. Integration of these data revealed an unexpected role for immuno-regulatory pathways in stem cell self-renewal and maintenance in KP^{trf}C tumors. In particular, Retinoic acid receptor-related orphan receptor gamma (ROR γ), a nuclear hormone receptor known for its role in inflammatory cytokine responses and T cell differentiation^{5,6}, emerged as a key regulator of stem cells. ROR γ was not only elevated with pancreatic cancer progression, but was also genomically amplified in a subset of pancreatic cancer patients. Functionally its inhibition via genetic approaches or small molecule inhibitors led to a striking defect in pancreatic cancer growth *in vitro* and *in vivo*, and mitigated its lethality. Collectively, these data reveal an unexpected co-option of immuno-regulatory signals by pancreatic cancer stem cells, and suggest that therapeutics currently being used for autoimmune indications should be considered for treatment of pancreatic cancer.

KEYWORDS

Cancer stem cells, stem cell signals, pancreatic cancer, ROR γ , retinoic acid receptor, CRISPR screen, Musashi, tumor heterogeneity, therapy resistance, super-enhancer, H3K27ac, intravital imaging

INTRODUCTION

While cytotoxic agents remain the standard of care for most cancers, their use is often associated with initial efficacy, followed by disease progression. This is particularly true for pancreatic cancer, a highly aggressive disease, where current multidrug chemotherapy regimens result in tumor regression in 30% of patients, quickly followed by disease progression in essentially all cases⁷. Even in patients that present with surgically resectable, localized disease, the 5-year survival rate remains under 40%, highlighting how difficult it is to effectively eradicate all tumor cells. Thus, to improve patient outcome and response to current therapies, it is important to first identify the fundamental drivers of tumor heterogeneity by determining which cells may be preferentially drug resistant and aggressive.

In previous work, we and others have shown that subpopulations within PDAC are enriched for the capacity to drive tumorigenesis, metastasis, and survive current therapies¹⁻⁴; these subpopulations bore hallmarks of stem cells^{8,9} including their enriched ability to propagate tumors and to recreate the heterogeneity of the primary tumor³. Although pancreatic cancer stem cells are epithelial in origin, they frequently possess mesenchymal-like features, which may in part explain their over-representation in circulation and ability to seed metastasis^{1,4,10,11}. Importantly, cancer stem cells have been shown to be highly resistant to cytotoxic therapies^{1,4,12} and patients with a high cancer stem cell signature have poorer prognosis compared to those with a low stem cell signature^{13,14}. Recent data suggests that cancer stem cells can also directly modulate the tumor microenvironment to be less responsive to immunotherapy¹⁴⁻¹⁶. Furthermore, targeted therapies aimed at the tumor microenvironment can lead to expansion of an aggressive cancer stem cell population^{17,18}, and result in worse outcome. These studies highlight the necessity to target pancreatic cancer stem cells given their capacity to survive current therapies, drive disease relapse, and modulate tumor behavior. Although pancreatic cancer stem cells are dependent on stem cell signals such as Musashi⁴, hedgehog³, and cMet¹⁹, and have unique metabolic requirements²⁰, these signals are currently difficult to effectively block and remain a clinical challenge²¹⁻²³.

Specifically PDAC stem cells are functionally distinct from the rest of the tumor not due to genetic differences but due to epigenetic differences that promote expression of stem cell signals and maintain a stem-like state. In certain contexts, the epigenome can determine the cell of origin of the cancer²⁴, permit

adaptation necessary to survive therapies^{25,26}, and promote a more metastatic phenotype^{27,28}. To this end, chromatin regions that are preferentially open, as defined by the epigenome, permits unique transcription factor accessibility which drives gene expression that defines the cell state²⁹⁻³². Together it is the combination of the chromatin landscape with transcriptional effector molecules that can sustain a cell population responsible for poor patient outcome. Elucidating the landscape and signals that are key to maintaining that population is crucial for achieving complete and durable responses.

Here we systematically define the pancreatic cancer stem cell landscape by conducting unbiased, genome-wide studies in primary stem and non-stem tumor cells. We utilized RNA-seq and H3K27ac ChIP-seq³² to characterize the epigenetic and transcriptomic signature that uniquely defines pancreatic cancer stem cells. These differentially expressed programs were then integrated with a genome-wide CRISPR dropout screen that was designed to identify broad tumor cell dependencies as well as dependencies specific to cancer stem cells. This comprehensive approach led to the identification of an unexpected role for immuno-regulatory signals in maintaining the pancreatic cancer stem cell state, many of which are therapeutically actionable. In particular, the retinoic acid receptor related orphan receptor gamma (ROR γ) was identified as a critical stem cell factor. Genetic or pharmacologic blockade of ROR γ led to a significant loss of tumor propagating capacity in both human and mouse models of pancreatic cancer by disrupting critical super-enhancer linked gene expression. Further, delivery of ROR γ antagonists in tumor-bearing autochthonous pancreatic cancer mice led to a significant depletion in stem cells and improved overall survival. Together, our studies offer a unique comprehensive map of pancreatic cancer stem cells and identified critical vulnerabilities that may be exploited to improve therapeutic targeting of aggressive tumor cells.

RESULTS

In previous work, we have used the KP^{ffC} mouse model³³⁻³⁶ of pancreatic ductal adenocarcinoma (PDAC) to show that a reporter mouse designed to mirror expression of the stem cell signal Musashi (Msi) could effectively identify tumor cells that preferentially harbor capacity for drug resistance and tumor re-growth⁴. Further, Msi2+ tumor cells were 209-fold enriched in the ability to give rise to organoids³⁷ in limiting dilution assays (**Figure Supplement 3.1A-B**). Because Msi+ cells were preferentially enriched for tumor propagation and drug resistance, classically defined properties of cancer stem cells, we postulated that these reporter mice could be used as a tool to understand the molecular underpinnings of this aggressive subpopulation within pancreatic cancer.

To map the functional landscape of the stem cell state, we utilized a combination of RNA-sequencing (RNA-seq), chromatin immunoprecipitation followed by deep sequencing (ChIP-seq) and genome-wide CRISPR screening^{38,39}. Pancreatic ductal adenocarcinoma (PDAC) cells were isolated from Msi2-reporter (REM2) KP^{ffC} mice⁴ based on GFP and EpCAM expression and analyzed by RNA-seq (**Figure 3.1A**). Principal component analysis showed that KP^{ffC} reporter+ tumor cells were strikingly distinct from reporter- tumor cells at a global transcriptional level, indicating that they were functionally driven by a unique set of programs defined by differential expression of over a thousand genes (**Figures 3.1B-C**). We focused on the ~600 genes enriched in stem cells (l_{fdr}<0.2) in order to understand the transcriptional programs that may functionally maintain the stem cell phenotype. Gene Set Enrichment Analysis (GSEA)⁴⁰ was used to compare this PDAC stem cell transcriptome signature with other cell signatures⁴¹; this revealed that the transcriptional state of PDAC stem cells mapped closely with other developmental and stem cell states, indicating molecular features aligned with their observed functional traits (**Figures 3.1D-E**). Additionally, the transcriptional signature of PDAC stem cells was inversely correlated with cell proliferation signatures (**Figures 3.1F-G**), consistent with our finding that stem cells are largely quiescent following chemotherapy while non-stem cells continue to cycle (**Figure Supplement 3.1C**). Moreover, stem cells were characterized by metabolic signatures associated with tumor aggressiveness including increased sulfur amino acid metabolism⁴², and enhanced glutathione synthesis, which can enable survival following radiation and chemotherapy⁴³⁻⁴⁵ (**Figures 3.1H-I**). Finally, the PDAC stem cell transcriptome bore striking

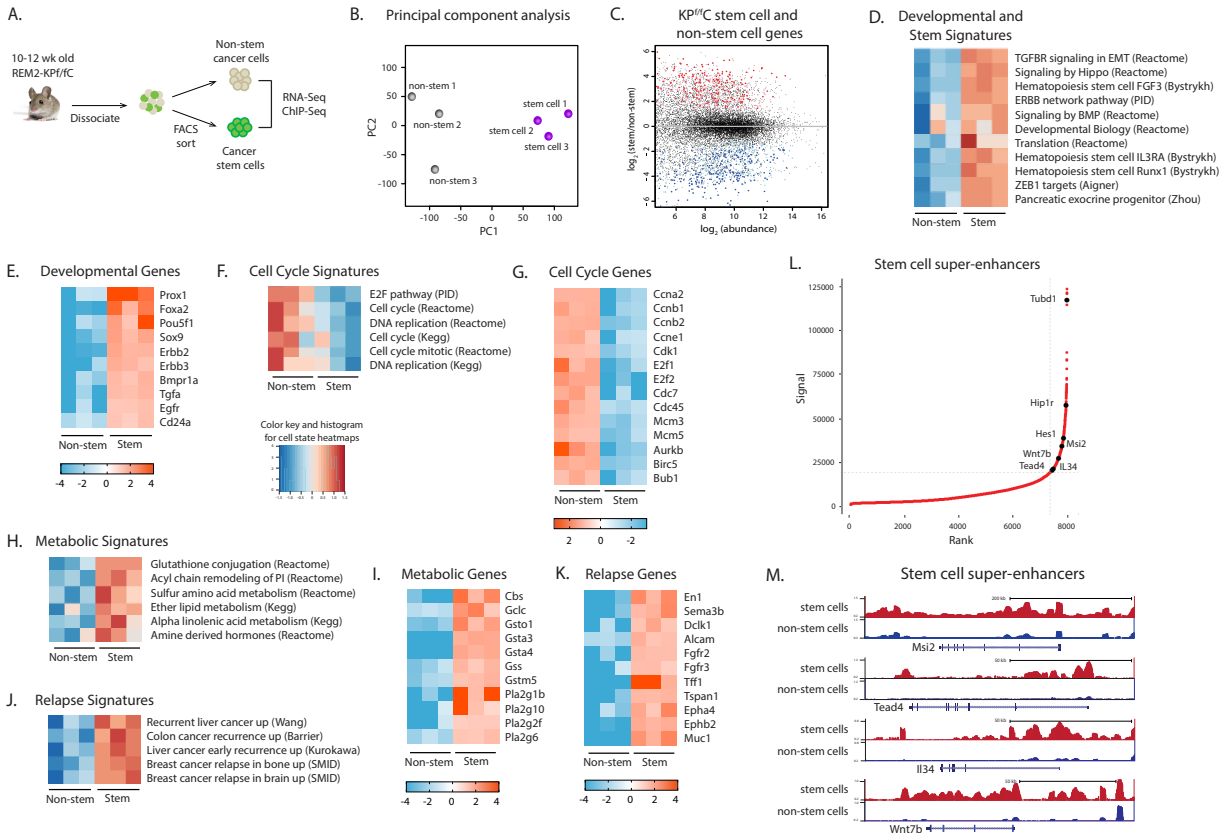


Figure 3.1. Transcriptomic and epigenetic tumor cell map reveals a unique stem cell state. (A) Schematic of overall strategy for RNA-seq and ChIP-seq of EpCAM+GFP+ (stem) and Epcam+GFP- (non-stem) tumor cells from REM2-KP^{fl/c} mice (n=3 for RNA-seq, n=1 for ChIP-seq) (B) Principal components analysis of KP^{fl/c} stem (blue) and non-stem (gray) cells. (C) Transcripts enriched in stem cells (red, pink) and non-stem cells (dark blue, light blue). Pink, light blue, lfd<0.3; red, dark blue, lfd<0.1. (D-K) Gene set enrichment analysis (GSEA) of stem and non-stem gene signatures. Cell states, and corresponding heat-maps of selected genes, associated with development and stem cells (D,E), cell cycle (F,G), metabolism (H,I), and cancer relapse (J,K). (D, F, H, J) Red denotes overlapping gene signatures; blue denotes non-overlapping gene signatures. (E, G, I, K) Red, over-represented gene expression; blue, under-represented gene expression; shades denote fold change from median values (L) Hockey stick plot of H3K27ac occupancy, ranked by signal density. Super-enhancers in stem cells are demarcated by highest ranking and intensity signals, above and right of dotted gray lines. Names of selected genes linked to super-enhancers are annotated. (M) H3K27ac ChIP-seq read counts across selected genes marked by super-enhancers unique to stem cells.

similarities to signatures from relapsed cancers of the breast, liver, and colon, programs that may underlie the ability of these cells to survive chemotherapy and drive tumor re-growth (**Figures 3.1J-K**).

In support of the significant molecular differences found in stem cells by transcriptomic analysis, the distribution of H3 lysine-27 acetylation (H3K27ac, **Figures 3.1A, Figure Supplement 3.2A**), a histone mark associated with active enhancers^{32,46}, revealed that the differential gene expression programs were driven by changes at the chromatin level. Thus, genomic regions enriched for H3K27ac specifically in either stem cells or non-stem cells coincided with regions where gene expression was increased in each cell type (**Figures Supplement 3.2B-D**). Because super-enhancers have been proposed to be key drivers of cell identity^{31,46,47}, we mapped shared and unique super-enhancers in stem and non-stem cells (**Figures 3.1L-M, Figure Supplement 3.2E-F**). Interestingly this revealed that not all epigenetic changes were equivalently different between the two populations: while most promoter and enhancer-associated H3K27ac marks were shared in both stem and non-stem tumor cells, with less than 5% being unique, super-enhancer associated H3K27ac marks were much more frequently restricted, with 65% of all super-enhancers being unique to each population. Further, super-enhancers in the stem cell population were clearly demarcated by peaks with substantially greater peak intensity and strength (**Figure 3.1M**) while those in non-stem cells were either shared with stem cells or only marginally more enriched in H3K27Ac than those in stem cells (Figure not shown). These data suggest that stem cells in pancreatic cancer have a more defined super-enhancer landscape than non-stem cells and raise the possibility that super-enhancers and their upstream transcriptional regulators may be preferential effectors of stem cell identity in pancreatic cancer. In support of this, key transcription factors and programs that underlie developmental and stem cell states, such as Klf7, Foxp1, Hmga1, Meis2, Tead4, Wnt7b and Msi2, were associated with super-enhancers in KP^{fl/c} stem cells (**Figures 3.1L-M**).

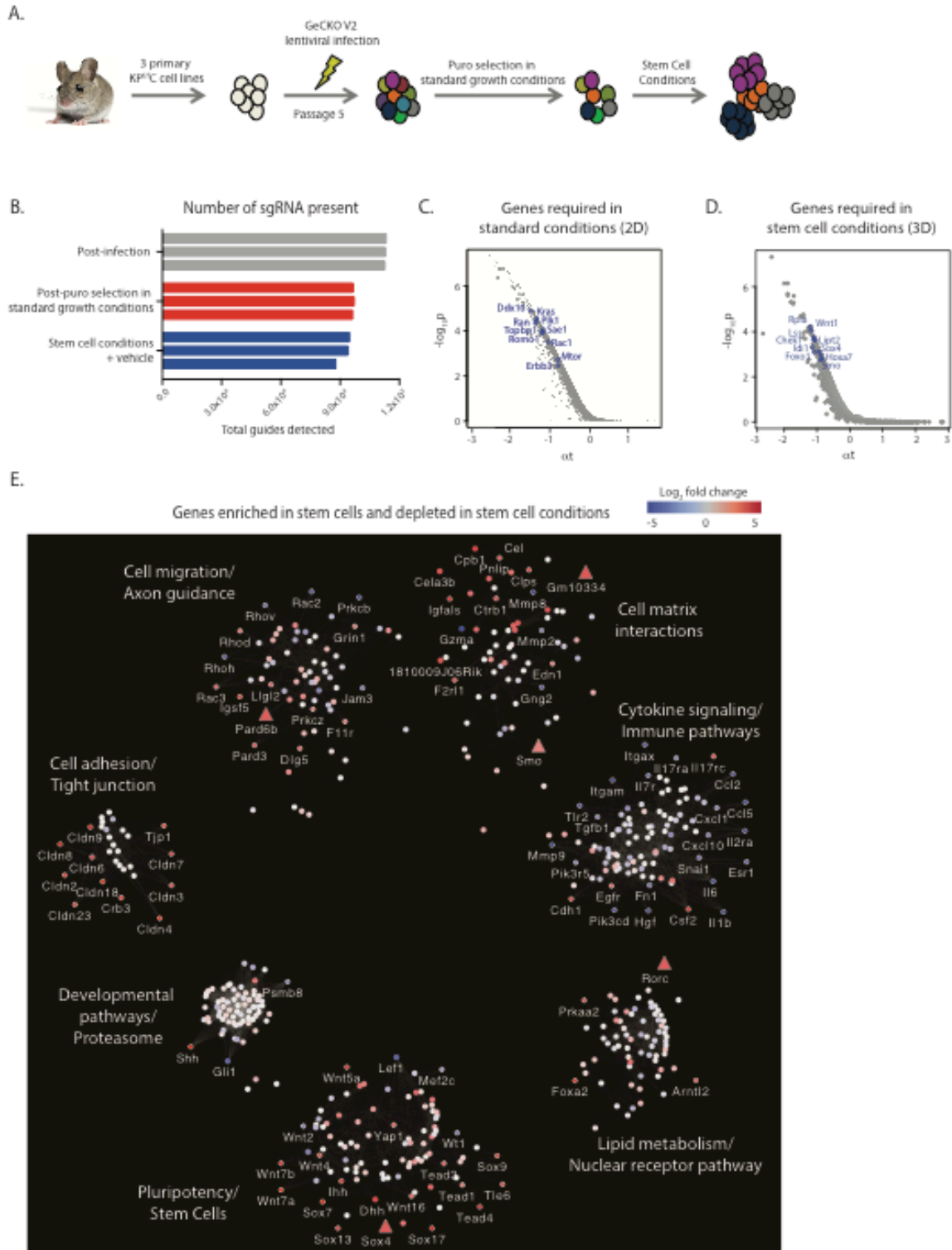
To define which of the programs uncovered by the transcriptional and epigenetic analyses represented true functional dependencies of stem cells, we carried out a genome-wide CRISPR screen^{38,39}. Thus, we established primary cell cultures highly enriched for stem cells (**Figure Supplement 3.3A**) from Msi reporter-KP^{fl/c} mice and transduced them with the mouse GeCKO CRISPRv2 sgRNA library³⁸ (**Figure 3.2A**). The screen was designed to be multiplexed in order to identify genes required in conventional 2-dimensional cultures, as well as in 3-dimensional sphere cultures⁴⁸ that selectively allow stem cell growth⁴

(**Figure 3.2A**). The screens showed clear evidence of selection, with 807 genes depleted (and thus essential) in conventional cultures (**Figures 3.2B-C**, $p < 0.005$) and an additional 178 in stem cell conditions (**Figures 3.2B, D**, $p < 0.005$). Importantly, the screens showed a loss of oncogenes and an enrichment of tumor suppressors in conventional cultures (**Figures 3.2C, Figure Supplement 3.3B**), and a loss of stem cell signals and gain of negative regulators of stem signals in stem cell conditions (**Figures 3.2D**, Data not shown).

Computational integration of the transcriptomic and CRISPR-based functional genomic data was carried out using a network propagation method similar to one developed previously⁴⁹. Here, the network was seeded with genes that were preferentially enriched in stem cells and also identified as essential for stem cell growth in 3-dimensional sphere cultures in the CRISPR assay (**Figure 3.2E**). The genes most proximal to the seeds were then determined using the mouse STRING interactome⁵⁰ based on known and predicted protein-protein interactions. The network was subsequently clustered into functional communities based on high interconnectivity between genes; this analysis identified seven subnetworks built around distinct biological pathways or 'core programs'. These core programs identified stem and pluripotency pathways, developmental and proteasome signals, lipid metabolism/nuclear receptors, cell adhesion/cell-matrix/cell migration, and immuno-regulatory signaling as pathways integral to the stem cell state (**Figure 3.2E**).

Ultimately the power of such a map is the ability to provide a systems level view of new dependencies. Thus we used the network map as a framework to select an integrated gene set based on the transcriptomic, epigenomic and the CRISPR functional genomic analysis (**Table 3.1**). For example, while many genes within the pluripotency and developmental core program were known to be important in pancreatic cancer (e.g. elements of the Wnt, Hedgehog and Hippo pathways), many had not yet been explored, and presented new opportunities for discovery (**Figures 3.3A, L, Figure Supplement 3.4A**) and investigation as novel targets (**Table 3.2**). In addition, novel metabolic factors such as Sptssb, a key contributor to sphingolipid metabolism⁵¹, and Lpin2, an enzyme involved in generation of pro-inflammatory very-low density lipoproteins⁵², were found to be critical new stem cell dependencies, implicating lipid metabolism as a key point of control (**Figures 3.3B, L**). The integrated analysis also identified new gene families as having broad regulatory patterns in pancreatic cancer: thus within the adhesion/cell-matrix core

Figure 3.2. Genome-scale CRISPR screen identifies core stem cell programs in PDAC. (A) Schematic of CRISPR screen. Three independent primary KP^{fl/c} lines were generated from end-stage REM2-KP^{fl/c} tumors and transduced with lentiviral GeCKO V2 library (MOI 0.3). Cells were plated in standard 2D conditions under puromycin selection, then in 3D stem cell conditions. **(B)** Number of guides detected in each replicate following lentiviral infection (gray bars), after puromycin selection in 2D (red bars), and after 3D sphere formation (blue bars). **(C, D)** Volcano plots of guides depleted in 2D (C) and 3D (D). Genes indicated on plots, $p < 0.005$. **(E)** Network propagation analysis integrating transcriptomic, epigenetic and functional analysis of stem cells. Genes enriched in stem cells by RNA-seq (stem/non-stem \log_2 fold-change > 2) and depleted in 3D stem cell growth conditions (FDR < 0.5) were used to seed the network (triangles), then analyzed for known and predicted protein-protein interactions. Each node represents a single gene; node color is mapped to the RNA-seq fold change; stem cell enriched genes, red; non-stem cell enriched genes, blue; genes not significantly differentially expressed, gray. Labels are shown for genes which are enriched in stem cells by RNA-seq and ChIP-seq (Up/Up) or enriched in non-stem cells by RNA-seq and ChIP-seq (Down/Down); RNA \log_2 fold change absolute value greater than 2.0, ChIP-seq FDR < 0.01 . Seven core programs were defined by groups of genes with high interconnectivity; each core program is annotated by Gene Ontology analysis (FDR < 0.05).



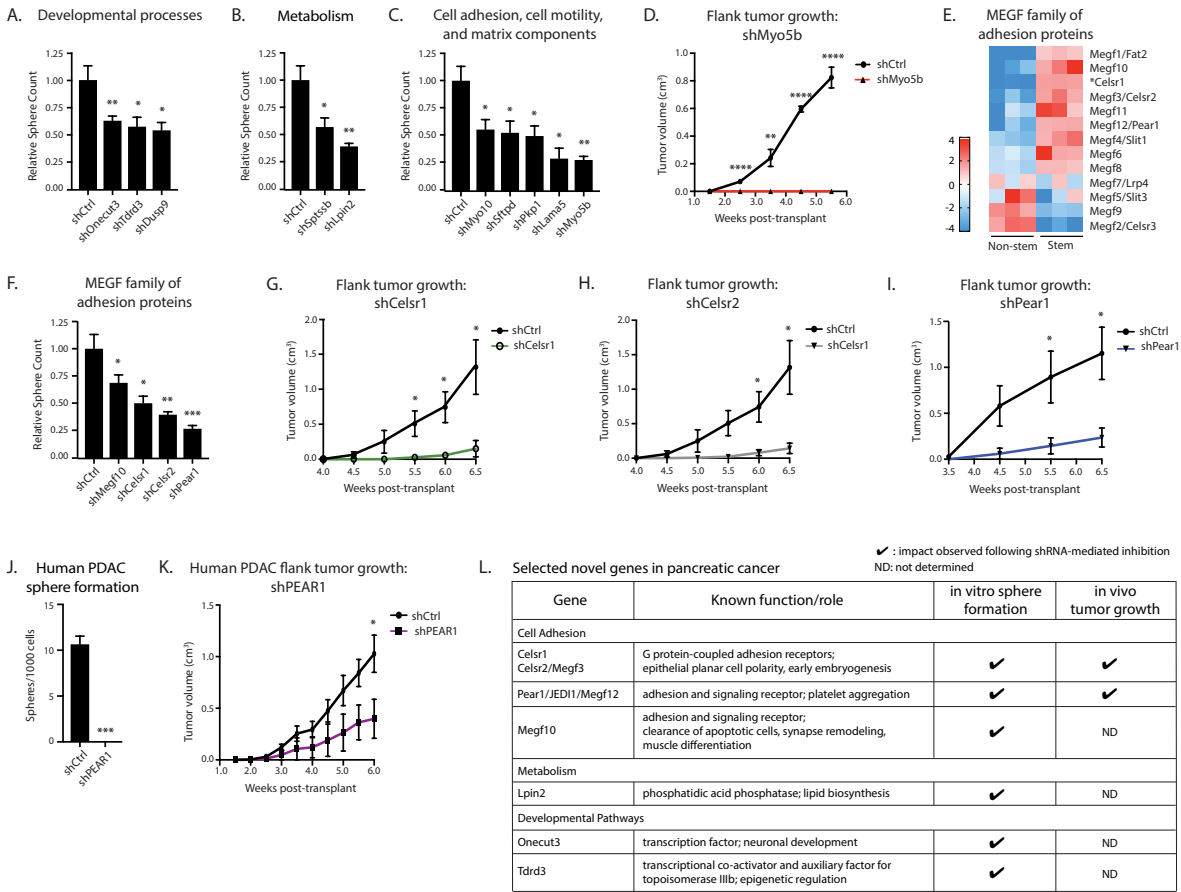


Figure 3.3. Identification of novel pathway dependencies of pancreatic cancer stem cells. (A-D) Functional impact of selected network genes on $KP^{fl/c}$ cell growth *in vitro* and *in vivo*. Genes from stem and developmental processes (A), lipid metabolism (B), and cell adhesion, motility, and matrix components (C-D), were inhibited via shRNA in $KP^{fl/c}$ cells, and impact on tumor propagation assessed by stem cell sphere assays *in vitro* or by tracking flank transplants *in vivo*. Sphere formation, n=3-6 per conditions; flank tumor transplant, n=4 per condition. (E-I) Identification of preferential dependence on MEGF family of adhesion proteins. (E) Heat map of relative RNA expression of MEGF family and related (*Celsr1) genes in $KP^{fl/c}$ stem and non-stem cells. Red, over-represented; blue, under-represented; color denotes fold change from median values. (F-I) Impact of inhibiting Celsr1, Celsr2, and Pear1 in sphere forming assays *in vitro* (F) and flank transplants *in vivo* (G-I). Sphere formation, n=3-6 per condition; flank tumor transplant, n=4 per condition. (J-K) Impact of shPEAR1 on human pancreatic cancer cell sphere formation (J) and *in vivo* tumor propagation (K). Sphere formation, n=3; flank tumor transplant, n=4 per condition. (L) Table summarizing identification of key new dependencies of pancreatic cancer growth and propagation. Check indicates significant impact following shRNA inhibition; ND, not determined.

program (**Figures 3.3C-L, Figure Supplement 3.4B**), several members of the multiple EGF repeat (MEGF) subfamily of orphan adhesion G protein coupled receptors (8 of 12 differentially expressed, **Figure 3.3E**) such as *Celsr1*, *Celsr2*⁵³, and *Pear1/Jedi*⁵⁴ emerged as new regulators of pancreatic cancer propagation as their inhibition potentially blocked cancer propagation *in vitro* and *in vivo* (**Figures 3.3F-K**). These pathways could be important to pursue in the future especially because GPCRs are frequently effective drug targets.

An unexpected discovery from this map was the identification of immune pathways/cytokine signaling as a core program. In line with this, retrospective analysis of the RNA-seq and ChIP-seq analysis revealed that multiple immuno-regulatory cytokines receptors were preferentially expressed on stem cells while their associated ligand were preferentially expressed by non-stem tumor cells (**Figure 3.4A**). This was of particular interest because many genes associated with this program, such as interleukin-10 (IL-10)⁵⁵, interleukin-34 (IL-34) and colony stimulating factor 1 receptor (CSF1R)⁵⁶, have been studied primarily in context of the tumor microenvironment, but have not been reported to be produced by, or to functionally impact, pancreatic epithelial cells directly. To more definitively identify whether these cytokines and cytokine receptors were co-expressed on epithelial cells, we carried out a single-cell RNA-seq from KPR^{172H/+}C tumor cells, an independent model of pancreatic cancer. This confirmed the presence of IL10rb, IL34 and Csf1r on epithelial tumor cells (**Figures 3.4B-C, Figure Supplement 3.4C**). shRNA-mediated inhibition of IL-10/IL10R and IL-34/CSF1R pathways, led to a striking loss of sphere forming capacity (**Figures 3.4D, G**), and impaired tumor growth and propagation *in vivo* (**Figures 3.4E-F, H**). These findings demonstrate an intriguing orthogonal co-option of inflammatory mediators by pancreatic cancer stem cells and suggest that agents that modulate cytokine networks may directly impact their function in pancreatic cancer propagation.

To understand how the gene networks defined above are controlled, we focused on transcription factors because of their powerful role in regulating broad hierarchical programs key to cell fate and identity^{57,58}. Of the 53 transcription factors identified within the map, 12 were found to be enriched in stem cells by transcriptomic and epigenetic parameters (**Figure Supplement 3.5A**), and included several pioneer factors^{31,59} known to promote tumorigenesis, such as *Sox9*^{60,61} and *Foxa2*⁶²⁻⁶⁴. Among transcription factors with no known role in pancreatic cancer (*Arntl2*, *Nr1d1* and *RORγ*), only *RORγ* was potentially actionable with clinical-grade antagonists available⁶⁵. Importantly, at the molecular level, motif enrichment

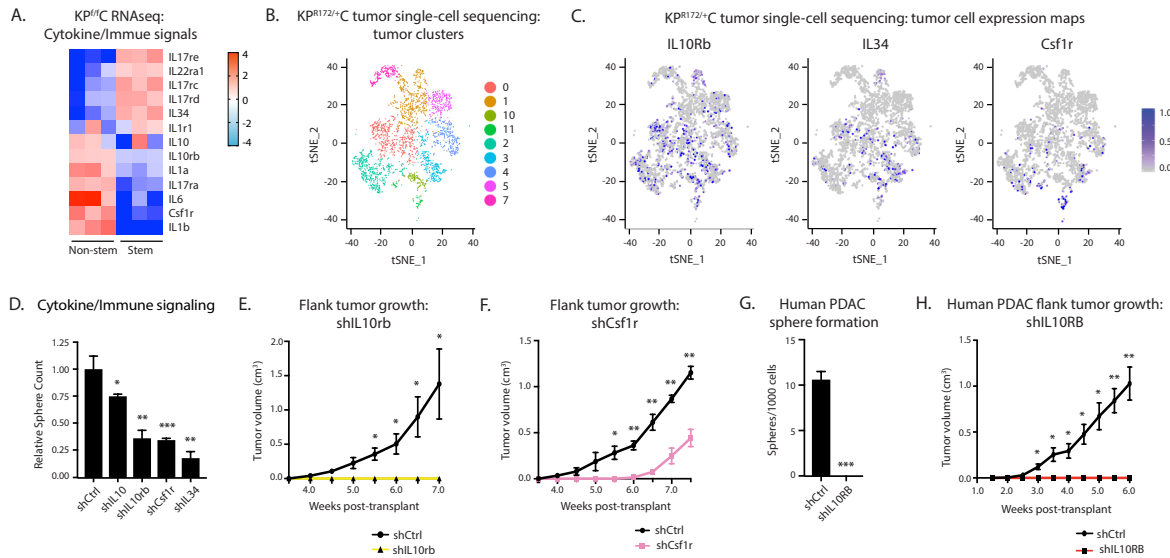


Figure 3.4. Pancreatic cancer stem cells are dependent on immune-type signaling. (A) Heat map of relative RNA expression of immune-related genes in KP^{fl}C stem and non-stem cells. Red, over-represented; blue, under-represented; color denotes fold change from median values. (B-C) Single cell RNA-sequencing analysis of KP^{R172H/+}C tumors. Tumor cells from 9 independent tumors (B) were assessed for IL10rb, IL34, and Csf1r expression (C); color denotes relative mRNA expression. (D-F) Direct impact of cytokine signaling inhibition on pancreatic cancer stem cell propagation. Sphere forming ability *in vitro* and tumor propagation *in vivo* of KP^{fl}C cells following shRNA knockdown of cytokine/immune signals (IL10/IL10rb, IL34/Csf1r). Sphere formation, n=3-6 per condition; flank tumor transplant, n=4 per condition. (G-H) Impact of shIL10RB on human pancreatic cancer cell sphere formation (G) and *in vivo* tumor propagation (H). Sphere formation, n=3; flank tumor transplant, n=4 per condition. Data represented as mean +/- S.E.M. * p<0.05, ** p<0.01, *** p<0.001 by Student's t-test or One-way ANOVA.

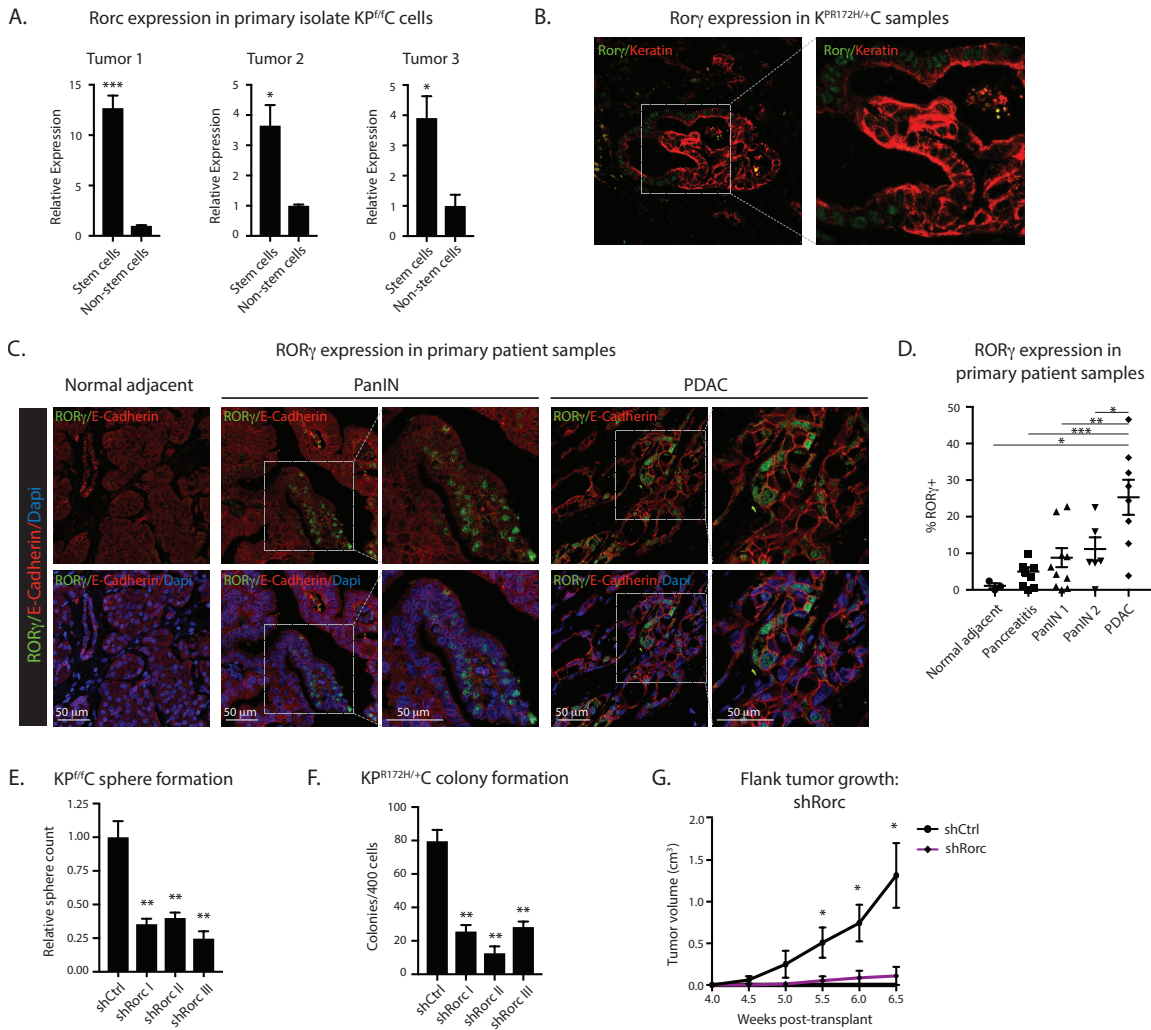


Figure 3.5. The immuno-regulatory gene ROR γ is a critical dependency of PDAC propagation. (A) Relative gene expression of mRorc in primary isolated stem and non-stem cells from 3 independent REM2- $KP^{fl/c}$ tumors. **(B)** Representative images of ROR γ expression in $KP^{R172H/+}$ C tumors. ROR γ (green), Keratin (red), Dapi (blue). **(C)** Representative images of ROR γ expression in normal adjacent human pancreas (left), PanINs (middle), and PDAC (right). ROR γ (green), E-Cadherin (red), Dapi (blue). **(D)** Quantification of ROR γ expression frequency in patient samples. Normal adjacent, n=3; pancreatitis, n=8; PanIN 1, n=10; PanIN 2, n=6; PDAC, n=8. **(E-G)** Functional impact of ROR γ inhibition on $KP^{fl/c}$ (E, G) and $KP^{R172H/+}$ C (F) tumor growth. Sphere forming capacity (E, F) and *in vivo* tumor propagation (G) following shRorc knockdown. Sphere formation, n=3 per shRNA; flank tumor transplant, n=4 per condition.

analysis revealed that ROR γ sites were preferentially enriched in chromatin regions uniquely open in stem cells relative to non-stem cells ($p=0.0087$, **Figure Supplement 3.5B**) and in open chromatin regions that corresponded with high gene expression in stem cells ($p=0.0032$, **Figure Supplement 3.5B**). These findings are consistent with the possibility that ROR γ may be important in controlling gene expression programs that are important for defining a stem cell state in pancreatic cancer.

ROR γ was an unanticipated dependency as it is a nuclear hormone receptor that has been predominantly studied in the context of T cell differentiation and T helper 17 (Th17) fate⁵; consistent with this, it mapped to both the hijacked cytokine signaling/immune subnetwork and the nuclear receptor/metabolism subnetwork (**Figure 3.2E**). Ror γ expression was low in normal murine pancreas (data not shown), but increased in KP^{ff}C tumors and largely overlapped with stem cell populations (**Figure 3.5A**). Ror γ was also expressed in tumor cells of KP^{R172H/+}C tumors by immunohistochemistry (**Figure 3.5B**) suggesting that it was not limited to one particular model of pancreatic cancer. Importantly Ror γ expression in both mouse models was predictive of expression in human pancreatic cancer: thus while ROR γ was low in normal human pancreas and pancreatitis samples, its expression increased significantly in epithelial tumor cells with progression (**Figures 3.5C-D, Figure Supplement 5C**). We used shRNA-mediated knockdown to confirm the role of ROR γ identified by the genetic CRISPR-based screen. ROR γ loss led to a 3-4 fold decrease in stem cell sphere formation *in vitro* in KP^{ff}C cells (**Figure 3.5E**) and a 3-6 fold decrease in KP^{R172H/+}C cells (**Figure 3.5F**); further, KP^{ff}C tumor cells lacking ROR γ showed a striking defect in tumor initiation and propagation *in vivo*, with an 11-fold reduction in final tumor volume (**Figure 3.5G**).

To understand the mechanism by which ROR γ could influence PDAC stem cells, we performed RNA-sequencing analysis of low-passage KP^{ff}C cells that had been transduced with shRNA targeting either Rorc or control sequence. Of the genes downregulated with loss of ROR γ , a large fraction (~26%) contained ROR γ binding motifs in associated promoter or enhancer regions marked by H3K27ac, suggesting they may be direct downstream targets of ROR γ (**Figure 3.6A**). Interestingly, nearly 28% of stem cell super-enhancer linked genes were downregulated in cells lacking ROR γ (**Figure 3.6A**). Further, ROR γ binding sites were disproportionately present in stem cell super-enhancers (**Figure 3.6B**), suggesting ROR γ may preferentially control a super-enhancer network in stem cells. These super-enhancer-associated stem cell genes that may be regulated by ROR γ included potent oncogenic signals that can control cell fate such as

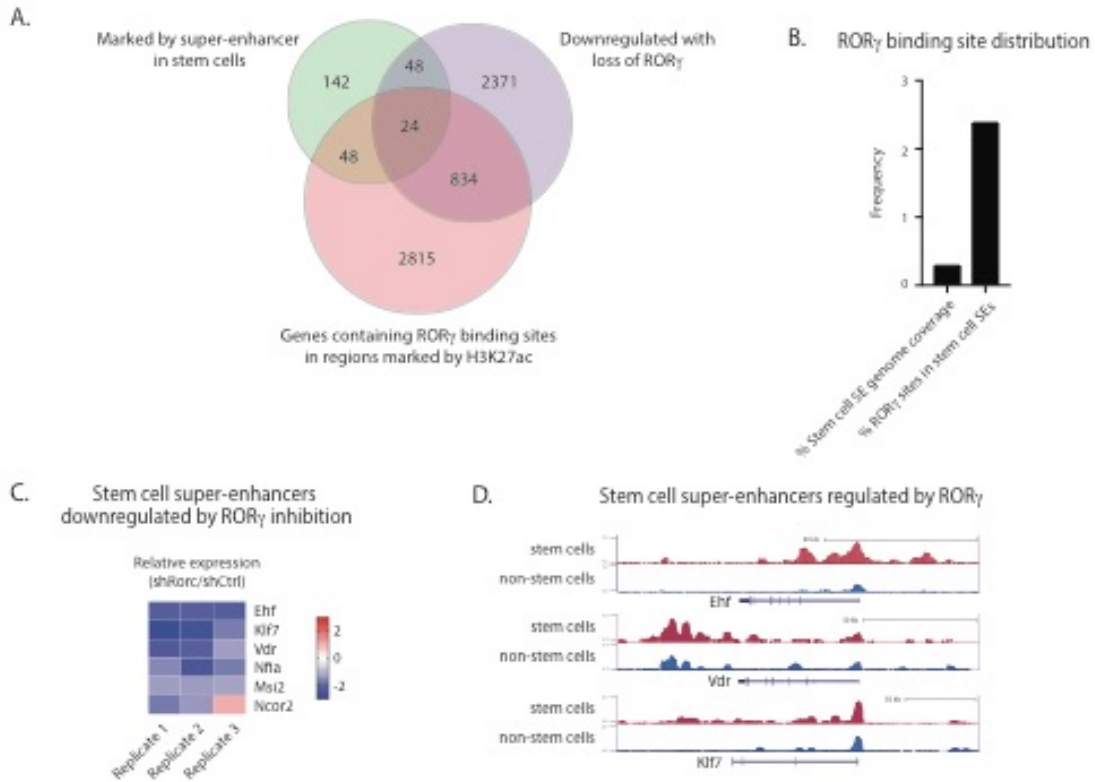


Figure 3.6. $ROR\gamma$ controls expression of super-enhancer associated oncogenes. (A) Venn diagram of genes downregulated with loss of $ROR\gamma$ (purple, 3277), genes associated with open chromatin regions containing $ROR\gamma$ binding sites (red, 3721), and genes marked by stem cell-specific super-enhancers (green, 262). (B) Analysis of $ROR\gamma$ binding site distribution: frequency of $ROR\gamma$ binding sites in stem cell-specific super-enhancers (right) and percent of genome comprised of stem cell-specific super-enhancers (left). (C) Heat map of relative RNA expression of genes with reduced expression in *Rorc*-depleted cells compared to control. Red, over-represented; blue, under-represented; color denotes fold change from shCtrl cells (heat map represents technical triplicate). (D) H3K27ac ChIP-seq read counts for genes marked by super-enhancers in stem cells that are downregulated following $ROR\gamma$ inhibition in $KP^{fl/c}$ cells.

Msi2, Klf7, Ehf, and Vdr (**Figures 3.6C-D**). Taken together, these data suggest that ROR γ is an upstream regulator of a powerful oncogenic effector network controlled by super-enhancers in PDAC stem cells.

The finding that ROR γ was a key dependency in pancreatic cancer was particularly exciting, as multiple inhibitors have been developed to target this pathway in autoimmune disease⁶⁶. Pharmacologic blockade of ROR γ using the reverse agonist SR2211⁶⁷ led to a ~3-fold decrease in sphere formation in KP^{ff}C cells (**Figure 3.7A**) and colony formation in KP^{R172H/+}C (**Figure 3.7B**). SR2211 was also effective in blocking KP^{ff}C cancer organoid propagation (**Figures 3.7C-D**). To assess the impact of the inhibitor *in vivo*, SR2211 alone or in combination with the standard of care chemotherapy gemcitabine was delivered to immunocompetent mice bearing established flank tumors derived from KP^{ff}C cells (**Figure 3.7E**). Combination therapy led to a 6-fold drop in total cell count and a 9.5-fold drop in total tumor cells (**Figures 3.7F-G**). Importantly, SR2211 effectively depleted cancer stem cells *in vivo*; while gemcitabine alone had no impact on cancer stem cell burden, SR2211 led to a 3-fold loss in stem cell content, and SR2211 in combination with gemcitabine led to an 11-fold loss (**Figure 3.7H**). Collectively, these data demonstrate that ROR γ is an essential dependency of pancreatic cancer stem cells and suggest that its inhibition may synergize with chemotherapy to more effectively control advanced desmoplastic tumors that are normally refractory to therapy.

To visualize whether ROR γ blockade impacts tumor progression by targeting stem cells, SR2211 was delivered into REM2-KP^{ff}C mice with late-stage autochthonous tumors and responses subsequently tracked via live imaging. In vehicle-treated mice, large stem cell clusters could be readily identified throughout the tumor based on GFP expression driven by the Msi reporter (**Figures 3.7I-J**). SR2211 led to a striking depletion of the majority of large stem cell clusters within 1 week of treatment (**Figures 3.7I-J**), with no increased necrosis observed in surrounding tissues. This provided a unique spatio-temporal view of the impact of ROR γ signal inhibition *in vivo*, and suggested that stem cell depletion is an early consequence of ROR γ blockade. Further, ROR γ blockade alone led to improved overall survival in autochthonous, tumor-bearing KP^{ff}C survival. While all 50% of vehicle treated mice succumbed to disease by 10 weeks of age, 100% of mice that received SR2211 remained alive (**Figure 3.7K**).

To explore the functional relevance of ROR γ to human pancreatic cancer, we inhibited ROR γ both genetically and through pharmacologic inhibitors. CRISPR based disruption of ROR γ using 5 independent

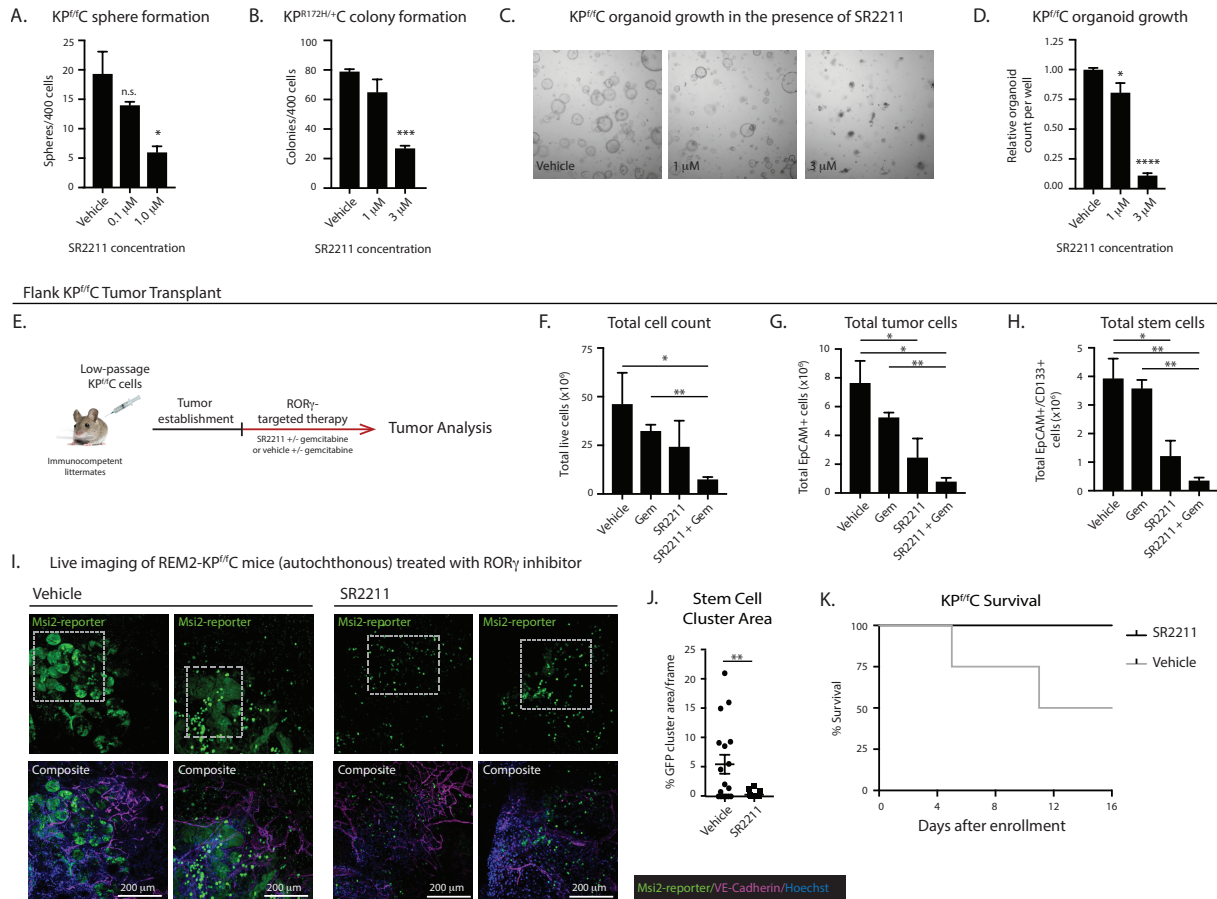


Figure 3.7. Pharmacologic blockade of ROR γ depletes pancreatic cancer stem cells.

(A-B) Sphere forming capacity of KP^{fl/c} cells (A) and colony forming capacity of KP^{R172H/+C} (B) in the presence of the ROR γ inverse agonist SR2211 or vehicle (n=3 per condition). (C-D) Representative images (C) and quantification (D) of KP^{fl/c} organoid growth in the presence of SR2211 or vehicle (n=3 per condition). (E) Schematic of strategy for analysis of flank tumor-bearing mice treated with gemcitabine or vehicle in combination with SR2211 or vehicle. (F-H) Analysis of flank tumor-bearing mice treated for 3 weeks. Total live cells (F), total EpCAM+ tumor epithelial cells (G), and total EpCAM+/CD133+ stem cells (H) (n=4 for vehicle, n=2 for vehicle + gemcitabine, n=4 for SR2211, n=3 for SR2211 + gemcitabine). (I) Live imaging of REM2-KP^{fl/c} mice with established tumors treated with vehicle or SR2211 for 8 days (n=2 per condition). Msi2-reporter (green), VE-Cadherin (magenta), Hoechst (blue); Msi2-reporter+ stem cells, gray box. (J) Quantification of stem cell clusters from REM2-KP^{fl/c} live imaging (n=2 per condition; 6-10 frames analyzed per mouse). (K) Survival of KP^{fl/c} mice at 10.5 weeks of age treated with either vehicle or SR2211 (n=4 per condition). Data represented as mean +/- S.E.M. * p<0.05, ** p<0.01, *** p<0.001 by Student's t-test or One-way ANOVA.

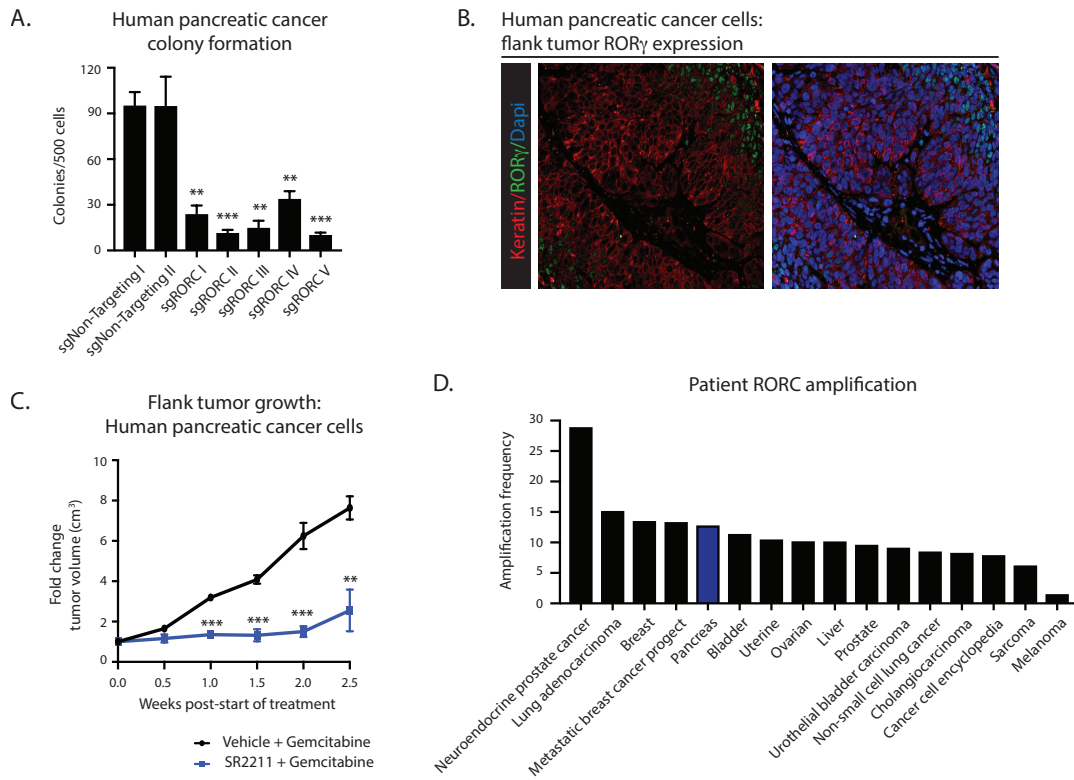


Figure 3.8. ROR γ is amplified in and required for human pancreatic cancer growth. (A) Colony formation of human pancreatic tumor cells following CRISPR mediated knockdown out RORC (sgRORC I-V) or non-targeting sequences (I-II). **(B)** Representative image of ROR γ expression in human pancreatic flank tumors. ROR γ (green), Keratin (red), Dapi (blue). **(C)** Flank tumor growth of human pancreatic cancer cells in immunocompromised mice treated with gemcitabine with either vehicle (black) or SR2211 (blue) (n=4 per condition). **(D)** Frequency of RORC amplification detected in cancer patients (cBioportal).

guides led to a ~3 to 9-fold loss of colony formation (**Figure 3.8A**). When transplanted into immunocompromised mice, human PDAC cells formed tumors with ROR γ expression in a sub-fraction in tumor cells (**Figure 3.8B**), which reflected expression patterns in primary patient samples (**Figure 3.5C**). To test if ROR γ inhibition could block human tumor growth *in vivo*, we transplanted human PDAC cells into the flank region of immunocompromised mice and allowed tumors to become palpable before beginning treatment. Compared to vehicle-treatment, SR2211 delivery was highly effective, and tumor growth was essentially extinguished with a nearly 6-fold reduction in growth rate in mice receiving SR2211 (**Figure 3.8C**). These data are particularly exciting in light of the fact that analysis of the genomic makeup of pancreatic cancer patients revealed systematic amplification of RORC in ~12% pancreatic cancer patients (**Figure 3.8D**). These data raise the intriguing possibility that RORC amplification can serve as a biomarker for patients who may be particularly responsive to RORC inhibition.

Discussion

It is an unfortunate truth that the most common outcome for pancreatic cancer patients following a response to cytotoxic therapy is not cure, but eventual disease progression and death driven by drug resistant stem cell-enriched populations^{4,68,69}. The work we report here has allowed us to develop a comprehensive molecular map of the core dependencies of pancreatic cancer stem cells by integrating their epigenetic, transcriptomic and functional genomic landscape. This analysis could be invaluable as a resource for understanding therapeutic resistance and relapse, and for discovering new vulnerabilities in pancreatic cancer. To this end, the MEGF family of orphan receptors represent a potentially actionable family of adhesion GPCRs, as this class of signaling receptors have been considered druggable in cancer and other diseases⁷⁰. Importantly our epigenetic analysis revealed a significant relationship between super-enhancer-associated genes and functional dependencies in stem cell conditions; stem cell-unique super-enhancer associated genes were ~3.5-fold more likely to drop out in the CRISPR screen in stem cell conditions compared to super-enhancer associated genes in non-stem cells (data not shown). This provides additional evidence for the epigenetic and transcriptomic link to functional dependencies in cancer stem cells, and further supports previous findings that super-enhancer linked genes may be more important for maintaining the cell state and more sensitive to perturbation³¹.

From the screens presented here, we identified an unexpected dependence of KP^{fl}C stem cells on inflammatory and immune mediators, such as the CSF1R/IL-34 axis and IL-10R signaling. While these have been previously thought to act primarily on immune cells in the microenvironment^{55,56}, our data suggest that stem cells may have evolved to co-opt this cytokine-rich milieu, allowing them to resist effective immune-based elimination. These findings also suggest that agents targeting CSF1R, which are under investigation for pancreatic cancer⁷¹, may act not only on the tumor microenvironment but also directly on pancreatic epithelial cells themselves. Our studies also raise the possibility that therapies designed to activate the immune system to attack tumors may have effects on tumor cells directly: just as we have learned chemotherapy can kill tumor cells but may also impair the immune system, therapies designed to activate the immune system such as IL-10 may also promote the growth of tumor cells. This dichotomy of action will need to be considered in order to better optimize immunomodulatory treatment strategies.

A major new discovery driven by the network map was the identification of ROR γ as a key immunoregulatory pathway hijacked in pancreatic cancer. Prior work implicating ROR γ in prostate cancer⁷² suggests that this pathway may not be restricted to pancreatic cancer but may be more broadly utilized in other epithelial cancers. Surprisingly, although cytokines such as IL17, IL21, IL22, and CSF2 are known targets of ROR γ in Th17 cells, none of these were downregulated in Rorc-deficient pancreatic tumor cells, suggesting that ROR γ has unique context specific targets in pancreatic cancer relative to Th17 cells. Indeed our analyses suggest that ROR γ is controlling a set of potent oncogenes that are marked by super-enhancers in stem cells, many of which are also regulators of transcription. This strongly suggests that ROR γ may be critical in defining the stem cell state in pancreatic cancer.

Finally, one particularly exciting aspect of this work is the possibility that ROR γ represents a potential therapeutic target for pancreatic cancer. Our data suggests that while ROR γ inhibitors alone deplete cancer stem cells *in vivo*, combination ROR γ therapy synergizes with standard induction chemotherapy, leading to a deeper depletion in total tumor burden and cancer stem cell content. Given inhibitors of ROR γ are currently in Phase II trials for autoimmune diseases⁶⁵, our findings suggest that repurposing of these agents as pancreatic cancer therapies warrants further investigation.

METHODS

Mice. REM2 ($Msi2^{eGFP/+}$) reporter mice were generated as previously described⁴; all of the reporter mice used in experiments were heterozygous for the *Msi2* allele. The LSL-Kras G12D mouse, B6.129S4-Kras^{tm4TyjJ} (Stock No: 008179) and the p53flox/flox mouse, B6.129P2- Trp53^{tm1Bm/J} (Stock No: 008462), were purchased from The Jackson Laboratory. Dr. Maike Sander provided Ptf1a-Cre mice as previously described³⁶. Mice were bred and maintained in the animal care facilities at the University of California San Diego. All animal experiments were performed according to protocols approved by the University of California San Diego Institutional Animal Care and Use Committee. No sexual dimorphism was noted in all mouse models. Therefore, males and females were equally used for experimental purposes and both sexes are represented in all data sets.

Tissue dissociation, cell isolation, and analysis. (A) Mouse pancreatic tumors were washed in MEM (Gibco, Life Technologies) and cut into 1-2 mm pieces immediately following resection. Tumor pieces were collected into a 50 ml Falcon tube containing 10 ml Gey's balanced salt solution (Sigma), 5 mg Collagenase P (Roche), 2 mg Pronase (Roche), and 0.2 μ g DNase I (Roche). Samples were incubated for 20 minutes at 37°C, then pipetted up and down 10 times and returned to 37°C. After 15 more minutes, samples were pipetted up and down 5 times, then passaged through a 100 μ m nylon mesh (Corning). Red blood cells were lysed using RBC Lysis Buffer (eBioscience) and the remaining tumor cells were washed, then resuspended in HBSS (Gibco, Life Technologies) containing 2.5% FBS and 2 mM EDTA for staining, FACS analysis, and cell sorting. Analysis and cell sorting were carried out on a FACSAria III machine (Becton Dickinson), and data were analyzed with FlowJo software (Tree Star). (B) For analysis of cell surface markers by flow cytometry, 5×10^5 cells were resuspended in HBSS containing 2.5% FBS and 2 mM EDTA, then stained with FC block followed by 0.5 μ l each antibody. The following antibodies were used: rat anti-mouse EpCAM-APC (eBioscience), rat anti-mouse CD133-PE (eBioscience), and rat anti-mouse CD45-PE and PE/Cy7 (eBioscience).

Human and mouse pancreatic cancer cell lines. (A) Mouse primary pancreatic cancer cell lines were

established from end-stage WT- and REM2-KP^{fl/c} mice as follows: tumors were isolated and dissociated into single cell suspension as described above, then plated in 1x DMEM containing 10% FBS, 1x pen/strep, and 1x non-essential amino acids. At the first passage, cells were collected and resuspended in HBSS (Gibco, Life Technologies) containing 2.5% FBS and 2 mM EDTA, then stained with FC block followed by 0.2 μ g/10⁶ cells anti-EpCAM APC (eBioscience). EpCAM⁺ tumor cells were sorted then re-plated for at least one additional passage. Functional studies were performed using cell lines between passage 2 and passage 6. (B) MIA PaCa-2 human pancreatic cancer cells were purchased from ATCC; FG and AA0779E human pancreatic cancer cell lines were provided by Dr. Andrew Lowy. Cell lines were cultured in 1x DMEM (Gibco, Life Technologies) containing 10% FBS, 1x pen/strep (Gibco, Life Technologies), and 1x non-essential amino acids (Gibco, Life Technologies).

Pancreatic tumorsphere formation assay. Pancreatic tumorsphere formation assays were performed on pancreatic tumor cells modified from Rovira, et al⁴⁸. Briefly, low-passage (<6 passages) WT or REM2-KP^{fl/c} cell lines, or human pancreatic cancer cell lines, were infected with lentiviral particles containing shRNAs; positively infected (red) cells were sorted 72 hours after transduction. 100-300 infected cells were suspended in 100 μ l DMEM F-12 (Gibco, Life Technologies) containing 1x B-27 supplement (Gibco, Life Technologies), 3% FBS, 100 μ M B-mercaptoethanol (Gibco, Life Technologies), 1x non-essential amino acids (Gibco, Life Technologies), 1x N2 supplement (Gibco, Life Technologies), 20 ng/ml EGF (Gibco, Life Technologies), 20 ng/ml bFGF₂ (Gibco, Life Technologies), and 10 ng/ml ESGRO mLIF (Thermo Fisher). Cells in media were plated in 96-well ultra-low adhesion culture plates (Costar) and incubated at 37°C for 7 days.

Organoid culture assays. (A) Limiting dilution assay in organoid culture conditions. Tumors from 10-12 week old end stage REM2-KP^{fl/c} mice were harvested and dissociated into a single cell suspension as described above. Tumor cells were stained with FC block then 0.2 μ g/10⁶ cells anti-EpCAM APC (eBioscience). REM2⁺/EpCAM⁺ (stem) and REM2⁻/EpCAM⁺ (non-stem) cells were sorted, resuspended in 20 μ l Matrigel (BD Biosciences, 354230) at indicated doses, and plated as a dome in a pre-warmed 48 well plate. After incubation at 37°C for 5 min, domes were covered with 300 μ l PancreaCult Organoid

Growth Media (Stemcell Technologies). Organoids were imaged and quantified 6 days later. Limiting dilution analysis was performed as previously described⁷³. (B) Organoids from REM2-KP^{fl}C were passaged at ~1:2 as previously described³⁷. Briefly, organoids were isolated using Cell Recovery Solution (Corning 354253), then dissociated using Accumax Cell Dissociation Solution (Innovative Cell Technologies AM105), and plated in 20 μ l matrigel (BD Biosciences, 354230) domes on a pre-warmed 48-well plate. After incubation at 37°C for 5 min, domes were covered with 300 μ l PancreaCult Organoid Growth Media (Stemcell Technologies). SR2211 (Cayman Chemicals 11972) was resuspended in DMSO at 20 mg/ml, diluted 1:10 in 0.9% NaCl containing 0.2% acetic acid, and further diluted in PancreaCult Organoid Media (Stemcell Technologies) to the indicated dilutions. Organoids were grown in the presence of vehicle or SR2211 for 4 days, then imaged and quantified. (C) Primary patient organoids were provided by Andrew Lowy, and passaged and maintained as previously described³⁷. Briefly, organoids were isolated using Cell Recovery Solution (Corning 354253), then dissociated into single cell suspension with TrypLE Express (ThermoFisher 12604) supplemented with 25 μ g/ml DNase I (Roche) and 14 μ M Rho Kinase Inhibitor (Y-27632, Sigma). Cells were split ~1:2 into 20 μ l domes plated on pre-warmed 48 well plates. Domes were incubated at 37°C for 5 min, then covered with human complete organoid feeding media³⁷ without Wnt3a-conditioned media. SR2211 was prepared as described in (B), added at indicated doses, and refreshed every 3 days. Organoids were grown in the presence of vehicle or SR2211 for 7 days, then imaged and quantified. Organoids were counted using ImageJ 1.51s software.

RNA-seq, data analysis, and visualization

Stem and non-stem tumor cell isolation followed by RNA-sequencing: Tumors from 10-12 week old REM2-KP^{fl}C mice were harvested and dissociated into a single cell suspension as described above. Tumor cells were stained with FC block then 0.2 μ g/10⁶ cells anti-EpCAM APC (eBioscience). 70,00-100,00 REM2+/EpCAM+ (stem) and REM2-/EpCAM+ (non-stem) cells were sorted and total RNA was isolated using RNeasy Micro kit (Qiagen). Total RNA was assessed for quality using an Agilent Tapestation, and all samples had RIN \geq 7.9. RNA libraries were generated from 65 ng of RNA using Illumina's TruSeq Stranded mRNA Sample Prep Kit following manufacturer's instructions, modifying the shear time to 5 minutes. RNA libraries were multiplexed and sequenced with 50 basepair (bp) single end reads (SR50) to a depth of

approximately 30 million reads per sample on an Illumina HiSeq2500 using V4 sequencing chemistry.

RNA-seq analysis: RNA-seq fastq files were processed into transcript-level summaries using *kallisto*, an ultrafast pseudo-alignment algorithm with expectation maximization⁷⁴. Transcript-level summaries were processed into gene-level summaries by adding all transcript counts from the same gene. Gene counts were normalized across samples using *DESeq* normalization⁷⁵, and the gene list was filtered based on mean abundance, which left 13,787 genes for further analysis. Differential expression was assessed with an *R* package *limma*⁷⁶ applied to log₂-transformed counts. Statistical significance of each test was expressed in terms of local false discovery rate *lfd*⁷⁷ using the *limma* function *eBayes*⁷⁸. *lfd*, also called posterior error probability, is the probability that a particular gene is not differentially expressed, given the data.

Cell state analysis: For cell state analysis, Gene Set Enrichment Analysis (GSEA)⁴⁰ was performed with the Bioconductor GSVA⁴¹ and the Bioconductor GSVAdata c2BroadSets gene set collection, which is the C2 collection of canonical gene sets from MsigDB3.0⁴⁰. GSEA was performed with the following parameters: mx.diff=TRUE, verbose=TRUE, parallel.sz=1, min.sz=5, max.sz=500, naseq=F.

ChIP-seq for histone H3K27ac

Stem and non-stem tumor cell isolation followed by H3K27ac ChIP-sequencing: 70,000 REM2+/EpCAM+ (stem) and REM2-/EpCAM+ (non-stem) cells were freshly isolated as described above. ChIP was performed as described previously⁷⁹. Cells were pelleted by centrifugation and crosslinked with 1% formalin in culture medium using the protocol described previously⁷⁹. Fixed cells were then lysed in SDS buffer and sonicated on a Covaris S2 ultrasonicator. The following settings were used: Duty factor: 20%, Intensity: 4 and 200 Cycles/burst, Duration: 60 seconds for a total of 10 cycles to shear chromatin with an average fragment size of 200-400 bp. ChIP for H3K27Acetyl was performed using the antibody ab4729 (Abcam, Cambridge, UK) specific to the H3K27Ac modification. Library preparation of eluted chromatin immunoprecipitated DNA fragments was performed using the NEBNext Ultra II DNA library prep kit (E7645S and E7600S- NEB) for Illumina as per the manufacturer's protocol. Library prepped DNA was then subjected to single-end, 75-nucleotide reads sequencing on the Illumina NexSeq500 sequencer at a sequencing depth of 20 million reads per sample.

H3K27ac signal quantification from ChIP-seq data: Pre-processed H3K27ac ChIP sequencing data was aligned to the UCSC mm10 mouse genome using the Bowtie2 aligner (version 2.1.0⁸⁰), removing reads with quality scores of <15. Non-unique and duplicate reads were removed using samtools (version 0.1.16) and Picard tools (version 1.98), respectively. Replicates were then combined using BEDTools (version 2.17.0). Absolute H3K27ac occupancy in stem cells and non-stem cells was determined using the SICER-df algorithm without an input control (version 1.1; ⁸¹), using a redundancy threshold of 1, a window size of 200bp, a fragment size of 150, an effective genome fraction of 0.75, a gap size of 200bp and an E-value of 1000. Relative H3K27ac occupancy in stem cells vs non-stem cells was determined as above, with the exception that the SICER-df-rb algorithm was used.

Determining the overlap between peaks and genomic features: Genomic coordinates for features such as coding genes in the mouse mm10 build were obtained from the Ensembl 84 build (Ensembl BioMart). The observed vs expected number of overlapping features and bases between the experimental peaks and these genomic features (datasets A and B) was then determined computationally using a custom python script, as described in Cole et al., 2017⁸². Briefly, the number of base pairs within each region of A that overlapped with each region of B was computed. An expected background level of expected overlap was determined using permutation tests to randomly generate >1000 sets of regions with equivalent lengths and chromosomal distributions to dataset B, ensuring that only sequenced genomic regions were considered. The overlaps between the random datasets and experimental datasets were then determined, and p values and fold changes were estimated by comparing the overlap occurring by chance (expected) with that observed empirically (observed). This same process was used to determine the observed vs expected overlap of different experimental datasets.

RNA-Seq/ChIP-Seq correlation

Overlap between gene expression and H3K27ac modification: Genes that were up- or down-regulated in stem cells were determined using the Cuffdiff algorithm, and H3K27ac peaks that were enriched or disfavoured in stem cells were determined using the SICER-df-rb algorithm. The H3K27ac peaks were then annotated at the gene level using the 'ChippeakAnno' and 'org.Mm.eg.db' packages in R, and genes with peaks that were either exclusively up-regulated or exclusively down-regulated (termed 'unique up' or

'unique down') were isolated. The correlation between up-regulated gene expression and up-regulated H3K27ac occupancy, or down-regulated gene expression and down-regulated H3K27ac occupancy, was then determined using the Spearman method in R.

Creation of composite plots: Composite plots showing RNA expression and H3K27ac signal across the length of the gene were created. Up- and down-regulated RNA peaks were determined using the FPKM output values from Tophat2, and up- and down-regulated H3K27ac peaks were determined using the SICER algorithm. Peaks were annotated with nearest gene information, and their location relative to the TSS was calculated. Data were then pooled into bins covering gene length intervals of 5%. Overlapping up/up and down/down sets, containing either up- or down-regulated RNA and H3K27ac, respectively, were created, and the stem and non-stem peaks within these sets were plotted in Excel.

Super-enhancer identification. Enhancers in stem and non-stem cells were defined as regions with H3K27ac occupancy, as described in Hnisz et al⁴⁶. Peaks were obtained using the SICER-df algorithm before being indexed and converted to .gff format. H3K27ac Bowtie2 alignments for stem and non-stem cells were used to rank enhancers by signal density. Super-enhancers were then defined using the ROSE algorithm, with a stitching distance of 12.5kb and a TSS exclusion zone of 2.5kb. The resulting super-enhancers for stem or non-stem cells were then annotated at the gene level using the R packages 'ChippeakAnno' and 'org.Mm.eg.db', and overlapping peaks between the two sets were determined using 'ChippeakAnno'. Super-enhancers that are unique to stem or non-stem cells were annotated to known biological pathways using the Gene Ontology (GO) over-representation analysis functionality of the tool WebGestalt⁸³.

Genome-wide CRISPR screen

CRISPR library amplification and viral preparation: The mouse GeCKO CRISPRv2 knockout pooled library^{38,39} was acquired from Addgene (catalog# 1000000052) as two half-libraries (A and B). Each library was amplified according to the Zhang lab library amplification protocol^{38,39} and plasmid DNA was purified using NucleoBond Xtra Maxi DNA purification kit (Macherey-Nagel). For lentiviral production, 24 x T225 flasks were plated with 21×10^6 293T each in 1x DMEM containing 10% FBS. 24 hours later, cells were

transfected with pooled GeCKOv2 library and viral constructs. Briefly, media was removed and replaced with 12.5 ml warm OptiMEM (Gibco). Per plate, 200 μ l PLUS reagent (Life Technologies), 10 μ g library A, and 10 μ g library B was mixed in 4 ml OptiMEM along with 10 μ g pRSV/REV (Addgene), 10 μ g pMDLg/pRRE (Addgene), and 10 μ g pHCMVG (Addgene) constructs. Separately, 200 μ l Lipofectamine (Life Technologies) was mixed with 4 ml OptiMEM. After 5 minutes, the plasmid mix was combined with Lipofectamine and left to incubate at room temperature for 20 minutes, then added dropwise to each flask. Transfection media was removed 22 hours later and replaced with DMEM containing 10% FBS, 5 mM MgCl₂, 1 U/ml DNase (Thermo Scientific), and 20mM HEPES pH 7.4. Viral supernatants were collected at 24 and 48 hours, passaged through 0.45 μ m filter (corning), and concentrated by ultracentrifugation at 20,000 rpm for 2 hours at 4°C. Viral particles were resuspended in DMEM containing 10% FBS, 5 mM MgCl₂, and 20 mM HEPES pH 7.4, and stored at -80°C.

CRISPR screen in primary KP^{fl/c} cells: 3 independent primary REM2-KP^{fl/c} cell lines were established as described above and maintained in DMEM containing 10% FBS, 1x non-essential amino acids, and 1x pen/strep. At passage 3, each cell line was tested for puromycin sensitivity and GeCKOv2 lentiviral titer was determined. At passage 5, 1.6x10⁸ cells from each cell line were transduced with GeCKOv2 lentivirus at an MOI of 0.3. 48 hours after transduction, 1x10⁸ cells were harvested for sequencing (“T0”) and 1.6x10⁸ were re-plated in the presence of puromycin according to previously tested puromycin sensitivity. Cells were passaged every 3-4 days for 3 weeks; at every passage, 5x10⁷ cells were replated to maintain library coverage. At 2 weeks post-transduction, cell lines were tested for sphere forming capacity. At 3 weeks, 3x10⁷ cells were harvested for sequencing (“2D; cell essential genes”), and 2.6x10⁷ cells were plated in sphere conditions as described above (“3D; stem cell essential genes”). After 1 week in sphere conditions, tumorspheres were harvested for sequencing.

DNA isolation, library preparation, and sequencing: Cells pellets were stored at -20°C until DNA isolation using Qiagen Blood and Cell Culture DNA Midi Kit (13343). Briefly, per 1.5x10⁷ cells, cell pellets were resuspended in 2 ml cold PBS, then mixed with 2 ml cold buffer C1 and 6 ml cold H₂O, and incubated on ice for 10 minutes. Samples were pelleted 1300 x g for 15 minutes at 4°C, then resuspended in 1 ml cold buffer C1 with 3 ml cold H₂O, and centrifuged again. Pellets were then resuspended in 5 ml buffer G2 and treated with 100 μ l RNase A (Qiagen 1007885) for 2 minutes at room temperature followed by 95 μ l

Proteinase K for 1 hour at 50°C. DNA was extracted using Genomic-tip 100/G columns, eluted in 50°C buffer QF, and spooled into 300 µl TE buffer pH 8.0. Genomic DNA was stored at 4°C. For sequencing, gRNA's were first amplified from total genomic DNA isolated from each replicate at T0, 2D, 3DV, and 3DG (PCR1). Per 50 µl reaction, 4 µg gDNA was mixed with 25 µl KAPA HiFi HotStart ReadyMIX (KAPA Biostystems), 1 µM reverse primer1, and 1 µM forward primer1 mix (including staggers). Primer sequences are available upon request. After amplification (98°C 20 seconds, 66°C 20 seconds, 72°C 30 seconds, × 22 cycles), 50 µl of PCR1 products were cleaned up using QIAquick PCR Purification Kit (Qiagen). The resulting ~200bp products were then barcoded with Illumina Adaptors by PCR2. 5 µl of each cleaned PCR1 product was mixed with 25 µl KAPA HiFi HotStart ReadyMIX (KAPA Biostystems), 10 µl H₂O, 1 µM reverse primer2, and 1 µM forward primer2. After amplification (98°C 20 seconds, 72°C 45 seconds, × 8 cycles), PCR2 products were gel purified, and eluted in 30 µl buffer EB. Final concentrations of the desired products were determined and equimolar amounts from each sample was pooled for Next Generation Sequencing.

Processing of the CRISPR screen data: Sequence read quality was assessed using fastqc (<http://www.bioinformatics.babraham.ac.uk/projects/fastqc/>). Prior to alignment, 5' and 3' adapters flanking the sgRNA sequences were trimmed off using cutadapt v1.11⁸⁴ with the 5'-adapter TCTTGTGGAAAGGACGAAACACCG and the 3' adapter GTTTTAGAGCTAGAAATAGCAAGTT, which came from the cloning protocols of the respective libraries deposited on Addgene (<https://www.addgene.org/pooled-library/>). Error tolerance for adapter identification was set to 0.25, and minimal required read length after trimming was set to 10 bp. Trimmed reads were aligned to the GeCKO mouse library using Bowtie2⁸⁰ in the --local mode with a seed length of 11, an allowed seed mismatch of 1 and the interval function set to 'S,1,0.75'. After completion, alignments are classified as either unique, failed, tolerated or ambiguous based on the primary ('AS') and secondary ('XS') alignment scores reported by Bowtie2. Reads with the primary alignment score not exceeding the secondary score by at least 5 points were discarded as ambiguous matches. Read counts were normalized by using the "size-factor" method as described in Love, et al. (2014)⁸⁵ and Li et al. (2014)⁸⁶. All of this was done using implementations in the PinAPL-Py webtool (Spahn, et al. 2017)⁸⁷, with detailed code available at <https://github.com/LewisLabUCSD/PinAPL-Py>.

gRNA growth and decay analysis: We use a parametric method in which the cell population with damaged gene i grows as $N_i(t) = N_i(0)e^{(\alpha_0 + \delta_i)t}$, where α_0 is the growth rate of unmodified cells and δ_i is the change of the growth rate due to the gene deletion. Since the aliquot extracted at each time point is roughly the same and represents only a fraction of the entire population, the observed sgRNA counts n_i do not correspond to N_i directly. The correspondence is only relative: if we define $c_i \equiv n_i / \sum_k n_k$ as the compositional fraction of sgRNA species i , the correspondence is $c_i = N_i / \sum_k N_k$. As a result, the exponential can only be determined up to a multiplicative constant, $e^{-\delta_i t} = A \cdot c_i(0) / c_i(t)$. The constant is determined from the assumption that a gene deletion typically does not affect the growth rate. Mathematically, $1 = A \text{ med}[c_i(0) / c_i(t)]$. We define the statistic that measures the effect of gene deletion as $x_i \equiv e^{-\delta_i t}$ and calculate it for every gene i from

$$x_i = A \frac{c_i(0)}{c_i(t)}.$$

Since we are interested in genes essential for growth, we will perform a single-tailed test for x_i . We collect the three values of x_i , one from each biological replicate, into a vector \mathbf{x}_i . A statistically significant effect will have all three values large (>1) and consistent. If \mathbf{x}_i were to denote position of a point in a three-dimensional space, we would be interested in points that lie close to the body diagonal and far away from the origin. A suitable statistic is $s = (\mathbf{x} \cdot \mathbf{n})^2 - [\mathbf{x} - (\mathbf{x} \cdot \mathbf{n})\mathbf{n}]^2$, where $\mathbf{n} = (1,1,1)/\sqrt{3}$ is the unit vector in the direction of the body diagonal and \cdot denotes scalar product. A q -value (false discovery rate) for each gene is estimated as the number of s -statistics not smaller than s_i expected in the null model divided by the observed number of s -statistics not smaller than s_i in the data. The null model is simulated numerically by permuting gene labels in \mathbf{x}_i for every experimental replicate, independently of each other, repeated 10^3 times.

STRING Interactome Network Analysis: The results from the CRISPR 3DV experiment were integrated with the RNA-seq results using a network approach. We identified likely CRISPR-essential genes by filtering to include genes which had a false-discovery rate corrected p-value of less than 0.5, resulting in 94 genes. We chose a relaxed filter here because the following filtering steps will help eliminate false positives, and our network analysis method helps to amplify weak signals. These genes were further filtered in two ways: first, we included only genes which were expressed in the RNA-seq data (this resulted in 57 genes), and

second, we further restricted by genes which had enriched expression in stem cells by >2 log fold change in the RNA-seq (this resulted in 10 genes). These results are used to seed the network neighborhood exploration. We used the STRING mouse interactome⁵⁰ as our background network, including only high confidence interactions (edge weight > 700). The STRING interactome contains known and predicted functional protein-protein interactions. The interactions are assembled from a variety of sources, including genomic context predictions, high throughput lab experiments, and co-expression databases. Interaction confidence is a weighted combination of all lines of evidence, with higher quality experiments contributing more. The high confidence STRING interactome contains 13,863 genes, and 411,296 edges. Because not all genes are found in the interactome, our seed gene sets are further filtered when integrated with the network. This results in 39 CRISPR-essential, RNA-expressed seed genes, and 5 CRISPR-essential, RNA differentially-expressed seed genes. After integrating the seed genes with the background interactome, we employed a network propagation algorithm to explore the network neighborhood around these seed genes. Network propagation is a powerful method for amplifying weak signals by taking advantage of the fact that genes related to the same phenotype tend to interact⁸⁸. We implement the network propagation method developed in⁴⁹, which simulates how heat would diffuse, with loss, through the network by traversing the edges, starting from an initially hot set of 'seed' nodes. At each step, one unit of heat is added to the seed nodes, and is then spread to the neighbor nodes. A constant fraction of heat is then removed from each node, so that heat is conserved in the system. After a number of iterations, the heat on the nodes converges to a stable value. This final heat vector is a proxy for how close each node is to the seed set. For example, if a node was between two initially hot nodes, it would have an extremely high final heat value, and if a node was quite far from the initially hot seed nodes, it would have a very low final heat value. This process is described by the following (as in Vanunu et al.⁴⁹):

$$F^t = W'F^{t-1} + (1 - \alpha)Y$$

Where F^t is the heat vector at time t, Y is the initial value of the heat vector, W' is the normalized adjacency matrix, and $\alpha \in (0,1)$ represents the fraction of total heat which is dissipated at every timestep. We examine the results of the subnetwork composed of the 500 genes nearest to the seed genes after network propagation. This will be referred to as the 'hot subnetwork'. In order to identify pathways and biological mechanisms related to the seed genes, we apply a clustering algorithm to the hot subnetwork, which

partitions the network into groups of genes which are highly interconnected within the group, and sparsely connected to genes in other groups. We use a modularity maximization algorithm for clustering⁸⁹, which has proven effective in detecting modules, or clusters, in protein-protein interaction networks^{90,91}. These clusters are annotated to known biological pathways using the over-representation analysis functionality of the tool WebGestalt⁸³. We use the 500 genes in the hot subnetwork as the background reference gene set. To display the networks, we use a spring-embedded layout, which is modified by cluster membership (along with some manual adjustment to ensure non-overlapping labels). Genes belonging to each cluster are laid out radially along a circle, to emphasize the within cluster and between cluster connections. VisJS2jupyter⁹² was used for network propagation and visualization. Node color is mapped to the RNAseq log fold change, with down-regulated genes displayed in blue, upregulated genes displayed in red, and genes with small fold changes displayed in gray. Labels are shown for genes which have a log fold change with absolute value greater than 3.0. Seed genes are shown as triangles with white outlines, while all other genes in the hot subnetwork are circles. The clusters have been annotated by selecting representative pathways from the enrichment analysis.

KP^{R172H}C single cell analysis. Freshly harvested tumors from KPC (*LSL-Kras^{G12D/+}; LSL-Trp53^{R172H/+}; Pdx-1-Cre*) mice were subjected to mechanical and enzymatic dissociation using a Miltenyi gentleMACS Tissue Dissociator to obtain single cells. The 10X Genomics Chromium Single Cell Solution was employed for capture, amplification and labeling of mRNA from single cells and for scRNA-Seq library preparation. Sequencing of libraries was performed on a Illumina *HiSeq* 2500 system. Sequencing data was input into the Cell Ranger analysis pipeline to align reads and generate gene-cell expression matrices. Finally, Custom R packages were used to perform gene-expression analyses and cell clustering projected using the t-SNE (t-Distributed Stochastic Neighbor Embedding) clustering algorithm.

scRNA-seq datasets from two independent KPC PDAC tumor tissues generated on 10xGenomics platform were merged and utilized to explore and validate the molecular signatures of the tumor cells under dynamic development. The tumor cells that are used to illustrate the signal of *Il10rb*, *Il34* and *Csf1r* etc. are characterized from the heterogeneous cellular constituents using SuperCT method developed by Dr. Wei Lin and confirmed by the Seurat FindClusters with the enriched signal of *Epcam*, *Krt19* and *Prom1* etc. The

tSNE layout of the tumor cells is calculated by Seurat pipeline using the single-cell digital expression profiles.

shRNA lentiviral constructs and production. Short hairpin RNA (shRNA) constructs were designed and cloned into pLV-hU6-mPGK-red vector by Biosettia. The target sequences are listed in Supplementary Table 1. Virus was produced in 293T cells transfected with 4 μg shRNA constructs along with 2 μg pRSV/REV, 2 μg pMDLg/pRRE, and 2 μg pHCMVG constructs. Viral supernatants were collected for two days then concentrated by ultracentrifugation at 20,000 rpm for 2 hours at 4°C.

RT-qPCR analysis. RNA was isolated using RNeasy Micro and Mini kits (Qiagen) and converted to cDNA using Superscript III (Invitrogen). Quantitative real-time PCR was performed using an iCycler (BioRad) by mixing cDNAs, iQ SYBR Green Supermix (BioRad) and gene specific primers. Primer sequences are available in Supplementary Table 2. All real time data was normalized to B2M or Gapdh.

Flank tumor transplantation studies. (A) shRNA-infected pancreatic tumor cell propagation *in vivo*. Cells were infected with lentiviral particles containing shRNAs, then positively infected (red) cells were sorted 72 hours after transduction. 1000 low passage, shRNA-infected KP^{ff}C or 2×10^5 shRNA-infected human pancreatic cancer cells were resuspended in 50 μl culture media, then mixed 1:1 with matrigel (BD Biosciences, 354230). Cells were injected subcutaneously into the left or right flank of 5-8 week-old NOD/SCID recipient mice. Subcutaneous tumor dimensions were measured with calipers 1-2x weekly for 6-8 weeks. (B) Drug-treated KP^{ff}C flank tumors. 2×10^4 low passage REM2-KP^{ff}C tumor cells were resuspended in 50 μl culture media, then mixed 1:1 with matrigel (BD Biosciences, 354230). Cells were injected subcutaneously into the left or right flank of 5-8 week-old non-tumor bearing, immunocompetent littermates. Tumor growth was monitored twice weekly; when tumors reached 0.1-0.3 cm^3 , mice began treatment and were treated for 3 weeks as described below. After 3 weeks of therapy, tumors were removed, weighed, dissociated, and analyzed by flow cytometry. Tumor volume was calculated using the standard modified ellipsoid formula $\frac{1}{2}$ (Length x Width²).

Immunofluorescence staining. (A) Pancreatic cancer tissue from KP^{ffC} mice was fixed in Z-fix (Anatech Ltd, Fisher Scientific) and paraffin embedded at the UCSD Histology and Immunohistochemistry Core at The Sanford Consortium for Regenerative Medicine according to standard protocols. 5 μ m sections were obtained and deparaffinized in xylene. (B) Human pancreas paraffin embedded tissue array was acquired from US Biomax, Inc (BIC14011a). For paraffin embedded mouse and human pancreas tissues, antigen retrieval was performed for 40 minutes in 95-100°C 1x Citrate Buffer, pH 6.0 (eBioscience). Sections were blocked in PBS containing 0.1% Triton X100 (Sigma- Aldrich), 10% Goat Serum (Fisher Scientific), and 5% bovine serum albumin (Invitrogen). (C) Human pancreatic cancer cell lines were suspended in DMEM (Gibco, Life Technologies) supplemented with 50% FBS and adhered to slides by centrifugation at 500 rpm. 24 hours later, cells were fixed with Z-fix (Anatech Ltd, Fisher Scientific), washed in PBS, and blocked with PBS containing 0.1% Triton X-100 (Sigma-Aldrich), 10% Goat serum (Fisher Scientific), and 5% bovine serum albumin (Invitrogen). All incubations with primary antibodies were carried out overnight at 4°C. Incubation with Alexafluor-conjugated secondary antibodies (Molecular Probes) was performed for 1 hour at room temperature. DAPI (Molecular Probes) was used to detect DNA and images were obtained with a Confocal Leica TCS SP5 II (Leica Microsystems). The following primary antibodies were used: chicken anti-GFP (Abcam, ab13970) 1:500; rabbit anti-ROR γ (Thermo Fisher, PA5-23148) 1:500, mouse anti-E-Cadherin (BD Biosciences, 610181).

In vivo and in vitro drug therapy. The ROR γ inverse agonists SR2211 (Cayman Chemicals, 11972) was resuspended in DMSO at 20 mg/ml, then mixed 1:20 in 8% Tween80-PBS, 1:20 in corn oil, or 1:10 in 0.9% NaCl with 0.2% acetic acid prior to use. Gemcitabine (Sigma, G6423) was resuspended in H₂O at 20 mg/ml, then mixed with PBS prior to use. (A) For in vitro drug studies, low passage (<6 passage) WT- or REM2- KP^{ffC} cells, (<10 passage) $KP^{R172H/+C}$ cells, or human pancreatic cancer cells were plated in non-adherent tumorsphere conditions or Matrigel colony conditions for 1 week in the presence of SR2211 or vehicle. (B) For flank tumor bearing KP^{ffC} littermates, mice were treated with either vehicle (PBS) or gemcitabine (25 mg/kg i.p., 1x weekly) alone, or in combination with vehicle (5% DMSO, 8% Tween80-PBS) or SR2211 (10 mg/kg i.p., daily) for 3 weeks. (C) For immunocompromised mice bearing flank human pancreatic (FG) cells, mice were treated with either vehicle (5% DMSO in corn oil) or SR2211 (10 mg/kg i.p., daily) for 2.5

weeks. All flank tumors were measured 2x weekly and mice were sacrificed if tumors were $>2\text{cm}^3$, in accordance with IACUC protocol. (D) For KP^{flC} autochthonous survival, 8 week old tumor bearing KP^{flC} mice were enrolled in either vehicle (10% DMSO, 0.9% NaCl with 0.2% acetic acid) or SR2211 (20 mg/kg i.p., daily), and treated until moribund.

Tumor imaging. 9.5-10.5 week old REM2- KP^{flC} mice were treated either vehicle or SR2211 (10 mg/kg i.p., daily) for 8 days. For imaging, mice were anesthetized by intraperitoneal injection of ketamine and xylazine (100/20 mg/kg). In order to visualize blood vessels and nuclei, mice were injected retro-orbitally with AlexaFluor 647 anti-mouse CD144 (VE-cadherin) antibody and Hoechst 33342 immediately following anesthesia induction. After 25 minutes, pancreatic tumors were removed and placed in HBSS containing 5% FBS and 2mM EDTA. 80-150 μm images in 1024 x 1024 format were acquired with an HCX APO L20x objective on an upright Leica SP5 confocal system using Leica LAS AF 1.8.2 software. GFP cluster sizes were measure using ImageJ 1.51s software.

cBioportal. RORC genomic amplification data from cancer patients was collected from the Memorial Sloan Kettering Cancer Center cBioPortal for Cancer Genomics (<http://www.cbioportal.org>).

Statistical analysis. Statistical analyses were carried out using GraphPad Prism software version 7.0d (GraphPad Software Inc.). Sample sizes were determined based on the variability of pancreatic tumor models used. Tumor bearing animals within each group were randomly assigned to treatment groups. Data are shown as the mean \pm SEM. Two-tailed unpaired Student's t-tests with Welch's correction or One-way analysis of variance (ANOVA) for multiple comparisons when appropriate were used to determine statistical significance (* $P < 0.05$, ** $P < 0.01$, *** $P < 0.001$, **** $P < 0.0001$).

Data availability. Further information on experimental design is available in the Nature Research Reporting Summary linked to this paper. The datasets generated during and/or analyzed during the current study are available from the corresponding author on reasonable request. H3K27ac ChIP sequencing data have been deposited at NCBI GEO (<https://www.ncbi.nlm.nih.gov/geo/query/acc.cgi?acc=GSE113712>).

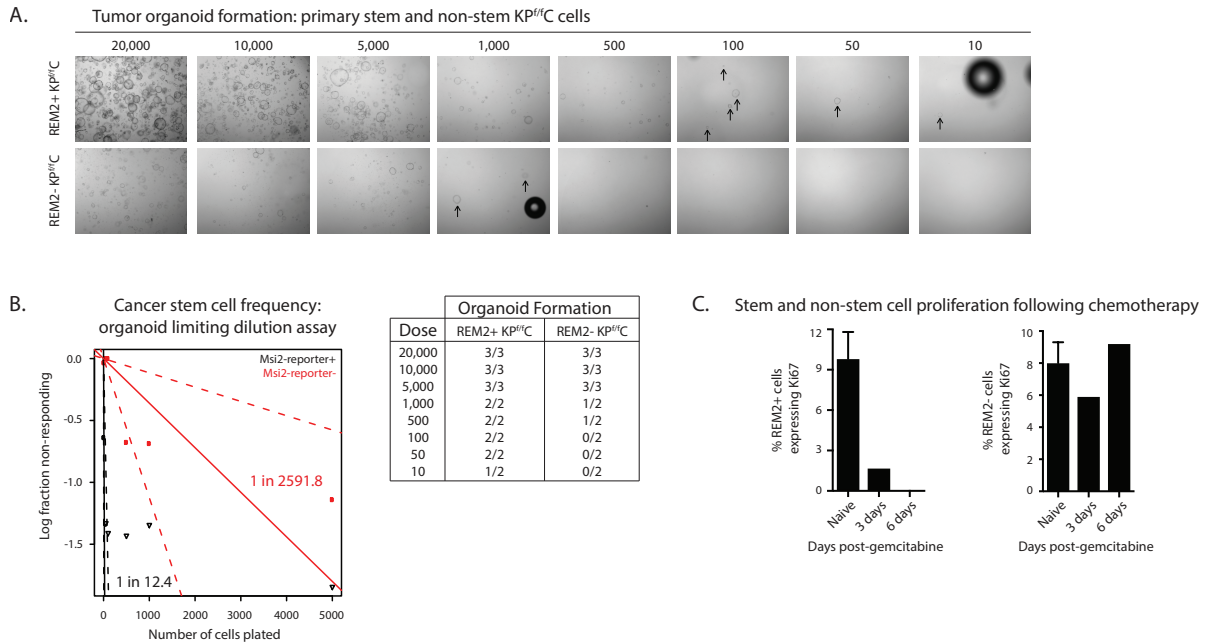


Figure Supplement 3.1. REM2+ tumor cells preferentially drive organoid establishment. (A) Representative images of primary isolated REM2+ and REM2- tumor cells plated in organoid growth conditions. **(B)** Organoid forming frequency of REM2+ (1 in 12.4) and REM2- (1 in 2591.8) tumor cells from limiting dilution analysis. **(C)** Histologic analysis of REM2+ and REM2- tumor cell proliferation frequency (% of cells expressing Ki67) from mice treated with gemcitabine every 3 days.

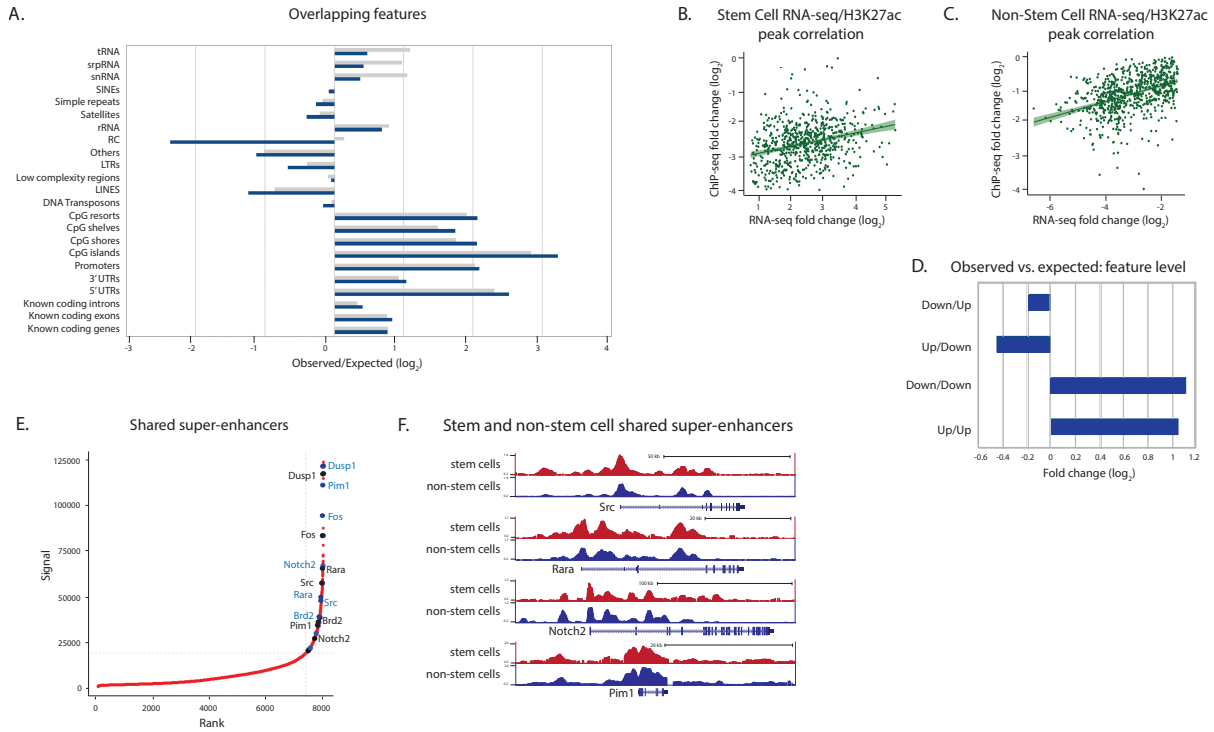


Figure Supplement 3.2. H3K27ac ChIP-seq is concordant with RNA-seq in stem and non-stem cells. (A) Overlap of H3K27ac peaks and genomic features. For each genomic feature, frequency of H3K27ac peaks in stem cells (blue) and non-stem cells (gray) are represented as ratio of observed peak distribution/expected random genomic distribution. (B) Concordance of H3K27ac peaks with RNA expression in stem (B; $p=7.1 \times 10^{-14}$) and non-stem cells (C; $p < 22 \times 10^{-16}$). (C) Ratio of observed/expected overlap in gene expression and H3K27ac enrichment comparing stem and non-stem cells. Down/Up, gene expression enriched in non-stem/H3K27ac enriched in stem; Up/Down, gene expression enriched in stem/H3K27ac enriched in non-stem; Down/Down, both gene expression and H3K27ac enriched in non-stem; Up/Up, both gene expression and H3K27ac enriched in stem. (E) Hockey stick plot of H3K27ac occupancy, ranked by signal density. Super-enhancers in stem and non-stem cells are demarcated by highest ranking and intensity signals, above and right of dotted gray lines. Names of selected genes linked to super-enhancers are annotated (stem, black; non-stem, blue). (F) H3K27ac ChIP-seq read counts across selected genes marked by super-enhancers shared in stem cells (red) and non-stem cells (blue).

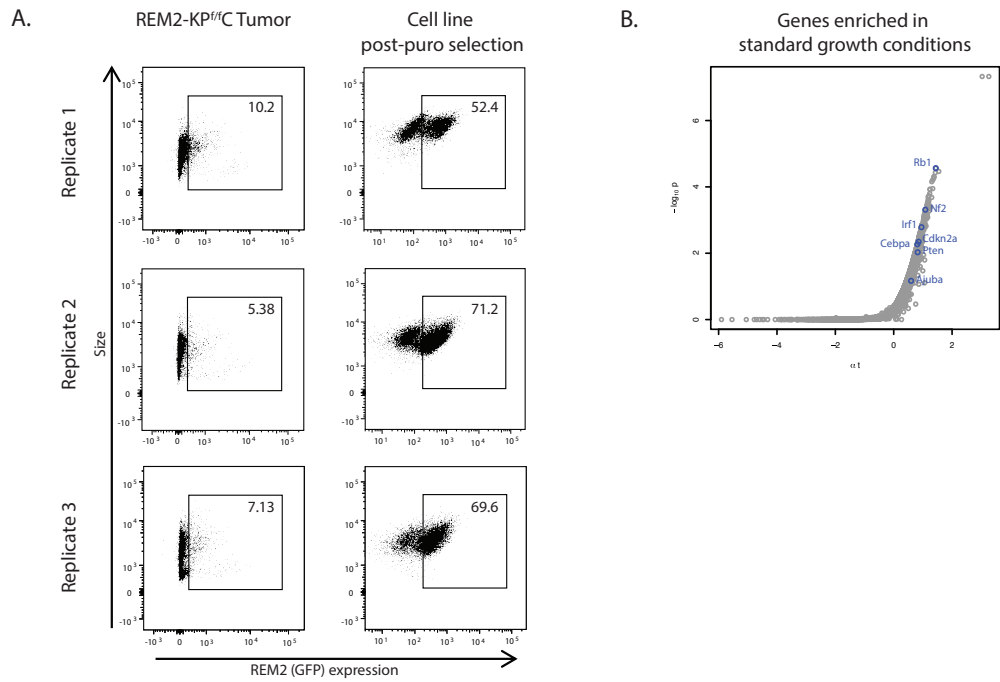


Figure Supplement 3.3. Cell line establishment for CRISPR screen . (A) Establishment of three independent REM2-KP^{fl/c} cell lines from end-stage REM2-KP^{fl/c} mice for genome-wide CRISPR-screen analysis Stem cell content of freshly-dissociated REM2-KP^{fl/c} tumors (A, left), and after puromycin selection in standard growth conditions (A, right). **(B)** Volcano plots of guides enriched for in 2D. Genes indicated on plots, $p < 0.01$.

Novel regulators of cancer stem cells

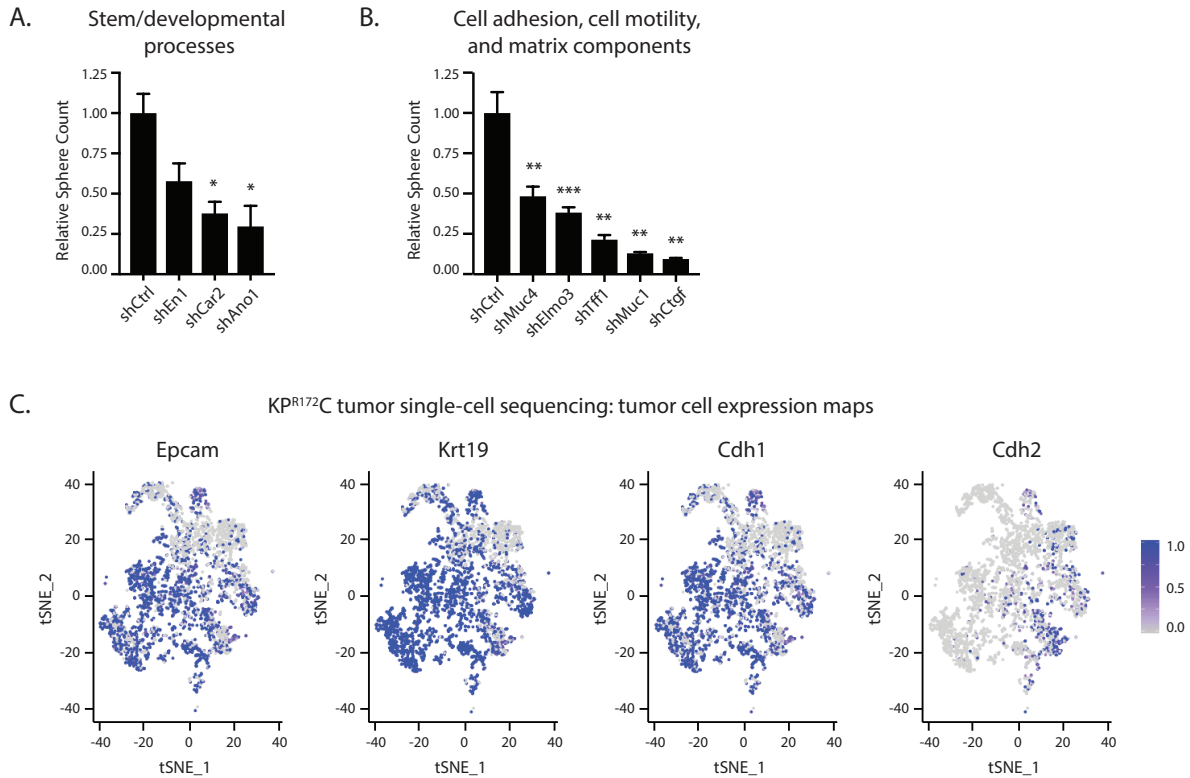
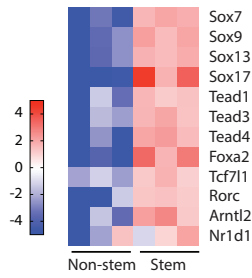


Figure Supplement 3.4. Identification of novel regulators of cancer stem cells. (A-B) Sphere forming capacity of KPR^{fl}C cells following shRNA knockdown. Selected genes involved in stem and developmental processes (A) or cell adhesion, cell motility, and matrix components (B). Data represented as mean +/- S.E.M. * $p < 0.05$, ** $p < 0.01$, *** $p < 0.001$ by Student's t-test or One-way ANOVA. (C) Single cell mRNA expression map of epithelial tumor markers (Epcam, Krt19, and Cdh1) and mesenchymal tumor cells (Cdh2) from KPR^{172H/+}C tumor single-cell sequencing. Color denotes relative mRNA expression.

A. Transcription factors identified in CRISPR screen network



B. ROR γ binding motif analysis

	p-value
"up/up" regions	0.0032
"down/down" regions	0.4842
Unique stem cell enriched H3K27ac	0.0087
Unique non-stem cell enriched H3K27ac	0.889

C. Stromal ROR γ expression in primary patient samples

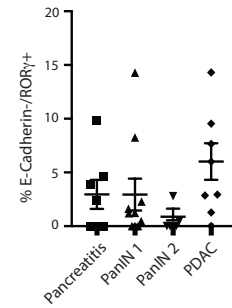


Figure Supplement 3.5. Transcription factors identified in CRISPR interactome. (A) Heat map of relative RNA expression of transcription factors identified in the CRISPR interactome and enriched in KP^{fl/c} stem cells. Red, over-represented; blue, under-represented; color denotes fold change from median values. **(B)** Analysis of ROR γ binding motifs in genomic regions marked by H3K27ac. Up/up, RNA expression and H3K27ac marks enriched in stem cells; down/down, RNA expression and H3K27ac enriched in non-stem cells. **(C)** Immunofluorescent analysis of ROR γ expression in stroma of pancreatitis, PanINs, or PDAC from human tissue samples.

Table 3.1. Selected genes from stem cell networks.

Cell migration/Cell adhesion/Cell matrix interactions

Gene name	RNA-seq fold change (stem/non-stem)	H3K27ac ChIP-seq	CRISPR screens
Sftpd	42.427	Up	-
Tff1	26.019	Stem cell SE	-
Muc4	24.882	Up	-
Crb3	10.083	Up	✓ 3D
Celsr1	9.194	Up	✓ 3D
Cldn6	8.211	Up	✓ 3D
Lama5	8.087	Stem cell SE	
Pard6b	7.549	Stem cell SE	✓✓✓ 3D ✓ 2D
Cldn3	7.254	Stem cell SE	✓ 3D
Celsr2	5.629	Up	-
Pear1	4.417	Up	✓ 3D
Smo	4.202	Up	✓✓✓ 3D
Rhof	1.789	Stem cell SE	✓✓✓ 3D
Lgl1	1.506	Up	✓ 3D
Calm1	-1.239	Stem cell SE	✓ 3D

Development/Pluripotency/Stem cell signals

Gene name	RNA-seq fold change (stem/non-stem)	H3K27ac ChIP-seq	CRISPR screens
Car2	22.3120000	Up	-
Onecut3	19.2840000	Stem SE	-
En1	12.0350000	Up	✓ 2D
Sox4	7.136	N.D.	✓✓✓ 3D
Smo	4.2020000	Up	✓✓✓ 3D
Mapk11	4.032	Stem SE	✓ 3D
Wnt9a	1.562		✓ 3D
Psmc4	1.299	Up	✓✓✓ 2D ✓ 3D
Psmb1	1.275	Up	✓✓✓ 2D ✓ 3D
Foxo1	1.1840000	Up	✓✓✓ 3D
Psmc3	1.045	Up	✓✓✓ 2D ✓ 3D
Psmc7	-1.110	N.D.	✓ 3D

Cytokine signaling/Immune pathways

Gene name	RNA-seq fold change (stem/non-stem)	H3K27ac ChIP-seq	CRISPR screens
Gkn1	39.77	Up	-
Gkn3	29.339	Up	-
Sult1c2	23.634	Up	-
Ii34	6.586	Stem cell SE	-
Akt1	-1.400	Stem cell SE	✓ 3D
Il15	-1.587	Down	✓ 3D

Lipid metabolism/Nuclear receptor pathways

Gene name	RNA-seq fold change (stem/non-stem)	H3K27ac ChIP-seq	CRISPR screens
Sptssb	30.999	Up	-
Rorc	7.598	Up	✓✓✓ 3D
Arntl2	6.592	Up	✓ 3D
Med18	2.077		✓ 3D
Lpin2	1.847	Shared SE	-
Bhlhe41	1.737	Stem cell SE	✓ 3D

Table 3.1. Table shows selected genes from stem cell networks identified by enriched gene expression in stem cells (RNA-seq), preferentially open (H3K27ac ChIP-seq), or essential for growth (CRISPR screens). RNA-seq: fold change indicates expression in stem/non-stem. H3K27ac ChIP-seq: up indicates H3K27ac peaks enriched in stem cells; Stem cell SE, super-enhancer unique to stem cells; Shared SE, super-enhancer in both stem and non-stem cells; N.D., H3K27ac not detected. CRISPR screens; 2D, conventional growth conditions; 3D, stem cell conditions; ✓✓✓, p<0.005; ✓, gene ranks in top 10% of depleted guides (p<0.049 for 2 p<0.092 for 3D); -, gene not in top 10% of depleted.

Table 3.2. Novel Drug Targets in Pancreatic Cancer

Target	Core program	Known function	Drug/Compound	in vitro sphere formation	in vivo tumor growth
ROR- γ	Immune/cytokine signaling	nuclear receptor	SR2211	✓✓✓✓	✓✓
IL-10	Immune/cytokine signaling	cytokine	AS101	✓✓✓	-
Dusp	Developmental pathways	phosphatase	BCI	✓✓	-
Wnk4	Developmental pathways	serine/threonine kinase	Wnk463	✓✓	ND
Myo5	Cell motility/migration	myosin	Pentabromopseudilin	✓✓	ND
IL-7	Immune/cytokine signaling	cytokine	Anti-IL7	✓	-
CD83	Immune/cytokine signaling	Ig superfamily membrane protein	GC7	✓	ND
Cxcl2	Immune/cytokine signaling	chemokine	Danirixin	-	ND
Drd2/3	Immune/cytokine signaling	dopamine receptor	Eticlopride	-	-

✓✓✓✓: dose response observed; growth suppressed by 8-fold or more relative to control

✓✓✓: dose response observed; growth suppressed between 4-fold and 8-fold relative to control

✓✓: dose response observed; growth suppressed by less than 4-fold relative to control

✓: response observed only at highest drug dose tested

- : no detectable response

ND: not determined

ACKNOWLEDGEMENTS

We are grateful to Olivier Harismendy, Prashant Mali and Kristen Jepsen for advice on the CRISPR screen, Christopher Wright for providing the Ptf1a-Cre mice, and Armin Ahmadi and Kendall Chambers for technical support. N.K.L. received support from T32 GM007752 and a National Research Service Award F31 CA206416; L.P.F received support from T32 GM007752; T.R. was supported by NIH grant R35 CA197699, Stand Up To Cancer–Cancer Research UK–Lustgarten Foundation Pancreatic Cancer Dream Team Research Grant (SU2C-AACR-DT-20-16), and PDAC R01 CA186043. The project described was partially supported by the National Institutes of Health, Grant UL1TR001442. The content is solely the responsibility of the authors and does not necessarily represent the official views of the NIH.

AUTHOR CONTRIBUTIONS

N.K.L designed and performed the CRISPR screen and in vitro and in vivo shRNA validation experiments, isolated cell populations for RNA-seq and ChIP-seq analysis, performed all functional experiments related to ROR-gamma inhibition in vitro and in vivo, performed all histologic analysis, and all live imaging experiments. L.P.F., R.F., N.R., T.G., and L.A.E. provided experimental help; P.S., N.L., K.F., R.S., and S.B.R. performed all bioinformatics analysis related to RNA-seq and CRISPR screen; A.D. (Anagha), and A.D. (Aniruddha) performed ChIP-seq; K.G., N.R., and P.A. performed all analysis related to ChIP-seq; T.I., A.M.L., and P.A. provided experimental advice and comments on the manuscript. N.K.L and T.R. wrote the paper. M.K. helped write the paper. T.R. conceived the project, and planned and guided the research.

DISSERTATION ACKNOWLEDGEMENTS

Chapter 3, in part, has been submitted for publication. Lytle NK, Ferguson LP, Fox RG, Gilroy K, Robertson N, Deshpande A, Rajbhandari N, Gilderman T, Esparza LA, Shima Y, Kritzik M, Spahn P, French R, Lin W, Noel P, Han H, Von Hoff D, Lewis N, Fisch KM, Sasik R, Rosenthal SB, Ideker T, Deshpande A, Lowy AM, Adams P, Reya T. A multiscale map of the stem cell state in pancreatic adenocarcinoma. The dissertation author is the primary author of this work.

REFERENCES

- 1 Hermann, P. C., Huber, S. L., Herrler, T., Aicher, A., Ellwart, J. W., Guba, M., Bruns, C. J. & Heeschen, C. Distinct populations of cancer stem cells determine tumor growth and metastatic activity in human pancreatic cancer. *Cell Stem Cell* **1**, 313-323, doi:10.1016/j.stem.2007.06.002 (2007).
- 2 Mueller, M. T., Hermann, P. C., Witthauer, J., Rubio-Viqueira, B., Leicht, S. F., Huber, S., Ellwart, J. W., Mustafa, M., Bartenstein, P., D'Haese, J. G., Schoenberg, M. H., Berger, F., Jauch, K. W., Hidalgo, M. & Heeschen, C. Combined targeted treatment to eliminate tumorigenic cancer stem cells in human pancreatic cancer. *Gastroenterology* **137**, 1102-1113, doi:10.1053/j.gastro.2009.05.053 (2009).
- 3 Li, C., Heidt, D. G., Dalerba, P., Burant, C. F., Zhang, L., Adsay, V., Wicha, M., Clarke, M. F. & Simeone, D. M. Identification of pancreatic cancer stem cells. *Cancer Res* **67**, 1030-1037, doi:10.1158/0008-5472.CAN-06-2030 (2007).
- 4 Fox, R. G., Lytle, N. K., Jaquish, D. V., Park, F. D., Ito, T., Bajaj, J., Koechlein, C. S., Zimdahl, B., Yano, M., Kopp, J., Kritzik, M., Sicklick, J., Sander, M., Grandgenett, P. M., Hollingsworth, M. A., Shibata, S., Pizzo, D., Valasek, M., Sasik, R., Scadeng, M., Okano, H., Kim, Y., MacLeod, A. R., Lowy, A. M. & Reya, T. Image-based detection and targeting of therapy resistance in pancreatic adenocarcinoma. *Nature* **534**, 407-411, doi:10.1038/nature17988 (2016).
- 5 Ivanov, I., McKenzie, B. S., Zhou, L., Tadokoro, C. E., Lepelley, A., Lafaille, J. J., Cua, D. J. & Littman, D. R. The orphan nuclear receptor ROR γ directs the differentiation program of proinflammatory IL-17+ T helper cells. *Cell* **126**, 1121-1133, doi:10.1016/j.cell.2006.07.035 (2006).
- 6 Nurieva, R., Yang, X. O., Martinez, G., Zhang, Y., Panopoulos, A. D., Ma, L., Schluns, K., Tian, Q., Watowich, S. S., Jetten, A. M. & Dong, C. Essential autocrine regulation by IL-21 in the generation of inflammatory T cells. *Nature* **448**, 480-483, doi:10.1038/nature05969 (2007).
- 7 Conroy, T., Desseigne, F., Ychou, M., Bouche, O., Guimbaud, R., Becouarn, Y., Adenis, A., Raoul, J. L., Gourgou-Bourgade, S., de la Fouchardiere, C., Bennouna, J., Bachet, J. B., Khemissa-Akouz, F., Pere-Verge, D., Delbaldo, C., Assenat, E., Chauffert, B., Michel, P., Montoto-Grillot, C., Ducreux, M., Groupe Tumeurs Digestives of, U. & Intergroup, P. FOLFIRINOX versus gemcitabine for metastatic pancreatic cancer. *N Engl J Med* **364**, 1817-1825, doi:10.1056/NEJMoa1011923 (2011).
- 8 Reya, T., Morrison, S. J., Clarke, M. F. & Weissman, I. L. Stem cells, cancer, and cancer stem cells. *Nature* **414**, 105-111, doi:10.1038/35102167 (2001).
- 9 Hanahan, D. & Weinberg, R. A. Hallmarks of cancer: the next generation. *Cell* **144**, 646-674, doi:10.1016/j.cell.2011.02.013 (2011).
- 10 Nomura, A., Banerjee, S., Chugh, R., Dudeja, V., Yamamoto, M., Vickers, S. M. & Saluja, A. K. CD133 initiates tumors, induces epithelial-mesenchymal transition and increases metastasis in pancreatic cancer. *Oncotarget* **6**, 8313-8322, doi:10.18632/oncotarget.3228 (2015).
- 11 Wellner, U., Schubert, J., Burk, U. C., Schmalhofer, O., Zhu, F., Sonntag, A., Waldvogel, B., Vannier, C., Darling, D., zur Hausen, A., Brunton, V. G., Morton, J., Sansom, O., Schuler, J., Stemmler, M. P., Herzberger, C., Hopt, U., Keck, T., Brabletz, S. & Brabletz, T. The EMT-activator ZEB1 promotes tumorigenicity by repressing stemness-inhibiting microRNAs. *Nat Cell Biol* **11**, 1487-1495, doi:10.1038/ncb1998 (2009).

- 12 Bailey, J. M., Alsina, J., Rasheed, Z. A., McAllister, F. M., Fu, Y. Y., Plentz, R., Zhang, H., Pasricha, P. J., Bardeesy, N., Matsui, W., Maitra, A. & Leach, S. D. DCLK1 marks a morphologically distinct subpopulation of cells with stem cell properties in preinvasive pancreatic cancer. *Gastroenterology* **146**, 245-256, doi:10.1053/j.gastro.2013.09.050 (2014).
- 13 Grosse-Wilde, A., Fouquier d'Herouel, A., McIntosh, E., Ertaylan, G., Skupin, A., Kuestner, R. E., del Sol, A., Walters, K. A. & Huang, S. Stemness of the hybrid Epithelial/Mesenchymal State in Breast Cancer and Its Association with Poor Survival. *PLoS One* **10**, e0126522, doi:10.1371/journal.pone.0126522 (2015).
- 14 Malta, T. M., Sokolov, A., Gentles, A. J., Burzykowski, T., Poisson, L., Weinstein, J. N., Kaminska, B., Huelsken, J., Omberg, L., Gevaert, O., Colaprico, A., Czerwinska, P., Mazurek, S., Mishra, L., Heyn, H., Krasnitz, A., Godwin, A. K., Lazar, A. J., Cancer Genome Atlas Research, N., Stuart, J. M., Hoadley, K. A., Laird, P. W., Noushmehr, H. & Wiznerowicz, M. Machine Learning Identifies Stemness Features Associated with Oncogenic Dedifferentiation. *Cell* **173**, 338-354 e315, doi:10.1016/j.cell.2018.03.034 (2018).
- 15 Spranger, S., Bao, R. & Gajewski, T. F. Melanoma-intrinsic beta-catenin signalling prevents anti-tumour immunity. *Nature* **523**, 231-235, doi:10.1038/nature14404 (2015).
- 16 Cheah, M. T., Chen, J. Y., Sahoo, D., Contreras-Trujillo, H., Volkmer, A. K., Scheeren, F. A., Volkmer, J. P. & Weissman, I. L. CD14-expressing cancer cells establish the inflammatory and proliferative tumor microenvironment in bladder cancer. *Proc Natl Acad Sci U S A* **112**, 4725-4730, doi:10.1073/pnas.1424795112 (2015).
- 17 Rhim, A. D., Oberstein, P. E., Thomas, D. H., Mirek, E. T., Palermo, C. F., Sastra, S. A., Dekleva, E. N., Saunders, T., Becerra, C. P., Tattersall, I. W., Westphalen, C. B., Kitajewski, J., Fernandez-Barrena, M. G., Fernandez-Zapico, M. E., Iacobuzio-Donahue, C., Olive, K. P. & Stanger, B. Z. Stromal elements act to restrain, rather than support, pancreatic ductal adenocarcinoma. *Cancer Cell* **25**, 735-747, doi:10.1016/j.ccr.2014.04.021 (2014).
- 18 Chiou, S. H., Risca, V. I., Wang, G. X., Yang, D., Gruner, B. M., Kathiria, A. S., Ma, R. K., Vaka, D., Chu, P., Kozak, M., Castellini, L., Graves, E. E., Kim, G. E., Mourrain, P., Koong, A. C., Giaccia, A. J. & Winslow, M. M. BLIMP1 Induces Transient Metastatic Heterogeneity in Pancreatic Cancer. *Cancer Discov* **7**, 1184-1199, doi:10.1158/2159-8290.CD-17-0250 (2017).
- 19 Li, C., Wu, J. J., Hynes, M., Dosch, J., Sarkar, B., Welling, T. H., Pasca di Magliano, M. & Simeone, D. M. c-Met is a marker of pancreatic cancer stem cells and therapeutic target. *Gastroenterology* **141**, 2218-2227 e2215, doi:10.1053/j.gastro.2011.08.009 (2011).
- 20 Bao, B., Wang, Z., Ali, S., Ahmad, A., Azmi, A. S., Sarkar, S. H., Banerjee, S., Kong, D., Li, Y., Thakur, S. & Sarkar, F. H. Metformin inhibits cell proliferation, migration and invasion by attenuating CSC function mediated by deregulating miRNAs in pancreatic cancer cells. *Cancer Prev Res (Phila)* **5**, 355-364, doi:10.1158/1940-6207.CAPR-11-0299 (2012).
- 21 Mo, H. N. & Liu, P. Targeting MET in cancer therapy. *Chronic Dis Transl Med* **3**, 148-153, doi:10.1016/j.cdtm.2017.06.002 (2017).
- 22 Rimkus, T. K., Carpenter, R. L., Qasem, S., Chan, M. & Lo, H. W. Targeting the Sonic Hedgehog Signaling Pathway: Review of Smoothed and GLI Inhibitors. *Cancers (Basel)* **8**, doi:10.3390/cancers8020022 (2016).

- 23 Bhaw-Luximon, A. & Jhurry, D. Metformin in pancreatic cancer treatment: from clinical trials through basic research to biomarker quantification. *J Cancer Res Clin Oncol* **142**, 2159-2171, doi:10.1007/s00432-016-2178-4 (2016).
- 24 Kaufman, C. K., Mosimann, C., Fan, Z. P., Yang, S., Thomas, A. J., Ablain, J., Tan, J. L., Fogley, R. D., van Rooijen, E., Hagedorn, E. J., Ciarlo, C., White, R. M., Matos, D. A., Puller, A. C., Santoriello, C., Liao, E. C., Young, R. A. & Zon, L. I. A zebrafish melanoma model reveals emergence of neural crest identity during melanoma initiation. *Science* **351**, aad2197, doi:10.1126/science.aad2197 (2016).
- 25 Sharma, S. V., Lee, D. Y., Li, B., Quinlan, M. P., Takahashi, F., Maheswaran, S., McDermott, U., Azizian, N., Zou, L., Fischbach, M. A., Wong, K. K., Brandstetter, K., Wittner, B., Ramaswamy, S., Classon, M. & Settleman, J. A chromatin-mediated reversible drug-tolerant state in cancer cell subpopulations. *Cell* **141**, 69-80, doi:10.1016/j.cell.2010.02.027 (2010).
- 26 Hata, A. N., Niederst, M. J., Archibald, H. L., Gomez-Caraballo, M., Siddiqui, F. M., Mulvey, H. E., Maruvka, Y. E., Ji, F., Bhang, H. E., Krishnamurthy Radhakrishna, V., Siravegna, G., Hu, H., Raof, S., Lockerman, E., Kalsy, A., Lee, D., Keating, C. L., Ruddy, D. A., Damon, L. J., Crystal, A. S., Costa, C., Piotrowska, Z., Bardelli, A., Iafrate, A. J., Sadreyev, R. I., Stegmeier, F., Getz, G., Sequist, L. V., Faber, A. C. & Engelman, J. A. Tumor cells can follow distinct evolutionary paths to become resistant to epidermal growth factor receptor inhibition. *Nat Med* **22**, 262-269, doi:10.1038/nm.4040 (2016).
- 27 Makohon-Moore, A. P., Zhang, M., Reiter, J. G., Bozic, I., Allen, B., Kundu, D., Chatterjee, K., Wong, F., Jiao, Y., Kohutek, Z. A., Hong, J., Attiyeh, M., Javier, B., Wood, L. D., Hruban, R. H., Nowak, M. A., Papadopoulos, N., Kinzler, K. W., Vogelstein, B. & Iacobuzio-Donahue, C. A. Limited heterogeneity of known driver gene mutations among the metastases of individual patients with pancreatic cancer. *Nat Genet* **49**, 358-366, doi:10.1038/ng.3764 (2017).
- 28 McDonald, O. G., Li, X., Saunders, T., Tryggvadottir, R., Mentch, S. J., Warmoes, M. O., Word, A. E., Carrer, A., Salz, T. H., Natsume, S., Stauffer, K. M., Makohon-Moore, A., Zhong, Y., Wu, H., Wellen, K. E., Locasale, J. W., Iacobuzio-Donahue, C. A. & Feinberg, A. P. Epigenomic reprogramming during pancreatic cancer progression links anabolic glucose metabolism to distant metastasis. *Nat Genet* **49**, 367-376, doi:10.1038/ng.3753 (2017).
- 29 Boyle, A. P., Davis, S., Shulha, H. P., Meltzer, P., Margulies, E. H., Weng, Z., Furey, T. S. & Crawford, G. E. High-resolution mapping and characterization of open chromatin across the genome. *Cell* **132**, 311-322, doi:10.1016/j.cell.2007.12.014 (2008).
- 30 Lamparter, D., Marbach, D., Rueedi, R., Bergmann, S. & Kutalik, Z. Genome-Wide Association between Transcription Factor Expression and Chromatin Accessibility Reveals Regulators of Chromatin Accessibility. *PLoS Comput Biol* **13**, e1005311, doi:10.1371/journal.pcbi.1005311 (2017).
- 31 Whyte, W. A., Orlando, D. A., Hnisz, D., Abraham, B. J., Lin, C. Y., Kagey, M. H., Rahl, P. B., Lee, T. I. & Young, R. A. Master transcription factors and mediator establish super-enhancers at key cell identity genes. *Cell* **153**, 307-319, doi:10.1016/j.cell.2013.03.035 (2013).
- 32 Creighton, M. P., Cheng, A. W., Welstead, G. G., Kooistra, T., Carey, B. W., Steine, E. J., Hanna, J., Lodato, M. A., Frampton, G. M., Sharp, P. A., Boyer, L. A., Young, R. A. & Jaenisch, R. Histone H3K27ac separates active from poised enhancers and predicts developmental state. *Proc Natl Acad Sci U S A* **107**, 21931-21936, doi:10.1073/pnas.1016071107 (2010).

- 33 Tuveson, D. A., Shaw, A. T., Willis, N. A., Silver, D. P., Jackson, E. L., Chang, S., Mercer, K. L., Grochow, R., Hock, H., Crowley, D., Hingorani, S. R., Zaks, T., King, C., Jacobetz, M. A., Wang, L., Bronson, R. T., Orkin, S. H., DePinho, R. A. & Jacks, T. Endogenous oncogenic K-ras(G12D) stimulates proliferation and widespread neoplastic and developmental defects. *Cancer Cell* **5**, 375-387 (2004).
- 34 Bardeesy, N., Aguirre, A. J., Chu, G. C., Cheng, K. H., Lopez, L. V., Hezel, A. F., Feng, B., Brennan, C., Weissleder, R., Mahmood, U., Hanahan, D., Redston, M. S., Chin, L. & Depinho, R. A. Both p16(Ink4a) and the p19(Arf)-p53 pathway constrain progression of pancreatic adenocarcinoma in the mouse. *Proc Natl Acad Sci U S A* **103**, 5947-5952, doi:10.1073/pnas.0601273103 (2006).
- 35 Hingorani, S. R., Petricoin, E. F., Maitra, A., Rajapakse, V., King, C., Jacobetz, M. A., Ross, S., Conrads, T. P., Veenstra, T. D., Hitt, B. A., Kawaguchi, Y., Johann, D., Liotta, L. A., Crawford, H. C., Putt, M. E., Jacks, T., Wright, C. V., Hruban, R. H., Lowy, A. M. & Tuveson, D. A. Preinvasive and invasive ductal pancreatic cancer and its early detection in the mouse. *Cancer Cell* **4**, 437-450 (2003).
- 36 Kawaguchi, Y., Cooper, B., Gannon, M., Ray, M., MacDonald, R. J. & Wright, C. V. The role of the transcriptional regulator Ptf1a in converting intestinal to pancreatic progenitors. *Nat Genet* **32**, 128-134, doi:10.1038/ng959 (2002).
- 37 Boj, S. F., Hwang, C. I., Baker, L. A., Chio, I., Engle, D. D., Corbo, V., Jager, M., Ponz-Sarvisé, M., Tiriác, H., Spector, M. S., Gracanin, A., Oni, T., Yu, K. H., van Boxtel, R., Huch, M., Rivera, K. D., Wilson, J. P., Feigin, M. E., Ohlund, D., Handly-Santana, A., Ardito-Abraham, C. M., Ludwig, M., Elyada, E., Alagesan, B., Biffi, G., Yordanov, G. N., Delcuze, B., Creighton, B., Wright, K., Park, Y., Morsink, F. H., Molenaar, I. Q., Borel Rinkes, I. H., Cuppen, E., Hao, Y., Jin, Y., Nijman, I. J., Iacobuzio-Donahue, C., Leach, S. D., Pappin, D. J., Hammell, M., Klimstra, D. S., Basturk, O., Hruban, R. H., Offerhaus, G. J., Vries, R. G., Clevers, H. & Tuveson, D. A. Organoid models of human and mouse ductal pancreatic cancer. *Cell* **160**, 324-338, doi:10.1016/j.cell.2014.12.021 (2015).
- 38 Sanjana, N. E., Shalem, O. & Zhang, F. Improved vectors and genome-wide libraries for CRISPR screening. *Nat Methods* **11**, 783-784, doi:10.1038/nmeth.3047 (2014).
- 39 Shalem, O., Sanjana, N. E., Hartenian, E., Shi, X., Scott, D. A., Mikkelsen, T., Heckl, D., Ebert, B. L., Root, D. E., Doench, J. G. & Zhang, F. Genome-scale CRISPR-Cas9 knockout screening in human cells. *Science* **343**, 84-87, doi:10.1126/science.1247005 (2014).
- 40 Subramanian, A., Tamayo, P., Mootha, V. K., Mukherjee, S., Ebert, B. L., Gillette, M. A., Paulovich, A., Pomeroy, S. L., Golub, T. R., Lander, E. S. & Mesirov, J. P. Gene set enrichment analysis: a knowledge-based approach for interpreting genome-wide expression profiles. *Proc Natl Acad Sci U S A* **102**, 15545-15550, doi:10.1073/pnas.0506580102 (2005).
- 41 Hanzelmann, S., Castelo, R. & Guinney, J. GSEA: gene set variation analysis for microarray and RNA-seq data. *BMC Bioinformatics* **14**, 7, doi:10.1186/1471-2105-14-7 (2013).
- 42 Ryu, C. S., Kwak, H. C., Lee, K. S., Kang, K. W., Oh, S. J., Lee, K. H., Kim, H. M., Ma, J. Y. & Kim, S. K. Sulfur amino acid metabolism in doxorubicin-resistant breast cancer cells. *Toxicol Appl Pharmacol* **255**, 94-102, doi:10.1016/j.taap.2011.06.004 (2011).
- 43 Belalcazar, A. D., Ball, J. G., Frost, L. M., Valentovic, M. A. & Wilkinson, J. t. Transsulfuration Is a Significant Source of Sulfur for Glutathione Production in Human Mammary Epithelial Cells. *ISRN Biochem* **2013**, 637897, doi:10.1155/2013/637897 (2014).

- 44 Chio, I. I. C., Jafarnejad, S. M., Ponz-Sarvise, M., Park, Y., Rivera, K., Palm, W., Wilson, J., Sangar, V., Hao, Y., Ohlund, D., Wright, K., Filippini, D., Lee, E. J., Da Silva, B., Schoepfer, C., Wilkinson, J. E., Buscaglia, J. M., DeNicola, G. M., Tiriach, H., Hammell, M., Crawford, H. C., Schmidt, E. E., Thompson, C. B., Pappin, D. J., Sonenberg, N. & Tuveson, D. A. NRF2 Promotes Tumor Maintenance by Modulating mRNA Translation in Pancreatic Cancer. *Cell* **166**, 963-976, doi:10.1016/j.cell.2016.06.056 (2016).
- 45 Lu, H., Chen, I., Shimoda, L. A., Park, Y., Zhang, C., Tran, L., Zhang, H. & Semenza, G. L. Chemotherapy-Induced Ca(2+) Release Stimulates Breast Cancer Stem Cell Enrichment. *Cell Rep* **18**, 1946-1957, doi:10.1016/j.celrep.2017.02.001 (2017).
- 46 Hnisz, D., Abraham, B. J., Lee, T. I., Lau, A., Saint-Andre, V., Sigova, A. A., Hoke, H. A. & Young, R. A. Super-enhancers in the control of cell identity and disease. *Cell* **155**, 934-947, doi:10.1016/j.cell.2013.09.053 (2013).
- 47 Loven, J., Hoke, H. A., Lin, C. Y., Lau, A., Orlando, D. A., Vakoc, C. R., Bradner, J. E., Lee, T. I. & Young, R. A. Selective inhibition of tumor oncogenes by disruption of super-enhancers. *Cell* **153**, 320-334, doi:10.1016/j.cell.2013.03.036 (2013).
- 48 Rovira, M., Scott, S. G., Liss, A. S., Jensen, J., Thayer, S. P. & Leach, S. D. Isolation and characterization of centroacinar/terminal ductal progenitor cells in adult mouse pancreas. *Proc Natl Acad Sci U S A* **107**, 75-80, doi:10.1073/pnas.0912589107 (2010).
- 49 Vanunu, O., Magger, O., Ruppin, E., Shlomi, T. & Sharan, R. Associating genes and protein complexes with disease via network propagation. *PLoS Comput Biol* **6**, e1000641, doi:10.1371/journal.pcbi.1000641 (2010).
- 50 Szklarczyk, D., Franceschini, A., Wyder, S., Forslund, K., Heller, D., Huerta-Cepas, J., Simonovic, M., Roth, A., Santos, A., Tsafou, K. P., Kuhn, M., Bork, P., Jensen, L. J. & von Mering, C. STRING v10: protein-protein interaction networks, integrated over the tree of life. *Nucleic Acids Res* **43**, D447-452, doi:10.1093/nar/gku1003 (2015).
- 51 Zhao, L., Spassieva, S., Gable, K., Gupta, S. D., Shi, L. Y., Wang, J., Bielawski, J., Hicks, W. L., Krebs, M. P., Naggert, J., Hannun, Y. A., Dunn, T. M. & Nishina, P. M. Elevation of 20-carbon long chain bases due to a mutation in serine palmitoyltransferase small subunit b results in neurodegeneration. *Proc Natl Acad Sci U S A* **112**, 12962-12967, doi:10.1073/pnas.1516733112 (2015).
- 52 Dwyer, J. R., Donkor, J., Zhang, P., Csaki, L. S., Vergnes, L., Lee, J. M., Dewald, J., Brindley, D. N., Atti, E., Tetradis, S., Yoshinaga, Y., De Jong, P. J., Fong, L. G., Young, S. G. & Reue, K. Mouse lipin-1 and lipin-2 cooperate to maintain glycerolipid homeostasis in liver and aging cerebellum. *Proc Natl Acad Sci U S A* **109**, E2486-2495, doi:10.1073/pnas.1205221109 (2012).
- 53 Formstone, C. J. & Little, P. F. The flamingo-related mouse Celsr family (Celsr1-3) genes exhibit distinct patterns of expression during embryonic development. *Mech Dev* **109**, 91-94 (2001).
- 54 Nanda, N., Bao, M., Lin, H., Clauser, K., Komuves, L., Quertermous, T., Conley, P. B., Phillips, D. R. & Hart, M. J. Platelet endothelial aggregation receptor 1 (PEAR1), a novel epidermal growth factor repeat-containing transmembrane receptor, participates in platelet contact-induced activation. *J Biol Chem* **280**, 24680-24689, doi:10.1074/jbc.M413411200 (2005).
- 55 Wang, X., Wong, K., Ouyang, W. & Rutz, S. Targeting IL-10 Family Cytokines for the Treatment of Human Diseases. *Cold Spring Harb Perspect Biol*, doi:10.1101/cshperspect.a028548 (2017).

- 56 Guillonneau, C., Bezie, S. & Anegon, I. Immunoregulatory properties of the cytokine IL-34. *Cell Mol Life Sci* **74**, 2569-2586, doi:10.1007/s00018-017-2482-4 (2017).
- 57 Roe, J. S., Hwang, C. I., Somerville, T. D. D., Milazzo, J. P., Lee, E. J., Da Silva, B., Maiorino, L., Tiriach, H., Young, C. M., Miyabayashi, K., Filippini, D., Creighton, B., Burkhart, R. A., Buscaglia, J. M., Kim, E. J., Grem, J. L., Lazenby, A. J., Grunkemeyer, J. A., Hollingsworth, M. A., Grandgenett, P. M., Egeblad, M., Park, Y., Tuveson, D. A. & Vakoc, C. R. Enhancer Reprogramming Promotes Pancreatic Cancer Metastasis. *Cell* **170**, 875-888 e820, doi:10.1016/j.cell.2017.07.007 (2017).
- 58 Neph, S., Stergachis, A. B., Reynolds, A., Sandstrom, R., Borenstein, E. & Stamatoyannopoulos, J. A. Circuitry and dynamics of human transcription factor regulatory networks. *Cell* **150**, 1274-1286, doi:10.1016/j.cell.2012.04.040 (2012).
- 59 Zaret, K. S. & Carroll, J. S. Pioneer transcription factors: establishing competence for gene expression. *Genes Dev* **25**, 2227-2241, doi:10.1101/gad.176826.111 (2011).
- 60 Kopp, J. L., von Figura, G., Mayes, E., Liu, F. F., Dubois, C. L., Morris, J. P. t., Pan, F. C., Akiyama, H., Wright, C. V., Jensen, K., Hebrok, M. & Sander, M. Identification of Sox9-dependent acinar-ductal reprogramming as the principal mechanism for initiation of pancreatic ductal adenocarcinoma. *Cancer Cell* **22**, 737-750, doi:10.1016/j.ccr.2012.10.025 (2012).
- 61 Adam, R. C., Yang, H., Rockowitz, S., Larsen, S. B., Nikolova, M., Oristian, D. S., Polak, L., Kadaja, M., Asare, A., Zheng, D. & Fuchs, E. Pioneer factors govern super-enhancer dynamics in stem cell plasticity and lineage choice. *Nature* **521**, 366-370, doi:10.1038/nature14289 (2015).
- 62 Qi, J., Nakayama, K., Cardiff, R. D., Borowsky, A. D., Kaul, K., Williams, R., Krajewski, S., Mercola, D., Carpenter, P. M., Bowtell, D. & Ronai, Z. A. Siah2-dependent concerted activity of HIF and FoxA2 regulates formation of neuroendocrine phenotype and neuroendocrine prostate tumors. *Cancer Cell* **18**, 23-38, doi:10.1016/j.ccr.2010.05.024 (2010).
- 63 Bailey, P., Chang, D. K., Nones, K., Johns, A. L., Patch, A. M., Gingras, M. C., Miller, D. K., Christ, A. N., Bruxner, T. J., Quinn, M. C., Nourse, C., Murtaugh, L. C., Harliwong, I., Idrisoglu, S., Manning, S., Nourbakhsh, E., Wani, S., Fink, L., Holmes, O., Chin, V., Anderson, M. J., Kazakoff, S., Leonard, C., Newell, F., Waddell, N., Wood, S., Xu, Q., Wilson, P. J., Cloonan, N., Kassahn, K. S., Taylor, D., Quek, K., Robertson, A., Pantano, L., Mincarelli, L., Sanchez, L. N., Evers, L., Wu, J., Pinese, M., Cowley, M. J., Jones, M. D., Colvin, E. K., Nagrial, A. M., Humphrey, E. S., Chantrill, L. A., Mawson, A., Humphris, J., Chou, A., Pajic, M., Scarlett, C. J., Pinho, A. V., Giry-Laterriere, M., Rooman, I., Samra, J. S., Kench, J. G., Lovell, J. A., Merrett, N. D., Toon, C. W., Epari, K., Nguyen, N. Q., Barbour, A., Zeps, N., Moran-Jones, K., Jamieson, N. B., Graham, J. S., Duthie, F., Oien, K., Hair, J., Grutzmann, R., Maitra, A., Iacobuzio-Donahue, C. A., Wolfgang, C. L., Morgan, R. A., Lawlor, R. T., Corbo, V., Bassi, C., Rusev, B., Capelli, P., Salvia, R., Tortora, G., Mukhopadhyay, D., Petersen, G. M., Australian Pancreatic Cancer Genome, I., Munzy, D. M., Fisher, W. E., Karim, S. A., Eshleman, J. R., Hruban, R. H., Pilarsky, C., Morton, J. P., Sansom, O. J., Scarpa, A., Musgrove, E. A., Bailey, U. M., Hofmann, O., Sutherland, R. L., Wheeler, D. A., Gill, A. J., Gibbs, R. A., Pearson, J. V., Waddell, N., Biankin, A. V. & Grimmond, S. M. Genomic analyses identify molecular subtypes of pancreatic cancer. *Nature* **531**, 47-52, doi:10.1038/nature16965 (2016).
- 64 Cirillo, L. A., Lin, F. R., Cuesta, I., Friedman, D., Jarnik, M. & Zaret, K. S. Opening of compacted chromatin by early developmental transcription factors HNF3 (FoxA) and GATA-4. *Mol Cell* **9**, 279-289 (2002).
- 65 Gege, C. Retinoid-related orphan receptor gamma t (RORgammat) inhibitors from Vitae Pharmaceuticals (WO2015116904) and structure proposal for their Phase I candidate VTP-43742. *Expert Opin Ther Pat* **26**, 737-744, doi:10.1517/13543776.2016.1153066 (2016).

- 66 Huh, J. R. & Littman, D. R. Small molecule inhibitors of ROR γ : targeting Th17 cells and other applications. *Eur J Immunol* **42**, 2232-2237, doi:10.1002/eji.201242740 (2012).
- 67 Kumar, N., Lyda, B., Chang, M. R., Lauer, J. L., Solt, L. A., Burris, T. P., Kamenecka, T. M. & Griffin, P. R. Identification of SR2211: a potent synthetic ROR γ -selective modulator. *ACS Chem Biol* **7**, 672-677, doi:10.1021/cb200496y (2012).
- 68 Hong, S. P., Wen, J., Bang, S., Park, S. & Song, S. Y. CD44-positive cells are responsible for gemcitabine resistance in pancreatic cancer cells. *Int J Cancer* **125**, 2323-2331, doi:10.1002/ijc.24573 (2009).
- 69 Van den Broeck, A., Vankelecom, H., Van Delm, W., Gremeaux, L., Wouters, J., Allemeersch, J., Govaere, O., Roskams, T. & Topal, B. Human pancreatic cancer contains a side population expressing cancer stem cell-associated and prognostic genes. *PLoS One* **8**, e73968, doi:10.1371/journal.pone.0073968 (2013).
- 70 Lappano, R. & Maggiolini, M. G protein-coupled receptors: novel targets for drug discovery in cancer. *Nat Rev Drug Discov* **10**, 47-60, doi:10.1038/nrd3320 (2011).
- 71 Sankhala KK, B. J.-Y., Ganjoo KN, Italiano A, Hassan AB, Kim TM, Ravi V, Cassier PA, Rutkowski P, Sankar N, Qazi I, Sikorski RS, Collins H, Zhang C, Shocron E, Genderblom H. A phase I/II dose escalation and expansion study of cabiralizumab (cabira; FPA-008), an anti-CSF1R antibody, in tenosynovial giant cell tumor (TGCT, diffuse pigmented villonodular synovitis D-PVNS). *J Clin Oncol* **35**, 11078 (2017).
- 72 Wang, J., Zou, J. X., Xue, X., Cai, D., Zhang, Y., Duan, Z., Xiang, Q., Yang, J. C., Louie, M. C., Borowsky, A. D., Gao, A. C., Evans, C. P., Lam, K. S., Xu, J., Kung, H. J., Evans, R. M., Xu, Y. & Chen, H. W. ROR- γ drives androgen receptor expression and represents a therapeutic target in castration-resistant prostate cancer. *Nat Med* **22**, 488-496, doi:10.1038/nm.4070 (2016).
- 73 Hu, Y. & Smyth, G. K. ELDA: extreme limiting dilution analysis for comparing depleted and enriched populations in stem cell and other assays. *J Immunol Methods* **347**, 70-78, doi:10.1016/j.jim.2009.06.008 (2009).
- 74 Bray, N. L., Pimentel, H., Melsted, P. & Pachter, L. Near-optimal probabilistic RNA-seq quantification. *Nat Biotechnol* **34**, 525-527, doi:10.1038/nbt.3519 (2016).
- 75 Anders, S. & Huber, W. Differential expression analysis for sequence count data. *Genome Biol* **11**, R106, doi:10.1186/gb-2010-11-10-r106 (2010).
- 76 Ritchie, M. E., Phipson, B., Wu, D., Hu, Y., Law, C. W., Shi, W. & Smyth, G. K. limma powers differential expression analyses for RNA-sequencing and microarray studies. *Nucleic Acids Res* **43**, e47, doi:10.1093/nar/gkv007 (2015).
- 77 Efron, B. & Tibshirani, R. Empirical bayes methods and false discovery rates for microarrays. *Genet Epidemiol* **23**, 70-86, doi:10.1002/gepi.1124 (2002).
- 78 I, L. & T, S. Replicated microarray data. *Statistica Sinica* **12**, 31-46 (2002).
- 79 Deshpande, A. J., Deshpande, A., Sinha, A. U., Chen, L., Chang, J., Cihan, A., Fazio, M., Chen, C. W., Zhu, N., Koche, R., Dzhekieva, L., Ibanez, G., Dias, S., Banka, D., Krivtsov, A., Luo, M., Roeder, R. G., Bradner, J. E., Bernt, K. M. & Armstrong, S. A. AF10 regulates progressive H3K79

- methylation and HOX gene expression in diverse AML subtypes. *Cancer Cell* **26**, 896-908, doi:10.1016/j.ccell.2014.10.009 (2014).
- 80 Langmead, B. & Salzberg, S. L. Fast gapped-read alignment with Bowtie 2. *Nat Methods* **9**, 357-359, doi:10.1038/nmeth.1923 (2012).
- 81 Zang, C., Schones, D. E., Zeng, C., Cui, K., Zhao, K. & Peng, W. A clustering approach for identification of enriched domains from histone modification ChIP-Seq data. *Bioinformatics* **25**, 1952-1958, doi:10.1093/bioinformatics/btp340 (2009).
- 82 Cole, J. J., Robertson, N. A., Rather, M. I., Thomson, J. P., McBryan, T., Sproul, D., Wang, T., Brock, C., Clark, W., Ideker, T., Meehan, R. R., Miller, R. A., Brown-Borg, H. M. & Adams, P. D. Diverse interventions that extend mouse lifespan suppress shared age-associated epigenetic changes at critical gene regulatory regions. *Genome Biol* **18**, 58, doi:10.1186/s13059-017-1185-3 (2017).
- 83 Wang, J., Vasaikar, S., Shi, Z., Greer, M. & Zhang, B. WebGestalt 2017: a more comprehensive, powerful, flexible and interactive gene set enrichment analysis toolkit. *Nucleic Acids Res* **45**, W130-W137, doi:10.1093/nar/gkx356 (2017).
- 84 Martin, M. Cutadapt removes adaptor sequences from high-throughput sequencing reads. *EMBnet.journal* **17**, 10-12 (2011).
- 85 Love, M. I., Huber, W. & Anders, S. Moderated estimation of fold change and dispersion for RNA-seq data with DESeq2. *Genome Biol* **15**, 550, doi:10.1186/s13059-014-0550-8 (2014).
- 86 Li, W., Xu, H., Xiao, T., Cong, L., Love, M. I., Zhang, F., Irizarry, R. A., Liu, J. S., Brown, M. & Liu, X. S. MAGeCK enables robust identification of essential genes from genome-scale CRISPR/Cas9 knockout screens. *Genome Biol* **15**, 554, doi:10.1186/s13059-014-0554-4 (2014).
- 87 Spahn, P. N., Bath, T., Weiss, R. J., Kim, J., Esko, J. D., Lewis, N. E. & Harismendy, O. PinAPL-Py: A comprehensive web-application for the analysis of CRISPR/Cas9 screens. *Sci Rep* **7**, 15854, doi:10.1038/s41598-017-16193-9 (2017).
- 88 Cowen, L., Ideker, T., Raphael, B. J. & Sharan, R. Network propagation: a universal amplifier of genetic associations. *Nat Rev Genet* **18**, 551-562, doi:10.1038/nrg.2017.38 (2017).
- 89 Blondel, V. D., J.L., G., R., L. & E., L. Fast unfolding of communities in large networks. *Journal of Statistical Mechanics* **10**, arXiv:0803.0476 (2008).
- 90 T., V. L. & E., M. Robust community detection methods with resolution parameter for complex detection in protein protein interaction networks. *Pattern Recognition in Bioinformatics*, 1-13 (2012).
- 91 S., F. Community detection in graphs. *Physics Reports* **486**, 75-174 (2010).
- 92 Rosenthal, S. B., Len, J., Webster, M., Gary, A., Birmingham, A. & Fisch, K. M. Interactive network visualization in Jupyter notebooks: visJS2jupyter. *Bioinformatics* **34**, 126-128, doi:10.1093/bioinformatics/btx581 (2018).

CHAPTER 4

Examination of tumor cell behavior in response to target inhibition using intravital imaging

Nikki K. Lytle

The following chapter is a compilation of imaging experiments that contributed to manuscripts published in *Cancer Cell* 2016, *Cell Stem Cell* 2015, *Proc Natl Acad Sci* 2014, and *Cancer Cell* 2018.

1. Bajaj J*, Konuma T*, Lytle NK, Kwon HY, Ablack JN, Cantor JM, Rizzieri D, Chuah C, Oehler VG, Broome EH, Ball ED, van der Horst EH, Ginsberg MH, Reya T. CD98-mediated adhesive signaling enables the establishment and propagation of acute myelogenous leukemia. *Cancer Cell*. 2016 Nov 14;30(5):792-805.
2. Kwon HY*, Bajaj J*, Ito T, Blevins A, Konuma T, Weeks J, Lytle NK, Koechlein CS, Rizzieri D, Chuah C, Oehler VG, Sasik R, Hardiman G, Reya T. Tetraspanin 3 is required for the development and propagation of acute myelogenous leukemia. *Cell Stem Cell*. 2015 Aug 6;17(2):152-164.
3. Wu X, Zhang W, Font-Burgada J, Palmer T, Hamil AS, Biswas SK, Poidinger M, Borchering N, Xie Q, Ellies LG, Lytle NK, Wu LW, Fox RG, Yang J, Dowdy SF, Reya T, Karin M. Ubiquitin-conjugating enzyme Ubc13 controls breast cancer metastasis through a TAK1-p38 MAP kinase cascade. *Proc Natl Acad Sci U.S.A.* 2014 Sep 23;111(38):13870-13875.
4. Dravis C*, Chung C-Y*, Lytle NK, Herrera-Valdez J, Luna G, Trejo CL, Reya T, Wahl GM. Epigenetic and transcriptomic profiling of mammary gland development and tumor models disclose regulators of cell state plasticity. *Cancer Cell*. Accepted 2018 Aug.

PREFACE TO CHAPTER 4:

Chapter 4, in part, is a compilation of experiments published in (1) *Cancer Cell* entitled “CD98-mediated adhesive signaling enables the establishment and propagation of acute myelogenous leukemia,” (2) *Cell Stem Cell* entitled “Tetraspanin 3 is required for the development and propagation of acute myelogenous leukemia,” (3) *Proc Natl Acad Sci* entitled “Ubiquitin-conjugating enzyme Ubc13 controls breast cancer metastasis through a TAK1-p38 MAP kinase cascade,” and (4) *Cancer Cell* entitled “Epigenetic and transcriptomic profiling of mammary gland development and tumor models disclose regulators of cell state plasticity.” Intravital imaging provides a unique and powerful platform to gain insight into signals that sustain and drive aggressive tumor cell behaviors. Early in my graduate training, I was able to learn *in vivo* imaging of calvarial bone marrow and normal pancreas. In both cases, mice are kept alive, but anesthetized, and the techniques were developed in a way to minimize disruption of blood flow and optimize tissue viability. I adapted these principals to image early stage KP^{fl}C tumors, which provided early tumorigenic insight in an autochthonous setting, and flank-transplanted tumors, which allowed me to track solid tumor cell metastatic behaviors. I am grateful to Joi Weeks, Claire Koechlein, and Ray Fox, who were all critical in developing the original intravital imaging techniques in the Reya lab, and were wonderful teachers to me and others.

ABSTRACT:

Metastatic Breast Cancer and Acute Myelogenous Leukemia, although seemingly very different in their disease development and trajectory, are both highly difficult to treat and associated with very poor prognosis. Moreover, studies in both of these cancers have suggested that tumor cell behaviors are dependent on signals from the tumor microenvironment. However, many of these studies were primarily based on *in vitro* co-culture experiments that may be heavily influenced by artificial growth conditions. The findings presented here first identified signals required for normal disease progression and maintenance in either metastatic breast cancer or leukemia. By performing intravital imaging in disease lacking these essential signals, we were able to uncover surprising tumor cell behaviors that provided insight into the functional role for each potential target. To this end, leukemia lacking either CD98 or Tspan3 was significantly mis-localized: the majority of disease was no longer in bone marrow regions with supportive niche factors necessary for leukemia stem cell maintenance. Ubc13 inhibition in metastatic breast cancer completely blocked lung metastases, but surprisingly had no impact on tumor cell intravasation, survival in circulation, or extravasation. Finally, breast cancer cells expressing Sox10, a factor that promotes high cell plasticity, were uniquely more migratory and invasive *in vivo*. Together, these findings highlight the power of disrupting microenvironmental or intrinsic signals that support an aggressive tumor cell phenotype.

KEYWORDS

Intravital imaging, cancer stem cells, stem cell signals, stem cell niche, Musashi, CD98, tetraspanin, acute myeloid leukemia, Sox10, Ubc13, circulating tumor cells, tumor cell dissemination, intravasation, tumor cell migration, breast cancer, cell state reprogramming

CD98-MEDIATED ADHESIVE SIGNALING ENABLES THE ESTABLISHMENT AND PROPAGATION OF ACUTE MYELOGENOUS LEUKEMIA

Introduction

The microenvironment that surrounds cancer cells can play a critical regulatory role in malignant growth and expansion. Early studies in breast cancer using both 3D cultures and in vivo approaches identified a role for stromal elements such as fibroblasts, vascular cells, and the extracellular matrix in sustaining tumor growth and dissemination, in part by activating transforming growth factor β , SDF1- α /CXCR4 signaling pathways, and through the release of metalloproteinases¹⁻³. Further, epithelial interactions with extracellular matrix components were subsequently shown to be necessary for effective dissemination and metastasis of breast cancers^{4,5}, and to contribute to chemoresistance⁶. Recent studies have challenged the dogma that the microenvironment is always supportive of oncogenesis by showing that targeted depletion of stromal cells can enhance pancreatic cancer growth⁷⁻⁹. Although leukemic cells experience less anchorage than solid tumor cells, and are often thought to not be as spatially restricted, they do grow and reside within the bone marrow surrounded by a large network of microenvironmental cells. However, the specific molecular cues that drive the engagement of leukemia cells with the microenvironment, and their role in sustaining and promoting oncogenesis, remain poorly understood.

To address these key questions we have focused on CD98, a molecule that amplifies adhesive signals induced by a variety of extracellular matrix components through interactions with integrins^{10,11}, and plays an important regulatory role in assembly of a fibronectin matrix¹². Because of its role in mediating signals from multiple integrins, blocking CD98 can impair a broad spectrum of adhesive signals and be a powerful approach to disrupting interactions of cancer cells with their microenvironment. CD98 is highly expressed in many solid tumors, and its expression associated with poor prognosis¹³. The functional relevance of CD98 has primarily been tested in context of solid cancer cell lines. For example, ectopic expression of CD98 can transform epithelial cell lines such as CHO¹⁴ and NIH3T3¹⁵ and promote their anchorage-independent growth and tumor formation in immunocompromised mice, while inhibitory antibodies against CD98 can block the proliferation of bladder cancer cell lines¹⁶. Further, the inhibition of a CD98 light chain (LAT1) can affect proliferation of breast and lung cancer cell lines by impairing amino acid transport^{17,18}. The development of a conditional *Slc3a2* (referred to as *Cd98hc*) allele¹² has allowed

genetic analysis of the role of CD98. *Cd98hc* deletion can prevent the formation of embryonic stem cell teratomas¹¹ and squamous cell carcinomas¹⁹, and heterozygous loss of *Cd98hc* reduces intestinal adenoma formation²⁰. However, the role of CD98 in hematologic malignancies and the relative contribution of adhesive signaling and amino acid transport functions to cancer have not been examined. To address this, we tested whether CD98 controls the establishment and propagation of primary leukemia cells within their native microenvironment by using both a genetic approach and the delivery of a newly developed therapeutic in the context of de novo acute myelogenous leukemia (AML).

Results

CD98 in De Novo AML Initiation and Maintenance

We tested the importance of CD98 in leukemogenesis using a mixed-lineage leukemia fusion protein (MLL)-driven model of de novo AML, a highly drug-resistant disease in adults and children. Because MLL-driven AML often presents with *NRAS* mutations, we used MLL-AF9 and *NRAS*^{G12V} oncogenes to establish myeloid leukemia with *Cd98hc*^{fl/fl} cells (**Figure Supplement 4.1A**). CD98 loss led to a marked increase in survival (55%) relative to controls (0%) (**Figure Supplement 4.1A**), indicating that CD98 is important for MLL-leukemia initiation. To determine whether continued AML propagation requires CD98, we assessed the capacity of sorted cKit⁺ leukemia cells to propagate disease (**Figure Supplement 4.1B**). Tamoxifen-induced CD98 loss led to a dramatic reduction in the number of leukemic colonies formed in vitro (**Figure Supplement 4.1C**) and significantly increased the median survival of mice transplanted with cKit⁺ AML cells from 21.5 days to 33 days (**Figure Supplement 4.1D**). These data indicate that abrogating CD98 expression reduced morbidity from established disease. Serial transplantation of CD98^{-/-} cKit⁺ leukemia cells not only impaired self-renewal but also led to a striking improvement in survival (0% for CD98^{+/+} versus 46% for CD98^{-/-}) (**Figure Supplement 4.1D**). Finally, because patients generally present with full-blown disease, we modeled a more clinically relevant setting by eliminating CD98 expression after AML establishment (**Figure Supplement 4.1E**). Loss of CD98 in this context led to a significant increase in survival (0% for CD98^{+/+} versus 66% for CD98^{-/-}, **Figure Supplement 4.1E**). CD98 appeared to be broadly required by non-MLL AML as well, with its loss improving survival dramatically in disease driven by AML-ETO9a and *NRAS*^{G12V} (**Figure Supplement 4.1F**). These data demonstrated a requirement for CD98

in the initiation, self-renewal, and propagation of de novo AML, and provided clear genetic evidence that targeting CD98 may be of therapeutic value.

CD98-Mediated Integrin Signaling Is Required for Leukemia Growth

Since CD98 can regulate both integrin-mediated signaling and amino acid transport, we tested the importance of each function for leukemia progression by reconstituting the two functions individually in CD98^{-/-} cells using chimeric human CD98-CD69 proteins (**Figures 4.1A**). These chimeric proteins separated CD98 functions by replacing either the integrin binding cytoplasmic and transmembrane domain or the extracellular amino acid transport domain of CD98 with parts of CD69, another type II transmembrane protein^{11,21}. Loss of colony-forming ability could be rescued almost completely by the full-length human CD98 heavy chain (as a control) as well as partially by the chimera that restored integrin binding and signaling (**Figure 4.1B**), indicating that downstream activation of integrin signaling is critical for leukemia growth. In contrast, the chimera that only restored amino acid transport failed to rescue the defect. Interestingly, rescue was most efficient when the chimera that preserves integrin binding was co-delivered with the chimera that restores amino acid transport. These data suggest that the integrin binding function of CD98 is critically required for leukemic growth and that the amino acid transport function can synergize with integrin binding to fully restore the normal function of LSCs. We should note that CD98 loss affected cells grown on semi-soft substrates such as methylcellulose or *in vivo*, but not when plated in liquid culture (**Figure Supplement 4.1C-D, and Figure 4.1B**; data not shown). This is consistent with previous work showing that CD98-mediated signaling is required for proliferation and survival on soft substrates but not stiff substrates¹⁹, possibly because there is enough tension on contact with stiff substrates (such as plastic) that CD98 is not needed to amplify integrin signaling.

As integrin-dependent adhesion mediates leukemia cell interactions with their microenvironment, we tested whether eliminating CD98 expression affected the dynamic *in vivo* associations of leukemic cells with their niche by real-time imaging. We first tested whether wild-type leukemia cells were capable of forming long-term interactions with blood vessels over time and found that about 25% of cells in the marrow space remained in close contact with vessels for 25 min or longer. The loss of CD98 reduced long-term interactions by 2-fold (**Figures 4.1C-D**), indicating that CD98 enables stable interactions of leukemia cells

with their niche *in vivo*. To define whether the interactions of leukemia cells with endothelium are physiologically important for maintaining stem cell properties, we used human umbilical vein endothelial cells (HUVECs) as a surrogate. Consistent with *in vivo* imaging analysis, the ability of cKit⁺ leukemia cells to adhere to HUVECs was reduced by ~40% with CD98 loss (**Figures 4.1E-F**). These data indicate that CD98-integrin-mediated interactions with endothelial cells are needed for survival and maintenance of LSCs.

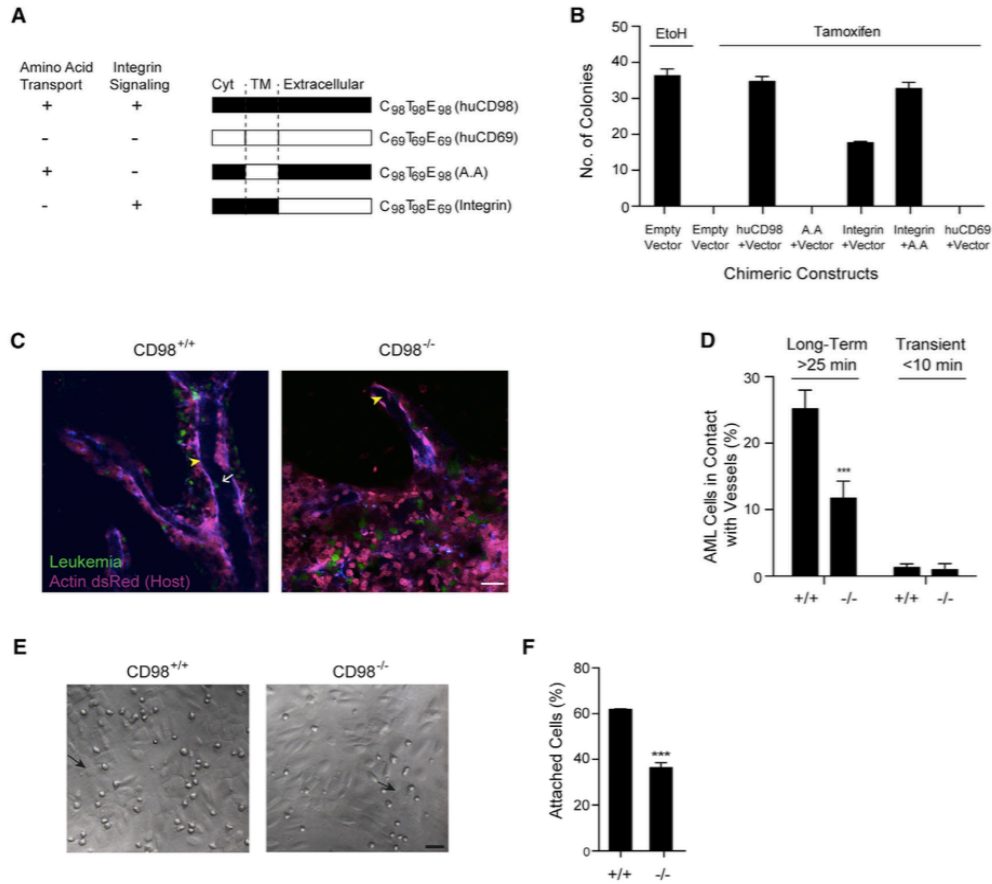


Figure 4.1. AML Is Dependent on CD98-Mediated Integrin Signaling

(A) Human CD98-CD69 chimeric constructs designed to specifically reconstitute either the amino acid transport or the integrin signaling function of CD98. (B) Average number of colonies formed by *Cd98hc^{fl/fl}* cKit⁺ cells transduced with human CD98 chimeric proteins and grown in the presence of ethanol (vehicle) or tamoxifen (to delete *Cd98hc*) ($n = 3$). (C) Representative images of calvarial bone marrow (magenta) of mice transplanted with CD98^{+/+} and CD98^{-/-} AML cells (green). Arrowheads indicate blood vessels (marked by VE-cadherin in blue), and arrow points to a leukemia cell adhering to vessel. Scale bar, 25 μ m. (D) Average frequency of CD98^{+/+} and CD98^{-/-} leukemia cells in contact with blood vessels (distance <0.5 mm) for 25 min or longer (stable/long-term) or for less than 10 min (transient/short-term) ($n = 12$ movies for each group, from 4 to 5 mice per cohort; data were compiled from two independent experiments). (E) Representative pictomicrographs show CD98^{+/+} and CD98^{-/-} leukemia cells (indicated by arrows) adhering to HUVECs. Scale bar, 25 μ m. (F) Average frequency of CD98^{+/+} and CD98^{-/-} cKit⁺ cells adhering to HUVECs ($n = 3$ from a representative experiment; similar results were obtained from two independent experiments). (Error bars represent \pm SEM. * $p < 0.05$, ** $p < 0.01$, *** $p < 0.001$, unpaired t test).

Methods

Generation of Experimental Mice. The conditional knockout mice (*Cd98hc^{fl/fl}*, also *Slc3a2-loxP*)¹² were mated with *Rosa26-CreER^{T2}* mice (Strain: B6;129-Gt(ROSA)26Sor^{tm1(cre/Esr1)Tyj}) mice to generate the *Cd98hc^{fl/fl};Rosa26-CreER* mice. B6-CD45.1 (Strain: B6.SJL-*Ptprc^aPtprc^b*/BoyJ) mice were used as transplant recipients. All mice were 6–16 weeks of age. Mice were bred and maintained in the animal care facilities at the University of California San Diego. All animal experiments were performed according to protocols approved by the UC San Diego Institutional Animal Care and Use Committee.

In Vivo Transplantation Assays. For bone marrow transplants, 500 LT-HSCs (KLS CD150⁺ CD48⁻ or KLSFlk2⁻ CD34⁺) isolated from bone marrow of mice expressing CD45.2 were transplanted into lethally irradiated (9.5 Gy) congenic recipient mice (expressing CD45.1) along with 2x10⁵ Sca1-depleted bone marrow rescue cells. Peripheral blood of recipient mice was collected every 4 weeks for 4–6 months after transplant. Where indicated, adult mice were administered tamoxifen (Sigma) in corn oil (20 mg/mL) daily by intraperitoneal injection (150 µg per gram of body weight) for 5 consecutive days.

Generation and Analysis of Leukemia Models. Bone marrow KLS cells were sorted from *Cd98hc^{fl/fl};Rosa26-CreER^{+/+}* mice and cultured overnight in RPMI medium (Life Technologies) supplemented with 20% fetal bovine serum (FBS), 50 mM 2-mercaptoethanol, 100 ng/mL stem cell factor (SCF) (R&D Systems), and 10 ng/mL interleukin-3 (IL-3) and 10 ng/mL IL-6 (R&D Systems). Cells were retrovirally infected with MSCV-MLL-AF9-IRES-tNGFR and MSCV-NRAS^{G12V}-IRES-YFP. Cells were harvested 48 hr after infection and retro-orbitally transplanted into cohorts of sublethally irradiated (6 Gy) B6-CD45.1 mice. For secondary transplants, cells from primary transplanted mice were sorted for cKit⁺ MLL-AF9-IRES-tNGFR⁺/MSCV-NRAS-IRES-YFP⁺ cells, and 2,000 to 4,000 cells were transplanted per mouse. Where indicated, adult mice were administered tamoxifen (Sigma) in corn oil (20 mg/mL) daily by intraperitoneal injection (150 µg per gram of body weight) for 5 consecutive days. Recipients were maintained on antibiotic water (sulfamethoxazole and trimethoprim) and evaluated daily for signs of

morbidity, weight loss, failure to groom, and splenomegaly. Premorbid animals were euthanized and relevant tissues harvested and analyzed by flow cytometry.

In Vivo Imaging. Imaging was done as described previously²²⁻²⁵. In brief, Actin-dsRed NOD SCID mice (Strain: NOD.Cg-*Prkdc*^{SCID} Tg(CAG-DsRed*MST)1Nagy/KupwJ) were transplanted with CD98^{+/+} or CD98^{-/-} MLL-leukemia cells and imaged 7–10 days post transplant. VE-Cadherin conjugated to Alexa Fluor 647 (eBiosciences) was administered at a concentration of 10 µg diluted in 100 µL, 15 min prior to imaging. Images were acquired by the Leica LAS AF 2.7.3 software with a TCS SP5 upright DM600 CFS Leica confocal system using an HCX APO L 203/1.00 W Leica Plan Apochromat objective. Images were continuously captured in 1,024 x 1,024 format (approximately 7 s per scan) for up to 1 hr. Images were analyzed using the Leica AF 2.7.3 software.

Additional methods can be found in: Bajaj J, Konuma T, Lytle NK, Kwon HY, Ablack JN, Cantor JM, Rizzieri D, Chuah C, Oehler VG, Broome EH, Ball ED, van der Horst EH, Ginsberg MH, Reya T. CD98-mediated adhesive signaling enables the establishment and propagation of acute myelogenous leukemia. *Cancer Cell*. 2016 Nov 14;30(5):792-805.

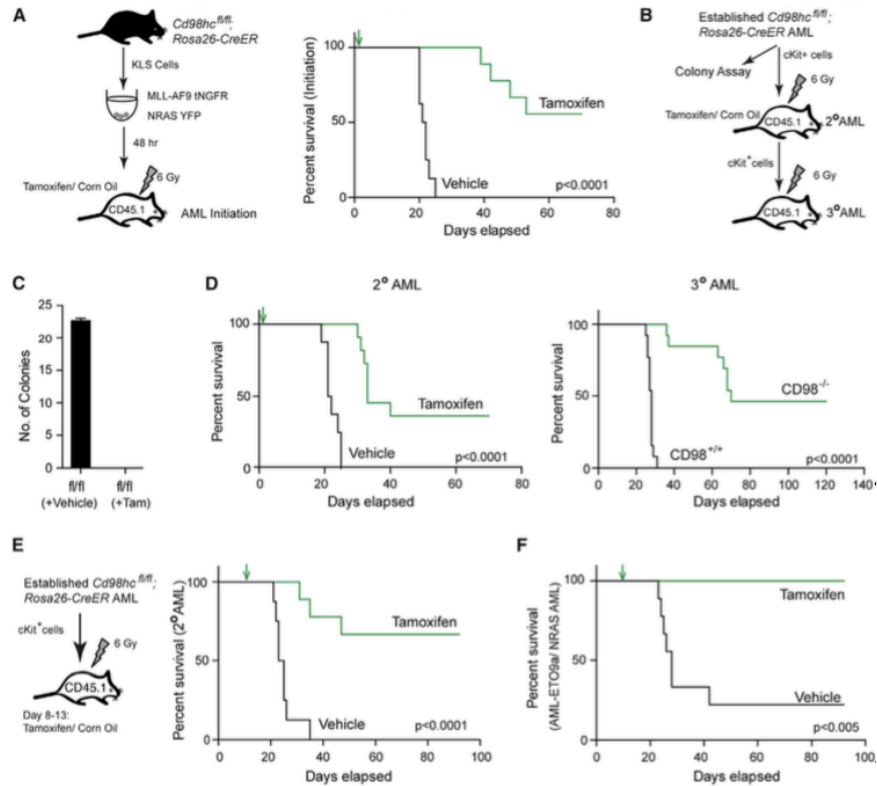


Figure Supplement 4.1. CD98 Loss Impairs AML Growth and Propagation

(A) KLS cells from *Cd98hc^{fl/fl};Rosa26-CreER* mice were retrovirally transduced with MLL-AF9-IRES-tNGFR and NRAS^{G12V}-IRES-YFP and transplanted to establish disease (schematic on the left). The start of treatment is indicated by an arrow on the survival curve (right; $n = 8-9$ for each cohort, data combined from two independent experiments). (B–D) cKit⁺ cells from established *Cd98hc^{fl/fl};Rosa26-CreER* leukemia (schematic in B) were isolated and cultured in vitro in the presence of tamoxifen or vehicle, and colony formation assessed (C). Cells were transplanted, 2 recipients treated with tamoxifen or vehicle, and survival monitored ($n = 8$ for vehicle and $n = 11$ for tamoxifen treatment, data combined from two independent experiments). The cKit⁺ CD98^{+/+} or CD98^{-/-} leukemia cells from 2 mice were also transplanted into 3 recipients to monitor in vivo self-renewal capacity (D). The start of treatment is indicated by an arrow on the survival curve ($n = 13$ for each cohort, data combined from two independent experiments). (E) cKit⁺ *Cd98hc^{fl/fl};Rosa26-CreER* AML cells were transplanted, recipients treated with tamoxifen or vehicle from day 8 to day 13 (schematic on the left), and survival monitored (right; $n = 8$ for control and $n = 9$ for tamoxifen treatment, data combined from two independent experiments). The start of treatment is indicated by an arrow on the survival curve. (F) KLS cells from *Cd98hc^{fl/fl};Rosa26-CreER* mice were isolated, infected with AML-ETO9a and NRAS oncogenes, and transplanted. Mice were subsequently treated with tamoxifen or corn oil, starting 8 days after transplant. The start of treatment is indicated by an arrow on the survival curve ($n = 9$ for vehicle and $n = 8$ for tamoxifen treatment, data combined from two independent experiments). Survival curves depict log-rank test p values. Error bars represent \pm SEM.

Acknowledgements

We are grateful to Annette Luo for technical support, Marcie Kritzik for help with manuscript preparation, and Sanford Shattil for advice on the project. We would like to thank Scott Armstrong, Scott Lowe, and Michael Cleary for providing MLL-AF9, AML1-ETO9a, and other plasmids. J.B. received a postdoctoral fellowship from the National Cancer Center; T.K. received a postdoctoral fellowship from the Japanese Society for the Promotion of Science; N.K.L. received support from NIH grant T32 GM007752 and National Research Service Award F31 CA206416; J.N.A. received a postdoctoral fellowship from the Arthritis Foundation; J.M.C. is funded in part by a Melanoma Research Alliance Young Investigator Award; T.R. was supported by a Lymphoma and Leukemia Society Scholar Award. This work was also supported by NIH grants HL078784 and HL117807 awarded to M.H.G. and HL097767, DK099335, DP1 CA174422, and R35 CA197699 awarded to T.R. E.H.v.d.H. is an employee of Igenica Biotherapeutics.

Author contributions

J.B. designed and performed experiments on human and murine leukemia progression, provided analysis of mAb impact, imaging, and mechanistic studies, and helped write the paper. T.K. designed and performed experiments on normal hematopoiesis and leukemia progression in mouse models. N.K.L., H.Y.K., J.N.A., and J.M.C. provided experimental data and help. D.R., C.C., V.G.O., E.H.B., and E.D.B. provided primary leukemia patient samples and experimental advice. E.H.v.d.H. provided the CD98 antibody and experimental advice. M.H.G. and T.R. conceived the project, planned and guided the research, and wrote the paper.

Dissertation Acknowledgements

Chapter 4, in part, a reprint of the material as it appears in *Cancer Cell*: Bajaj J, Konuma T, Lytle NK, Kwon HY, Ablack JN, Cantor JM, Rizzieri D, Chuah C, Oehler VG, Broome EH, Ball ED, van der Horst EH, Ginsberg MH, Reya T. CD98-mediated adhesive signaling enables the establishment and propagation of acute myelogenous leukemia. *Cancer Cell*. 2016 Nov 14;30(5):792-805. The dissertation author performed all live imaging experiments for this publication and assisted in analysis.

TETRASPANIN 3 IS REQUIRED FOR THE DEVELOPMENT AND PROPAGATION OF ACUTE MYELOGENOUS LEUKEMIA

Introduction

Acute Myelogenous Leukemia (AML) is a cancer marked by the rapid and uncontrolled growth of immature cells of the myeloid lineage²⁶. Because it is a heterogeneous disease involving a wide array of chromosomal translocations and/or mutations, response to therapy differs widely between subclasses of AML. For example, while leukemias with FIt3 mutations or MLL-translocations are generally associated with poor prognosis in both adults and children, those driven by PML/RAR translocations respond well to therapy²⁷⁻³¹. However, despite improvements in therapy for some subtypes of AML, current treatments which include chemotherapy and bone marrow transplantation, remain ineffective for a vast majority of AML patients. Thus, identifying new approaches to more effectively target common regulators of therapy resistant AML remains critically important.

In an effort to identify pathways that mediate the aggressive growth of AML and other hematologic malignancies, we have focused on stem cell programs that are subverted to drive the oncogenic state. One important regulator of such programs is the RNA binding protein Musashi. Musashi 2 (Msi2) has been shown to predict poor prognosis in patients with Chronic Myelogenous Leukemia (CML), and is critical for progression to the blast crisis phase of the disease³². Msi2 is also highly expressed in several AML lines and can serve as an indicator of poor outcome^{33,34}. The fact that multiple hematologic malignancies require Msi2 suggested that identifying stem cell programs triggered by Msi2 could lead to the discovery of pathways important for establishing and sustaining disease. Genome wide expression analysis of Msi-deficient cancer stem cell from blast crisis CML and *de novo* AML identified genes commonly regulated in both leukemias. This strategy identified Tetraspanin 3 (Tspan3), a recently identified member of the tetraspanin family, as a key downstream target of Msi2 and a potential functional element in myeloid leukemia.

The tetraspanin (tetraspan or TM4SF) family forms a large group of integral membrane proteins possessing four membrane-spanning domains separated by short intracellular and extracellular domains, as well as one long extracellular domain³⁵. Although tetraspanins are expressed across a wide variety of cells and tissue types and are involved in diverse cellular processes such as cell adhesion, proliferation, and immune responses³⁶, many tetraspanins remain understudied and the roles they play in normal stem

cell biology and in disease remain unknown. This is particularly true of Tspan3, which has been studied in context of oligodendrocyte migration³⁷, and about which little else is known. The regulation of Tspan3 by Msi2 in AML led us to test its role in leukemia development and propagation.

Results

Tspan3 is required for AML development and propagation in mouse models

To define the role of Tspan3 in leukemia, hematopoietic stem/progenitor cells (KLS) from wild type or Tspan3 null mice were infected with MLL-AF9/NRAS and transplanted (**Figure Supplement 4.2A**). Whereas 90% of recipients transplanted with wild type cells died of leukemia and only 10% survived, 53% of those transplanted with Tspan3 null cells survived, indicating a 5-fold increase in survival (**Figure Supplement 4.2B**). The cKit⁺ Gr1⁻ leukemic stem cell population expressed Tspan3 at higher levels relative to bulk leukemia, suggesting Tspan3 may be specifically important for these cells (**Figure Supplement 4.2C**). To directly test whether loss of Tspan3 impaired self-renewal of leukemic stem cells, we serially transplanted cKit⁺ cells from wild type or Tspan3 null tumors. As shown in Figure Supplement 4.2D, 100% of the mice transplanted with wild type leukemia cells developed leukemia within 69 days, whereas only 31% of mice transplanted with Tspan3 null cKit⁺ cells developed leukemia. Tspan3 loss not only significantly reduced the incidence of leukemia but also markedly increased the latency of disease (**Figure Supplement 4.2D**). These data indicate that Tspan3 is required for maintaining the self-renewal of leukemic stem cells and tumor-propagating ability of *de novo* AML.

To determine whether Tspan3 is also required in established AML, and to rule out the possibility that impaired AML propagation in Tspan3 knockouts could be due to developmental defects, we used shRNA to knock down Tspan3 in established leukemia. AML cells were transduced with control or Tspan3 shRNA and transplanted (**Figure Supplement 4.2E-F**). Whereas almost all mice transplanted with control leukemia succumbed to disease, leukemia formation was significantly impaired with Tspan3 inhibition (**Figure Supplement 4.2E**), with only 50-68% of mice transplanted with Tspan3-knock down MLL-AF9 or MLL-AF9/ NRAS AML succumbing to disease. Consistent with this, Tspan3 deficient leukemia cells were less able to form colonies *in vitro* (**Figure Supplement 4.2G**). These data indicate that Tspan3 is critical

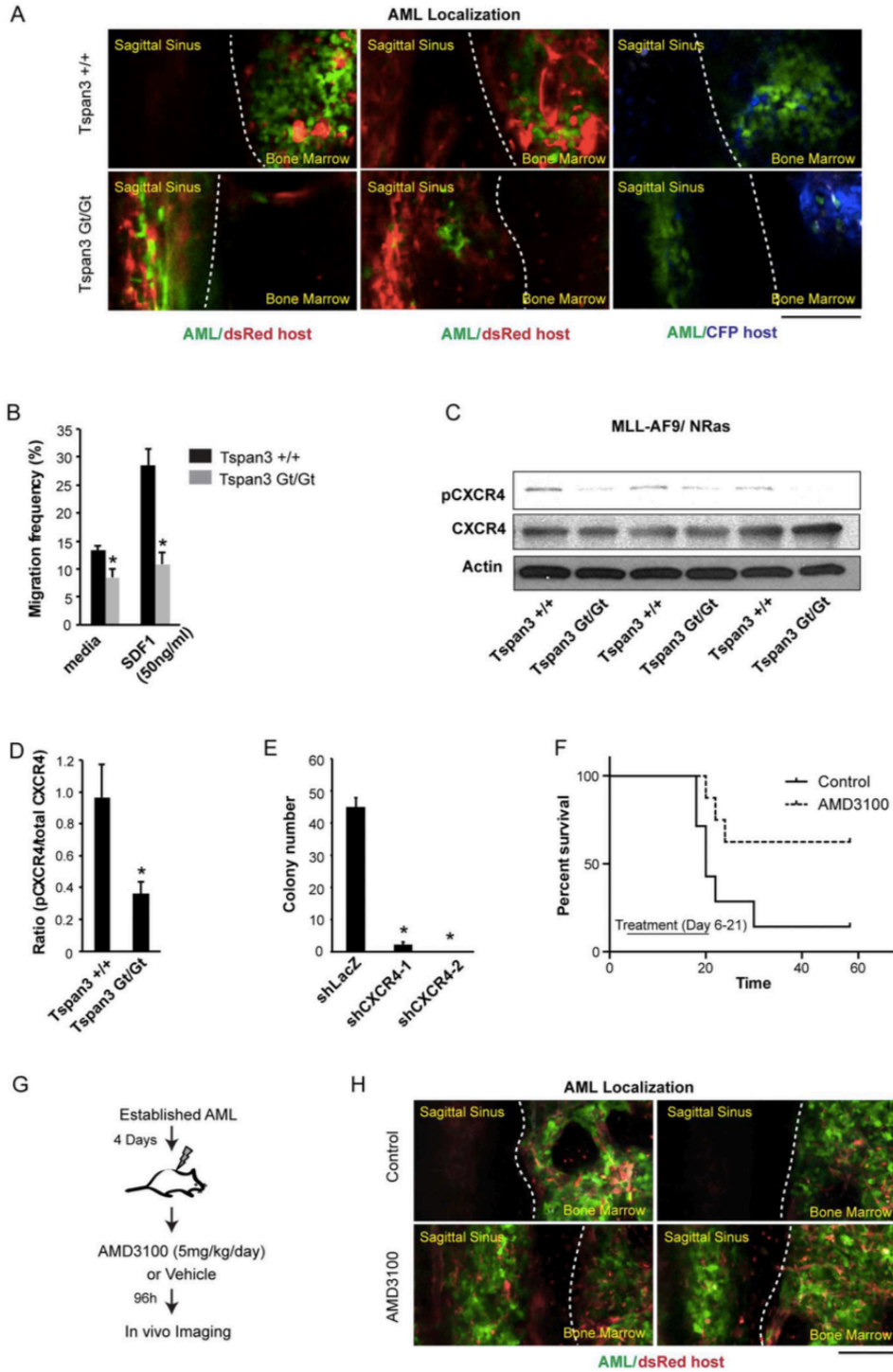
for MLL-driven leukemia, and that its inhibition can impair propagation of established AML *in vitro* and *in vivo*.

Tspan3 is required for a normal response to the chemokine CXCL12/SDF-1

The fact that neither the defects in proliferation or cell survival in Tspan3 null cells were as severe as defects observed in AML propagation (data not shown) suggested that Tspan3 may operate through additional mechanisms in context of the microenvironment *in vivo*. We thus tracked the spatial distribution of wild type and Tspan3 null leukemic cells within the bone marrow through *in vivo* imaging in real time. While control AML cells localized to an area with vascular beds known to be rich in SDF-1 on both sides of the central sinus within the calvarium³⁸⁻⁴⁰, Tspan3 null AML cells were located predominantly in the central sinus distant from SDF-1 enriched areas (**Figure 4.2A**). Consistent with these defects *in vivo*, Tspan3 deletion impaired the capacity of leukemic cells to migrate toward SDF *in vitro*. While 28% of the wild type leukemia cells migrated towards SDF-1 within 4 hours in a Boyden chamber assay, 2.5 fold fewer Tspan3 null cells (11%) migrated within the same period of time (**Figure 4.2B**). Defects in chemokine responsiveness were couple with defects in receptor activation, as loss of Tspan3 led to significantly reduced levels of activated (Ser339 phosphorylated) CXCR4 (**Figure 4.2C-D**). To test if CXCR4 acts functionally downstream of Tspan3, we inhibited CXCR4 using shRNAs and AMD3100, a small-molecule inhibitor of CXCR4-signaling. Inhibition of CXCR4 through either strategy resulted in a marked loss of colony forming ability of cKit⁺ AML cells (**Figure 4.2E**). Further, *in vivo* delivery of AMD3100 showed significantly prolonged survival (**Figure 4.2F**), and profoundly altered the *in vivo* localization of AML cells (**Figure 4.2G-H**), phenocopying the effects of Tspan3 deletion. Collectively, these data suggest that Tspan3 may influence AML growth, at least in part, by controlling CXCR4-mediated chemokine responsiveness.

Figure 4.2. Tspan3 is required for normal migration and SDF responsiveness of AML cells

(A) *In vivo* image of bone marrow region in mouse calvarium. MLL-AF9/NRAS-driven leukemic cells obtained from wild type or Tspan3 null leukemia were injected retro-orbitally into sublethally irradiated dsRed or CFP mice and the calvarial bone marrow analyzed 8 to 15 days afterward to assess localization within the bone marrow niche. The images shown were acquired in a single plane. Tspan3Gt/Gt images focus on central sinusoid region to show aberrant enrichment of cells. (B) Migration of wild type and Tspan3 null MLL-AF9/ NRAS leukemic cells to SDF1 was measured 4 hours after exposure. Error bars represent s.e.m., *p<0.05. (C-D) Protein lysates from wild type and Tspan3 null -driven leukemia were analyzed by western blot for phosphorylated CXCR4 (C) and band intensity was quantified using Image J (D). (E) Colony-forming ability of cKit⁺ MLL-AF9/NRAS leukemia transduced with either firefly luciferase shRNA as a control (shLuc) or two independent CXCR4 shRNAs (shCXCR4). (F) Survival curve of mice transplanted with established cKit⁺ MLL-AF9/NRAS leukemic wild type or Tspan3 null cells. Mice were treated with 5mg/kg/day AMD3100 or vehicle (water) for 15 days, starting 6 days post- transplant (n=8 for each cohort, data compiled from two independent experiments), p<0.05 (G) Experimental scheme for imaging leukemia localization *in vivo* following CXCR4 inhibition (E) *In vivo* image of bone marrow region (red) showing defects in localization of MLL-AF9/NRAS- leukemia cells (green) following AMD3100 treatment. Dotted white line demarcates the boundary between central sinusoid and bone marrow regions. Images are maximum intensity projections of on average 60µm z-stacks. Scale bar represents 100µm. Error bars represent s.e.m., *p<0.05.



Methods

Mice. C57BL6/J mice were used as transplant donors, B6-CD45.1 (B6.SJL-*Ptprc^aPtprc^b*/BoyJ) and C57BL6/J were used as transplant recipients. All mice were 1-5 months of age unless otherwise specified. Mice were bred and maintained in the animal care facility at University of California San Diego. All animal experiments were performed according to protocols approved by Duke University and University of California San Diego Institutional Animal Care and Use Committees.

Generation of Tspan3 knockout mice. Tspan3 knockout mice were generated from mouse embryonic stem cell line NPX312 (strain 129/Ola; Baygenomics, <http://www.mmrrc.org>). The gene trap vector (pGT1 TMpfs) was inserted between exons 3 and 4. These cells were injected into C57BL/6 blastocysts, which were then implanted into pseudo pregnant females. High-contribution chimeras were obtained. Chimeric mice were backcrossed to C57BL/6 mice and knockout mice were generated by breeding offspring of heterozygous mice. Experiments were performed with mice of mixed genetic background.

Generation and analysis of leukemic mice, and cell isolation and FACS analysis. See above in methods for Bajaj J, et al. *Cancer Cell*. 2016 Nov 14;30(5):792-805.

In vivo imaging of leukemia cells. MLL-AF9/ NRas leukemic WT and Tspan null cells (50,000 to 200,000 cells/mouse) were injected into sublethally irradiated Actin-dsRed or Actin-CFP mice. The calvarial bone marrow was imaged 8 to 15 days after transplants. Images were acquired by the Leica LAS AF 2.7.3 software with TCS SP5 upright DM600 CFS Leica confocal system using the HCX APO L 20x/1.00 W Leica Plan Aplanachromat objective.

Additional methods can be found in: Kwon HY, Bajaj J, Ito T, Blevins A, Konuma T, Weeks J, Lytle NK, Koechlein CS, Rizzieri D, Chuah C, Oehler VG, Sasik R, Hardiman G, Reya T. Tetraspanin 3 is required for the development and propagation of acute myelogenous leukemia. *Cell Stem Cell*. 2015 Aug 6;17(2):152-164.

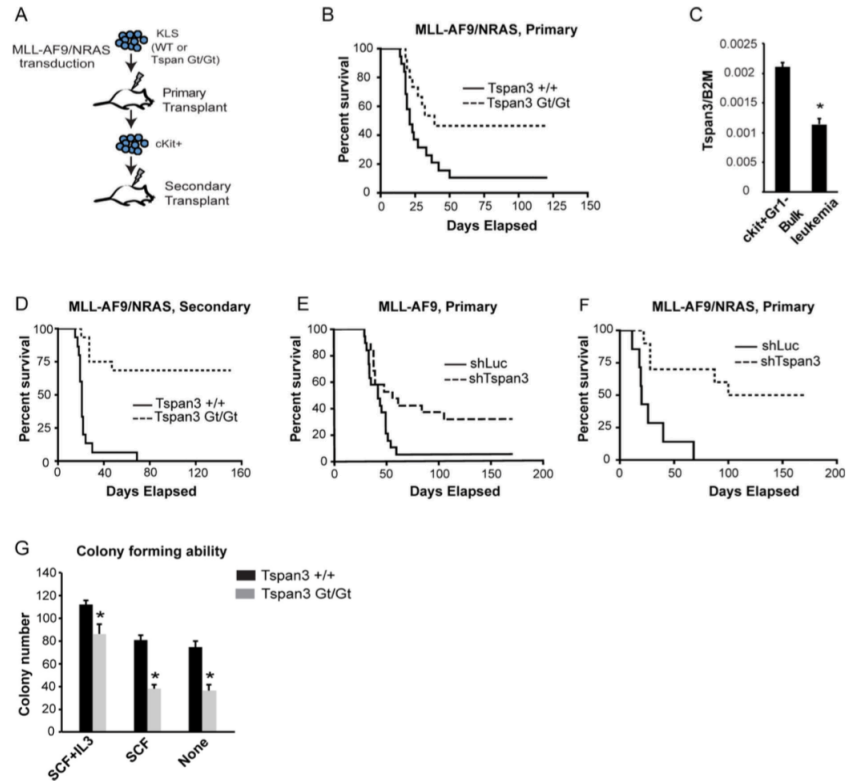


Figure Supplement 4.2. Loss of Tspan3 impairs the development and propagation of AML

(A) Experimental strategy to generate MLL-AF9/NRAS-driven leukemia from wild type or Tspan3 null mice. (B) Survival curve of mice receiving MLL-AF9/NRAS-infected wild type or Tspan3 null KLS cells. Data shown are from four independent experiments (wild type, n=19; Tspan3 null, n=15; p=0.0152). (C) Relative expression of *Tspan3* mRNA in cKit⁺ Gr1⁻ cells isolated from MLL-AF9/NRAS and in bulk leukemia (p<0.05). (D) Survival curve of mice receiving established MLL-AF9/NRAS cKit⁺ leukemic cells derived from wild type or Tspan3 null mice. Data shown are from three independent experiments (wild type, n=15; Tspan3 null, n=16; p<0.0001). (E-F) Survival curve of mice receiving established MLL-AF9 (E) or MLL-AF9/NRAS cells (F) infected with either control shLuc or shTspan3 virus; (E, n=19, p=0.02; F, n=7 for control, n=10 for shTspan3, p=0.0011). (G) MLL-AF9/NRAS-driven leukemic cKit⁺ cells were obtained from wild type or Tspan3 null leukemic mice, plated in methylcellulose in the presence of the indicated cytokines for 7 days and colony formation assessed. Error bars represent s.e.m., *p<0.05.

Acknowledgements

We are grateful to Jonathan Yang for technical support, Marcie Kritzik for help with manuscript preparation. We would also like to thank Scott Armstrong for the MLL-AF9 construct; Scott Lowe for the AML-ETO9a construct and Dong-Er Zhang for experimental advice; Warren Pear and Ann Marie Pendergast for the BCR-ABL construct; Gary Gilliland for the NUP98-HOXA9 construct. J.B. is supported by a postdoctoral fellowship from the National Cancer Center, T.I. is a recipient of a CIRM interdisciplinary stem cell training program fellowship, T.K. is supported by a postdoctoral fellowship from the Japanese Society for the Promotion of Science, C.S.K. and N.L. received support from the NIH Pharmacological Sciences Training Program (T32 GM007752), and H.Y.K was supported by the Basic Science Research Program through the National Research Foundation of Korea (NRF) funded by the Ministry of Education (2014R1A1A2A16052133). This work was also supported by a Lymphoma and Leukemia Society Scholar Award and the University of California San Diego Moores Cancer Center NCI Core Grant, P30CA23100, as well as by NIH grants DK63031, HL097767 and DP1 CA174422 awarded to T.R.

Author contributions

H.Y.K. and J.B. planned, designed and performed the majority of experiments and helped write the manuscript. T.I. carried out all genomic scale analysis of wild type and Msi2 null AML and bcCML. A.B., T.K., J.W., N.K.L. and C.S.K. provided experimental data and help. D.R., C.C. and V.G.O. provided primary leukemia patient samples and experimental advice. R.S. and G.H. carried out all bioinformatics analysis on microarray data. T.R. planned and guided the project and wrote the manuscript.

Dissertation Acknowledgements

Chapter 4, in part, a reprint of the material as it appears in *Cell Stem Cell*: Kwon HY, Bajaj J, Ito T, Blevins A, Konuma T, Weeks J, Lytle NK, Koechlein CS, Rizzieri D, Chuah C, Oehler VG, Sasik R, Hardiman G, Reya T. Tetraspanin 3 is required for the development and propagation of acute myelogenous leukemia. *Cell Stem Cell*. 2015 Aug 6;17(2):152-164. The dissertation author performed all live imaging experiments for this publication and assisted in analysis.

UBIQUITIN-CONJUGATING ENZYME UBC13 CONTROLS BREAST CANCER METASTASIS THROUGH A TAK1-P38 MAP KINASE CASCADE

Introduction

Breast cancer (BCa) is the leading invasive cancer among women worldwide. BCa-related mortality is usually caused by distant metastases rather than primary tumors^{41,42}. The spread of cancer cells from primary tumors to distant organs, termed metastasis, is a multistep process in which cancer cells must (i) invade through the extracellular matrix (ECM), (ii) disseminate into the bloodstream, (iii) survive in the circulation, and (iv) extravasate and successfully colonize distant sites⁴³. Conventional therapeutic strategies have limited success in preventing and treating metastatic cancer, and BCa metastases can recur many years after removal of the primary tumor. This phenomenon could be due to the complex nature of metastasis itself, and, more realistically, the limitation of current treatments that are effective against primary BCa, i.e., surgical removal and localized radiotherapy, but do little to prevent metastatic recurrence. Even chemotherapy is not very effective against metastatic tumors⁴⁴. Unfortunately, the pharmaceutical industry has been reluctant to conduct metastasis prevention trials on patients with early stage cancer using survival and reduction of metastatic load as end points, because such studies are lengthy and require a large number of patients with otherwise relatively good survival prospects⁴⁴. Consequently, the development of agents that prevent metastasis from occurring and trigger regression of established metastatic lesions is an urgent unmet need.

It was reported that expression of the ubiquitin conjugating enzyme (E2) Ubc13 is up-regulated in metastatic BCa⁴⁵. Ubc13, which heterodimerizes with Uev1a, catalyzes formation of lysine 63 (K63)-linked polyubiquitin chains, which control protein–protein interactions involved in DNA damage repair and protein kinase activation^{46,47}. In certain immune cells, Ubc13 is required for I κ B kinase (IKK)–nuclear factor κ B (NF- κ B) activation, but a more ubiquitous role for Ubc13 was observed in the activation of MAPK signaling⁴⁸⁻⁵⁰. We found that Ubc13 is required for activation of mitogen-activated protein kinase kinase kinase 1 (MEKK1), transforming growth factor β (TGF β)-activating kinase 1 (TAK1), and downstream MAPK cascades on CD40 engagement in B cells⁵¹. Importantly, MEKK1 and TAK1 are also required for BCa metastasis^{52,53}. Of the numerous signaling pathways affecting BCa metastasis, the TGF β pathway has some of the strongest effects, and it promotes metastasis by inducing migration, intravasation, and epithelial-mesenchymal transition (EMT) of carcinoma cells⁵⁴. TGF β signaling is mediated through SMAD-

dependent and -independent (non-SMAD) pathways^{55,56}. Non-SMAD TGF β signaling is positively regulated by multiple molecules including TAK1⁵⁷, tumor necrosis factor receptor-associated factor 6 (TRAF6)⁵⁸, and TRAF4⁵⁹. The p38 MAPK also participates in different steps of metastasis, including ECM invasion by primary cancer cells, migration across the surrounding tissue, entry into the circulation, and colonization of distant sites⁶⁰. p38 inhibitors are not toxic and were found effective in prevention and attenuation of inflammatory pain in humans^{61,62}. Here we show that a Ubc13-controlled TAK1–p38 cascade controls BCa metastatic dissemination and that a p38 inhibitor can cause regression of established metastases.

Results

To address if Ubc13 controls metastasis, we used an inducible shRNA lentivirus that allows gene silencing on doxycycline (Dox) treatment while labeling transduced cells with red fluorescent protein (RFP)⁶³. In LM2 cells transduced with this construct, Dox led to stable inhibition of Ubc13 expression within 3 d, and Dox withdrawal restored Ubc13 expression as early as day 3 with full expression on day 5 (**Figure Supplement 4.3A**). Flow cytometry and immunofluorescence (IF) microscopy confirmed that both p10-shCtrl– and p10-shUbc13– transduced cells were uniformly RFP positive after Dox addition (**Figure Supplement 4.3B**). To address whether Ubc13 is required for entry of BCa cells into the lung, p10-shControl– and shUbc13– transduced LM2 cells were cultured with Dox for 4 d, and tail vein injected into NOD/SCID mice that were kept on Dox-containing water for 1 wk and switched to regular drinking water for 3 wk. Lung metastasis was monitored weekly by a bioluminescence assay. Curiously, no differences in lung metastasis were observed between the two groups (**Figure Supplement 4.3C**), indicating that Ubc13 activity is not required for lung seeding, a process that was probably completed within the first 24 h. We also injected p10-shControl and shUbc13 LM2 cells into NOD/SCID mice that were kept on regular water for 1 wk, allowing the cells to enter the lung and colonize it. The mice were then given Dox-containing water to silence Ubc13 expression. Whereas p10-shControl cells formed detectable lung metastases as early as 2 wk after injection, p10-shUbc13 cells did not form detectable metastases in Dox-treated mice (**Figure Supplement 4.3D**). Microscopic analysis under bright field (BF) and red fluorescence (RFP) confirmed that shUbc13-LM2 cells formed much fewer and smaller lung nodules than shControl-LM2 cells (**Figure**

Supplement 4.3E). These data demonstrate that while Ubc13 is dispensable for BCa extravasation from the peripheral blood to lung tissue, it is required for establishment of macroscopic metastatic growth.

To further study how Ubc13 affects metastatic growth, we performed tumorsphere formation assays on control and shUbc13 cells and found that Ubc13 silencing had no effect on these properties (**Figure 4.3A-B**). These results are consistent with the finding that Ubc13 is generally dispensable for primary tumor growth (data not shown). Loss of Ubc13 in BCa cells also did not affect their proliferation as evident by carboxyfluorescein succinimidyl ester (CFSE) labeling (**Figure 4.3C**). Importantly, loss of Ubc13 also did not affect LM2 cell intravasation or extravasation quantified by qPCR (**Figure 4.3D**). Through real-time *in vivo* imaging, we observed no difference in frequencies of circulating tumor cells between shControl and shUbc13 LM2 transplanted mice (**Figure 4.3E-F, Table 4.1**). We therefore reasoned that Ubc13 could specifically control metastatic BCa growth properties. Indeed, shUbc13 BCa cells residing in small lung lesions were less proliferative than shControl cells in lung lesions and were more likely to show caspase 3 activation (**Figure Supplement 4.3F**). In keeping with Ubc13 being dispensable for primary tumor growth, we did not observe a difference in proliferation and apoptosis of BCa cells within primary tumors formed by shControl- or shUbc13-LM2 cells (data not shown).

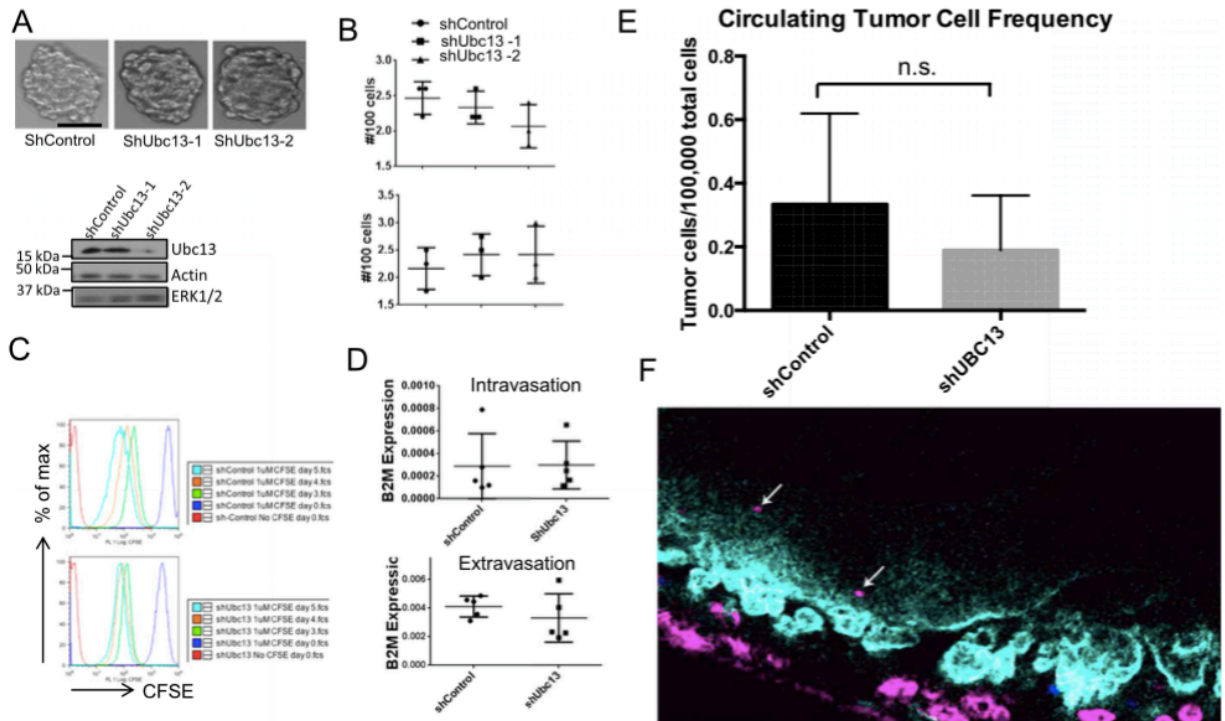


Figure 4.3. Ubc13 is not required for BCa tumorsphere formation, intravasation, or extravasation. (A-B) Tumorsphere formation assays of shControl- and shUbc13-PyMT (Py8119) cells. (A) Representative images showing tumorspheres formed by the indicated cells (Left) and their Ubc13 protein content (Right). (B) Frequencies of primary (Upper) and secondary (Lower) tumorsphere formation by indicated cells. (C) Histogram of CFSE dilution assays of shControl (Upper) and shUbc13 (Lower) PyMT cells at the indicated time points. (D) Comparison of intravasation (Upper) and extravasation (Lower) by shControl- and shUbc13-LM2 cells. Data are presented in arbitrary units, and the expression of human specific $\beta 2$ microglobulin (B2M) was normalized to that of mouse specific β -actin. Results are shown as averages \pm SEM. (E) Average circulating tumor cell frequencies imaged in mice transplanted with control and UBC13 knockdown tumor cells in 100,000 total blood cells. ($n = 6$ independent tumors for shControl and shUbc13 each, $P = 0.6757$). Total blood volume for duration of imaging was determined by multiplying the vessel cross-sectional area with the speed of blood flow; total cell count for each movie was determined from the cell number per nanoliter of mouse peripheral blood; circulating tumor cells were scored positively if $8 \mu\text{m}$ or larger in diameter. (F) Representative image showing tumor cell in blood vessel. Endothelial cells marking vessel wall (cyan), EGFP transplant recipient (blue), and tumor cells (magenta).

Methods

Cells, plasmids, and lentiviral infection. MDA-MB-231 4175 LM2, PyMT, and MT2 cells were maintained as previously described⁶⁴⁻⁶⁶. 4T1 cells were cultured in DMEM containing 10% FBS and Penn Strep. Primary carcinoma cells were obtained from spontaneous tumors grown in MMTV-cNeu/ErbB2 mice through a mincing, digestion, and filtration process as previously described⁶⁶. Lentiviral shGFP (designated as shControl) and shUbc13 constructs were described⁶⁷ and confirmed by sequencing. Scrambled shRNA was from Addgene (Plasmid 17920: pLKO.1 shSCR). The inducible lentiviral shRNA constructs p10-shControl and p10-shUbc13 were cloned as previously described⁶³. Briefly, the hairpin oligos were designed following instructions available on the website (<http://katahdin.mssm.edu/siRNA/RNAi.cgi?type=shRNA>). The sequence of p10-shUbc13 is as follows: TGCTGTTGACAGTGAGCGATAAAGTACGTTTCATGACCAATAGTGAAGCCACAGATGTATTGGTCAT GAAACGTA CTTTAGTGCCTACTGCCTCGGA. The sequence of p10-shControl (targeting *Drosophila* row gene) is as follows: TGCTGTTGACAGTGAGCGATAATGGAATATCTGCGACGGATAGTGAAGCCAC AGATGTATCCGTCGCAGATATTCCATTACTGCCTACTGCCTCGGA. The oligos were used as templates for PCR using primers: forward (CAGAAGGCTCGAGAAGGTATATTGCTGTTGACAGTGAGCG); reverse (CTAAAGTAGCCCCTTGAATTCCGAGGCAGTAGGCA). The PCR products were then purified and digested with XhoI/EcoRI followed by ligation to the XhoI/EcoRI-linearized pINDUCER-10 vector⁶³. Positive clones were verified by Sanger sequencing. An RNAi-resistant form of Ubc13 (RR) was produced by introducing sense mutations (no alteration of amino acids) at the small interfering RNA (siRNA)-binding site. To generate a Ubc13-expressing lentiviral construct, the cDNA was cloned into pLA-CMV lentiviral vector that contains a neomycin resistance cassette. The C87A mutation was introduced through site-directed mutagenesis (Stratagene). MKK3(EE) cDNA with Flag epitope at its N-terminal (7) was inserted into a pLA-CMV vector with neomycin selection marker. The shRNA or lentiviral expression constructs were transfected along with pLV-CMV delta (Inder Verma, Salk Institute) and pVSV-G (Clontech) into 293FT cells to produce viral particles⁶⁸ used to infect indicated breast cancer (BCa) cells. The transduced cells were selected and maintained in growth medium containing puromycin or neomycin. For the p10-shRNA-infected cells, doxycycline (Dox) was supplemented into the puromycin-containing medium.

In Vivo Live Imaging of Circulating Tumor Cells. Four- to 6-wk-old female NOD/SCID mice with constitutive expression of GFP under the control of the actin promoter (Jackson Laboratories) were used. LM2 cells (2×10^5) expressing Dox-inducible shRNA-RFP were suspended in PBS, mixed with matrigel in a 1:1 ratio, and injected into the fourth mammary fat pads. Tumors were allowed to develop for 4–5 wk while mice were maintained on Dox (2 mg/mL in drinking water, ad libitum). For imaging, each mouse was anesthetized by i.p. injection of ketamine and xylazine (100/20 mg/kg) and maintained under anesthesia throughout the procedure using 1–2% isoflurane gas mixed with oxygen. To visualize blood vessels, each mouse was injected retro-orbitally with AlexaFluor 647 anti-mouse CD144 (VE-cadherin) antibody immediately following anesthesia induction. Tumors were exposed by carefully removing hair, skin, and connective tissue while keeping tumor vasculature intact. The mouse was then placed inverted on an imaging apparatus, and each tumor was elevated and stabilized on a glass slide to reduce breathing artifacts. Movies were acquired by Leica LAS AF 1.8.2 software with an upright Leica SP5 confocal system. An HCX APO L20 \times objective with a 1.0 numerical aperture was used to continuously acquire images in 1,024 \times 512 format. GFP, RFP, and AlexaFluor 647 were excited with an Argon/2 laser, a diode-pumped solid-state laser, and a HeNe 633 laser, respectively. Multicolor imaging was captured simultaneously for GFP and AlexaFluor 647 and sequentially for RFP.

Additional methods can be found in: Wu X, Zhang W, Font-Burgada J, Palmer T, Hamil AS, Biswas SK, Poidinger M, Borchering N, Xie Q, Ellies LG, Lytle NK, Wu LW, Fox RG, Yang J, Dowdy SF, Reya T, Karin M. Ubiquitin-conjugating enzyme Ubc13 controls breast cancer metastasis through a TAK1-p38 MAP kinase cascade. *Proc Natl Acad Sci U.S.A.* 2014 Sep 23;111(38):13870-13875.

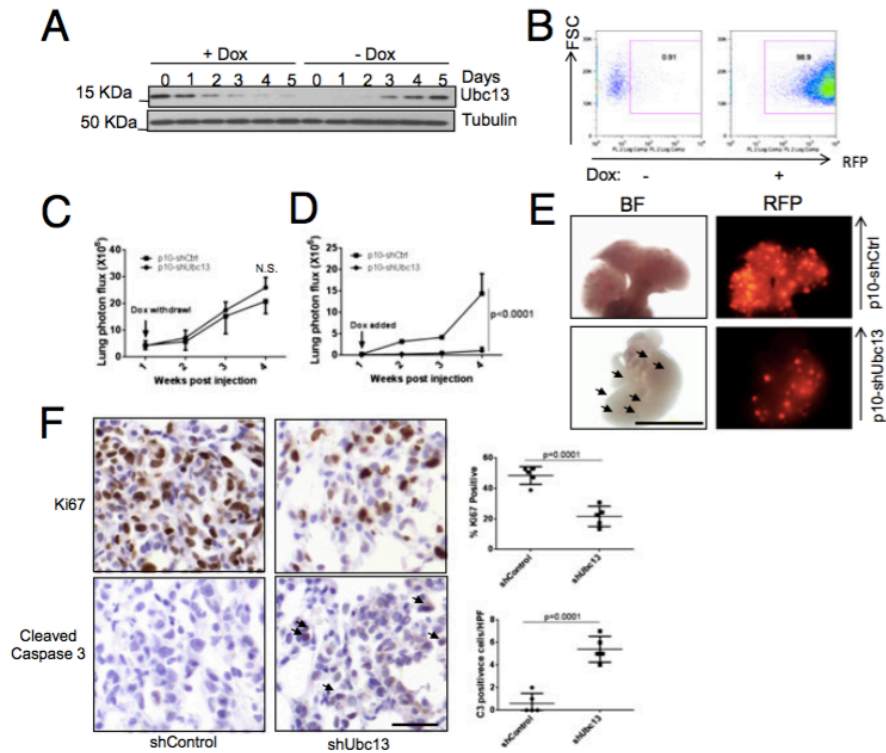


Figure Supplement 4.3. Ubc13 is required for lung colonization by BCa cells. (A) Dynamic, doxycycline (Dox)-regulated, Ubc13 silencing in p10-shUbc13-infected LM2 cells. (B) Analysis of RFP expression by p10-shCtrl or p10-shUbc13-infected LM2 cells cultured in the absence (–) or presence (+) of Dox for 4 d. (C) BLI measurement of mice injected with Dox-treated p10-Ctrl or p10-shUbc13 LM2 cells, given Dox in water for the first week and switched to regular water for the following 3 wk. (D) BLI measurement of mice injected with p10-shCtrl or p10-shUbc13 LM2 cells that were not treated with Dox. Mice were given regular water for the first week and switched to Dox-containing water for the following 3 wk. Data in C and D are averages \pm SEM; $n = 3$ mice. (E) Representative bright field and RFP images of lungs from mice transplanted with p10-shCtrl (Upper) or p10-shUbc13 (Lower) LM2 cells and treated as in D. (Scale bar, 1 cm.) (F) Ki67 and cleaved caspase 3 staining of lung lesions in mice that were i.v. inoculated with shControl- or shUbc13-LM2 cells (4 wk after injection). Five independent high-power fields were quantitated, and the results are shown on the right as averages \pm SEM. (Scale bar, 100 μ m.)

Table 4.1. Summary of circulating tumor cells in shCtrl and shUbc13 breast tumors

shControl							
Experiment	1	2	3	4	5	6	Total
Time (min)	29.5	60	60	92.7	130.2	30	402.4
Blood volume (nl)	37.5	179.2	88.6	1020.6	1370.5	70.2	2766.6
Total cells	397256	1899288	939493	1.1E+07	1.5E+07	744008	2.9E+07
Tumor cells >8mm	1	0	0	0	0	13	14

shUBC13							
Experiment	1	2	3	4	5	6	Total
Time (min)	60	44.2	60.1	64.9	98.2	60	387.5
Blood volume (nl)	44.9	113.4	1012.2	218.8	831.9	325.2	2546.3
Total cells	475490	1202150	1.1E+07	2318831	7968044	3446844	2.6E+07
Tumor cells >8mm	5	0	5	0	3	0	13

Acknowledgements

We thank Santa Cruz Biotechnology, Cell Signaling Technology, and GeneTex for providing antibodies, K. Taniguchi for help with histological analysis, J. Massague (Memorial Sloan Kettering Cancer Center) for sharing MDA-231 LM2 cells, S. Elledge (Harvard Medical School, Brigham and Women's Hospital) for sharing the inducible lentiviral shRNA vector, P. Sun (The Scripps Research Institute) for pBabeMKK3(EE), F. Zozzoli and J. Lum [Functional Genomics platform, Singapore Immunology Network, Agency for Science, Technology and Research (A*STAR)] for help with the microarray study, Y. Yang and M. Kelliher (University of Massachusetts Medical School) for sharing shUbc13 plasmids, M. Fujimuro (Kyoto Pharmaceutical University) for Ubc13 expression constructs, Jeevisha Bajaj for help with analysis of real time imaging, and J. Xu and E. Theodorakis (University of California, San Diego) for chemical inhibitor synthesis. S.K.B. and M.P. are grateful for funding from the Biomedical Research Council, A*STAR. X.W. was supported by a postdoctoral fellowship from Susan G. Komen for the Cure (KG111506). Funding was provided by National Institutes of Health (NIH) Grants 1R01CA168689 (to J.Y.), 3R01CA168689-02W1 (to T.P.), DP1CA174422 (to T.R.), T32 CA009523-29 (to R.G.F.), T32 GM007752-36 (to N.K.L.). Work was also supported by NIH Grants CA163798 and AI043477 and a San Diego Cancer Center Council Collaborative Translational Grant sponsored by Pedal the Cause San Diego (to M.K.). M.K. is an American Cancer Society Research Professor and holds the Ben and Wanda Hildyard Chair for Mitochondrial and Metabolic Diseases.

Author contributions

X.W. designed research; X.W., A.S.H., S.K.B., M.P., and N.K.L. performed research; W.Z., J.F.-B., T.P., L.G.E., L.-W.W., R.G.F., J.Y., and S.F.D. contributed new reagents/analytic tools; X.W., W.Z., N.B., Q.X., N.K.L., T.R., and M.K. analyzed data; and X.W. and M.K. wrote the paper.

Dissertation Acknowledgements

Chapter 4, in part, a reprint of the material as it appears in *PNAS*. Wu X, Zhang W, Font-Burgada J, Palmer T, Hamil AS, Biswas SK, Poidinger M, Borchering N, Xie Q, Ellies LG, Lytle NK, Wu LW, Fox RG, Yang J, Dowdy SF, Reya T, Karin M. Ubiquitin-conjugating enzyme Ubc13 controls breast cancer

metastasis through a TAK1-p38 MAP kinase cascade. *Proc Natl Acad Sci U.S.A.* 2014 Sep 23;111(38):13870-13875. The dissertation author performed and analyzed all live imaging experiments for this publication.

EPIGENETIC AND TRANSCRIPTOMIC PROFILING OF MAMMARY GLAND DEVELOPMENT AND TUMOR MODELS DISCLOSE REGULATORS OF CELL STATE PLASTICITY

Introduction

At diagnosis, most tumors present as heterogeneous collections of tumor cells and stroma. Many factors promote the cell state changes that contribute to tumor heterogeneity, drug resistance, tumor metastasis, and poor patient outcomes^{69,70}. Recent studies reveal that some oncogene-induced cell state changes that occur during tumor progression can be traced to mechanisms enabling cancer cells to adopt behaviors that are not part of their homeostatic repertoire⁷¹. This behavior, which we will refer to as cell state instability or plasticity, has some of the characteristics of the lineage infidelity acquired during wound healing⁷², or inflammation or oncogene associated reprogramming to a multi-potential embryonic or stem-like state⁷³. Better understanding of the mechanisms that underlie cell state instability in tumor progression could create opportunities for therapeutic intervention.

The cancer stem cell (CSC) hypothesis was initially attractive because it predicted the existence of a cellular subpopulation uniquely able to generate intra-tumoral heterogeneity, and that therapeutic targeting of these cells would prevent subsequent tumor evolution. However, it is now established that even differentiated cells can be reprogrammed into stem-like cells, suggesting that cell state reprogramming is more common and occurs in more diverse cell types than previously thought^{74,75}. Indeed, this type of reprogramming can be used to re-establish stem-like hierarchies in tumors even after elimination of putative CSCs^{76,77}. These data suggest that eliminating phenotypically unstable cells will likely be fruitless, as other cells will take their place. Rather, abrogating the mechanisms by which tumor cells gain cell state plasticity may be more productive.

We focused on the relationship between mammary gland development and aggressive breast cancers to better understand the mechanisms by which differentiated cells revert to other cell states, and by which intra-tumoral heterogeneity and malignancy arise. Despite its structural simplicity, the mammary gland undergoes impressive growth and invasive phases during development, cyclical expansive and apoptotic phases controlled by estrus cycles, and massive tissue expansion and involution associated with pregnancy and lactation⁷⁸. Clearly, mammary ducts must contain cells with significant growth, invasive, and multi-lineage potential. The coordinated cell state changes these cells undergo make the mammary tissue an excellent system in which to study mechanisms of cell state plasticity.

Whether adult mammary gland homeostasis requires a hierarchical relationship involving multipotent mammary stem cells (MaSCs) has been controversial. The capacity for basal cells to form reconstituted glands in transplantation assays has supported the notion that multipotent MaSCs reside in the basal fraction of the adult mammary gland^{79,80}. However, lineage tracing studies have produced conflicting results as to whether adult basal cells are multipotent or unipotent⁸¹⁻⁸⁶. On the other hand, studies have supported the conclusion that bipotent MaSCs are present in the fetus (i.e., fMaSCs)^{84,87,88}. Because lineage tracing experiments measure cell fate only in the context of a native structure, and functional assays only measure the developmental potential of cells under non-native conditions, the development of agnostic molecular approaches may better predict the differentiation potential of mammary cells and enable identification of differentiation state regulators.

Cancer has been referred to as a caricature of normal development and of tissue renewal (see Wahl and Spike, 2017 for references⁷³). Therefore, to ascertain development correlates of breast cancer, we designed this study with three goals: 1) to generate epigenetic and transcriptomic maps of the developmentally plastic, bipotent fetal mammary stem cell (fMaSC) and the adult lineages descended from them; 2) to identify genes, transcriptional regulators, and control regions associated with fetal mammary stem cell (fMaSC) bipotentiality that are altered upon adult lineage specification; 3) and to test whether such regulators are altered during cancer progression, and contribute to the genesis of intra-tumoral heterogeneity.

Results

Sox10 is associated with the developmental plasticity and bipotentiality of fMaSCs:

We first performed ATAC-seq and RNA-seq on biological replicates of mammary cell populations enriched for E18 fMaSCs, adult basal cells, luminal progenitor cells (LPs), and mature luminal cells (MLs) using FACS-based purification with previously established cell surface markers and corresponding phenotypic characterization (**Figure Supplement 4.4A**)^{87,89}. ATAC-seq maps chromatin accessibility and indicates the potential of a flanking gene to be expressed. By contrast, RNA-seq maps transcript levels, and hence correlates more directly with cellular phenotype at the time of analysis. We identified chromatin regions that are uniquely open or closed in each of the four mammary cell populations (Uniquely Accessible

Region, UAR, and Uniquely Repressed Region, URR, respectively) and identified transcription factor (TF) motifs within the UARs and URRs. Homer revealed expected enrichment of the P63 and TEAD4 DNA binding motifs in basal cells, the ELF5 DNA binding motif in LPs, and the FOXA1 and Jun-AP1 DNA binding motifs in MLs (**Figure Supplement 4.4B**). These TF DNA binding motifs have also been mapped to uniquely active enhancers of the analogous populations of human mammary cells⁹⁰. Notably, binding motifs for SOX4, SOX9, SOX10, and NF1 were significantly enriched in fMaSC UARs compared to the other cell types (**Figure Supplement 4.4B**). Moreover, many regions containing these SOX motifs were specifically closed in MLs (enriched in ML URRs), which are the most differentiated (least developmentally plastic) of the four mammary cell types (**Figure Supplement 4.4C**). Of these SOX factors, SOX10 uniquely exerts potent cell reprogramming capacities in vitro⁹¹ and is most differentially upregulated in the developmentally plastic fMaSC population (**Figure Supplement 4.4B**). Further, in fMaSCs, UARs adjacent to highly expressed genes contained more SOX10 binding motifs than UARs adjacent to genes expressed at lower levels (a trend that was not observed with other TFs, such as NF1, P63, and FRA1). These data suggest an association between SOX10 binding and chromatin activation in fMaSCs. Collectively, these data associate SOX factors (SOX10 in particular) with the developmental plasticity and bipotentiality of fMaSCs.

We then developed Sox10 reporters to enable the visualization and recovery of SOX10^{high} and SOX10^{low} tumor cells to evaluate correlations between SOX10 levels and gene expression changes (**Figure Supplement 4.4D**). RNA-seq analysis was performed on SOX10^{high} and SOX10^{low} luminal-like fractions from PY230 orthotopic and C3-1 autochthonous tumors. We built transcriptome profiles of SOX10^{high} and SOX10^{low} luminal-like cell populations, and ascertained stem/progenitor relatedness using Gene Set Enrichment Analysis (GSEA) with signature gene lists representing stem/progenitor populations from the normal mammary gland. We also used Spearman correlation to compare chromatin accessibility in SOX10^{high} and SOX10^{low} tumor cell populations with the UARs and URRs found in normal mammary cells. The chromatin accessibility of the SOX10^{high} PY230 tumor cells correlated significantly with unique chromatin features in LPs and fMaSCs (and to a smaller extent, basal cells) (**Figure Supplement 4.4E**). On the other hand, SOX10^{low} PY230 tumor cells correlated strongly with LP and ML UARs. Thus, while the chromatin features of SOX10^{high} PY230 tumor cells correlate better with stem/progenitor populations than

do SOX10^{low} tumor cells, both of these cell types possess blended chromatin features that are not apparent in the normal adult mammary cells from which they are derived.

We determined whether chromatin accessibility reflects gene expression using GSEA of the transcriptomes of SOX10^{high} and SOX10^{low} tumor cells. We used gene sets associated with UARs and URRs for fMaSCs, basal cells, LPs and MLs. These analyses revealed that SOX10^{high} cells up-regulated genes uniquely open in fMaSCs and LPs, and genes uniquely closed in MLs (**Figure Supplement 4.4F**). By contrast, SOX10^{low} tumor cells up-regulated genes uniquely open in MLs. Thus, stem/progenitor identity, as indicated by chromatin accessibility in SOX10^{high} vs. SOX10^{low} cells, correlated strongly with the transcriptome profiles of these cells. We infer that SOX10 contributes to the observed stem/progenitor identity, as there is significant enrichment in the SOX10^{high} tumor fraction for genes we previously showed are upregulated following SOX10 overexpression in an in vitro organoid culture model (**Figure Supplement 4.4F**)⁹².

SOX10^{high} cells within mammary tumors exhibit de-differentiated and EMT-like features

Ectopic overexpression of SOX10 reprograms mammary epithelial cells into a mesenchymal-like cell state⁹². Strikingly, analysis of sections from C3-1 mammary tumors revealed that SOX10^{high} cells expressed low levels of epithelial cytokeratins, whereas cells with lower SOX10 expression retained epithelial markers (**Figures 4.4A-B**). To better quantify the relationship between SOX10 and epithelial markers, we dissociated C3-1 mammary tumors to single cells, and found that >80–90% of SOX10^{high} cells had undetectable levels of KRT8 and KRT14 (**Figures 4.4C-D**). SOX10^{high} tumor cells form tumorspheres in 3-D culture conditions at low efficiency, and these tumorspheres exhibited high levels of SOX10 and low levels of cytokeratins (**Figure 4.4E**). Thus SOX10^{high} cells in these basal-like mammary tumors showed reduced levels of keratin markers associated with the epithelial state and mammary cell differentiation.

We analyzed the PY230 mammary tumor model to determine the generality of the relationship between Sox10 expression and loss of epithelial features. Notably, SOX10^{high} PY230 mammary tumor cells also exhibited significant decreases in multiple epithelial and luminal mammary cell markers compared to SOX10^{low} mammary tumor cells (**Figure 4.4F**). SOX10^{high} cells also had increased expression of the mesenchymal/EMT markers Vim, Snai2, and Twist1. As ectopic expression of SOX10 in normal mammary

cells also elicits de-differentiation and mesenchymal-like features with similar corresponding gene expression changes⁹², we infer that SOX10 directly contributes to this cell state change. Because SOX10 over-expression can also induce motility and mammary cell delamination in 3D culture⁹², we determined whether SOX10^{high} cells also locally invade in mouse tumor models in vivo. Strikingly, significant numbers of SOX10^{high} cells in PY230 tumors were found outside the primary tumor margin and in close proximity to tumor vasculature (**Figure 4.4G**).

We examined the TCGA database to determine if SOX10 is similarly linked to EMT and de-differentiation in human breast cancer. We generated a rank-order list of human genes based on the correlation of their expression with SOX10 expression across a panel of human breast tumors. Many EMT-related genes positively correlated with SOX10 expression, whereas many epithelial/differentiation related genes negatively correlated with SOX10 expression (**Figure 4.4H**). Moreover clear expression of the mesenchymal marker VIM could also be detected in many of the SOX10⁺ tumor cells (**Figure 4.4I**).

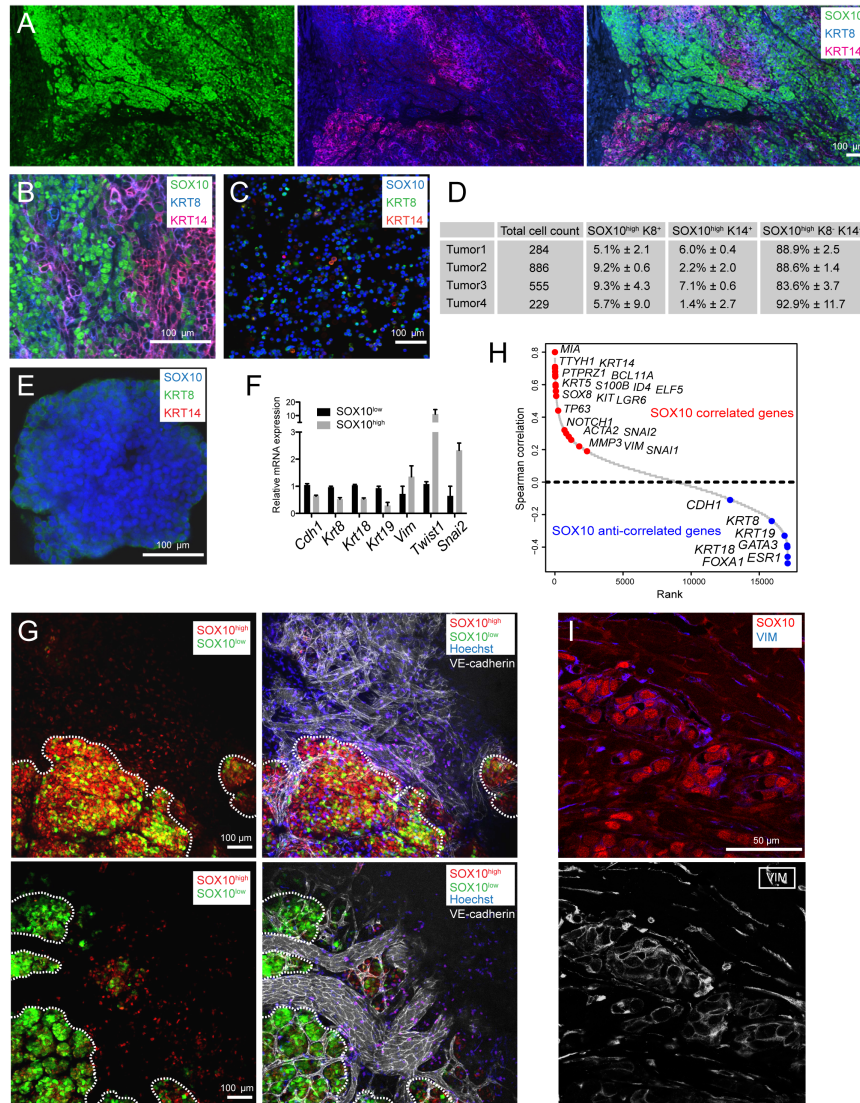


Figure 4.4. SOX10⁺ tumor cells exhibit de-differentiation and mesenchymal features.

(A-B) Low (A) and high (B) magnification image of C3-1; Sox10-H2BVenus mammary tumors immunostained for K8, K14, and GFP (SOX10). (C) Single cell dissociation of a C3-1; Sox10-H2BVenus mammary tumor immunostained for K8 and K14. (D) Quantification of keratin status in four C3-1; Sox10-H2BVenus mammary tumors. Average percentage and 95% confidence interval from two images for each tumor are shown. (E) Tumorsphere grown from C3-1; Sox10-H2BVenus mammary cells plated in 3-D culture, immunostained for K8 and K14. (F) Relative expression of differentiation and mesenchymal genes in PY230 tumor cells. Mean ± SEM (n=2). (G) PY230 Sox10^{tdTomato} tumor showing SOX10⁺ cells (red) in the primary tumor margin and near vasculature (white). PY230 Sox10^{tdTomato} tumor cells were labeled with a LV-GFP to visualize tumor cells not expressing SOX10 (green). (H) Rank order list of SOX10 co-expression genes in human breast tumors with epithelial (blue) and EMT-associated (red) genes highlighted. (I) Tissue section from an ER⁻ PR⁻ HER2⁻ human breast tumor immunostained for SOX10 and VIM.

Methods

Mice. The Sox10-H2BVenus⁹³, Sox10^{flox}⁹⁴, C3-1-TAg⁹⁵, and Trp53^{flox};Brca1^{flox} (Perou CM et al., manuscript in progress) mice have been previously described. For tumor studies, mice were maintained in an FVB background, except for the Sox10^{flox};C3-1-TAg study in which mice were in a mixed CD1/FVB/B6 background. The Sox10^{flox} LoxP cassette was deleted by a Zp3-Cre mouse⁹⁶. Orthotopic transplantation of PY230 cells were performed with 6-10 week old adult wild-type C57bl/6 mice. All animals were handled in accordance with Salk Institute IACUC and AAALAC approved protocols and other ethics guidelines.

Mammary tumor cell transplantation. PY230 cells grown in 2-D culture were orthotopically transplanted into the #4 fat pads of 6-10 week old syngeneic mice. 10,000-200,000 cells were used per transplantation, unless otherwise indicated in text. Surgery and recovery of animals followed strict and IACUC-approved protocols.

PY230 CRISPR-based genome modification. PY230 cells were grown in media conditions that have previously been described⁹⁷. For genome modification of PY230 cells, the PY230 cells were first infected at <3 MOI with CD0616, a lentivirus containing a floxed Cas9-2A-G418^R cassette modified from LentiCrisprV2⁹⁸. G418-resistant cells were expanded as PY230-Cas9 cells. To target the Sox10 locus for tdTomato, a targeting vector was designed in an AAV backbone sequentially containing: an sgRNA cassette vs. genomic sequence proximally downstream of the stop codon (AGGCCAAGCCCTGACTGAGC), 268 bp 5' homology arm, in-frame AVI-V5-V5-2A-tdTomatoNLS cassette, LoxP-EFS-TagBFP-CW3SL-LoxP, 394 bp 3' homology arm. AAV was generated by transfection with PEI (Polysciences) in 293A cells with the AAV SOX10 TV, transfer plasmid, and DJ cap plasmid. PY230-Cas9 cells were infected with the AAV, TagBFP⁺ cells were isolated by FACS and plated at clonal density, and PY230 clones were picked, expanded, screened by PCR, and sequenced to validated candidates. AAV-Cre was then used to remove the Cas9 and the TagBFP cassette. Protein lysates from PY230-Sox10^{tdTomato} mammary tumors that were immunoprecipitated with streptavidin and immunoblotted with a V5 antibody confirmed the specific presence of a single protein at SOX10's expected size of 60-70 kDa. To produce null alleles of Sox10 in

PY230 cells, a similar strategy was used to identify Sox10^{null} clones, except the PY230-Cas9 cells were infected with an AAV sequentially containing: two sgRNAs cassettes targeting necessary coding regions near the start codon (CCAGCGACGGCGCGCTGCCT) and (GGCGGCGGCCGGGAGCGACA), and an EFS-tdTomatoNLS-WPRE cassette. Viability of resulting clones was confirmed by plating 100,000 cells Sox10^{null} cells in 2-D culture and quantifying their cell proliferation after 4 days, in comparison to the parental PY230 cell line.

Intravital imaging. Sox10^{tdTomatoNLS} PY230 cells infected with LV-CMV-eGFP were orthotopically transplanted into 6-10 week- old female syngeneic mice. Tumors were allowed to develop until they reached approximately 0.25cm³. For imaging, mice were anesthetized by IP injection of ketamine and xylazine (100/20 mg/kg) and maintained under anesthesia throughout the procedure using 1-2% (vol/vol) isoflurane gas mixed with oxygen. In order to visualize blood vessels and nuclei, mice were injected retro-orbitally with AlexaFluor 647 anti-mouse CD144 (VE-cadherin) antibody and Hoechst 33342 immediately following anesthesia induction. Tumors were exposed by carefully removing hair, skin, and connective tissue while keeping tumor vasculature intact. Mice were then placed inverted on an imaging apparatus, and each tumor was elevated and stabilized on a glass slide to reduce breathing artifacts. 80-150 micron images in 1024 × 1024 format were acquired with an HCX APO L20x objective on an upright Leica SP5 confocal system using Leica LAS AF 1.8.2 software. Videos were generated using Volocity 3D Image Analysis Software and compressed using Microsoft Video 1 compression.

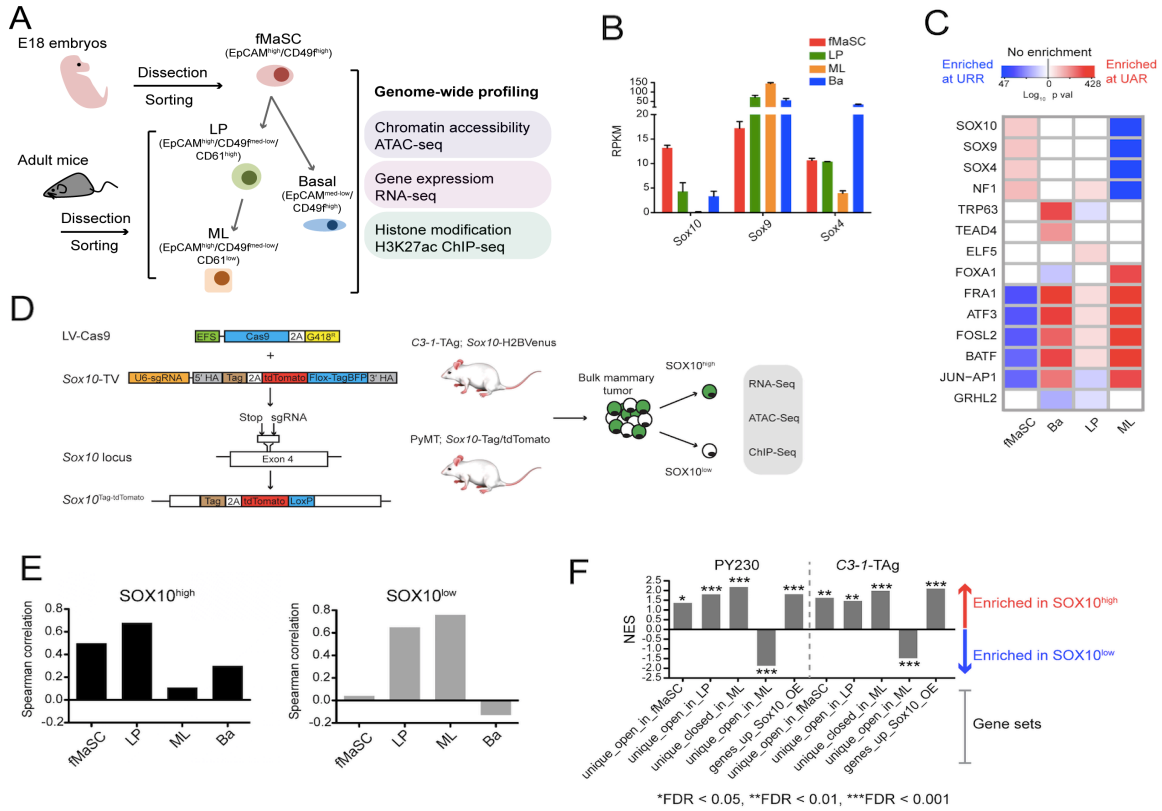


Figure Supplement 4.4. Sox10⁺ tumor cells exhibit mammary stem/progenitor features. (A) Experimental strategy for epigenetic and transcriptional profiling of mammary cells. **(B)** Transcript level of Sox factors. Mean \pm SEM (n=2). **(C)** Enrichment of transcription factor motifs at UAR/URR across mammary cell subpopulations. **(D)** Strategy to modify the Sox10 locus and characterize SOX10^{high} and SOX10^{low} tumor cells. **(E)** Correlation of chromatin accessibility in PY230 tumor cells with UARs and URRs in normal mammary cells. **(F)** GSEA of UAR or URR associated gene sets, and genes upregulated following Sox10^{OE} in SOX10^{high} and SOX10^{low} tumor cells.

Acknowledgements

We thank Charlene Huang for lab assistance, Rose Rodewald, Cynthia Ramos, and Luke Wang for lab management, Karissa Huang, Alexis Roth, and Jasmine Padilla for genotyping, Alfredo Molinolo in the Moores Cancer Center Biorepository and Tissue Technology Shared Resource for human tumor samples, Conor Fitzpatrick and Caz O'Connor in the Salk Flow Cytometry Core, Max Shokirev in the Salk Bioinformatics Core, Manching Ku in the Salk Next Generation Sequencing Core, John Naughton in the Viral Vector Core, Bing Ren, David Gorkin, Sebastian Preissl and Sven Heinz for assistance with ATAC- and ChIP-seq, and Jeff Rosen, Raj Girardi, and David O'Keefe for critical evaluation of the manuscript. GW was supported by a Cancer Center Core Grant (CA014195), NIH/NCI (R35 CA197687), the Susan G. Komen Foundation (SAC110036), and the BCRF. CD was supported by NRSA fellowship F32CA174430. NKL was supported by GM007752 and CA206416, and TR by CA186043 and CA197699.

Author contributions

CD, CC, and GW designed the experiments. CD, CC, NL, JHV, GL, CT performed the studies, and all authors contributed to result interpretation. CD, CC, and GW wrote the manuscript. TR and GW provided funding.

Dissertation Acknowledgements

Chapter 4, in part, a reprint of the material accepted to *Cancer Cell*. Dravis C*, Chung C-Y*, Lytle NK, Herrera-Valdez J, Luna G, Trejo CL, Reya T, Wahl GM. Epigenetic and transcriptomic profiling of mammary gland development and tumor models disclose regulators of cell state plasticity. *Cancer Cell* 2018. The dissertation author performed and analyzed all live imaging experiments for this publication.

REFERENCES

- 1 Bissell, M. J. & Radisky, D. Putting tumours in context. *Nat Rev Cancer* **1**, 46-54, doi:10.1038/35094059 (2001).
- 2 Orimo, A., Gupta, P. B., SgROI, D. C., Arenzana-Seisdedos, F., Delaunay, T., Naeem, R., Carey, V. J., Richardson, A. L. & Weinberg, R. A. Stromal fibroblasts present in invasive human breast carcinomas promote tumor growth and angiogenesis through elevated SDF-1/CXCL12 secretion. *Cell* **121**, 335-348, doi:10.1016/j.cell.2005.02.034 (2005).
- 3 Petersen, O. W., Ronnov-Jessen, L., Howlett, A. R. & Bissell, M. J. Interaction with basement membrane serves to rapidly distinguish growth and differentiation pattern of normal and malignant human breast epithelial cells. *Proc Natl Acad Sci U S A* **89**, 9064-9068 (1992).
- 4 Desgrosellier, J. S., Barnes, L. A., Shields, D. J., Huang, M., Lau, S. K., Prevost, N., Tarin, D., Shattil, S. J. & Cheresch, D. A. An integrin alpha(v)beta(3)-c-Src oncogenic unit promotes anchorage-independence and tumor progression. *Nat Med* **15**, 1163-1169, doi:10.1038/nm.2009 (2009).
- 5 Desgrosellier, J. S. & Cheresch, D. A. Integrins in cancer: biological implications and therapeutic opportunities. *Nat Rev Cancer* **10**, 9-22, doi:10.1038/nrc2748 (2010).
- 6 Nakasone, E. S., Askautrud, H. A., Kees, T., Park, J. H., Plaks, V., Ewald, A. J., Fein, M., Rasch, M. G., Tan, Y. X., Qiu, J., Park, J., Sinha, P., Bissell, M. J., Frengen, E., Werb, Z. & Egeblad, M. Imaging tumor-stroma interactions during chemotherapy reveals contributions of the microenvironment to resistance. *Cancer Cell* **21**, 488-503, doi:10.1016/j.ccr.2012.02.017 (2012).
- 7 Lee, J. J., Perera, R. M., Wang, H., Wu, D. C., Liu, X. S., Han, S., Fitamant, J., Jones, P. D., Ghanta, K. S., Kawano, S., Nagle, J. M., Deshpande, V., Boucher, Y., Kato, T., Chen, J. K., Willmann, J. K., Bardeesy, N. & Beachy, P. A. Stromal response to Hedgehog signaling restrains pancreatic cancer progression. *Proc Natl Acad Sci U S A* **111**, E3091-3100, doi:10.1073/pnas.1411679111 (2014).
- 8 Ozdemir, B. C., Pentcheva-Hoang, T., Carstens, J. L., Zheng, X., Wu, C. C., Simpson, T. R., Laklai, H., Sugimoto, H., Kahlert, C., Novitskiy, S. V., De Jesus-Acosta, A., Sharma, P., Heidari, P., Mahmood, U., Chin, L., Moses, H. L., Weaver, V. M., Maitra, A., Allison, J. P., LeBleu, V. S. & Kalluri, R. Depletion of carcinoma-associated fibroblasts and fibrosis induces immunosuppression and accelerates pancreas cancer with reduced survival. *Cancer Cell* **25**, 719-734, doi:10.1016/j.ccr.2014.04.005 (2014).
- 9 Rhim, A. D., Oberstein, P. E., Thomas, D. H., Mirek, E. T., Palermo, C. F., Sastra, S. A., Dekleva, E. N., Saunders, T., Becerra, C. P., Tattersall, I. W., Westphalen, C. B., Kitajewski, J., Fernandez-Barrena, M. G., Fernandez-Zapico, M. E., Iacobuzio-Donahue, C., Olive, K. P. & Stanger, B. Z. Stromal elements act to restrain, rather than support, pancreatic ductal adenocarcinoma. *Cancer Cell* **25**, 735-747, doi:10.1016/j.ccr.2014.04.021 (2014).
- 10 Fenczik, C. A., Sethi, T., Ramos, J. W., Hughes, P. E. & Ginsberg, M. H. ComplementatIOn of dominant suppression implicates CD98 in integrin activation. *Nature* **390**, 81-85, doi:10.1038/36349 (1997).
- 11 Feral, C. C., Nishiya, N., Fenczik, C. A., Stuhlmann, H., Slepak, M. & Ginsberg, M. H. CD98hc (SLC3A2) mediates integrin signaling. *Proc Natl Acad Sci U S A* **102**, 355-360, doi:10.1073/pnas.0404852102 (2005).

- 12 Feral, C. C., Zijlstra, A., Tkachenko, E., Prager, G., Gardel, M. L., Slepak, M. & Ginsberg, M. H. CD98hc (SLC3A2) participates in fibronectin matrix assembly by mediating integrin signaling. *J Cell Biol* **178**, 701-711, doi:10.1083/jcb.200705090 (2007).
- 13 Cantor, J. M. & Ginsberg, M. H. CD98 at the crossroads of adaptive immunity and cancer. *J Cell Sci* **125**, 1373-1382, doi:10.1242/jcs.096040 (2012).
- 14 Henderson, N. C., Collis, E. A., Mackinnon, A. C., Simpson, K. J., Haslett, C., Zent, R., Ginsberg, M. & Sethi, T. CD98hc (SLC3A2) interaction with beta 1 integrins is required for transformation. *J Biol Chem* **279**, 54731-54741, doi:10.1074/jbc.M408700200 (2004).
- 15 Hara, K., Kudoh, H., Enomoto, T., Hashimoto, Y. & Masuko, T. Malignant transformation of NIH3T3 cells by overexpression of early lymphocyte activation antigen CD98. *Biochem Biophys Res Commun* **262**, 720-725, doi:10.1006/bbrc.1999.1051 (1999).
- 16 Yagita, H., Masuko, T. & Hashimoto, Y. Inhibition of tumor cell growth in vitro by murine monoclonal antibodies that recognize a proliferation-associated cell surface antigen system in rats and humans. *Cancer Res* **46**, 1478-1484 (1986).
- 17 Imai, H., Kaira, K., Oriuchi, N., Shimizu, K., Tominaga, H., Yanagitani, N., Sunaga, N., Ishizuka, T., Nagamori, S., Promchan, K., Nakajima, T., Yamamoto, N., Mori, M. & Kanai, Y. Inhibition of L-type amino acid transporter 1 has antitumor activity in non-small cell lung cancer. *Anticancer Res* **30**, 4819-4828 (2010).
- 18 Shennan, D. B. & Thomson, J. Inhibition of system L (LAT1/CD98hc) reduces the growth of cultured human breast cancer cells. *Oncol Rep* **20**, 885-889 (2008).
- 19 Estrach, S., Lee, S. A., Boulter, E., Pisano, S., Errante, A., Tissot, F. S., Cailleteau, L., Pons, C., Ginsberg, M. H. & Feral, C. C. CD98hc (SLC3A2) loss protects against ras-driven tumorigenesis by modulating integrin-mediated mechanotransduction. *Cancer Res* **74**, 6878-6889, doi:10.1158/0008-5472.CAN-14-0579 (2014).
- 20 Nguyen, H. T., Dalmaso, G., Torkvist, L., Halfvarson, J., Yan, Y., Laroui, H., Shmerling, D., Tallone, T., D'Amato, M., Sitaraman, S. V. & Merlin, D. CD98 expression modulates intestinal homeostasis, inflammation, and colitis-associated cancer in mice. *J Clin Invest* **121**, 1733-1747, doi:10.1172/JCI44631 (2011).
- 21 Fenczik, C. A., Zent, R., Dellos, M., Calderwood, D. A., Satriano, J., Kelly, C. & Ginsberg, M. H. Distinct domains of CD98hc regulate integrins and amino acid transport. *J Biol Chem* **276**, 8746-8752, doi:10.1074/jbc.M011239200 (2001).
- 22 Fox, R. G., Lytle, N. K., Jaquish, D. V., Park, F. D., Ito, T., Bajaj, J., Koechlein, C. S., Zimdahl, B., Yano, M., Kopp, J., Kritzik, M., Sicklick, J., Sander, M., Grandgenett, P. M., Hollingsworth, M. A., Shibata, S., Pizzo, D., Valasek, M., Sasik, R., Scadeng, M., Okano, H., Kim, Y., MacLeod, A. R., Lowy, A. M. & Reya, T. Image-based detection and targeting of therapy resistance in pancreatic adenocarcinoma. *Nature* **534**, 407-411, doi:10.1038/nature17988 (2016).
- 23 Koechlein, C. S., Harris, J. R., Lee, T. K., Weeks, J., Fox, R. G., Zimdahl, B., Ito, T., Blevins, A., Jung, S. H., Chute, J. P., Chourasia, A., Covert, M. W. & Reya, T. High-resolution imaging and computational analysis of haematopoietic cell dynamics in vivo. *Nat Commun* **7**, 12169, doi:10.1038/ncomms12169 (2016).

- 24 Kwon, H. Y., Bajaj, J., Ito, T., Blevins, A., Konuma, T., Weeks, J., Lytle, N. K., Koechlein, C. S., Rizzieri, D., Chuah, C., Oehler, V. G., Sasik, R., Hardiman, G. & Reya, T. Tetraspanin 3 Is Required for the Development and Propagation of Acute Myelogenous Leukemia. *Cell Stem Cell* **17**, 152-164, doi:10.1016/j.stem.2015.06.006 (2015).
- 25 Zimdahl, B., Ito, T., Blevins, A., Bajaj, J., Konuma, T., Weeks, J., Koechlein, C. S., Kwon, H. Y., Arami, O., Rizzieri, D., Broome, H. E., Chuah, C., Oehler, V. G., Sasik, R., Hardiman, G. & Reya, T. Lis1 regulates asymmetric division in hematopoietic stem cells and in leukemia. *Nat Genet* **46**, 245-252, doi:10.1038/ng.2889 (2014).
- 26 Shipley, J. L. & Butera, J. N. Acute myelogenous leukemia. *Exp Hematol* **37**, 649-658, doi:10.1016/j.exphem.2009.04.002 (2009).
- 27 Chen, Y., Cortes, J., Estrov, Z., Faderl, S., Qiao, W., Abruzzo, L., Garcia-Manero, G., Pierce, S., Huang, X., Kebriaei, P., Kadia, T., De Lima, M., Kantarjian, H. & Ravandi, F. Persistence of cytogenetic abnormalities at complete remission after induction in patients with acute myeloid leukemia: prognostic significance and the potential role of allogeneic stem-cell transplantation. *J Clin Oncol* **29**, 2507-2513, doi:10.1200/JCO.2010.34.2873 (2011).
- 28 Fernandez, H. F., Sun, Z., Yao, X., Litzow, M. R., Luger, S. M., Paietta, E. M., Racevskis, J., Dewald, G. W., Ketterling, R. P., Bennett, J. M., Rowe, J. M., Lazarus, H. M. & Tallman, M. S. Anthracycline dose intensification in acute myeloid leukemia. *N Engl J Med* **361**, 1249-1259, doi:10.1056/NEJMoa0904544 (2009).
- 29 Krivtsov, A. V. & Armstrong, S. A. MLL translocations, histone modifications and leukaemia stem-cell development. *Nat Rev Cancer* **7**, 823-833, doi:10.1038/nrc2253 (2007).
- 30 Roboz, G. J. Current treatment of acute myeloid leukemia. *Curr Opin Oncol* **24**, 711-719, doi:10.1097/CCO.0b013e328358f62d (2012).
- 31 Zeisig, B. B., Kulasekararaj, A. G., Mufti, G. J. & So, C. W. SnapShot: Acute myeloid leukemia. *Cancer Cell* **22**, 698-698 e691, doi:10.1016/j.ccr.2012.10.017 (2012).
- 32 Ito, T., Kwon, H. Y., Zimdahl, B., Congdon, K. L., Blum, J., Lento, W. E., Zhao, C., Lagoo, A., Gerrard, G., Feroni, L., Goldman, J., Goh, H., Kim, S. H., Kim, D. W., Chuah, C., Oehler, V. G., Radich, J. P., Jordan, C. T. & Reya, T. Regulation of myeloid leukaemia by the cell-fate determinant Musashi. *Nature* **466**, 765-768, doi:10.1038/nature09171 (2010).
- 33 Byers, R. J., Currie, T., Tholouli, E., Rodig, S. J. & Kutok, J. L. MSI2 protein expression predicts unfavorable outcome in acute myeloid leukemia. *Blood* **118**, 2857-2867, doi:10.1182/blood-2011-04-346767 (2011).
- 34 Kharas, M. G., Lengner, C. J., Al-Shahrour, F., Bullinger, L., Ball, B., Zaidi, S., Morgan, K., Tam, W., Paktinat, M., Okabe, R., Gozo, M., Einhorn, W., Lane, S. W., Scholl, C., Frohling, S., Fleming, M., Ebert, B. L., Gilliland, D. G., Jaenisch, R. & Daley, G. Q. Musashi-2 regulates normal hematopoiesis and promotes aggressive myeloid leukemia. *Nat Med* **16**, 903-908, doi:10.1038/nm.2187 (2010).
- 35 Hemler, M. E. Tetraspanin functions and associated microdomains. *Nat Rev Mol Cell Biol* **6**, 801-811, doi:10.1038/nrm1736 (2005).

- 36 Wright, M. D., Moseley, G. W. & van Spruel, A. B. Tetraspanin microdomains in immune cell signalling and malignant disease. *Tissue Antigens* **64**, 533-542, doi:10.1111/j.1399-0039.2004.00321.x (2004).
- 37 Tiwari-Woodruff, S. K., Buznikov, A. G., Vu, T. Q., Micevych, P. E., Chen, K., Kornblum, H. I. & Bronstein, J. M. OSP/claudin-11 forms a complex with a novel member of the tetraspanin super family and beta1 integrin and regulates proliferation and migration of oligodendrocytes. *J Cell Biol* **153**, 295-305 (2001).
- 38 Colmone, A., Amorim, M., Pontier, A. L., Wang, S., Jablonski, E. & Sipkins, D. A. Leukemic cells create bone marrow niches that disrupt the behavior of normal hematopoietic progenitor cells. *Science* **322**, 1861-1865, doi:10.1126/science.1164390 (2008).
- 39 Paxinos G, F. K. Paxinos and Franklin's the Mouse Brain in Steriotaxic Coordinates. (2012).
- 40 Sipkins, D. A., Wei, X., Wu, J. W., Runnels, J. M., Cote, D., Means, T. K., Luster, A. D., Scadden, D. T. & Lin, C. P. In vivo imaging of specialized bone marrow endothelial microdomains for tumour engraftment. *Nature* **435**, 969-973, doi:10.1038/nature03703 (2005).
- 41 DeSantis, C., Ma, J., Bryan, L. & Jemal, A. Breast cancer statistics, 2013. *CA Cancer J Clin* **64**, 52-62, doi:10.3322/caac.21203 (2014).
- 42 Ferlay, J., Steliarova-Foucher, E., Lortet-Tieulent, J., Rosso, S., Coebergh, J. W., Comber, H., Forman, D. & Bray, F. Cancer incidence and mortality patterns in Europe: estimates for 40 countries in 2012. *Eur J Cancer* **49**, 1374-1403, doi:10.1016/j.ejca.2012.12.027 (2013).
- 43 Fidler, I. J. The pathogenesis of cancer metastasis: the 'seed and soil' hypothesis revisited. *Nat Rev Cancer* **3**, 453-458, doi:10.1038/nrc1098 (2003).
- 44 Wan, L., Pantel, K. & Kang, Y. Tumor metastasis: moving new biological insights into the clinic. *Nat Med* **19**, 1450-1464, doi:10.1038/nm.3391 (2013).
- 45 Pestlin G, e. a. US Patent 20060257950A. (2006).
- 46 Bhoj, V. G. & Chen, Z. J. Ubiquitylation in innate and adaptive immunity. *Nature* **458**, 430-437, doi:10.1038/nature07959 (2009).
- 47 Wang, G., Gao, Y., Li, L., Jin, G., Cai, Z., Chao, J. I. & Lin, H. K. K63-linked ubiquitination in kinase activation and cancer. *Front Oncol* **2**, 5, doi:10.3389/fonc.2012.00005 (2012).
- 48 Yamamoto, M., Sato, S., Saitoh, T., Sakurai, H., Uematsu, S., Kawai, T., Ishii, K. J., Takeuchi, O. & Akira, S. Cutting Edge: Pivotal function of Ubc13 in thymocyte TCR signaling. *J Immunol* **177**, 7520-7524 (2006).
- 49 Yamamoto, M., Okamoto, T., Takeda, K., Sato, S., Sanjo, H., Uematsu, S., Saitoh, T., Yamamoto, N., Sakurai, H., Ishii, K. J., Yamaoka, S., Kawai, T., Matsuura, Y., Takeuchi, O. & Akira, S. Key function for the Ubc13 E2 ubiquitin-conjugating enzyme in immune receptor signaling. *Nat Immunol* **7**, 962-970, doi:10.1038/ni1367 (2006).
- 50 Tseng, P. H., Matsuzawa, A., Zhang, W., Mino, T., Vignali, D. A. & Karin, M. Different modes of ubiquitination of the adaptor TRAF3 selectively activate the expression of type I interferons and proinflammatory cytokines. *Nat Immunol* **11**, 70-75, doi:10.1038/ni.1819 (2010).

- 51 Matsuzawa, A., Tseng, P. H., Vallabhapurapu, S., Luo, J. L., Zhang, W., Wang, H., Vignali, D. A., Gallagher, E. & Karin, M. Essential cytoplasmic translocation of a cytokine receptor-assembled signaling complex. *Science* **321**, 663-668, doi:10.1126/science.1157340 (2008).
- 52 Cuevas, B. D., Winter-Vann, A. M., Johnson, N. L. & Johnson, G. L. MEKK1 controls matrix degradation and tumor cell dissemination during metastasis of polyoma middle-T driven mammary cancer. *Oncogene* **25**, 4998-5010, doi:10.1038/sj.onc.1209507 (2006).
- 53 Safina, A., Ren, M. Q., Vandette, E. & Bakin, A. V. TAK1 is required for TGF-beta 1-mediated regulation of matrix metalloproteinase-9 and metastasis. *Oncogene* **27**, 1198-1207, doi:10.1038/sj.onc.1210768 (2008).
- 54 Padua, D. & Massague, J. Roles of TGFbeta in metastasis. *Cell Res* **19**, 89-102, doi:10.1038/cr.2008.316 (2009).
- 55 Derynck, R. & Zhang, Y. E. Smad-dependent and Smad-independent pathways in TGF-beta family signalling. *Nature* **425**, 577-584, doi:10.1038/nature02006 (2003).
- 56 Massague, J. TGFbeta in Cancer. *Cell* **134**, 215-230, doi:10.1016/j.cell.2008.07.001 (2008).
- 57 Sorrentino, A., Thakur, N., Grimsby, S., Marcusson, A., von Bulow, V., Schuster, N., Zhang, S., Heldin, C. H. & Landstrom, M. The type I TGF-beta receptor engages TRAF6 to activate TAK1 in a receptor kinase-independent manner. *Nat Cell Biol* **10**, 1199-1207, doi:10.1038/ncb1780 (2008).
- 58 Yamashita, M., Fatyol, K., Jin, C., Wang, X., Liu, Z. & Zhang, Y. E. TRAF6 mediates Smad-independent activation of JNK and p38 by TGF-beta. *Mol Cell* **31**, 918-924, doi:10.1016/j.molcel.2008.09.002 (2008).
- 59 Zhang, L., Zhou, F., Garcia de Vinuesa, A., de Kruijf, E. M., Mesker, W. E., Hui, L., Drabsch, Y., Li, Y., Bauer, A., Rousseau, A., Sheppard, K. A., Mickanin, C., Kuppen, P. J., Lu, C. X. & Ten Dijke, P. TRAF4 promotes TGF-beta receptor signaling and drives breast cancer metastasis. *Mol Cell* **51**, 559-572, doi:10.1016/j.molcel.2013.07.014 (2013).
- 60 del Barco Barrantes, I. & Nebreda, A. R. Roles of p38 MAPKs in invasion and metastasis. *Biochem Soc Trans* **40**, 79-84, doi:10.1042/BST20110676 (2012).
- 61 Yong, H. Y., Koh, M. S. & Moon, A. The p38 MAPK inhibitors for the treatment of inflammatory diseases and cancer. *Expert Opin Investig Drugs* **18**, 1893-1905, doi:10.1517/13543780903321490 (2009).
- 62 Anand, P., Shenoy, R., Palmer, J. E., Baines, A. J., Lai, R. Y., Robertson, J., Bird, N., Ostefeld, T. & Chizh, B. A. Clinical trial of the p38 MAP kinase inhibitor dilmapiomod in neuropathic pain following nerve injury. *Eur J Pain* **15**, 1040-1048, doi:10.1016/j.ejpain.2011.04.005 (2011).
- 63 Meerbrey, K. L., Hu, G., Kessler, J. D., Roarty, K., Li, M. Z., Fang, J. E., Herschkowitz, J. I., Burrows, A. E., Ciccio, A., Sun, T., Schmitt, E. M., Bernardi, R. J., Fu, X., Bland, C. S., Cooper, T. A., Schiff, R., Rosen, J. M., Westbrook, T. F. & Elledge, S. J. The pINDUCER lentiviral toolkit for inducible RNA interference in vitro and in vivo. *Proc Natl Acad Sci U S A* **108**, 3665-3670, doi:10.1073/pnas.1019736108 (2011).
- 64 Minn, A. J., Gupta, G. P., Siegel, P. M., Bos, P. D., Shu, W., Giri, D. D., Viale, A., Olshen, A. B., Gerald, W. L. & Massague, J. Genes that mediate breast cancer metastasis to lung. *Nature* **436**, 518-524, doi:10.1038/nature03799 (2005).

- 65 Biswas, T., Gu, X., Yang, J., Ellies, L. G. & Sun, L. Z. Attenuation of TGF-beta signaling supports tumor progression of a mesenchymal-like mammary tumor cell line in a syngeneic murine model. *Cancer Lett* **346**, 129-138, doi:10.1016/j.canlet.2013.12.018 (2014).
- 66 Tan, W., Zhang, W., Strasner, A., Grivennikov, S., Cheng, J. Q., Hoffman, R. M. & Karin, M. Tumour-infiltrating regulatory T cells stimulate mammary cancer metastasis through RANKL-RANK signalling. *Nature* **470**, 548-553, doi:10.1038/nature09707 (2011).
- 67 Yang, Y., Yin, C., Pandey, A., Abbott, D., Sasseti, C. & Kelliher, M. A. NOD2 pathway activation by MDP or Mycobacterium tuberculosis infection involves the stable polyubiquitination of Rip2. *J Biol Chem* **282**, 36223-36229, doi:10.1074/jbc.M703079200 (2007).
- 68 Chumakov, A. M., Silla, A., Williamson, E. A. & Koeffler, H. P. Modulation of DNA binding properties of CCAAT/enhancer binding protein epsilon by heterodimer formation and interactions with NFkappaB pathway. *Blood* **109**, 4209-4219, doi:10.1182/blood-2005-09-031963 (2007).
- 69 Marusyk, A., Almendro, V. & Polyak, K. Intra-tumour heterogeneity: a looking glass for cancer? *Nat Rev Cancer* **12**, 323-334, doi:10.1038/nrc3261 (2012).
- 70 Wainwright, E. N. & Scaffidi, P. Epigenetics and Cancer Stem Cells: Unleashing, Hijacking, and Restricting Cellular Plasticity. *Trends Cancer* **3**, 372-386, doi:10.1016/j.trecan.2017.04.004 (2017).
- 71 Ge, Y. & Fuchs, E. Stretching the limits: from homeostasis to stem cell plasticity in wound healing and cancer. *Nat Rev Genet* **19**, 311-325, doi:10.1038/nrg.2018.9 (2018).
- 72 Ge, Y., Gomez, N. C., Adam, R. C., Nikolova, M., Yang, H., Verma, A., Lu, C. P., Polak, L., Yuan, S., Elemento, O. & Fuchs, E. Stem Cell Lineage Infidelity Drives Wound Repair and Cancer. *Cell* **169**, 636-650 e614, doi:10.1016/j.cell.2017.03.042 (2017).
- 73 Wahl, G. M. & Spike, B. T. Cell state plasticity, stem cells, EMT, and the generation of intra-tumoral heterogeneity. *NPJ Breast Cancer* **3**, 14, doi:10.1038/s41523-017-0012-z (2017).
- 74 Schwitalla, S., Fingerle, A. A., Cammareri, P., Nebelsiek, T., Goktuna, S. I., Ziegler, P. K., Canli, O., Heijmans, J., Huels, D. J., Moreaux, G., Rupec, R. A., Gerhard, M., Schmid, R., Barker, N., Clevers, H., Lang, R., Neumann, J., Kirchner, T., Taketo, M. M., van den Brink, G. R., Sansom, O. J., Arkan, M. C. & Greten, F. R. Intestinal tumorigenesis initiated by dedifferentiation and acquisition of stem-cell-like properties. *Cell* **152**, 25-38, doi:10.1016/j.cell.2012.12.012 (2013).
- 75 Tata, P. R., Mou, H., Pardo-Saganta, A., Zhao, R., Prabhu, M., Law, B. M., Vinarsky, V., Cho, J. L., Breton, S., Sahay, A., Medoff, B. D. & Rajagopal, J. Dedifferentiation of committed epithelial cells into stem cells in vivo. *Nature* **503**, 218-223, doi:10.1038/nature12777 (2013).
- 76 de Sousa e Melo, F., Kurtova, A. V., Harnoss, J. M., Kljavin, N., Hoeck, J. D., Hung, J., Anderson, J. E., Storm, E. E., Modrusan, Z., Koeppen, H., Dijkgraaf, G. J., Piskol, R. & de Sauvage, F. J. A distinct role for Lgr5(+) stem cells in primary and metastatic colon cancer. *Nature* **543**, 676-680, doi:10.1038/nature21713 (2017).
- 77 Shimokawa, M., Ohta, Y., Nishikori, S., Matano, M., Takano, A., Fujii, M., Date, S., Sugimoto, S., Kanai, T. & Sato, T. Visualization and targeting of LGR5(+) human colon cancer stem cells. *Nature* **545**, 187-192, doi:10.1038/nature22081 (2017).

- 78 Inman, J. L., Robertson, C., Mott, J. D. & Bissell, M. J. Mammary gland development: cell fate specification, stem cells and the microenvironment. *Development* **142**, 1028-1042, doi:10.1242/dev.087643 (2015).
- 79 Shackleton, M., Vaillant, F., Simpson, K. J., Stingl, J., Smyth, G. K., Asselin-Labat, M. L., Wu, L., Lindeman, G. J. & Visvader, J. E. Generation of a functional mammary gland from a single stem cell. *Nature* **439**, 84-88, doi:10.1038/nature04372 (2006).
- 80 Stingl, J., Eirew, P., Ricketson, I., Shackleton, M., Vaillant, F., Choi, D., Li, H. I. & Eaves, C. J. Purification and unique properties of mammary epithelial stem cells. *Nature* **439**, 993-997, doi:10.1038/nature04496 (2006).
- 81 Davis, F. M., Lloyd-Lewis, B., Harris, O. B., Kozar, S., Winton, D. J., Muresan, L. & Watson, C. J. Single-cell lineage tracing in the mammary gland reveals stochastic clonal dispersion of stem/progenitor cell progeny. *Nat Commun* **7**, 13053, doi:10.1038/ncomms13053 (2016).
- 82 Girardi, R. R., Shehata, M., Gallardo, M., Blasco, M. A., Simons, B. D. & Stingl, J. Stem and progenitor cell division kinetics during postnatal mouse mammary gland development. *Nat Commun* **6**, 8487, doi:10.1038/ncomms9487 (2015).
- 83 Rios, A. C., Fu, N. Y., Lindeman, G. J. & Visvader, J. E. In situ identification of bipotent stem cells in the mammary gland. *Nature* **506**, 322-327, doi:10.1038/nature12948 (2014).
- 84 Van Keymeulen, A., Rocha, A. S., Ousset, M., Beck, B., Bouvencourt, G., Rock, J., Sharma, N., Dekoninck, S. & Blanpain, C. Distinct stem cells contribute to mammary gland development and maintenance. *Nature* **479**, 189-193, doi:10.1038/nature10573 (2011).
- 85 Wang, D., Cai, C., Dong, X., Yu, Q. C., Zhang, X. O., Yang, L. & Zeng, Y. A. Identification of multipotent mammary stem cells by protein C receptor expression. *Nature* **517**, 81-84, doi:10.1038/nature13851 (2015).
- 86 Wuidart, A., Ousset, M., Rulands, S., Simons, B. D., Van Keymeulen, A. & Blanpain, C. Quantitative lineage tracing strategies to resolve multipotency in tissue-specific stem cells. *Genes Dev* **30**, 1261-1277, doi:10.1101/gad.280057.116 (2016).
- 87 Makarem, M., Kannan, N., Nguyen, L. V., Knapp, D. J., Balani, S., Prater, M. D., Stingl, J., Raouf, A., Nemirovsky, O., Eirew, P. & Eaves, C. J. Developmental changes in the in vitro activated regenerative activity of primitive mammary epithelial cells. *PLoS Biol* **11**, e1001630, doi:10.1371/journal.pbio.1001630 (2013).
- 88 Spike, B. T., Engle, D. D., Lin, J. C., Cheung, S. K., La, J. & Wahl, G. M. A mammary stem cell population identified and characterized in late embryogenesis reveals similarities to human breast cancer. *Cell Stem Cell* **10**, 183-197, doi:10.1016/j.stem.2011.12.018 (2012).
- 89 Asselin-Labat, M. L., Sutherland, K. D., Barker, H., Thomas, R., Shackleton, M., Forrest, N. C., Hartley, L., Robb, L., Grosveld, F. G., van der Wees, J., Lindeman, G. J. & Visvader, J. E. Gata-3 is an essential regulator of mammary-gland morphogenesis and luminal-cell differentiation. *Nat Cell Biol* **9**, 201-209, doi:10.1038/ncb1530 (2007).
- 90 Pellacani, D., Bilenky, M., Kannan, N., Heravi-Moussavi, A., Knapp, D., Gakkhar, S., Moksa, M., Carles, A., Moore, R., Mungall, A. J., Marra, M. A., Jones, S. J. M., Aparicio, S., Hirst, M. & Eaves, C. J. Analysis of Normal Human Mammary Epigenomes Reveals Cell-Specific Active Enhancer

- States and Associated Transcription Factor Networks. *Cell Rep* **17**, 2060-2074, doi:10.1016/j.celrep.2016.10.058 (2016).
- 91 Kim, Y. J., Lim, H., Li, Z., Oh, Y., Kovlyagina, I., Choi, I. Y., Dong, X. & Lee, G. Generation of multipotent induced neural crest by direct reprogramming of human postnatal fibroblasts with a single transcription factor. *Cell Stem Cell* **15**, 497-506, doi:10.1016/j.stem.2014.07.013 (2014).
- 92 Dravis, C., Spike, B. T., Harrell, J. C., Johns, C., Trejo, C. L., Southard-Smith, E. M., Perou, C. M. & Wahl, G. M. Sox10 Regulates Stem/Progenitor and Mesenchymal Cell States in Mammary Epithelial Cells. *Cell Rep* **12**, 2035-2048, doi:10.1016/j.celrep.2015.08.040 (2015).
- 93 Corpening, J. C., Deal, K. K., Cantrell, V. A., Skelton, S. B., Buehler, D. P. & Southard-Smith, E. M. Isolation and live imaging of enteric progenitors based on Sox10-Histone2BVenus transgene expression. *Genesis* **49**, 599-618, doi:10.1002/dvg.20748 (2011).
- 94 Finzsch, M., Schreiner, S., Kichko, T., Reeh, P., Tamm, E. R., Bosl, M. R., Meijer, D. & Wegner, M. Sox10 is required for Schwann cell identity and progression beyond the immature Schwann cell stage. *J Cell Biol* **189**, 701-712, doi:10.1083/jcb.200912142 (2010).
- 95 Maroulakou, I. G., Anver, M., Garrett, L. & Green, J. E. Prostate and mammary adenocarcinoma in transgenic mice carrying a rat C3(1) simian virus 40 large tumor antigen fusion gene. *Proc Natl Acad Sci U S A* **91**, 11236-11240 (1994).
- 96 de Vries, W. N., Binns, L. T., Fancher, K. S., Dean, J., Moore, R., Kemler, R. & Knowles, B. B. Expression of Cre recombinase in mouse oocytes: a means to study maternal effect genes. *Genesis* **26**, 110-112 (2000).
- 97 Bao, L., Cardiff, R. D., Steinbach, P., Messer, K. S. & Ellies, L. G. Multipotent luminal mammary cancer stem cells model tumor heterogeneity. *Breast Cancer Res* **17**, 137, doi:10.1186/s13058-015-0615-y (2015).
- 98 Sanjana, N. E., Shalem, O. & Zhang, F. Improved vectors and genome-wide libraries for CRISPR screening. *Nat Methods* **11**, 783-784, doi:10.1038/nmeth.3047 (2014).